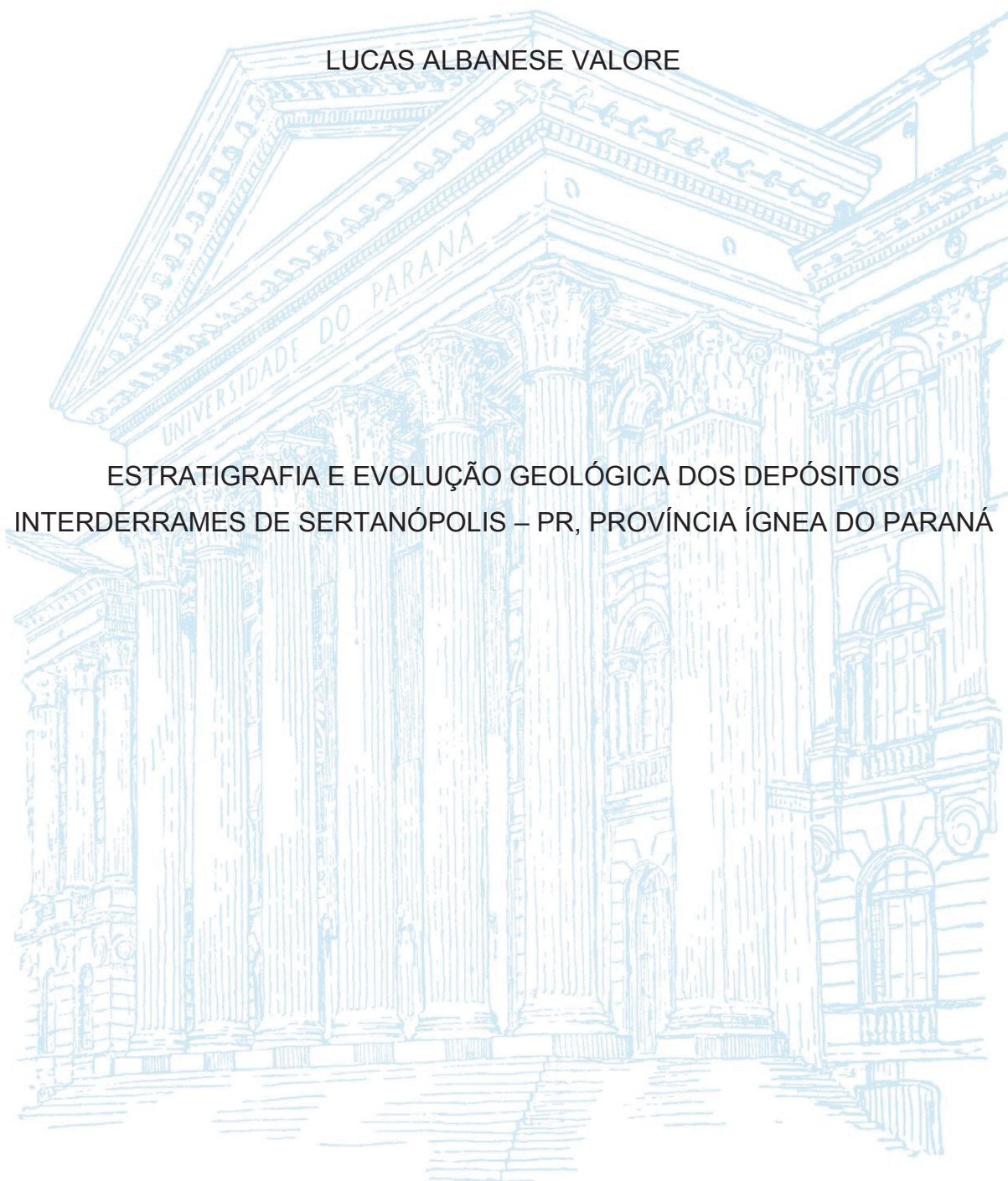UNIVERSIDADE FEDERAL DO PARANÁ

LUCAS ALBANESE VALORE

ESTRATIGRAFIA E EVOLUÇÃO GEOLÓGICA DOS DEPÓSITOS
INTERDERRAMES DE SERTANÓPOLIS – PR, PROVÍNCIA ÍGNEA DO PARANÁ

CURITIBA

2020

LUCAS ALBANESE VALORE

ESTRATIGRAFIA E EVOLUÇÃO GEOLÓGICA DOS DEPÓSITOS
INTERDERRAMES DE SERTANÓPOLIS – PR, PROVÍNCIA ÍGNEA DO PARANÁ

Dissertação apresentada ao Programa de Pós-Graduação em Geologia, Setor de Ciências da Terra, Universidade Federal do Paraná, como requisito parcial à obtenção do título de Mestre em Geologia.

Orientador: Prof. Dr. Otavio Augusto Boni Licht

Coorientadora: Prof. Dra. Eleonora Maria Gouvea Vasconcellos

CURITIBA

2020

MINISTÉRIO DA EDUCAÇÃO
SETOR DE CIENCIAS DA TERRA
UNIVERSIDADE FEDERAL DO PARANÁ
PRÓ-REITORIA DE PESQUISA E PÓS-GRADUAÇÃO
PROGRAMA DE PÓS-GRADUAÇÃO GEOLOGIA -
40001016028P5

TERMO DE APROVAÇÃO

Os membros da Banca Examinadora designada pelo Colegiado do Programa de Pós-Graduação em GEOLOGIA da Universidade Federal do Paraná foram convocados para realizar a arguição da Dissertação de Mestrado de **LUCAS ALBANESE VALORE** intitulada: **ESTRATIGRAFIA E EVOLUÇÃO GEOLÓGICA DO DEPÓSITO INTERDERRAMES DE SERTANÓPOLIS - PR, PROVÍNCIA ÍGNEA DO PARANÁ**, sob orientação do Prof. Dr. OTAVIO AUGUSTO BONI LICHT, que após terem inquirido o aluno e realizada a avaliação do trabalho, são de parecer pela sua APROVAÇÃO no rito de defesa.

A outorga do título de mestre está sujeita à homologação pelo colegiado, ao atendimento de todas as indicações e correções solicitadas pela banca e ao pleno atendimento das demandas regimentais do Programa de Pós-Graduação.

CURITIBA, 13 de Abril de 2020.

Assinatura Eletrônica
13/04/2020 12:29:31.0
OTAVIO AUGUSTO BONI LICHT
Presidente da Banca Examinadora (UNIVERSIDADE FEDERAL DO PARANÁ)

Assinatura Eletrônica
13/04/2020 12:28:00.0
CARLOS CONFORTI FERREIRA GUEDES
Avaliador Interno (UNIVERSIDADE FEDERAL DO PARANÁ)

Assinatura Eletrônica
13/04/2020 14:59:29.0
LUCIA CASTANHEIRA DE MORAES
Avaliador Externo (CENTRO FEDERAL DE EDUCAÇÃO TECN. DE MINAS GERAIS)

D E C L A R A Ç Ã O

Declaramos para os devidos fins que **LUCAS ALBANESE VALORE** realizou sua defesa de dissertação intitulada "**ESTRATIGRAFIA E EVOLUÇÃO GEOLÓGICA DO DEPÓSITO INTERDERRAMES DE SERTANÓPOLIS - PR, PROVÍNCIA ÍGNEA DO PARANÁ**" em 13 de abril de 2020, no Programa de Pós-Graduação em Geologia da Universidade Federal do Paraná, área Geologia Exploratória, nível Mestrado, e que por sugestão da banca examinadora, o título foi alterado para "**ESTRATIGRAFIA E EVOLUÇÃO GEOLÓGICA DOS DEPÓSITOS INTERDERRAMES DE SERTANÓPOLIS - PR, PROVÍNCIA ÍGNEA DO PARANÁ**".

Curitiba, 22 de junho de 2020

Carlos Conforti Ferreira Guedes
Coordenador do Programa
Pós-Graduação em Geologia

Dedico esta dissertação a todos os educadores e educadoras do Brasil.

AGRADECIMENTOS

"Give me the liberty to know, to utter, and to argue freely according to conscience, above all liberties."

— John Milton, Areopagitica

RESUMO

A Província Ígnea do Paraná (PIP), situada no sudeste da plataforma continental sulamericana, é geralmente destacada como a segunda maior Província Continental Basáltica (PCB) do mundo. No entanto, seu arcabouço estratigráfico ainda carece de investigações que possibilitem alcançar um entendimento pleno e integrado entre diferentes linhas e grupos de pesquisa. O estudo de camadas interderrames pode auxiliar consideravelmente nesta tarefa, uma vez que permite a elaboração de modelos faciológicos mais completos de produtos vulcânicos, favorecendo inferências sobre condições paleoambientais. Neste sentido, os depósitos interderrames de Sertanópolis, no norte do Paraná, representam uma importante oportunidade de pesquisa estratigráfica e sedimentológica na PIP. Nesta região, foram realizadas etapas de mapeamento geológico, com levantamento de seções e descrição de 96 afloramentos. Amostras de camadas interderrames e basaltos foram coletadas para preparo de seções delgadas, e análises litogeoquímicas foram realizadas em amostras de basaltos a partir da fluorescência de raios-x. Materiais interderrames foram analisados em microscopia eletrônica de varredura com espectrômetro de energia dispersiva acoplado (MEV-EDS). Os resultados indicam que quatro distintas camadas interderrames afloram na transição entre a Formação Pitanga e Paranapanema, sendo separadas por unidades vulcânicas de 20 a 50 m de espessura. Estas unidades correspondem a campos de lava compostos típicos (Fm. Pitanga) e campos de lava com derrames tabulares espessos (Fm. Paranapanema). Foram descritas 13 fácies interderrames, que incluem brechas, lapilli-tufos, tufos e depósitos vulcanogênicos retrabalhados. As fácies de granulação fina apresentam frequente vesiculação, além de estratificações difusas a estruturas características de migração e agradação de dunas, como laminação cruzada em *sets* decimétricos, laminações onduladas e estratificação em *backsets*. As fácies finas (tufos, lapilli-tufos) são ricas em material siliclástico (30 - 80 %), mica hidrotermal (<5 - 40 %), agregados de cinza com argilominerais (5 – 20 %) e fragmentos de vidro e basalto (<5 – 15 %). Estas fácies são interpretadas como tufos ricos em material acessório, com contribuição juvenil representada por fragmentos basálticos (holo ou hipohialinos) densos a moderadamente vesiculares, cristaloclastos de augita e agregados de cinza extremamente fina maciços ou acamadados, ricos em vidro alterado hidrotermalmente. Já as fácies mais grossas são brechas basálticas de arcabouço escoriáceo, com matriz siliciclástica comumente laminada e rítmica, de arranjo independente do arcabouço. Todas estas fácies são interpretadas como piroclásticas e hidrovulcânicas. Por fim, são descritas também brechas autoclásticas e peperitos, associados a topos e bases de derrame, respectivamente. As rochas piroclásticas interderrames de Sertanópolis apresentam características sugestivas de colocação a partir de múltiplas correntes piroclásticas de densidade (CDPs) com plumas úmidas cognatas e menor contribuição de deposição exclusivamente por queda. De maneira geral, as características dos depósitos vulcanoclásticos em Sertanópolis são semelhantes às de várias outras ocorrências no Paraná, o que favorece a hipótese de que fenômenos hidrovulcânicos explosivos devem ter sido tão frequentes na PIP quanto em diversas outras províncias continentais basálticas.

PALAVRAS-CHAVE: Províncias basálticas, vulcanologia, hidrovulcanismo.

ABSTRACT

The Paraná Igneous Province is a continental flood basalt province (CFBP) located in the southeastern part of South America, being correlated to Etendeka in Southwest Africa. Its lithostratigraphic framework is still being assessed by several different research groups, which need to come up with a regionally robust and integrated proposal. The study of sedimentary and volcaniclastic interflow deposits can considerably assist this, given that it allows for better chrono and lithostratigraphic correlations, while also helping interpret the palaeoenvironmental and volcanological evolution of the province. In northern Paraná, interflow beds exposed near the city of Sertanópolis represent an important research opportunity. In this region, we have conducted geological mapping, describing geological sections and a total of 96 outrcrops. Samples of interflow deposits and basalts were collected for thin section studies, and geochemical analyses of flows were conducted with X-ray fluorescence. Interflow materials were also examined with the help of scanning electron microscopy. Results indicate that four distinct interflow deposits are exposed at the transition from Pitanga to Paranapanema formations, and these units are separated by 20 – 50 m thick effusive volcanic intervals, which correspond to typical compound flow fields (Pitanga Fm.) and sheet flood flow fields (Paranapanema Fm.). Thirteen clastic facies were recognized, including breccias, lapilli-tuffs, tuffs and epiclastic volcanogenic sandstones. Fine-grained facies are frequently vesiculated and show diffuse stratification to well-defined dune-bedding structures, such as cross-laminated decimetric sets, wavy lamination and backset-lamination. These facies are composed mostly by fine siliciclastic material (30 – 80 %), hydrothermal mica crystals (<5 - 40 %), clay-mineral-rich ash aggregates (5 – 20 %) and glass and basalt fragments (<5 – 15 %). These facies are interpreted as hydromagmatic and pyroclastic accessory-crystal-rich tuffs/lapilli-tuffs with lesser amounts of juvenile fragments, which correspond to dense to moderately vesicular glass and basalt fragments (ash to lapilli), augite crystals and extremely fine ash in massive and layered aggregates. Coarse-grained facies are basalt breccias with scoriaceous framework, hosted by a commonly laminated siliciclastic matrix, which is also interpreted as pyroclastic. Lastly, autoclastic breccias and peperites are described close to flow-top and flow-base zones, respectively. Pyroclastic rocks at Sertanópolis have features that suggest emplacement by multiple pyroclastic density currents (PDCs) with cognate wet drifting plumes and lesser contribution of exclusive fallout. Pyroclastic breccias represent proximal PDC and ballistic curtain deposits that occur near a possible conduit, at the eastern section. Their scoriaceous framework suggests influence of magmatic-like fragmentation or vesiculation before explosive magma-water interaction. Stratigraphic and compositional characteristics of interflow deposits suggest that explosions occurred in confined permeable aquifers below the Sertanópolis succession, most likely other interflow deposits up to 250 m deep. This setting favored lateral explosion *loci* migration, generating a wide and polycyclic maar-like complex. In conclusion, features of volcaniclastic beds in Sertanópolis are similar to many other interflow deposits in the province, which suggests that explosive hydrovolcanic phenomena were as frequent in the PIP as in many other continental flood basalt provinces.

KEYWORDS: Flood basalts, physical volcanology, hydrovolcanism.

LISTA DE FIGURAS

CAPÍTULO I

CAPÍTULO II

CAPÍTULO III

CAPÍTULO IV

LISTA DE TABELAS

SUMÁRIO

1 CAPÍTULO I - INTRODUÇÃO

Províncias Continentais Basalticas (PCBs, ou *Continental Flood Basalt Province*s em inglês) são imensas acumulações de rochas vulcânicas máficas (com comuns contrapartes intrusivas e vulcanoclásticas) presentes em quase todos os continentes do planeta (Jerram e Widdowson, 2005; White *et al.,* 2009). PCBs formam o que podem ser denominadas bacias vulcânicas, e comumente se encontram associadas e intercaladas a registros sedimentares continentais (Single e Jerram, 2004; Jerram e Widdowson, 2005; White *et al.*, 2009). Algumas das PCBs mais conhecidas e estudadas incluem os Trapps Siberianos (Permiano - Triássico, Rússia), a Província do Deccan (Cretáceo – Paleoceno, Índia), a Província Columbia River (Mioceno, Estados Unidos), parte da Província Ígnea do Atlântico Norte (Paleoceno) e a Província Ígnea do Paraná, tema desta dissertação.

Os grandes volumes de magmatismo máfico que dão origem a PCBs têm sido entendidos como resultados da fusão anômala do manto superior, em situações que diferem consideravelmente da criação de crosta oceânica típica a partir de vulcanismo do tipo *mid ocean ridge* ou mesmo do vulcanismo em áreas de subducção (Coffin e Eldholm, 1994; Ernst *et al.*, 2005; Jerram e Widdownson, 2005; Bryan e Ernst, 2008). Estes elevados níveis de fusão vêm sendo associados a modelos de origem distintos, que incluem desde a clássica teoria das plumas mantélicas originadas na transição núcleo-manto (Fodor, 1987; Campbell, 2007) até novas hipóteses, baseadas em fenômenos como a fusão do manto "fértil" ou enriquecido sem anomalias térmicas (Anderson, 2005, 2007) e a conexão entre fraturas litosféricas e grandes reservatórios de magma basáltico sublitosférico (Silver *et al*., 2006).

A Província Ígnea do Paraná (PIP) é uma PCB localizada no centro-sudeste do continente sul-americano, em uma área de quase 1 milhão de km^2 que se estende desde boa parte do centro-sul brasileiro até porções do Uruguai, Paraguai, Argentina – a PIP é geralmente considerada a segunda maior PCB do planeta, possuindo área menor apenas que os Trapps Siberianos (Frank *et al.*, 2009). A província está colocada sobre cerca de 6000 m de sedimentos fanerozoicos da Bacia do Paraná, sendo também coberta por uma delgada (~300 m) sucessão pós-vulcânica cretácica (Piccirillo e Melfi, 1988; Peate, 1989, 1997; Machado *et al.* 2007; Fernandes *et al*., 2015) Os derrames que formam esta PCB recebem tipicamente a nomenclatura

estratigráfica "Formação Serra Geral" no Brasil, nome que se encontra agora formalmente elevado à categoria de Grupo (Rossetti *et al*., 2018; Licht e Arioli, 2018).

A Província Ígnea do Paraná e a Bacia do Paraná foram evidências chave de pesquisas que validaram a existência da então chamada "Deriva Continental" e a hipótese de abertura do Atlântico Sul durante o Cretáceo, o que se deve à correlação da PIP à Província Ígnea Etendeka e da Bacia do Paraná às sequências sedimentares de Karoo e Huab na África Ocidental, documentadas nos importantes trabalhos de du Toit (1927,1937), Bigarella (1970) e Bigarella e Van Eeden (1970) e intensamente estudadas até os dias atuais (Erlank *et al.,* 1984; Milner *et al*., 1995; Peate, 1997; Milani e De Wit, 2008).

O arcabouço litológico e vulcanológico da PIP tem interessado geocientistas desde o final do século XIX, conforme registrado nas clássicas descrições de Derby (1878), Oliveira (1916), Baker (1923), Washburne (1930) e Leinz (1949). De acordo com Licht (2014), estes estudos clássicos, produzidos desde esta época até pouco mais da metade do século XX, estabeleceram parte considerável das noções básicas sobre a geologia da província, muitas das quais são mantidas até hoje. Após a publicação desses trabalhos pioneiros, com o início do uso de técnicas analíticas como a fluorescência de raios X e datações pelo método ^{40}K/^{40}Ar, foram realizadas as primeiras investigações geoquímicas e geocronológicas na PIP, que constituem uma importante fase do desenvolvimento da pesquisa sobre sua geologia e petrogênese regional. Alguns destes estudos, publicados dos anos 60 a 80 em parcerias com pesquisadores internacionais, produziram dados e classificações que também são utilizados até hoje (Creer *et al.* 1965; Macdougall e Rüegg, 1966; Rüegg, 1970; Bellieni, *et al*., 1984; Fodor *et al.,* 1985a, 1985b; Fodor, 1987; Mantovani *et al*., 1985, 1988; Piccirilo *et al*., 1988; Peate, 1989).

Nas últimas duas décadas, diferentes escolas nacionais organizaram-se em linhas de pesquisa voltadas à investigação mais detalhada de temas que incluem a vulcanologia física da PIP (Lima *et al*., 2012; Barreto *et al*., 2014; Machado *et al*., 2015, Rossetti *et al*., 2018), o refinamento da sua tipologia geoquímica e petrogênese (Rocha-Júnior *et al*., 2013; Barreto *et al*., 2016; Licht, 2018; Gomes *et al*., 2018) e a delimitação geocronológica dos derrames basálticos, à luz de novas técnicas como a datação ^{40}Ar/^{39}Ar por aquecimento pontual incremental a laser e

datação U-Pb por microssonda de alta resolução (*SHRIMP*) (Thiede e Vasconcelos, 2010; Pinto *et al.,* 2011; Baksi, 2018).

Há, por fim, como resultado da convergência dessas vertentes de pesquisa, o tema que concerne à estratigrafia da PIP. Este assunto vem sendo considerado um dos objetivos essenciais de futuras investigações geológicas na província, tendo revelado complexidade crescente à medida que novas dúvidas são levantadas por pesquisas nas áreas citadas acima.

Nesse cenário, há um objeto de estudo em especial que pode auxiliar consideravelmente a caracterização estratigráfica da PIP, e que recentemente passou a receber maior atenção em investigações geológicas a seu respeito. É o caso das camadas depositadas entre os derrames vulcânicos (comumente denominadas *red beds* ou *boles* na literatura internacional), que incluem litofácies diversas, com origens que vêm sendo remetidas a processos desde piroclásticos (Licht, 2012; Licht *et al*. 2015) até essencialmente sedimentares e vulcanoclásticos efusivos (Waichel *et al*., 2007; Luchetti *et al*., 2014; Machado *et al*., 2015), e cuja existência é mencionada já nos importantes trabalhos de White (1908), Oliveira (1916) e Washburne (1930). No entanto, por mais que o tema tenha sido retomado nas últimas décadas por pesquisadores preocupados com o entendimento da vulcanologia e estratigrafia da província de maneira geral (Waichel *et al*., 2007; Licht, 2012; Luchetti *et al*., 2014; Licht *et al*., 2015; Machado *et al*., 2015; Riccomini *et al.,* 2016; Rossetti *et al*., 2018; Moraes e Seer, 2018; Moraes *et al*., 2018), permanecem ainda dúvidas à respeito da expressão, gênese e deposição destas camadas interderrames, especialmente no que concerne ao controle destas características por fatores ambientais (climáticos e fisiográficos), estratigráficos e magmáticos. Além disso, considerando-se que a relevância em expressão física destas camadas pode ser comparável às camadas de derrames básicos (Licht, 2012), julga-se ainda haver espaço para novas propostas de caracterização e delimitação formal das camadas interderrames.

Ademais, conforme passamos a entender a PIP e a Bacia do Paraná como representantes de um verdadeiro sistema vulcanossedimentar (Leinz, 1949, Licht, 2012; Rossetti *et al*., 2019), torna-se cada vez mais evidente a importância do estudo da íntima interrelação entre a sedimentação interderrames e os episódios de magmatismo estilo PCB (Ross *et al*., 2005; White *et al*., 2009; Manville *et al*., 2009;

Nemeth e Palmer, 2019). É digno de nota ainda que o sistema vulcanossedimentar Paraná-Etendeka apresenta uma ainda indefinida correlação com o vulcanismo basáltico que parece ter condicionado geoquímica e fisiograficamente a evolução das bacias do pré-sal, formadas durante a abertura do Atlântico Sul (Almeida *et al*., 1996; Mohriak *et al*., 2008; Stica *et al*., 2014; Thompson *et al*., 2015; Szatmari e Milani, 2016; Rogerson *et al*., 2017). Este intervalo de sedimentos sin-rifte e carbonatos lacustres, que sabidamente é o *play* responsável por mais da metade da atual produção de óleo brasileira (Petersohn, 2018), apresenta também episódios de vulcanismo sin-sedimentar (Mohriak *et al*., 2008; Thomaz *et al*., 2015; Lobo *et al*., 2016; Szatmari e Milani, 2016; Goldberg *et al*., 2017; Fornero *et al*., 2019) que são ainda pouco compreendidos, e cuja distribuição pode afetar consideravelmente a exploração dos intervalos petrolíferos (Mohriak *et al*., 2002; Millet *et al*, 2016; Fornero *et al*., 2019; Amthor, J. com. pess., 2019).

Nesse contexto, o entendimento da paleogeografia vulcânica permite o estabelecimento de modelos de fácies preditivos (Nemeth e Palmer, 2019), que ajudam a contornar problemas gerados pela baixa resolução (sísmica) e representatividade (poços) dos dados geralmente utilizados para delimitação de alvos exploratórios. Embora a PIP tenha sido gerada em um contexto tectônico e deposicional distinto daquele registrado no pré-sal do Atlântico Sul, a continuidade espaço-temporal das províncias e a correlação entre seus sistemas vulcânicos criam uma importante possibilidade de estudos comparativos, cuja integração deve contribuir significativamente para um modelo faciológico mais completo de ambas as províncias (Rossetti *et al*., 2019; Fornero *et al*., 2019).

Nas regiões Norte e Noroeste do Paraná, uma série de camadas interderrames e depósitos vulcanoclásticos máficos (*mafic volcaniclastic deposits* ou *MVD*s, *sensu* Ross *et al*., 2005) são reportados (Valore e Licht, 2016; Valore *et al*., 2017). Estas ocorrências apresentam uma arquitetura de fácies regional particular, sugestiva de complexas e frequentes interações entre sistemas magmáticos, sedimentares e hidrológicos (interação lava-água-sedimento). Entre elas, os depósitos interderrames de Sertanópolis caracterizam em conjunto uma das ocorrências de maior extensão lateral (cerca de 250 km²) e mais complexa sucessão estratigráfica entre os exemplos citados, demandando estudo estratigráfico detalhado, conforme análises de caráter regional (Valore *et al*., 2017, Licht e Arioli, 2018). A partir dessa análise

preliminar, supõe-se que estes depósitos interderrames provavelmente resultam da atuação de condicionantes ambientais e magmáticos importantes, relacionados principalmente a fenômenos hidrovulcânicos (ver Capítulo III), e que podem ser utilizados tanto para aprimorar correlações e mapas litoestratigráficos (Williamson e Bell, 1994; Single e Jerram, 2004; Martí *et al*., 2018; Rossetti *et al*., 2018; Licht e Arioli, 2018) como para avançar na elaboração de modelos de fácies na PIP como um todo (Nemeth e Palmer, 2019). Nesse contexto, e considerando-se as particularidades desta região, os depósitos interderrames de Sertanópolis foram selecionados como objeto de estudo desta dissertação.

1.1 Objetivos

Tendo em vista o cenário exposto acima, pretende-se investigar a estratigrafia e origem dos depósitos interderrames de Sertanópolis, de maneira a contemplar a associação entre sistemas deposicionais e magmáticos (vulcanoclásticos) e sua evolução ao longo do intervalo de tempo geológico estudado, possivelmente indentificando controles que ajudem a reestabelecer partes da história da PIP e a melhorar seu entendimento litoestratigráfico.

Como objetivos específicos, almeja-se a caracterização dos aspectos texturais, composicionais e morfológicos das fácies interderrames, bem como o seu entendimento petrológico e a interpretação do significado do arcabouço faciológico para a evolução e empilhamento estratigráfico dos depósitos.

1.2 Localização da área de estudo

Este estudo foi desenvolvido em uma região de cerca de 250 km² a norte de Londrina, no norte do Paraná. Os afloramentos estudados estão situados em uma área rural entre os municípios de Bela Vista do Paraíso, Sertanópolis e Primeiro de Maio, acessada pelas estradas PR-090, PR-323, PR-445 (atravessando o Rio Tibagi), PR-160 e BR-369, além de estradas rurais, trilhas e drenagens (Figura 1.1).
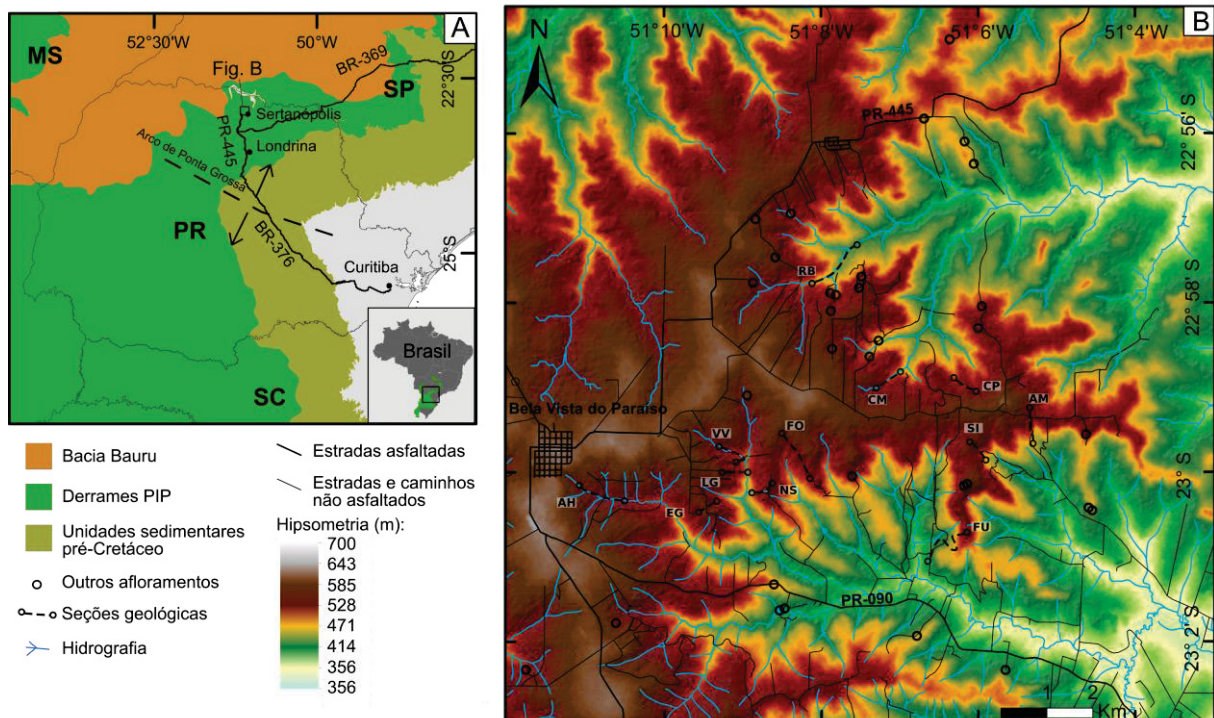
Figura 1.1 – A) Contexto geológico-geográfico da área de estudo. B) Localização da área de estudo e mapa hipsométrico derivado do modelo digital de elevação desenvolvido a partir de imagens do satélite *ALOS PALSAR* (*Advanced Land Observing Satellite Phased Array type L-band Synthetic Aperture Radar*).

1.3 Estrutura da dissertação

Esta dissertação está organizada em cinco capítulos. O Capítulo I introduz o tema, a justificativa e os objetivos desta pesquisa. O Capítulo II apresenta os materiais e dados utilizados para o seu desenvolvimento e uma síntese dos métodos com que foram tratados. O Capítulo III trata do contexto geológico regional da área de estudo, com ênfase para a caracterização da Província Ígnea do Paraná e comparação com os modelos mais atuais sobre províncias continentais basálticas, abrangendo sua vulcanologia, quimioestratigrafia e evolução magmática. O Capítulo IV inclui o artigo científico intitulado "*Hydrovolcanic eruptions of the Paraná Igneous Province: insights from mafic volcaniclastic deposits at Sertanópolis, Paraná, Brazil*", que corresponde aos resultados obtidos nesta pesquisa. Este capítulo foi formatado de acordo com normas da revista internacional *Journal of Volcanology and Geothermal Research*, para o qual o artigo será submetido. Por fim, o Capítulo V contém as considerações finais e referências da pesquisa.

2 CAPÍTULO II - MATERIAIS E MÉTODOS

Para investigação dos processos geológicos responsáveis pela origem das camadas interderrames em Sertanópolis, foi necessário um trabalho de múltiplas etapas e abordagens, que, em suma, consistiu em: análise estratigráfica de campo; análise petrográfica por microscopia óptica de luz transmitida; microscopia eletrônica de varredura e análise geoquímica das rochas vulcânicas associadas.

2.1 Análise estratigráfica e mapeamento geológico

Para determinar a constituição do arcabouço estratigráfico, foi necessário o mapeamento geológico da região, em uma escala que se aproxima ao semi-detalhe (1:25000) de maneira geral, mas que contou com maior ênfase nas regiões de ocorrência das camadas interderrames. Para tal, procedeu-se inicialmente o sensoriamento remoto da região por meio de fotografias aéreas (Instituto de Terras, Cartografia e Geologia - ITCG) e imagens de satélite *ASTER – Advanced Spaceborne Thermal Emission and Reflection Radiometer* com resolução espacial de 15 m (*NASA – North American Space Agency*), *SRTM - Shuttle Radar Topographic Mission* com resolução de 30 m (*NASA*) e *ALOS PALSAR - Advanced Land Observing Satellite Phased Array type L-band Synthetic Aperture Radar* de 12,5 m (*JAXA – Japan Aerospace Exploration Agency* e *JAROS - Japan Resources Observation System Organization*). Foram utilizados também mapas topográficos, hipsométricos e mapas de declividade produzidos pelo tratamento das imagens de satélite para delimitação preliminar das extensões dos depósitos interderrames. A interpretação das feições topográficas e morfológicas de terreno se baseou na fotointerpretação geológica, conforme descrito em Nadalin (2016). Para regiões da PIP, buscou-se identificar sistemas de quebras de relevo indicativos de respostas diferenciais aos processos erosivos e geomorfológicos, que foram usados para traçar preliminarmente os contatos entre derrames (mais suscetíveis à erosão, especialmente em regiões vesiculares) e interderrames (menos suscetíveis à erosão quando silicificados), de acordo com o método proposto por Licht e Arioli (2018).

As atividades de campo totalizaram 19 dias e foram realizadas em 2018 e 2019. Durante estas etapas, foram descritos 96 afloramentos de camadas interderrames e também dos basaltos associados. Foram levantados perfis geológicos de afloramentos, tendo sido posteriormente elaboradas seções

estratigráficas compostas dos depósitos interderrames. A partir disto, foi definido um arcabouço de fácies, que foi comparado a modelos e propostas da literatura para determinação de processos deposicionais. Para isto, foi necessário reconhecer os produtos de diferentes mecanismos de transporte e deposição e associá-los a fenômenos de fragmentação vulcanoclástica ou a fragmentação derivada de intemperismo e erosão.

Neste sentido, para classificação de rochas vulcanoclásticas, optou-se por utilizar a nomenclatura definida por White e Houghton (2006) em continuidade à proposta de McPhie *et al.* (1993), com subdivisão em litotipos vulcanoclásticos primários (produzidos por fragmentação e deposição vulcânica direta) e secundários (ressedimentados e remobilizados sin-eruptivamente), classificados de acordo com esquemas das figuras 2.1 e 2.2. A classificação distingue e separa os produtos vulcanoclásticos dos chamados depósitos epiclásticos, produzidos por erosão e intemperismo de rochas vulcânicas ou vulcanoclásticas, sendo desta maneira consideradas rochas sedimentares. A distinção entre esses três grandes grupos supõe muitas vezes um grau avançado de conhecimento dos processos envolvidos na formação de cada depósito, o que se buscou durante este trabalho, mas que nem sempre é possível no registro geológico antigo (McPhie *et al.*, 1993).

Processo	Adjetivo (substantivo)
Sedimentação a partir de plumas e correntes piroclásticas	Piroclástico (vários)
Deposição de fragmentos de lava, resfriados no ar	Autoclástico (autobrecha)
Deposição de fragmentos de lava, resfriados na água	Hialoclástico (hialoclastito)
Mistura de magma e sedimento úmido, ~in situ	Peperítico (peperito)
Nota: Todos os nomes devem ser baseados na granulação e grau de litificação	

Figura 2.1 – Classificação genética de depósitos vulcanoclásticos primários segundo White e Houghton (2006).
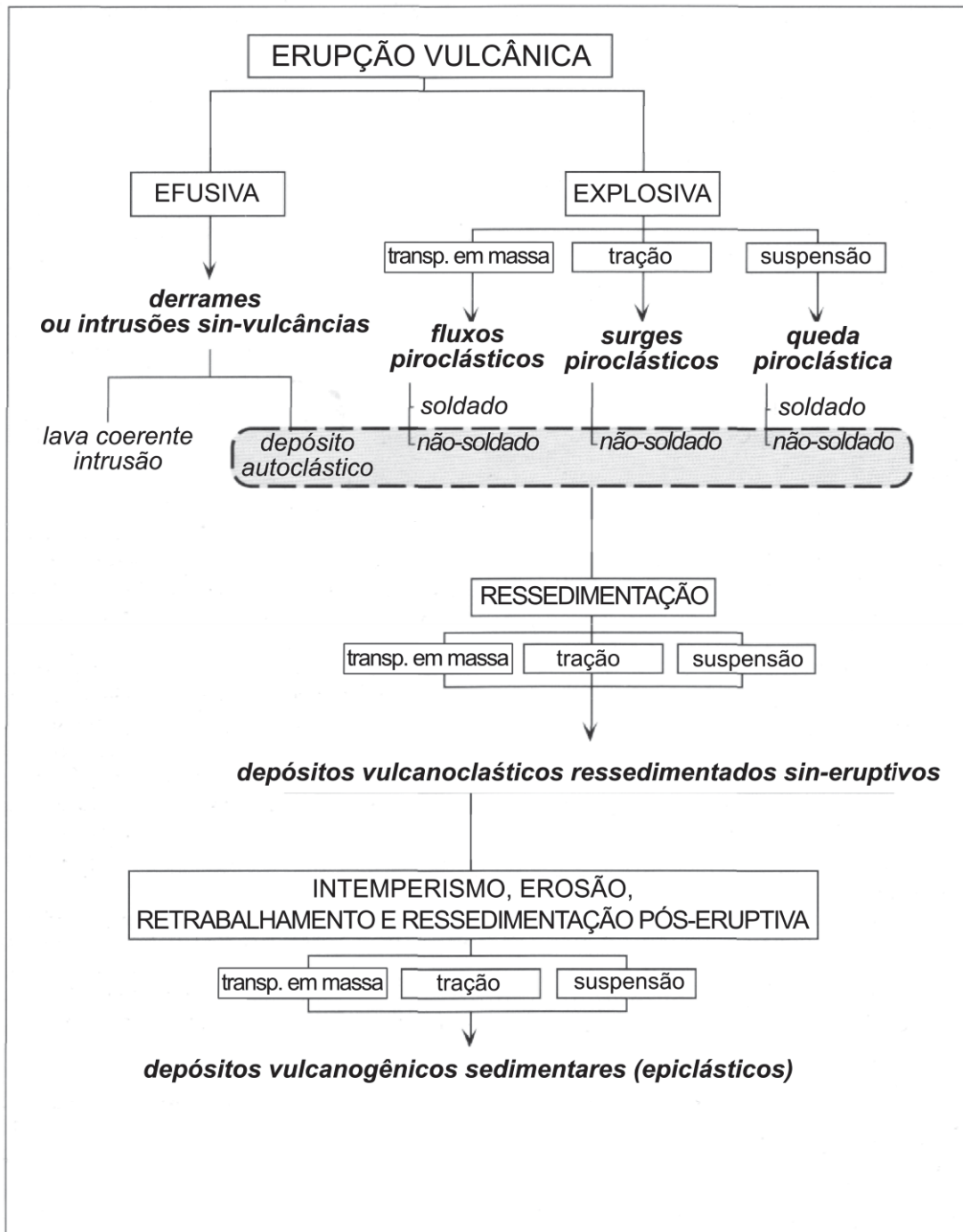
Figura 2.2 – Esquema de classificação genética de depósitos vulcânicos e vulcanogênicos, modificado de McPhie *et al.*(1993).

Além disso, para nomenclatura de classes granulométricas de piroclastos foi adotada a proposta de White e Houghton (2006, Figura 2.3), que faz equivalência (para grãos mais grossos que o silte) com a clássica proposta de Wentworth (1922) para rochas sedimentares, diferindo assim da proposta de Fisher (1961). No entanto, para constituintes de granulação equivalente às classes silte e argila, também foi utilizada uma nomenclatura baseada em Wentworth (1922), uma vez que a proposta

de White e Houghton (2006) não diferencia classes granulométricas menores que 0,0625 mm - que recebem apenas a designação de "cinza extremamente fina". Assim, ao se tratar de constituintes menores que 0,0625 mm, serão utilizados os termos "equivalente a silte" e "equivalente a argila", ou ainda "equivalente a lama". Isto se deve também à dificuldade de se determinar, para fácies piroclásticas, se o material desta granulação possui origem efetivamente envolvida em processos explosivos ou origem sedimentar (Cas e Wright, 1987).

Figura 2.3 – A) Classificação granulométrica de componentes vulcanoclásticos, segundo White e Houghton (2006). B) Classificação granulométrica de depósitos vulcanoclásticos, a partir de Fisher (1961), modificado de White e Houghton (2006). L – *lapilli;* LT – *lapilli*-tufo; T – tufo; C- cinza; TB – tufo-brecha; B – brecha; B&B – blocos e bombas. Divisões em 25% e 75%

2.2 Análise petrográfica por microscopia óptica de luz transmitida

Devido ao grau de consolidação das amostras interderrames estudadas, a análise petrográfica de seções delgadas em microscópio de luz transmitida configura-se como um dos melhores e mais práticos métodos para determinação mais detalhada de componentes e texturas das respectivas fácies descritas. Esta análise permite a determinação dos constituintes de grão fino e distinção de aspectos texturais como seleção, laminação e arranjo, que podem ser utilizados para inferir graus de transporte, maturidade e processos deposicionais. No caso de constituintes vulcanogênicos, esta técnica torna-se especialmente importante, uma vez que permite o reconhecimento de clastos vítreos, fragmentos líticos e cristaloclastos oriundos de fragmentação primária ou retrabalhados (Fisher e Schminke, 1984; Cas e Wright, 1987; McPhie *et al*., 1993). Além disso, como existem muitas sobreposições de certos aspectos composicionais e texturais entre litofácies vulcanoclásticas, considera-se aqui que a análise microscópica deve ser

intrínseca ao próprio processo de determinação do arcabouço faciológico, conforme já observado em estudos de camadas interderrames da PIP (Valore, 2017). A análise petrográfica foi feita com base em propostas consolidadas de caracterização e classificação faciológica e petrográfica de rochas vulcanoclásticas, sedimentares e vulcânicas, com ênfase em trabalhos como Fisher e Schminke (1984), Cas e Wright (1987), Walker e James (1992), McPhie *et al.* (1993), Reading (1996), Tucker (2001), White e Hougton (2006).

Para fins de nomenclatura de constituintes vulcanoclásticos, foi utilizada a nomenclatura de Cas e Wright (1987), que inclui piroclastos juvenis (formados diretamente por magma fragmentado), piroclastos acessórios (derivados de rochas encaixantes e ejetados explosivamente) e piroclastos acidentais (incluídos aleatoriamente durante o transporte), com exclusão dos piroclastos cognatos (Múrcia *et al.*, 2013). A escala granulométrica utilizada durante análise ao microscópio foi a mesma citada na seção anterior.

Para esta etapa, foram confeccionadas 30 seções delgadas no Laboratório de Laminação Petrográfica (LAMIN) da Universidade Federal do Paraná e no Laboratório de Análise de Minerais e Rochas (LAMIR – UFPR). Também foram descritas 5 seções elaboradas pelo antigo Serviço Geológico do Paraná (Mineropar, agora parte do ITCG). Para a descrição foram utilizados microscópios disponíveis nos laboratórios do Departamento de Geologia da UFPR, entre eles o LAPEM (Laboratório de Pesquisa em Microscopia) e o LAMIR-UFPR. Para obtenção de fotomicrografias, foram utilizadas a câmera acoplada ao microscópio petrográfico Leica (modelo DFC-295) no LAPEM e a câmera acoplada ao microscópio petrográfico ZEISS Imager. A2m no LAMIR.

2.3 Microscopia Eletrônica de Varredura (MEV)

Além de permitir caracterizar aspectos morfológicos e mineralógicos de materiais clásticos de maneira geral, a análise por microscopia eletrônica de varredura é especialmente útil para determinação da morfologia e consequentemente origem de constituintes vulcanoclásticos (Buttner *et al.*, 2002; White e Houghton, 2006; Jordan *et al.*, 2014).

Para se descrever a morfologia de clastos, é comumente utilizado o detector de elétrons secundários (*secondary electron image* ou *SEI*) do MEV, que permite

obtenção de imagens com contraste. Esta análise foi realizada em amostras com relevo (fragmentos de rocha). O detector de elétrons retroespalhados (*backscattered electrons*, ou *BSE*) foi utilizado em seções delgadas. A imagem assim obtida representa em tons de cinza a variação da composição atômica média imageada, de forma que materiais de peso atômico maior produzem tons de cinza mais claros, enquanto materiais de baixo peso atômico produzem tonalidades mais escuras (Postek *et al*., 1980). Além disso, foi utilizado o espectrômetro de raios X de energia dispersiva (*energy dispersive spectrometry* ou *EDS*) acoplado ao MEV para caracterização química elementar semi-quantitativa pontual das amostras e obtenção de mapas elementares, que permitem melhor diferenciação mineralógica e composicional dos materiais observados no MEV.

Foram analisadas 6 amostras de fragmentos de rocha e 8 seções delgadas, preparadas com metalização a ouro. As análises foram feitas no LAMIR, no equipamento JEOL 6010LA, com *EDS* modelo EX-94410T1L11. Foram utilizados feixes de eletrons de 20 kV.

2.4 Análises litogeoquímicas

A análise geoquímica por fluorescência de raios X teve como objetivo testar a correlação estratigráfica entre depósitos vulcanoclásticos máficos e a transição entre o domínio de derrames enriquecidos em elementos incompatíveis do Tipo 4 (SiO_2 < 62,02%, Zr < 522,15 ppm, TiO_2 ≥2,85%, P_2O_5 ≥ 0,413%) para derrames de baixo TiO_2 do Tipo 1 (SiO_2 < 62,02%, Zr < 522,15 ppm, TiO_2 < 2,85%, P_2O_5 < 0,413%) na PIP de acordo com a classificação de Licht (2018) e observações do mapeamento geológico regional da província no Paraná (Licht e Arioli, 2018).

A análise de FRX foi realizada em pastilhas de pó prensado e pérolas fundidas para determinação de elementos traço e óxidos, respectivamente. A perda ao fogo foi obtida com aquecimento em estufa a 1000º C por duas horas. Foram feitas 10 análises de amostras de núcleos de derrames e unidades de fluxo das unidades vulcânicas mapeadas. As análises foram realizadas no LAMIR no equipamento Axios Max da PANalytical, tubo de raio-x Rh.

3 CAPÍTULO III - CONTEXTO GEOLÓGICO

3.1 Bacia do Paraná

Situada na América do Sul, a Bacia do Paraná é uma extensa região de cobertura sedimentar intracratônica que abrange grande parte do território sul-brasileiro, bem como o leste do Paraguai, norte do Uruguai e nordeste da Argentina. Sua área atual encontra-se na ordem de 1.500.000 km^2, e a espessura completa da sucessão sedimentar soma em torno de 7000 metros (Zalán *et al*., 1990; Milani *et al*., 2007).

A lito e cronoestratigrafia da bacia vêm sendo debatidas desde as seminais contribuições de cientistas como White (1908) e Maack (1947), sendo abordadas em trabalhos importantes na segunda metade do século passado, incluindo propostas de divisão aloestratigráficas (Vail *et al*., 1977) bastante distintas entre si, como as de Schneider *et al.* (1974), Soares *et al.* (1978), Zalán *et al.* (1990) e Milani (1997). Esses trabalhos consolidaram alguns temas de consenso como conceitos chave para o entendimento da Bacia do Paraná, mas ainda existem algumas questões irresolutas quanto à natureza de alguns de seus ambientes de sedimentação, da divisão estratigráfica e de aspectos relativos à tectônica formadora da Bacia.

Milani (1997) reconheceu, na Bacia do Paraná, seis sequências aloestratigráficas de segunda ordem - ou supersequências em Vail *et al.* (1977), que correspondem a algumas dezenas de milhões de anos de registro sedimentar, e são separadas por hiatos deposicionais de magnitude semelhante. Segundo o autor, essas supersequências se dividem em: Rio Ivaí (Ordoviciano - Siluriano), Paraná (Devoniano), Gondwana I (Carbonífero - Eotriássico), Gondwana II (Meso a Neotriássico), Gondwana III (Neojurássico-Eocretáceo) e Bauru (Neocretáceo). De acordo com Milani *et al.* (2007), as três primeiras refletem grandes ciclos tectono-eustáticos bem definidos de transgressão e regressão, possibilitados pela incursão marinha na Bacia do Paraná durante o Paleozóico, enquanto as últimas três correspondem a um registro sedimentar essencialmente continental (Figura 3.1).
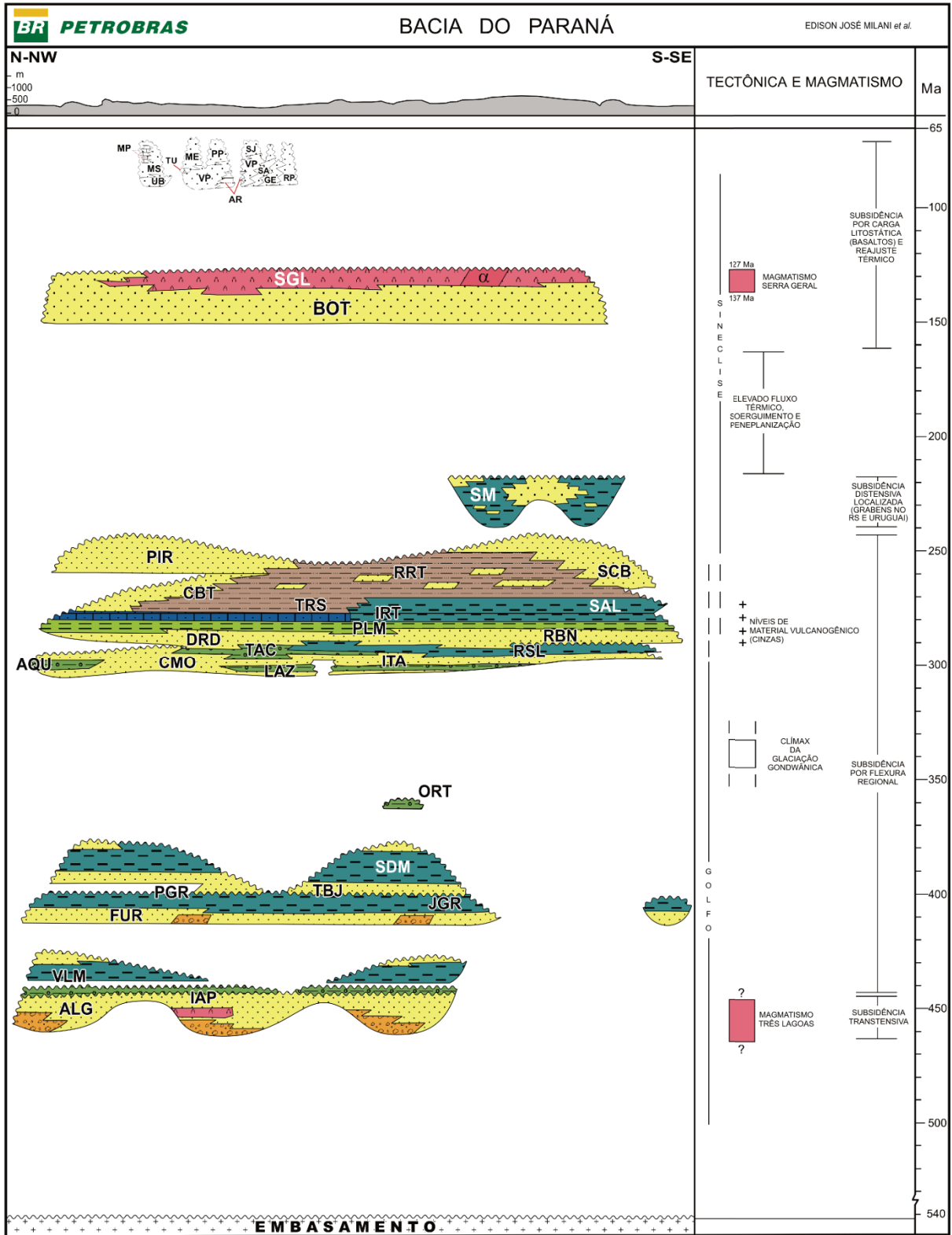
Figura 3.1 – Carta tectono e cronoestratigráfica da Bacia do Paraná, de Milani *et al.* (2007).

A história deposicional da Bacia se iniciou algum tempo após as orogêneses do Ciclo Brasiliano (responsável pela aglutinação do continente Gondwana no final do Neoproterozóico) e tanto a geração de espaço quanto o condicionamento do aporte

sedimentar estiveram associados à herança estrutural desses orógenos brasilianos. No entanto, esses parâmetros foram controlados primeiramente pela atividade tectônica de orógenos fanerozóicos que se formavam nas margens do Gondwana, a qual resultou em diferentes ciclos de subsidência na Bacia do Paraná (Zalán *et al*., 1987, 1990; Milani e Ramos, 1998).

Para Zalán *et al.* (1990) a sedimentação ocorreu sob influência de lineamentos tectônicos de direção NW e NE, sendo marcada por blocos limitados por falhas de atividade sutil, mas suficiente para o controle de depocentros e geração de altos estruturais intrabacinais. Zalán *et al*. (1990) citam a existência de um núcleo cratônico central no embasamento da Bacia do Paraná - hipótese já levantada por Cordani *et al*. (1984) -, embora Milani (1997) considere paradoxal que as regiões de maiores acúmulos sedimentares coincidam geograficamente com a região de implantação da Bacia no Neo-ordoviciano, pressupondo a existência de uma "Faixa Móvel Rio Paraná" que poderia responder mais ativamente aos mecanismos de subsidência regional.

Segundo Zalán *et al.* (1987, 1990) o início da sedimentação na Bacia do Paraná pode ser explicado pela subsidência termal causada pelo arrefecimento do recém formado "escudo Gondwana", largamente afetado por deformação e granitogênese associadas ao fim do Ciclo Brasiliano. Estes autores também admitem que parte da subsidência pode relacionar-se à extensão crustal e distensão resultantes do fim dos esforços compressionais do Brasiliano, sugerindo que uma calha N-S poderia ter condicionado a deposição da formação Rio Ivaí. Para os autores, este primeiro mecanismo, predominantemente de subsidência termal, poderia explicar a deposição daquilo que chamam de Sequência Siluriana e Sequência Devoniana. Já Milani (1997) e Milani e Ramos (1998) associam a fase inicial de subsidência da bacia à geração de grábens transtensivos em zonas de fraqueza neoproterozoicas reativadas (orientadas segundo NE-SW), provavelmente relacionada a algum tipo de rifteamento.

Para Assine (1996), Milani (1997) e Milani e Ramos (1998), o ápice da subsidência de cada ciclo deve ter coincidido com o ápice de cada evento orogenético nas margens do Gondwana, enquanto o soerguimento e a erosão das sucessões sedimentares devem ter ocorrido nos momentos de menor atividade

tectônica entre as orogenias, visão essencialmente oposta às ideias de Zalán *et al.* (1987, 1990) e Zalán (1991).

Para Assine (1996), Milani (1997) e Milani e Ramos (1998) existe uma relação causal entre a Orogenia Oclóyica (que envolveu a colisão do terreno Precordilheira com o Gondwana e teve seu ápice durante o Meso a Neo-Ordoviciano) e as taxas de subsidência iniciais, na fase correspondente à deposição da Supersequência Rio Ivaí. Neste mesmo sentido, para Milani (1997) e Milani e Ramos (1998), a supersequência devoniana (Supersequência Paraná) começou a se depositar em um contexto de lenta subsidência e substrato plano, possibilitado pelo desenvolvimento de uma superfície erosiva e de peneplanação regional sobre a Supersequência Rio Ivaí. Essa fase mais calma corresponderia ao intervalo de deposição dos arenitos da Formação Furnas. Durante o Emsiano, porém, implantou-se uma taxa de subsidência mais acelerada, que culminou na máxima inundação da bacia neste ciclo e na deposição dos folhelhos na base da Formação Ponta Grossa. Esta, por sua vez, apresenta pontuais progradações arenosas até seu limite superior, no Frasniano, onde há registro de sedimentação ainda majoriamente pelítica. Novamente, este ápice de subsidência poderia ser correlacionado ao clímax da Orogenia Chanica, nas margens ocidentais do paleocontinente (Assine, 1996).

A discordância que separa a supersequência devoniana da terceira fase de subsidência da bacia é uma das mais conhecidas e notáveis em todo o registro sedimentar do Gondwana (Assine, 1996). Esta discordância, que precede a deposição da Supersequência Gondwana I (Carbonífero – Eotriássico), é marcada por um hiato no registro sedimentar de 40 Ma (Assine, 1996) a até 70 Ma (Milani *et al.*, 2007) e sua origem também está sujeita a algumas discussões. Para Zalán *et al.* (1990) e Zalán (1991), está ligada principalmente a fatores tectônicos relacionados à Orogenia Eoherciniana, que teria dado fim à fase inicial de subsidência da bacia. Para Milani (1997) e Milani e Ramos (1998), no entanto, este hiato é resultado das condições paleogeográficas da Bacia do Paraná durante o final do Devoniano e início do Carbonífero, sendo mais plausível sua associação ao desenvolvimento de calotas de gelo próximas à bacia e também sobre partes dela, com conseqüente rebaixamento do nível do mar e perda do registro sedimentar mississipiano.

A Supersequência Gondwana I de Milani (1997) representa um capítulo especialmente importante da história deposicional da Bacia do Paraná. Esta

supersequência registra as últimas incursões do Panthalassa na bacia e, por conseguinte, seu último ciclo trangressivo-regressivo completo (Milani *et al.*, 1998). A sedimentação na porção basal da supersequência está em grande parte relacionada a um contexto paleoambiental de degelo, que resultou na deposição do Grupo Itararé (Milani e Ramos, 1998). Uma tendência transgressiva está registrada em toda a sucessão sobrejacente, referente ao Grupo Guatá, e a máxima inundação deste ciclo ocorreu durante o Artinskiano, durante a deposição dos folhelhos da Formação Palermo. Na medida em que este ciclo de subsidência de segunda ordem se aproximou do seu fim, no começo do Triássico, foram registrados sedimentos produzidos por sistemas deposicionais progressivamente mais continentais e áridos (Milani *et al.,* 2007), numa espessa (1400 m) sequência regressiva representada pelo Grupo Passa Dois.

Após o acúmulo da sequência sedimentar do Carbonífero-Eotriássico, a deposição na Bacia do Paraná teve prosseguimento no Mesotriássico, durante o início do episódio de distensão responsável pela quebra do Gondwana na porção sul do paleocontinente (Milani *et al.*, 2007). Esta porção de sedimentação meso a neotriássica – a Supersequência Gondwana II de Milani (1997) - pode ter sido controlada por grábens restritos às regiões do Rio Grande do Sul e do Uruguai, estando ausente em outros estados. Neste contexto foram depositados os sedimentos da Formação Santa Maria em uma rápida transgressão sobre o topo da Supersequência Gondwana I.

É certo que parte considerável dos sedimentos da Supersequência Gondwana II foi erodida, no entanto, durante uma fase de soerguimento pronunciado que culminou no desenvolvimento da ampla superfície de deflação do deserto Botucatu. É a este contexto que está associada a Supersequência Gondwana III, de idade neojurássica a eocretácica (Milani *et al.*, 2007). Durante esta fase continental da Bacia do Paraná, foram formados os amplos depósitos de arenitos da Formação Botucatu, considerados exemplos típicos de arenitos eólicos de ambiente desértico. No entanto, estão preservadas também intercalações de fácies fluviais-aluviais e lacustres restritas que, ao ocorrerem próximas de seu contato basal, acabam por dificultar o reconhecimento de seu limite inferior. Isso se deve ao fato de a Formação Botucatu muitas vezes estar posicionada diretamente acima da Formação Pirambóia – de paleoambientes fluviais-eólicos. Para Milani *et al.* (2007), no entanto, a grande

lacuna existente entre as duas formações não permite que seu contato seja considerado transicional, já que a Formação Pirambóia teria idade eotriássica e faria parte de sua Supersequência Gondwana I.

A unidade que completa a Supersequência Gondwana III de Milani (1997) corresponde ao Grupo Serra Geral, nome litoestratigráfico dos derrames que formam a Província Ígnea do Paraná. Sua importância no contexto da sedimentação da Bacia do Paraná vai além de implicações tectônicas e paleoambientais sin-magmáticas, uma vez que a subsidência termal pós-vulcanismo também deu origem a uma sucessão sedimentar, a Supersequência Bauru (Milani, 1997). Por este motivo, alguns autores consideram-na como parte de outra bacia (Bacia Bauru em Fernandes e Coimbra, 1996, 2000) que, por sua vez, compreende sedimentos depositados em condições paleoambientais de semi-aridez, semelhantes às exibidas no registro da Supersequência Gondwana III, antes do vulcanismo basáltico. No entanto, estão preservados também sedimentos de sistemas fluviais entrelaçados e de leques aluviais, em especial nas fases finais de evolução da bacia (após sedimentação desértica, Fernandes *et al*., 2015).

A conexão entre os ambientes deposicionais e regimes tectônicos durante as fases pré, sin e pós-vulcânicas ainda não é bem entendida. Inicialmente, assumia-se que os ambientes áridos pré-vulcânicos persistiram durante e após o magmatismo da PIP - o que explicaria, em partes, a ausência de magmatismo explosivo hidrovulcânico e também de um evento de extinção em massa contemporâneo (Ross *et al*., 2005). No entanto, a presença relativamente comum de intervalos de deposição subaquosa (ou de sedimentos e material vulcanoclástico formados por fenômenos hidrovulcânicos) sugere que esse panorama precisa ser revisto (Waichel *et al*., 2006, 2007; Luccheti *et al*., 2014; Machado *et al*., 2015; Moraes e Seer, 2018; Rossetti *et al*., 2018).

3.2 Vulcanologia física dos derrames da PIP

O extenso sistema de rochas vulcânicas extrusivas e intrusivas que compõem a Província Ígnea do Paraná (Figura 3.2) foi originado durante o Eocretáceo, na região da Bacia do Paraná, no sudeste do continente sulamericano (Piccirillo e Melfi, 1988; Peate, 1997). Este grande episódio magmático está compreendido temporal e fisicamente entre sedimentos das duas supersequências continentais mesozoicas

(Gondwana III e Bauru) que completam a história deposicional da bacia (Milani, 1997; Milani *et al*., 2007; Fernandes *et al*., 2015). Além da presença na forma de espessa sequência de derrames, as rochas da PIP são também encontradas como diques, soleiras e intrusivas rasas (gabros) dentro e fora da área da Bacia do Paraná, como nos enxames de diques de Ponta Grossa, da Serra do Mar e de Florianópolis (Almeida *et al*., 2012; Florisbal, 2014; Almeida *et al*., 2018, 2019). Assim, a área original da província possivelmente já foi maior do que a atual, uma vez que provavelmente incluía regiões agora erodidas no planalto atlântico, o que é evidenciado pela correlação dos derrames com a província Etendeka na África e com o Platô de São Paulo na margem continental brasileira (Szatmari e Milani, 2016; Svensen *et al*., 2018; Foulger, 2018).
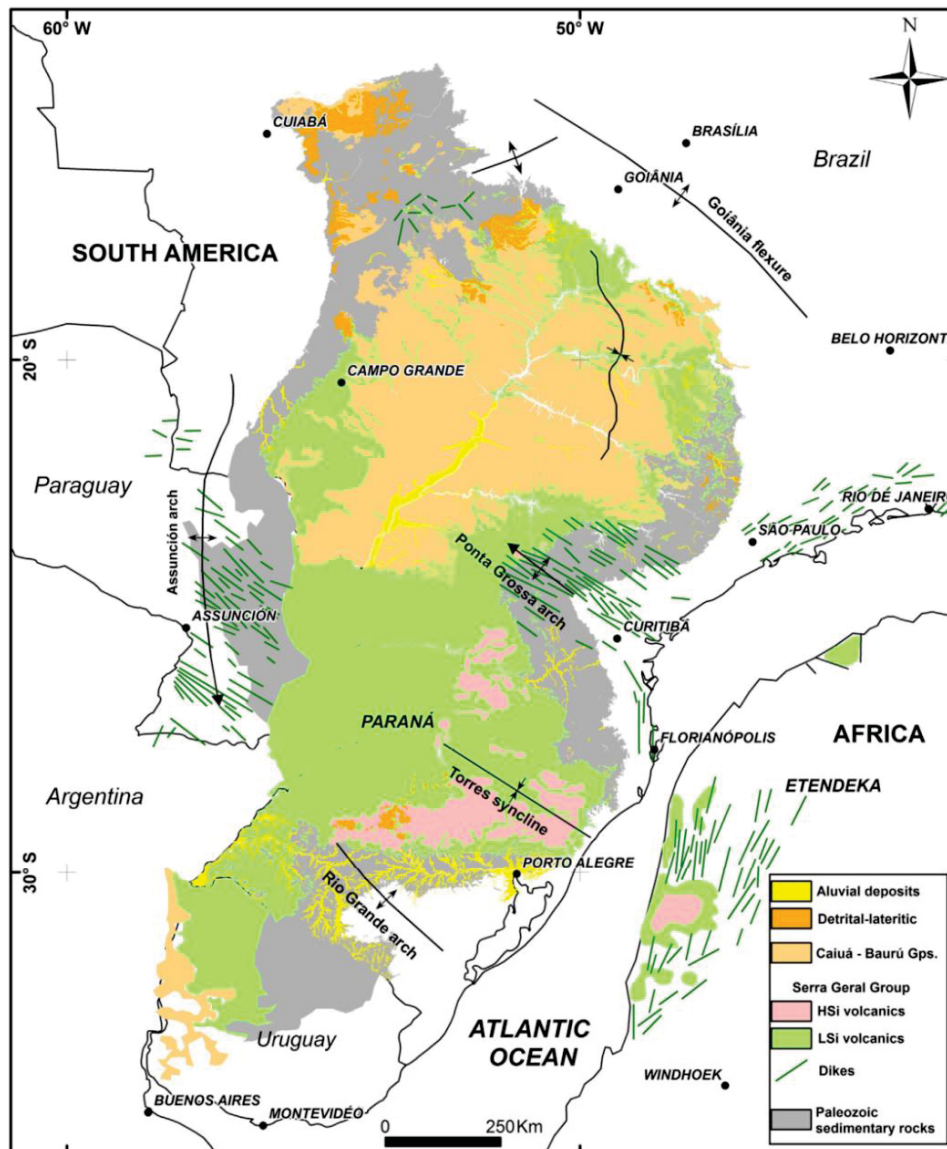
Figura 3.2 – Mapa de conjuntos litogeoquímicos simplificado da PIP, de Licht (2018).

Conforme descrito no Capítulo I, a PIP pode ser entendida como um sistema de grandes derrames basálticos continentais, que constitui um evento singular de extravasamento de material básico em região continental intraplaca. Tanto na PIP como em outras Províncias Continentais Basálticas, a colocação e expansão de volumes tão grandes de lavas pelo que pareciam ser algumas dezenas de espessos derrames (*layer-cake stratigraphy* em Jerram e Widdowson, 2005) foram historicamente questões problemáticas, muito melhor entendidas a partir das importantes contribuições de Walker (1971, 1973, 1987, 1989, 1991), Rowland e Walker (1990), Hon *et al*. (1994), Self *et al*. (1996, 1997, 1998), Thordarson e Self (1998), Kauahikawa *et al*. (1998) e Cashman *et al*. (1999).

De maneira geral, quando se comparam os derrames de PCBs com episódios de vulcanismo recentes, fica claro que há disparidades consideráveis que dificultaram, durante algum tempo, o emprego da hipótese atualística (Self *et al*., 1998). Este descompasso foi minimizado a partir do entendimento do processo de inflação, pelo qual se supõe que lobos vulcânicos semelhantes aos observados em campos de derrames basálticos modernos tenham obtido espessuras e extensões (ou apenas razões de aspecto) compatíveis com as observadas em imensos derrames tabulares do registro geológico (Walker, 1991; Hon *et al*., 1994; Self *et al*., 1996, 1997, 1998; Thordarson e Self, 1998), especialmente quando associados a taxas de efusão relativamente altas e contínuas (da ordem de milhares de m³/s). Não obstante, taxas de efusão ainda mais altas (100000 m³/s) também têm sido utilizadas para explicar geometrias de alguns *flood basalts* que parecem ter acomodado pouca ou nenhuma inflação, tendo provavelmente avançado rapidamente como verdadeiros "muros" espessos de lava (Bondre *et al*., 2004; Duraiswami *et al*., 2008; Óskarsson e Riishuus, 2014; Marshall *et al*., 2016). Essa hipótese se aproxima de alguns modelos mais antigos para lavas *pahoehoe* (Walker, 1971, 1973), em especial a algumas ideias desenvolvidas na Província Columbia River (PCR) (Shaw e Swanson, 1970, Swanson *et al*., 1975) posteriormente rejeitadas por Self *et al*. (1996) e Thordarson e Self (1998). De acordo com Óskarsson e Riishuus (2014), a principal evidência deste processo nos *flood basalts* do Mioceno na Islândia seria a formação de derrames sem as estruturas internas e morfologias gerais associadas a processos de inflação, como *breakouts* (protrusões de novos lobos em frentes de derrame), tubos de lava (condutos alimentadores

isolados termicamente) e *tumuli* (condutos de lava preenchidos que invertem a topografia), além de não serem encontrados horizontes de vesículas sobrepostos em crostas vesiculares.

A partir de estudos como os mencionados acima, foi possível compreender e analisar melhor as diferentes morfologias de derrames de lavas - muitas vezes características de situações intermediárias entre os mais conhecidos membros extremos *pahoehoe e a'ä* - que são produzidas por variações em fatores comumente inter-relacionados como taxas de alimentação, velocidade de fluxo, viscosidade, taxas de *strain,* e tensão de escoamento, reconhecíveis em derrames de ambos os contextos (Cashman *et al*., 1999; Griffiths, 2000; Gregg, 2017).

Na PIP, os avanços mais recentes na vulcanologia física se referem à caracterização regional dos principais tipos de lavas e dos fenômenos responsáveis por sua colocação. De acordo com Lima *et al.* (2012), Barreto *et al.* (2014), Rossetti *et al.* (2014, 2018) e Machado *et al.* (2015), parece haver um predomínio de campos de lava compostos *pahoehoe* (no sentido de Thordarson e Self, 1998; Self *et al*., 1997, 1998; Jerram e Widdowson, 2005) entre os derrames que compõem as fases iniciais do magmatismo em diferentes regiões da PIP, de maneira semelhante ao que é descrito em outras PCBs (Single e Jerram, 2004; Jerram e Widdowson, 2005). Segundo estes autores, esses campos de lava são formados por complexos entrelaçamentos de unidades de fluxo predominantemente do tipo P (*sensu* Walker, 1987; Wilmoth e Walker, 1993) em morfologias variadas, como lobos *pahoehoe* típicos, *lava toes* e *lava fingers* (Figura 3.3). De modo geral, estas morfologias são explicadas por processos menos pronunciados de inflação e taxas de alimentação baixas e intermitentes (Barreto *et al*., 2014; Rossetti *et al*., 2014). Associados a esses campos de lava compostos, no entanto, são descritos lobos tabulares (*sheet lobes*, *sensu* Self *et al*., 1997, 1998) mais inflados (3-15 m), possivelmente formados por coalescência de lobos e taxas de efusão ligeiramente maiores e mais contínuas (Barreto *et al*., 2014; Rossetti *et al*., 2014, 2018), que se tornam mais frequentes e espessos estratigrafia acima (Jerram *et al.* 1999; Lima *et al*., 2012; Rossetti *et al*., 2018). Segundo os autores, estas litofácies estão associadas a estruturas e variações texturais típicas de campos de lava inflados como *inflation clefts,* topos com horizontes vesiculares, núcleos com cilindros de vesículas e bases com vesículas em *pipe*.
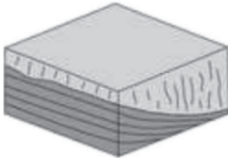
Associações de fácies	Descrição	Desenho	Interpretação
Lavas confinadas	Derrames espessos com disjunções colunares irregulares a bem desenvolvidas		Lava confinada em região interdunas
Pahoehoe composto	Pequenos lobos (dm - m) pahoehoe empilhados em padrões complexos		Baixas taxas de efusão em derrames de baixo volume
Pahoehoe tabular	Derrames tabulares de 5 - 8 m, com estrutura interna marcada por zonas vesiculares basal e de topo e núcleo maciço		Baixas taxas de efusão em derrames de volume maior, erupções prolongadas. Inflação e coalescência de lobos menores
Rubbly pahoehoe	Derrames espessos tabulares com núcleo maciço e topo brechado		Altas taxas de efusão, fragmentação autoclástica de topo de derrame

Figura 3.3 – Morfologias de campos de lava da PIP, modificado de Rossetti *et al*. (2014).

Outras classificações possíveis dizem respeito às chamadas morfologias de superfície, *i.e.* o aspecto e grau de coesão das superfícies de topo e base das unidades de fluxo. Nos derrames compostos da PIP, relata-se um predomínio de morfologias *slabby pahoehoe* e *pahoehoe* típica (Waichel *et al*., 2006; Barreto *et al*., 2014; Rossetti *et al*., 2014, 2018; Machado *et al*., 2015) características de baixas taxas de efusão e *strain.*

Segundo Waichel *et al*. (2006), Lima *et al*. (2012), Barreto *et al*. (2014) e Rossetti *et al*. (2018) além destas morfologias, estes campos de lava compostos também incluem lobos de núcleos vesiculares do tipo S (*spongy lobes* em Walker, 1989), que representariam unidades de fluxo praticamente isentas de inflação e ricas em vesículas de solidificação relativamente rápida (Walker, 1989; Wilmoth e Walker, 1993; Self *et al*., 1998). Segundo Walker (1989) esta morfologia é característica de regiões mediais a distais de campos de lava *pahoehoe* modernos no Hawaii, enquanto que Thordarson e Self (1998) consideram que lobos do tipo S fazem parte de associações proximais e de conduto na PCR.

Em conjunto, estas litofácies se assemelham consideravelmente às observadas nos campos de lava compostos da PCR por Self *et al*. (1996), Thordarson e Self (1998), onde estes mesmos autores realizaram trabalho detalhado de caracterização de fácies proximais e distais em relação a sistemas de alimentação. Na PIP, a dificuldade imposta à identificação sistemática de associações proximais e *near-vent*

como depósitos de *spatter* e cones de escória (White *et al*., 2009) complica tentativas de caracterização semelhantes que, não obstante, começam a ser esboçadas com auxílio da quimioestratigrafia de detalhe (Hartmann *et al*., 2013, Fernandes *et al*., 2018). Além disso, alguns condutos magmáticos, como as estruturas de Água Vermelha (Rio Grande, divisa de Minas Gerais – São Paulo), estão começando a ser mais bem caracterizados a partir de mapeamento de detalhe (Pacheco *et al*., 2018), especialmente em regiões onde lineamentos podem ter condicionado significativamente a atividade efusiva (Seer, H.J., com. pess., 2019).

Os campos de lava compostos e "transicionais" (no sentido de Single e Jerram, 2004) que formam a base da sucessão de lavas da PIP passam gradualmente para derrames tabulares mais espessos do tipo "simples" (*sensu* Walker, 1971; Self *et al*. 1998; Jerram e Widdowson, 2005), o que sugere aumento considerável nas taxas de alimentação durante a fase principal de vulcanismo (Lima *et al*., 2012; Barreto *et al*., 2014; Rossetti *et al*., 2018). Estes espessos derrames do tipo simples são as morfologias mais marcantes nas PCBs e caracterizam sua estratigrafia "*step-like*" ou "*layer-cake*" típica. No entanto, torna-se claro por essas descrições que o simples empilhamento de derrames tabulares de dimensões "infinitas" não configuraria uma concepção estratigráfica real de todas as morfologias vulcânicas da PIP, o que é reforçado por Self *et al*. (1998) quando citam que "todos os derrames do tipo 'simples' são compostos em alguma escala" – ideia que, no entanto, não foi acompanhada integralmente por autores como Harris e Rowland (2009) e Óskarsson e Riishus (2014), que, de maneira semelhante a Walker (1971), consideram as fácies do tipo simples como elementos definitivamente distintos dos campos de lava compostos.

Além disso, mesmo os intervalos de derrames tabulares típicos de PCBs também podem apresentar variações verticais e laterais complexas de morfologias como *breakouts* e tubos de lava (Waichel *et al*., 2006, 2012; Óskarsson e Riishus, 2014) que podem ser utilizadas para conceber uma verdadeira *estratigrafia de sequências vulcânicas* (Nemeth e Palmer, 2019) em PCBs. Além disso, variações nas morfologias de superfície acompanham controles como taxas de efusão e morfologia do terreno que são presentes também em erupções que formam derrames do tipo simples (Duraiswami *et al*., 2008; Óskarsson e Riishuus, 2014).

Associada às altas taxas de efusão e velocidades de fluxo responsáveis pela colocação destes derrames, parece ter sido frequente a produção de morfologias do tipo *rubbly pahoehoe* (*sensu* Keszthelyi *et al*., 2001), utilizadas para definir litofácies (Barreto *et al*., 2014; Rossetti *et al*., 2014) e unidades litoestratigráficas (Rossetti *et al*., 2018) características na PIP, em seguimento com os estudos de Duraiswami *et al*. (2008, 2014) nos derrames *rubbly pahoehoe* da Província do Deccan. Essa litofácies é caracterizada por derrames com bases coesas e brechas autoclásticas de topo que incluem desde fragmentos de superfícies cordadas até fragmentos de *clinker* (fragmentos vesiculares) com sinais de abrasão, semelhantes a brechas de topo de lavas *a'ä*. Segundo Rossetti *et al*. (2018), estes derrames simples *rubbly pahoehoe* estão associados a fase principal de vulcanismo (Fm. Vale do Sol) e formam parte considerável da PIP no Rio Grande do Sul.

De acordo com Jerram e Widdowson (2005) e Rossetti *et al*. (2018), o ápice do magmatismo representado pela erupção de derrames tabulares é produzido por altíssimas taxas de efusão e atividade vulcânica muito rápida, que ocorre em um período de 1 a 3 milhões de anos. Após esse período, uma correspondente diminuição da taxa de efusão produziria morfologias características de campos de lava compostos de derrames mais enriquecidos em sílica, em épocas de atividade vulcânica decrescente (Jerram e Widdowson, 2005), com aumento do espaço de tempo entre as erupções e consequente aumento do número de camadas interderrames preservadas (Rossetti, L., com. pess. 2019).
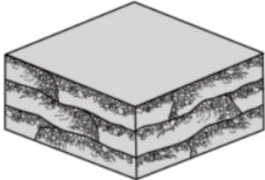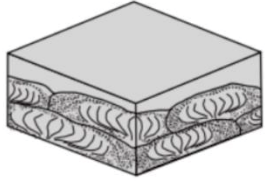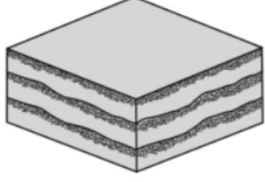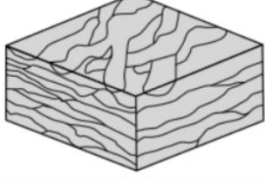
Associações de fácies de derrames	Bloco diagrama	Tipo de derrame predominante	Espessura unidades de fluxo	Espessura total
Tabular/lobado escoriáceo		Derrames rubbly pahoehoe*	10-15 m	~250
Domo ou escudo de lava		Domos ácidos	até 30 m	~150 m
Tabular clássica		Derrames pahoehoe simples	10-20 m	~500 m
Composto-entrelaçado		Derrames pahoehoe compostos (regiões de dunas)	0,3 - 1 m	100 - 200 m
		Derrames confinados (regiões interdunas)	até 40 m	

Figura 3.4 – Associações de fácies características da PIP na região do Sinclinal de Torres, Rio Grande do Sul, modificado de Waichel *et al*. (2012). * - *originalmente descritos como derrames do tipo a'ä, modificado em Rossetti et al. (2014, 2018).*

A partir do mapeamento geológico em escala 1:250.000 dos derrames da PIP (Grupo Serra Geral) no Paraná, algumas variações importantes deste modelo foram caracterizadas por Licht e Arioli (2018), em especial devido à subdivisão da PIP em duas subprovíncias (ver seção 3.3), ambas presentes e interdigitadas no estado (Figura 3.5). Apesar de muitas propostas considerarem que as lavas ácidas e evoluídas devem estar sobrepostas às lavas primitivas e aos derrames tabulares da fase efusiva principal, os autores observam que os derrames ácidos (Mb. Salto do Apucaraninha e Mb. Ourinhos) encontram-se muitas vezes em contato com a Fm. Botucatu no Paraná, tendo sido posteriormente cobertos pelas lavas básicas de alto TiO$_2$ da Formação Pitanga. Esta formação por sua vez transiciona para os derrames tabulares da Formação Paranapanema, que encerram a estratigrafia da província no Paraná sem o registro de uma fase de atividade vulcânica decrescente. De mesmo modo, os intervalos interderrames, frequentes na Fm. Pitanga e na base da Fm.

Paranapanema, tornam-se cada vez menos comuns em direção ao topo da sucessão vulcânica.
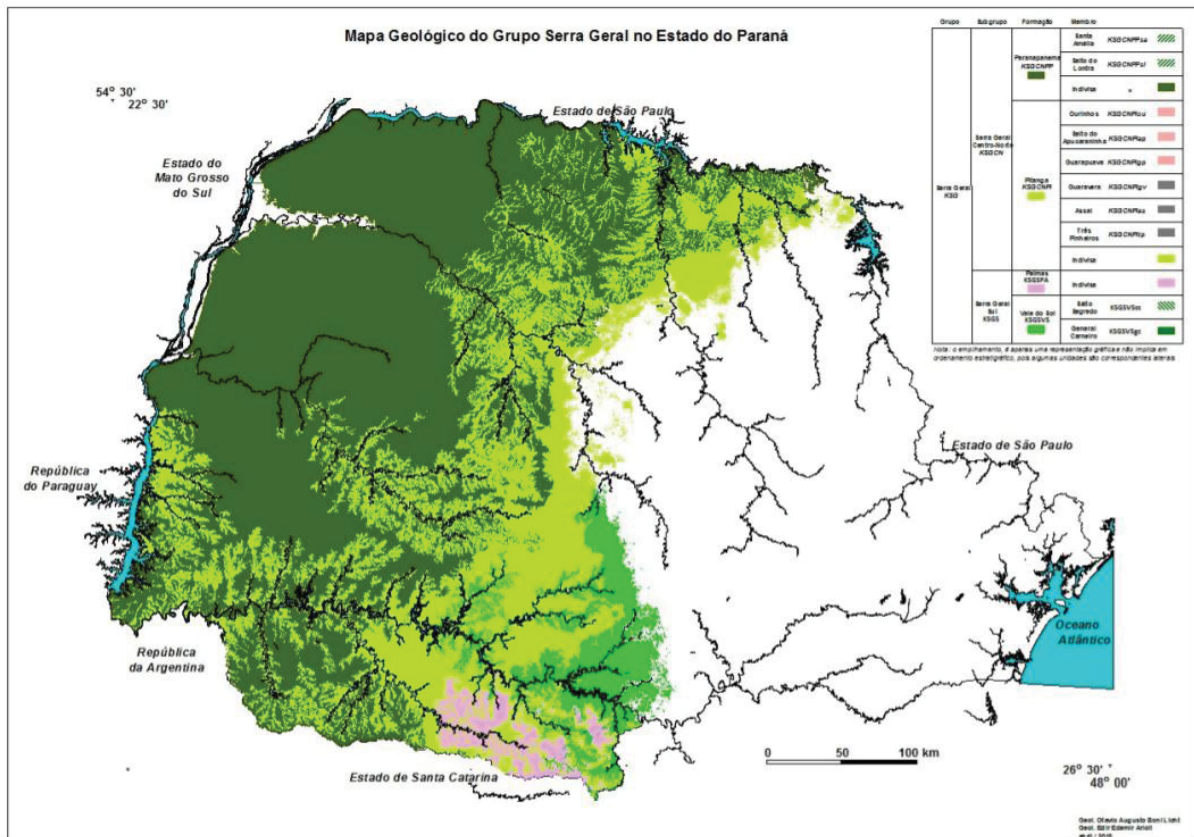
Figura 3.5 – Mapa geológico do Grupo Serra Geral no Paraná, com omissão das unidades da Bacia Bauru, de Licht e Arioli (2018). Unidades do Subgrupo Centro-Norte: Formação Pitanga (verde claro); Formação Paranapanema (verde escuro). Unidades do Subgrupo Sul: Formação Vale do Sol (verde médio); Formação Palmas (rosa claro).

3.3 Quimioestratigrafia e petrogênese da PIP

Pesquisas voltadas para o entendimento da quimioestratigrafia e evolução magmática da província tiveram início nas décadas de 60 a 80, a partir de importantes contribuições de pesquisadores internacionais. Com suporte de algumas delas, definiu-se um modelo tradicional que, salvo algumas atualizações e inclusão de subdivisões, ainda é o mais utilizado até hoje. Este modelo envolve a divisão das lavas extravasadas em oito magmas-tipo, definidos a partir limites interpretativos e petrológicos nos teores de SiO_2, TiO_2, P_2O_5, Zr, Y e Sr, propostos por Peate (1989, 1997) e Peate *et al.* (1992), em continuidade com trabalhos como Mantovani *et al.* (1985,1988) e Piccirillo *et al.* (1988). Na proposta de Peate *et al.* (1992) há dois grandes grupos de lavas, que separam rochas ácidas (com dois magmas-tipo) e básicas (com seis magmas-tipo). As rochas básicas, que eram até então divididas

em essencialmente dois grandes grupos, de alto (>2%) e baixo (<2%) TiO_2 (Bellieni *et al.*, 1984; Mantovani *et al.*, 1985), passaram a ser classificadas em três magmas tipo dentro de cada grupo, separados com base em intervalos nos teores de SiO_2, TiO_2, P_2O_5, Zr, Sr, Y, e Ba, que apresentam certas sobreposições nos seus valores (Tabela 3.1).

	"Baixo" TiO_2			"Alto" TiO_2		
	Gramado	Esmeralda	Ribeira	Paranapanema	Pitanga	Urubici
SiO_2	49 - 60	48 - 55	49 – 52	48 - 53	> 47	> 49
TiO_2	0,7 - 2	1,1 - 2,3	1,5 - 2,3	1,7 - 3,2	> 2,8	> 3,3
P_2O_5	0,05 - 0,4	0,1 - 0,35	0,15 - 0,50	0,2 - 0,8	> 0,35	> 0,45
Sr (ppm)	140 - 400	< 250	200 - 375	200 - 450	> 350	> 550
Ba (ppm)	100 - 700	90 - 400	200 - 600	200 - 650	> 200	> 500
Zr (ppm)	65 - 275	65 - 210	100 - 200	120 - 250	> 200	> 250
Ti/Zr	< 70	> 60	> 65	> 65	> 60	> 57
Ti/Y	< 330	< 330	> 300	> 350	> 350	> 500
Zr/Y	3,5 - 6,5	2,0 - 5,0	3,5 – 7	4,0 - 7,0	> 5,5	> 6,5
Sr/Y	< 13	< 9	5,0 – 17	4,5 - 15	> 8	> 14
Ba/Y	< 19	< 12	6,0 – 19	5,0 - 19	> 9	> 14

Tabela 3.1 - Resumo dos critérios de classificação dos magmas-tipo básicos de Peate *et al*. (1992).

Em trabalhos recentes, interpretações da evolução do magmatismo regional da PMP têm se baseado na união da quimioestratigrafia de Peate (1989) e Peate *et al*. (1992) com as idades obtidas por autores como Renne *et al*. (1992), Thiede e Vasconcelos (2010) e Baksi (2018), que sugerem rápido extravasamento do material vulcânico entre 135 – 131 Ma com um pulso principal de duração de aproximadamente 1 milhão de anos, o que se aproxima à duração do magmatismo proposta para grandes províncias ígneas de basaltos continentais em geral (Coffin e Eldholm, 1994, Ernst *et al*., 2005, Jerram e Widdowson, 2005; Silver *et al*., 2006, Bryan e Ernst, 2008). Esta proposta quimioestratigráfica se baseia na hipótese de migração do magmatismo de sul para norte, com uma tendência geral de enriquecimento em TiO_2, representada pelos magmas-tipo Ribeira, Pitanga e Paranapanema, que recobrem os tipos de baixo TiO_2 aflorantes a sul (Figura 3.6). Esta organização é, em grande parte, possibilitada pela ideia de que os limites entre os magmas-tipo devem se aproximar consideravelmente aos limites estratigráficos

físicos entre episódios ou sequências vulcânicas principais da PIP (Peate *et al*. 1992).
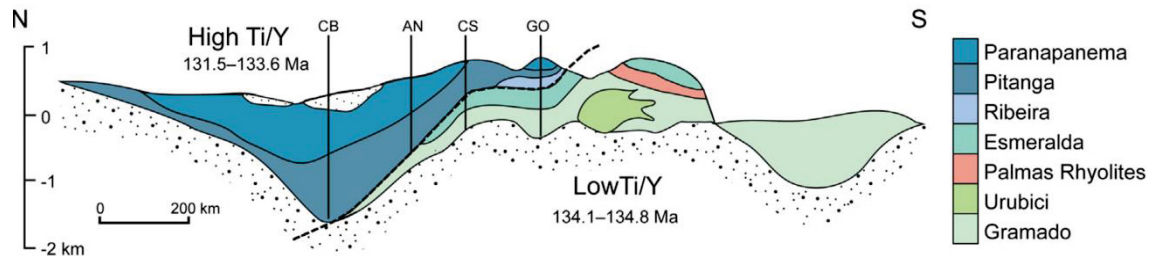
Figura 3.6 – Perfil geológico da PMP, utilizando a quimioestratigrafia de Peate (1997), além de isócronas construídas a partir de dados geocronológicos, citados por Rosseti *et al.* (2018). Adaptado do mesmo artigo.

Ao efetuar uma tentativa de classificação de 4895 amostras de basaltos da PIP considerando a proposta supracitada, Licht (2018) relata que quase metade das amostras não puderam ser classificadas, devido a problemas como sobreposições entre critérios para a classificação por etapas estabelecidos por Peate *et al.* (1992), que foram definidos a partir de um número consideravelmente menor de amostras. A partir disto, Licht e Arioli (2012) e Licht e Lima (2014), seguidos de Licht (2018) e Gomes *et al*. (2018) propõem uma caracterização geoquímica baseada na distribuição estatística dos teores de diversos elementos e suas combinações, entre os quais mantém-se a importância dos teores de SiO_2, TiO_2, P_2O_5 e Zr. A principal diferença desta abordagem é que as subpopulações definidas foram separadas por *gaps* naturais nas curvas de distribuição dos elementos e não por limites arbitrários com sobreposições de critérios de classificação (Figura 3.7).
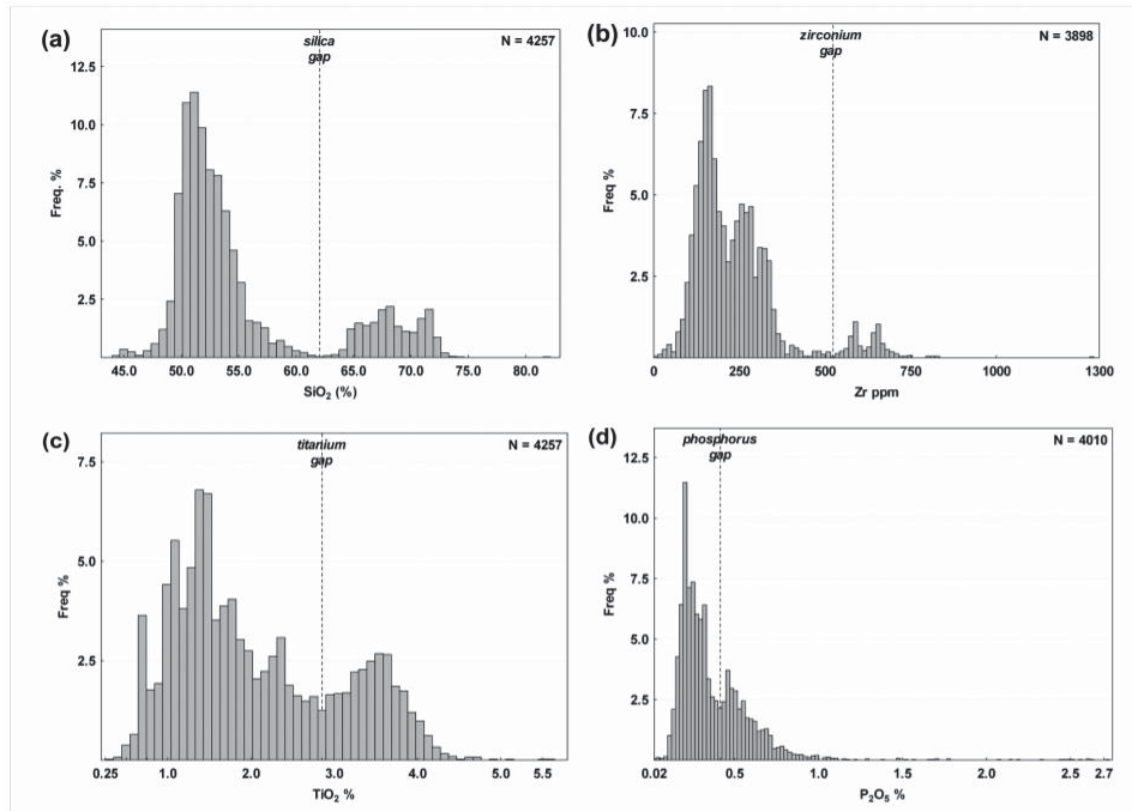
Figura 3.7 – Histogramas dos quatro elementos discriminantes SiO_2, Zr, TiO_2 e P_2O_5 com os respectivos limites naturais (Licht e Arioli, 2018).

Nessa abordagem, os limites naturais ou *gaps* presentes nessas curvas de distribuição foram utilizados para separar 16 combinações de subpopulações associadas a baixos e altos valores desses elementos, como pode ser observado na Figura 3.8.
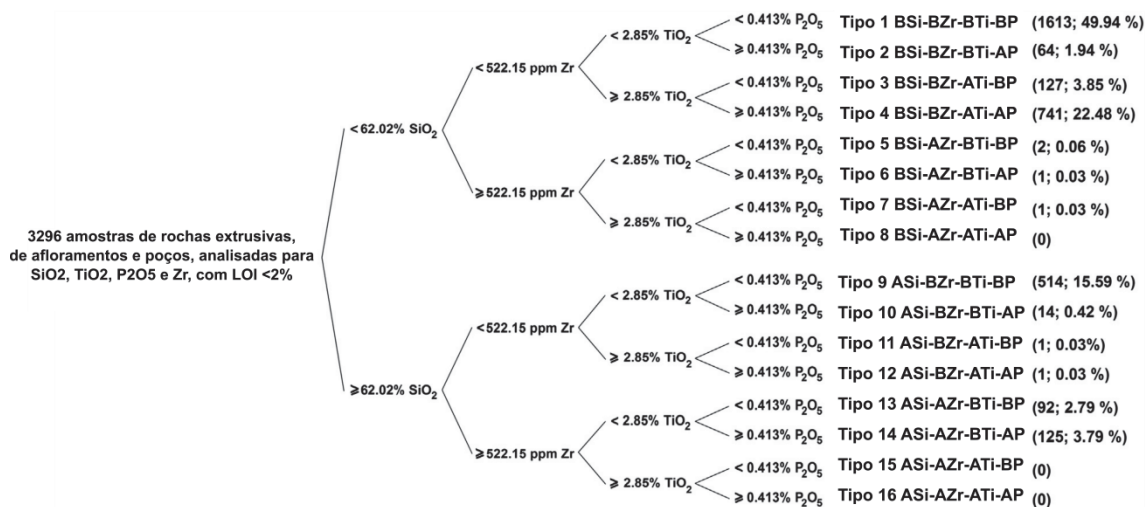
Figura 3.8 – Esquema representativo dos critérios estatísticos que definem cada subpopulação e quantidade de amostras em cada tipo, modificado de Licht (2018).

Das 16 associações formadas a partir desse método, sete são consideradas representativas de tipos geoquímicos reais, enquanto que as restantes são contrapartes estatísticas geoquimicamente impossíveis naturalmente derivadas da combinação dos critérios de classificação (como o tipo 8, com BSi-AZr-ATi-AP), tipos extremamente raros ou ainda possíveis erros analíticos. Assim, as 4 associações de baixa sílica (SiO$_2$ <62,02%) principais são os tipos 1, 2, 3 e 4, enquanto que as rochas de alta sílica são classificadas nos tipos 9, 10, 13 e 14 (Figura 3.8).

A partir desta análise estatística, Licht (2018) e Gomes *et al.* (2018) propõem um modelo quimioestratigráfico para a PIP consideravelmente distinto da proposta tradicional de Peate *et al.* (1992) e Peate (1997). Este modelo considera a existência de duas subprovíncias individuais, resultantes de focos de magmatismo atuantes em momentos e posições inicialmente diferentes, hipótese semelhante aos modelos já apresentados por Rüegg (1970) e Bellieni *et al.* (1984). Com o avanço do magmatismo e eventual sobreposição das lavas, gerou-se então o padrão de empilhamento de lavas de baixo TiO$_2$ (Tipo 1 CN, *sensu* Licht, 2018) sobre as lavas de alto TiO$_2$ (Tipo 4) na província centro-norte, que por sua vez recobriram as lavas de baixo TiO$_2$ da subprovíncia sul (Figura 3.9). De acordo com a quimioestratigrafia de Licht (2018), as lavas de alto TiO$_2$ e alto P$_2$O$_5$ do tipo 4 são representantes do início do sistema de magmatismo na subprovíncia centro-norte, o que constrasta significativamente com a ideia de que as lavas de alto TiO$_2$ representam os episódios vulcânicos finais em toda a PIP.
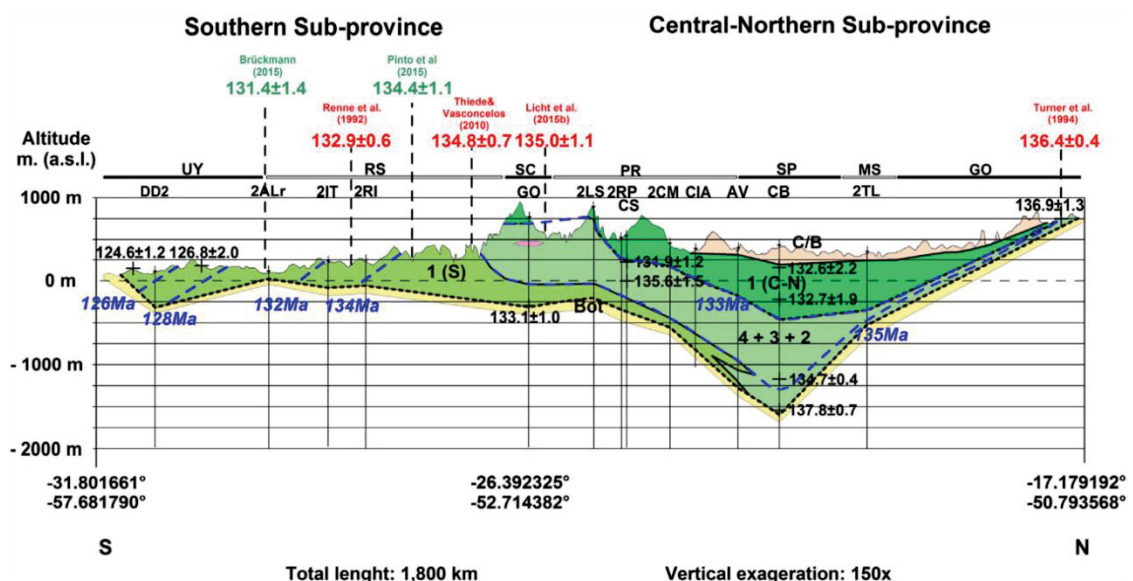
Figura 3.9 – Perfil quimio e cronoestratigráfico das subprovíncias Centro-Norte e Sul segundo Licht (2018).

Segundo a proposta quimioestratigráfica de Licht (2018), a área de estudo está compreendida na transição entre o domínio de lavas alto TiO_2 do Tipo 4 para a região de baixo TiO_2 do Tipo 1 (CN). Ainda, segundo quimioestratigrafia de detalhe de amostras de calha em poços (Gomes *et al*., 2018) é possível que os depósitos de Sertanópolis estejam situado em uma região próxima a intercalações entre derrames do Tipo 1 (CN) e Tipo 3.

Alinhada à quimioestratigrafia, a petrogênese dos magmas da província também tem sido um tema de importantes avanços e intensas discussões em anos recentes. Muitas das tentativas iniciais de explicação para a origem e divisão dos conjuntos de alto e baixo TiO_2 foram feitas já na época em que foram realizadas as primeiras análises químicas sistemáticas, algumas baseadas não só em geoquímica de rocha total como também em isótopos de Sr, Pb e O (Fodor *et al*., 1985a, 1985b, Fodor, 1987; Hawkesworth *et al*., 1988). Entre elas, destacava-se a percepção de distintos comportamentos em relação a parâmetros como: (i) teores de incompatíveis (como K, Rb e Ba), nos quais as lavas de alto TiO_2 são consideravelmente mais enriquecidas, possivelmente devido à fusão de regiões do manto muito distintas (Bellieni *et al*., 1984; Mantovani *et al*., 1985; Hawkesworth *et al*., 1988) ou a variações nos teores de fusão (Fodor *et al*., 1985a, Fodor, 1987); (ii) número de Mg, sugerindo que magmas primitivos oriundos de fusão parcial mais proeminente teriam gerado as lavas de baixo TiO_2 (Fodor, 1987); (iii) razões $^{87}Sr/^{86}Sr$, que sugerem alguma derivação crustal em especial para as lavas mais ácidas, o que é indicativo de processos *AFC (assimilation and fractional crystallization)* (Mantovani *et al*., 1985; Hawkesworth *et al*., 1988).

Atualmente, a causa da fusão responsável pelo magmatismo ainda não é um tema de consenso. Embora a correlação com o evento de rifteamento que deu fim ao Gondwana e abriu o Atlântico Sul seja clara (Szatmari e Milani, 2016; Foulger, 2018), a possibilidade de associação do magmatismo à ação da pluma mantélica de Tristão da Cunha (Fodor, 1987, Hawkesworth *et al*., 1992; Peate, 1997) vem sendo revisada, tendo sido descartada por Marques e Ernesto (2004) e posteriormente também por autores como Rocha-Júnior *et al*. (2012, 2013), Marques *et al*. (2016, 2018) e Foulger (2018).

Em um primeiro momento, Marques e Ernesto (2004) argumentam que a distância estabelecida em reconstruções paleomagnéticas de mais de 1.000 km

entre Tristão da Cunha e os derrames da província no Eocretáceo descartaria essa possibilidade. Neste sentido, Rocha-Junior *et al*. (2012, 2013) e Marques *et al*. (2016, 2018) argumentam que características composicionais e isotópicas (Sr, Nd, Pb e Os) da PIP não podem ser explicadas nem pela ação de uma pluma mantélica e nem por fusão exclusiva de rochas de um manto litosférico subcontinental (*SCLM*) antigo e homogêneo, sugerindo a contribuição de material astenosférico. Este, por sua vez, teria sido enriquecido e metassomatizado pela ação de fluidos ou magma relacionados a processos de subducção neoproterozoicos ou ainda mais antigos.

Foulger (2018), em uma extensa revisão sobre os modelos petrogenéticos da PIP, relata que variações espaciais e temporais do magmatismo vêm sendo explicadas por modelos de plumas mantélicas de características conflitantes entre si e aponta alguns problemas com esta interpretação, sugerindo que outras hipóteses sejam contempladas. Entre elas, o autor propõe que variações nos regimes de extensão litosférica que acompanharam o *breakup* do Gondwana Sul devem ter condicionado a erosão térmica ou mecânica do *SCLM* e a convecção na astenosfera, responsáveis pelo *emplacement* em lineamentos e *trends* vulcânicos específicos.

Em relação à origem dos magmas de baixo e alto TiO_2, De Min *et al*., (2018) sugerem alimentação a partir de dois distintos e separados reservatórios de magma, produzidos a partir de diferentes condições de fusão parcial, cristalização fracionada e assimilação crustal. Para os autores, a geração de magma foi impactada por contribuições significativas do material do *SCLM*, e as lavas de baixo TiO_2 foram afetadas por 5 – 30% de contaminação e assimilação de rochas supracrustais graníticas. Já as lavas de alto TiO_2 teriam sofrido pouca contaminação crustal, e sua assinatura isotópica seria indicativa de contribuição e mistura de magmas mantélicos e carbonatíticos na fonte próxima ao *SCLM*.

3.4 Camadas interderrames e depósitos vulcanoclásticos máficos (MVDs)

Segundo relatos de Licht (2014) e Cañon-Tapía (2018), pesquisas que fazem alusão à existência de camadas interderrames na PIP datam do início do século XX. Na segunda metade do século passado, no entanto, devido à maior ênfase dada à tipologia geoquímica e quimioestratigrafia dos derrames, menções a esse tema tornaram-se escassas na literatura. Com a intensificação das pesquisas em

vulcanologia física de derrames na PIP, camadas interderrames passaram novamente a receber atenção de maneira indireta (Jerram *et al*., 1999; Waichel *et al*., 2006, Lima *et al*., 2012), e recentemente tem sido objeto principal de estudos mais detalhados (Licht, 2012; Licht e Arioli, 2013; Lucchetti *et al*. 2014; Moraes e Seer, 2018). A maioria dos primeiros estudos sobre o assunto nas últimas décadas foca na ocorrência de arenitos eólicos resultantes da intercalação entre os primeiros derrames de basalto e o árido *paleoerg* Botucatu, que foi gradualmente afogado pela atividade vulcânica cada vez mais intensa na PIP (Jerram *et al*., 2000; Scherer, 2002; Jerram e Stollhofen, 2002; Petry *et al*., 2007), situação que também já fora reconhecida por Leinz (1949). Neste contexto, Jerram e Stollhofen (2002) e Petry *et al*. (2007) relatam que a interação passiva entre derrames e dunas do deserto Botucatu teria gerado brechas ígneas de matriz sedimentar idênticas a peperitos, termo mais comumente utilizado até então para denominar a litofácies produzida pela interação e mistura *in situ* entre intrusões e sedimentos encaixantes (Busby-Spera e White, 1987; Mueller *et al*., 2000; Martin e Nemeth, 2004, 2007) ou bases de derrame e sedimentos subjacentes (White *et al*., 2000; White e Houghton, 2006) – úmidos em ambas as situações.

Diante disso, Waichel *et al*. (2006, 2007) reconhecem peperitos em regiões centrais da província, associando-os a interações entre derrames e sedimentos úmidos depositados em ambientes fluvio-lacustres durante períodos de quiescência da atividade efusiva – interpretação que é seguida por Luccheti *et al*. (2014) também para brechas em derrames ácidos e por Rossetti *et al*. (2018) para interderrames do meio da sequência de baixo TiO_2 no Rio Grande do Sul. Do mesmo modo, esta hipótese foi utilizada para explicar conjuntos de brechas e sedimentos lamosos encontrados em proximidade com o contato com o *paleoerg* Botucatu, evidenciando heterogeneidades desse paleoambiente à época do início do magmatismo (Machado *et al*., 2015; Moraes e Seer, 2018).

A identificação de litofácies autoclásticas – *i.e*, formadas por fragmentação passiva de derrames e resfriamento em contato com ar (White e Houghton, 2006) – seguiu linhas interpretativas semelhantes. De acordo com a arquitetura de fácies vulcânicas que vem sendo proposta (Waichel *et al*., 2006; Barreto *et al*., 2014; Rossetti *et al*. 2014, 2018) rochas autoclásticas de topo de derrame associadas a morfologias como *rubbly* e *slabby pahoehoe* são feições comuns na PIP,

especialmente em intervalos de derrames simples produzidos por altíssimas taxas de efusão (Rossetti *et al*., 2018). Brechas de topo de derrames *rubbly pahoehoe* apresentam porosidade e espaços intergranulares consideráveis, que são comumente preenchidos por materiais clásticos eventualmente depositados acima delas (Duraiswami *et al*., 2014; Rosa *et al*., 2016; Marshall *et al*., 2016; Valore, 2017). Este arranjo se assemelha consideravelmente às fácies de brechas convencionadas como peperitos (Rosa *et al*., 2016), o que significa que intervalos autoclásticos podem ter sido subrepresentados em algumas propostas de caracterização iniciais na PIP.

A classificação dos fragmentos autoclásticos relacionados a derrames por si só como camadas interderrames propriamente ditas levaria a confusões de cunho faciológico e estratigráfico (Capítulo IV), mas o mesmo não pode ser dito sobre o material que pode preencher a porosidade intergranular das brechas autoclásticas e dar origem a uma rocha de composição mista. Em muitos intervalos, na realidade, o material depositado entre derrames só está preservado desta maneira na PIP (Valore, 2017, Rossetti *et al*., 2018) e também em outras PCBs (Óskarsson e Riishus, 2014; Marshall *et al*., 2016). Na PIP, este material clástico também tem sido interpretado como produto de deposição fluvio-lacustre e eólica alternada com a atividade vulcânica que, além de formar a matriz de algumas brechas autoclásticas, também é reportado como material de preenchimento de fraturas de inflação (*inflation clefts*) e superfícies irregulares de derrames, de maneira geral (Rossetti *et al*., 2014, 2018).

Conforme discutido em White *et al*. (2000), Rosa *et al*. (2016), Marshall *et al*. (2016), Valore (2017) e Nemeth e Palmer (2019), existem diversos processos que podem dar origem a brechas de arcabouço vulcânico e matriz clástica. Neste sentido, é questionável se fácies de brecha com arranjo de clastos isolados e sustentados por matriz, sugestivo de derivação alóctone ou de transporte do arcabouço em algum grau, podem ser satisfatoriamente explicadas pelo fenômeno de fragmentação autoclástica seguida de preenchimento da porosidade intergranular por material detrítico. Uma das possibilidades que podem explicar a gênese de camadas de brecha com graus variados de transporte primário inclui a formação de hialoclastitos, derivados da fragmentação da lava em situações de vulcanismo subaquoso, acompanhados de características *pillow lavas* (Moraes e Seer, 2018).

Até o momento, esta situação foi registrada em Araguari – MG próximo ao contato dos derrames com a Fm. Botucatu, em uma clara indicação da presença de paleoambientes consideravelmente úmidos.

Independente de maiores interpretações, o aparecimento de intervalos de deposição subaquosa entre diferentes horizontes vulcânicos é um dado intrigante, e sua relação com paleoambientes vulcânicos, sistemas deposicionais e variações do clima regional configuram um tema que, conforme mencionado previamente, necessita de mais estudos.

Em um contexto global, ao estudarem a conexão existente entre as idades de PCBs e extinções em massa, Ross *et al*. (2005) sugeriram que episódios de vulcanismo basáltico explosivo - capazes de afetar consideravelmente os ecossistemas globais (Svensen *et al*., 2009; Black *et al*., 2015; Jerram *et al*., 2016) - devem ser consideravelmente mais frequentes e importantes no registro geológico global do que o suposto previamente. Ross *et al.* (2005) compilaram dados de várias PCBs de diferentes contextos no mundo, mostrando que depósitos vulcanoclásticos máficos (*mafic volcaniclastic deposits*, ou simplesmente *MVD*s) oriundos principalmente de eventos explosivos seriam descritos em todas elas, com exceção da Província Magmática Paraná – Etendeka (Figura 3.10). Segundo os autores, a origem destes fenômenos estaria vinculada principalmente à interação entre os produtos magmáticos em si e os ambientes afetados por eles, especialmente no que se refere à presença de água externa ao sistema vulcânico – isto é, água meteórica, freática ou marinha. Tendo em vista que o vulcanismo basáltico geralmente apresenta explosividade inata relativamente restrita (Newhall e Self, 1982; Fisher e Schminke, 1984, Houghton *et al*., 2013), tem sido possível correlacionar satisfatoriamente boa parte dos *MVD*s primários a atividades explosivas hidromagmáticas (Ross e White, 2005; Ross *et al*., 2005; McClintock e White, 2006; White *et al.,* 2009; White e Ross, 2011), que teriam produzido diversos tipos de rochas piroclásticas (*sensu* White e Houghton, 2006). Estas, por sua vez, podem ter sido posteriormente ou mesmo sin-eruptivamente retrabalhadas por diversos processos sedimentares (McPhie *et al*., 1993; Nemeth e Palmer, 2019).

	Columbia River	Afro-Arabia	E Greenl.	Ireland+Skye	North Sea	Deccan	Ontong-Java	Ferrar	Karoo	Siberian	Emeishan	E Pilbara
Observations												
Cumulative MVD thickness locally >100 m	x	x		✓		✓	✓	✓	✓	✓	✓	✓
Structureless deposits			✓	✓				✓	✓	✓		
Layered deposits	✓	✓	✓	✓	✓	✓	✓	✓	✓	✓	✓	✓
Tuff-breccias and lapilli-tuffs (including 'agglomerates')	✓	✓	✓	✓	x	✓	✓	✓	✓	✓	✓	✓
Tuffs	✓	✓	✓	✓	✓	✓	✓	✓	✓	✓	✓	✓
Non-to poorly-vesicular blocky sideromelane (or former basaltic glass) clasts	✓		✓	✓	✓	✓	✓	✓	✓			✓
Vesicular basaltic clasts	✓		✓			✓	✓	✓	✓			rare
Abundant country rock fragments	✓		✓			✓		✓	✓	✓	✓	✓
Quartz grains (ash fraction)			✓					✓	✓			
Presence of accretionary lapilli		✓	✓			✓	✓	✓	✓			✓
Interpretations												
Primary volcaniclastic deposits	✓		✓	✓	✓	✓	✓	✓	✓			✓
Reworking syn- or post-volcanism	✓		✓		✓	✓		✓	✓			✓
Vent-filling deposits	✓[1]			✓		✓		✓	✓			
Phreatomagmatic fragmentation	✓		✓		✓	✓	✓	✓	✓			✓
'Magmatic' fragmentation	✓								✓			
Subaerial eruptions	✓		✓	✓		✓		✓	✓			✓
Subaqueous eruptions	✓		✓									
Subaerial deposition	✓	✓	✓	✓			✓	✓	✓	✓		
Subaqueous deposition	✓	✓	✓	✓	✓			✓	✓	✓		✓

✓=present; x=probably absent; left blank=insufficient information available; 1=Asotin craters only; 2=Gronau alkaline tuff.

Figura 3.10 – Resumo de feições características de *MVD*s encontradas em várias PCBs no mundo (Ross *et al.*, 2005).

Cabe dizer que em Ross *et al*. (2005) e White *et al*. (2009) o termo "freatomagmatismo" foi utilizado com a intenção de descrever quaisquer fenômenos explosivos derivados de hidrovulcanismo, em concordância com o uso mais comum do termo (Fischer e Schminke, 1984; Cas e Wright, 1987; Morrisey *et al*. 2000; White e Ross, 2011; Zimanowski *et al*., 2015; Nemeth e Palmer, 2019). De mesmo modo, os termos "hidrovulcanismo" e "hidromagmatismo" referem-se genericamente a interação passiva ou ativa entre magma e água externa, subterrânea ou em superfície, também seguindo os usos em Wohletz e Sheridan (1983) e Cas e Wright (1987). Ou seja, dentre as diferentes possibilidades da interação hidrovulcânica, o freatomagmatismo ou o hidrovulcanismo explosivo seriam então responsáveis por parte considerável da fragmentação de material juvenil e regional que compõem os *MVD*s nas diversas PCBs do mundo.

Embora tradicionalmente a PIP tenha sido entendida como uma exceção no tangente à presença de *MVD*s (Ross *et al*., 2005), a observação, dentre outros

fatores, de que muitas das fácies interderrames não podem ser explicadas por fenômenos de fragmentação passiva e *in situ* reforça e abre espaço para novos modelos, que se assemelham às ocorrências de hidrovulcanismo explosivo (Licht, 2012; Licht *et al*., 2015; Valore *et al*., 2017) e hidrovulcanismo subaquoso (Moraes e Seer, 2018) em outras PCBs.

Além disto, cabe mencionar que segundo Ross *et al*. (2005) e White *et al*. (2009), peperitos gerados por interações lava-sedimento úmido e hialoclastitos também são considerados *MVD*s primários, embora estes devam ser volumetricamente menos importantes do que rochas piroclásticas em depósitos hidrovulcânicos de PCBs (White e McClintock, 2001; Ross *et al*., 2005). Além disso, a ocorrência dessas fácies na PIP também indica que fenômenos hidrovulcânicos aconteceram com uma frequência maior do que os vulcanólogos entendiam até o momento da publicação de Ross *et al*. (2005). Ou seja, outras fácies vulcanoclásticas hidrovulcânicas (*i.e.,* fácies piroclásticas) devem ter expressão no registro geológico proporcional ao número de intervalos de deposição de peperitos e hialoclastitos (White e McClintock, 2001; Ross *et al*., 2005; McClintock e White, 2006), como as já mencionados descrições de Waichel *et al*. (2006, 2007), Luchetti *et al*. (2014) e Moraes e Seer (2018).

Para explicar os fenômenos hidrovulcânicos explosivos, uma das hipóteses mais utilizadas é a da interação combustível – refrigerante, ou *fuel – coolant interaction* (*FCI*, ou ainda *molten fuel-coolant intercation - MFCI*), derivada da engenharia metalúrgica e da ciência dos materiais. A hipótese se baseia no comportamento termodinâmico de um fluido supercrítico ou superaquecido - condições metaestáveis nas quais um fluido como a água apresenta propriedades mistas entre líquido e vapor (supercrítico) ou permanece líquido mesmo acima do seu ponto de ebulição (superaquecido) (Wohletz, 1983, 1986; Morrissey *et al*., 2000). Nestas condições, a água (na realidade, um fluido impuro, rico em material particulado e sais dissolvidos – White, 1996; Schipper e White, 2016) pode abruptamente transformar-se em vapor após atingir temperatura superior à da nucleação espontânea de bolhas de vapor (cerca de 590 K ou ~316 ºC em pressão atmosférica normal), devido a instabilidades termodinâmicas do sistema ou por influência de uma onda de choque. Essa transição abrupta é responsável por uma rápida expansão termohidráulica do sistema, que está subordinada à pressão

confinante, e pode ocorrer em uma taxa explosiva (Wohletz, 1983, 1986; Zimanowski *et al*., 1997; 2015; Morrissey *et al*., 2000).

Estes autores descrevem a sequência de eventos associada à *MFCI* em quatro estágios distintos, que podem formar uma espécie de ciclo de retroalimentação. Este ciclo é responsável por aumentar a taxa de transferência de calor, que depende do tamanho da superfície de contato entre combustível e refrigerante. Os estágios podem ser resumidos nos seguintes processos:

(i) Contato e mistura "grosseira" entre combustível e refrigerante, gerando um filme de vapor estável entre os dois;

(ii) Colapso quase simultâneo de todos os filmes de vapor devido a alguma instabilidade externa ou interna (sismos, condensação muito rápida do vapor), combustível e refrigerante são pareados térmica e mecanicamente;

(iii) Contato direto da lava com a água, onda de choque termohidráulico e aumento incremental da taxa de transferência de calor devido à fragmentação fina da lava, que leva ao superaquecimento da água sob pressão. Expansão do refrigerante cria tensão na lava, que é aliviada rúptil e explosivamente;

(iv) Expansão volumétrica da mistura combustível-refrigerante durante transformação da água em vapor superaquecido. Combustível e refrigerante não estão mais pareados. Nesta fase, interações dúcteis (passivas) com lava em outras regiões do sistema podem dar origem a fragmentos arredondados.

De maneira secundária dentro da *MFCI* ocorre um fenômeno que se convencionou como *quenching* ("arrefecimento"), em referência à fragmentação da lava pelo seu resfriamento e contração (Kokelaar, 1986; Cas e Wright, 1987; van Otterloo, 2015). Este fenômeno geralmente é associado à chamada "fragmentação passiva" – i.e. fragmentação que não envolve contato direto da lava com água, e que ocorre de maneira subordinada nos estágios 3 e 4 da *MFCI* (van Otterloo, 2015, Zimanowski *et al*., 2015). Já a expressão *thermal granulation* (granulação térmica) faz referência ao *quenching* estritamente passivo e não explosivo, que dá origem, por exemplo, a hialoclastitos e peperitos (Kokelaar, 1986; Busby-Spera e White, 1987; White *et al*., 2000; Skilling *et al*., 2002). Muitos autores concordam que a *MFCI* explosiva está condicionada à ocorrência do ciclo de eventos até além do estágio 2, e que a interação passiva geralmente está associada à impossibilidade de

manutenção da expansão termohidráulica ou sua completa ausência no sistema hidrovulcânico (Martin e Nemeth, 2007; van Otterloo, 2015).

A partir de uma série de extensivos experimentos e cálculos, Wohletz (1983, 1986) sugere que a interação hidrovulcânica explosiva ou freatomagmática é controlada pela razão entre magma e água no sistema e pelo consequente grau de superaquecimento da água. Estas variáveis estão, portanto, diretamente relacionadas à eficiência do sistema explosivo, bem como ao tamanho e ao tipo dos fragmentos e dos depósitos vulcanoclásticos gerados. Para Wohletz (1983, 1986) e Sheridan e Wohletz (1983) há um ponto crítico relativo à eficiência de transferência de calor no sistema, em função de uma razão entre massa de água/magma próxima a 0,3 (Figura 3.11).
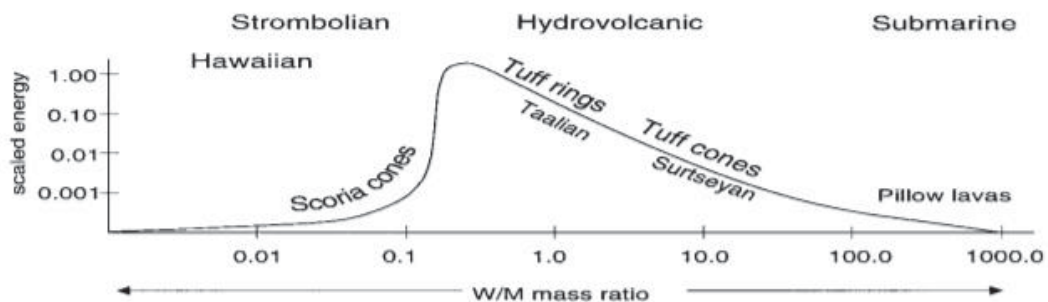
Figura 3.11 – Diagrama de razão água/magma *vs* energia explosiva. O máximo energético encontra-se em uma razão próxima a 0,2-0,3, correspondente ao tipo "Taaliano", que produz anéis de tufos. Cones de tufos são produzidos por razões mais altas (vulcanismo do tipo "Surtseyano"). Razões maiores tendem a progressivamente diminuir a explosividade (Wohletz e Sheridan, 1983; Morrisey *et al*., 2000).

Para Cas e Wright (1987) as explosões hidrovulcânicas podem ser enquadradas em dois tipos principais, designadas explosões freatomagmáticas e freáticas. Para uma razão água/magma menor que 0,2, considera-se que a quantidade de água seja muito baixa para efetivamente manter ciclos de superaquecimento, de modo que o sistema favorecerá uma explosão magmática comum (caso haja predisposição para tal) ou uma explosão freática. A explosão freática consiste na ejeção de vapor acompanhado essencialmente de fragmentos da rocha encaixante, com pouco ou nenhum material juvenil, em temperaturas geralmente menores do que as de explosões freatomagmáticas (Stearns e MacDonald, 1946; Muffler *et al*., 1971; Fischer e Schminke, 1984; Cas e Wright, 1987; Wohletz, 1998). Nas últimas décadas, no entanto, erupções de vapor e material acessório vêm sendo mais frequentemente denominadas explosões

hidrotermais, em detrimento do termo "freático" (Wohletz, 1998; White e Ross, 2011; Lube *et al*., 2014). Independente de questões terminológicas, sabe-se que estes estilos eruptivos comumente se alternam em sistemas hidrovulcânicos explosivos (White e Houghton, 2000; Sottili *et al*., 2009; White e Ross, 2011), o que contribui para a característica complexidade faciológica dos depósitos associados.

      Conforme o gráfico da Figura 3.11, a MFCI pode ser suprimida em razões água/magma muito maiores, dando origem apenas a fragmentos gerados por granulação térmica - o que, no caso do vulcanismo subaquoso, também comumente se deve a pressões hidroestáticas demasiadamente baixas (White e Houghton, 2000) ou altas (van Otterloo, 2015). Ainda, segundo Wohletz (1983, 1986) e Sheridan e Wohletz (1983), a eficiência explosiva do sistema é máxima quando a razão é igual ou ligeiramente superior a 0,3, o que possibilita a ocorrência de uma explosão freatomagmática propriamente dita. Essa explosão é caracterizada pela ejeção de material juvenil intensamente fragmentado, que pode eventualmente dar origem a grandes plumas e nuvens piroclásticas, como as descritas em vulcões poligenéticos com episódios freatoplinianos (Self e Sparks, 1978; Smith e Kokelaar, 2013; Van Eaton e Wilson, 2013; Houghton *et al*., 2015).

      De maneira geral, erupções hidrovulcânicas eficientes dão origem a piroclastos juvenis predominantemente finos (cinza fina a extremamente fina) (Wohletz, 1983, 1986; Cas e Wright, 1987, Sohn, 1996), embora a participação de partículas de granulação grossa possa ser subrepresentada nos depósitos de tefra hidrovulcânica devido à retenção destas dentro do próprio conduto (Graettinger *et al*., 2015; White e Valentine, 2016; Valentine *et al*., 2017). De maneira correspondente, a análise da morfologia destas partículas finas em depósitos vulcanoclásticos é considerada crucial para a determinação mais precisa da natureza dos fenômenos de fragmentação (magmática ou hidromagmática), bem como sua diferenciação de processos de fragmentação não-explosivos (Zimanowski *et al*., 1997, 2015; Dellino *et al*., 2001; Büttner *et al*., 2002; Dürig *et al*., 2012; Graettinger *et al*., 2013; van Otterloo *et al*., 2013, 2015; Jordan *et al*., 2013, 2014; White *et al*., 2015; Liu *et al*., 2017). Neste sentido, é importante investigar tanto as partículas produzidas pelo contato direto entre lava e água (partículas ativas) quanto as fragmentadas pela tensão termohidráulica dele resultante (partículas passivas), uma vez que as primeiras podem corresponder a apenas um terço dos volumes de material juvenil

ejetado (Zimanowski *et al.*, 1997; Buttner *et al.*, 2002; White e Valentine, 2016) e que ambas ocorrem juntas em depósitos hidromagmáticos (Graettinger *et al.*, 2013; Jordan *et al.*, 2014; Zimanowski *et al.*, 2015).

Partículas ativas (Figura 3.12) tipicamente exibem formatos relativamente equidimensionais e angulosos, com características quebras superficiais "em degrau" irregulares (produzidas pela fragmentação rúptil) e redes de fraturas internas relacionadas ao *quenching* (que ocorre sem hidratação da lava) (Heiken, 1972; Zimanowski *et al.*, 1997; Buttner *et al.*, 2002; Durig *et al.*, 2012). Também são descritos padrões "em musgo" criados pela aglutinação de fragmentos extremamente finos (< 20 µm) (Wohletz, 1983; Morrisey *et al.*, 2000). Partículas passivas (Figura 3.13) apresentam morfologias arredondadas produzidas por fragmentação em regime dúctil da lava, semelhantes a cabelos e lágrimas de "*Pele*" (Graettinger *et al.*, 2013; Jordan *et al.*, 2014). Também são características de granulação térmica ou fragmentação magmática as partículas angulosas com superfícies mais conchoidais ou planas lisas, com formatos comumente alongados e cuspados (Buttner *et al.*, 2002; Durig *et al.*, 2012; Jordan *et al.*, 2014; van Otterloo, 2015). Além disto, a interação lava-água posterior à MFCI que ocorre na coluna eruptiva ou no interior de correntes piroclásticas de densidade (CDPs, ou *PDCs* em inglês) úmidas também dá origem a feições características, como superfícies com inúmeros minúsculos buracos, filmes de hidratação enriquecidos em ferro e magnésio e filmes de minúsculas partículas aderentes em clastos maiores (Capaccioni e Coniglio, 1996; Zimanowski *et al.*, 2015).
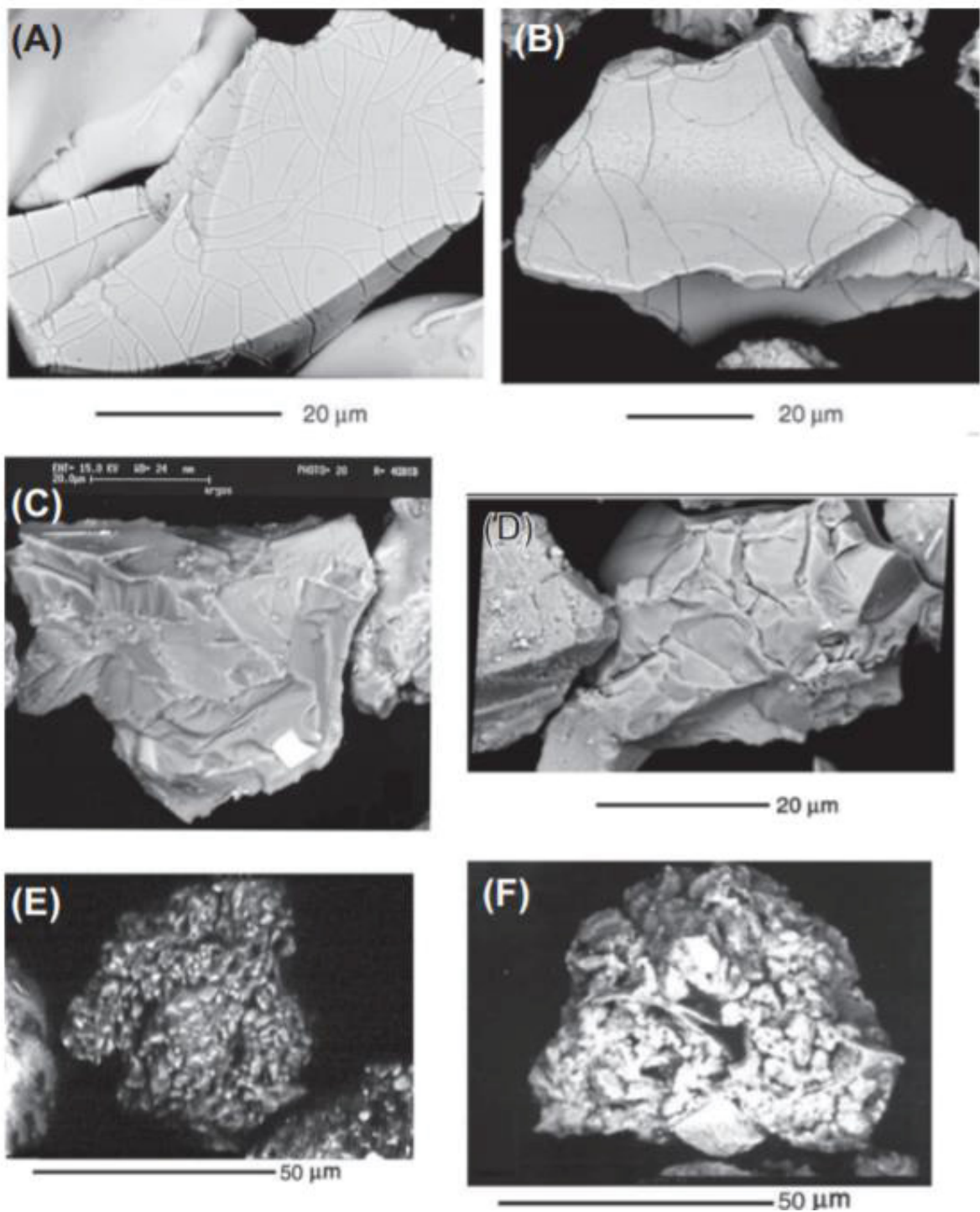
Figura 3.12 – Morfologia de partículas ativas ao microscópio eletrônico de varredura: A) Partícula com quebras perlíticas de experimento MFCI; B) Partícula angulosa com quebras perlíticas de depósito natural; C) Partícula basáltica com quebras em degrau; D) Partícula riolítica com quebras em degrau. E) Partícula tipo "musgo", experimento MFCI. F) Partícula natural com morfologia tipo "musgo". Modificado de Zimanowski *et al*. (2015).
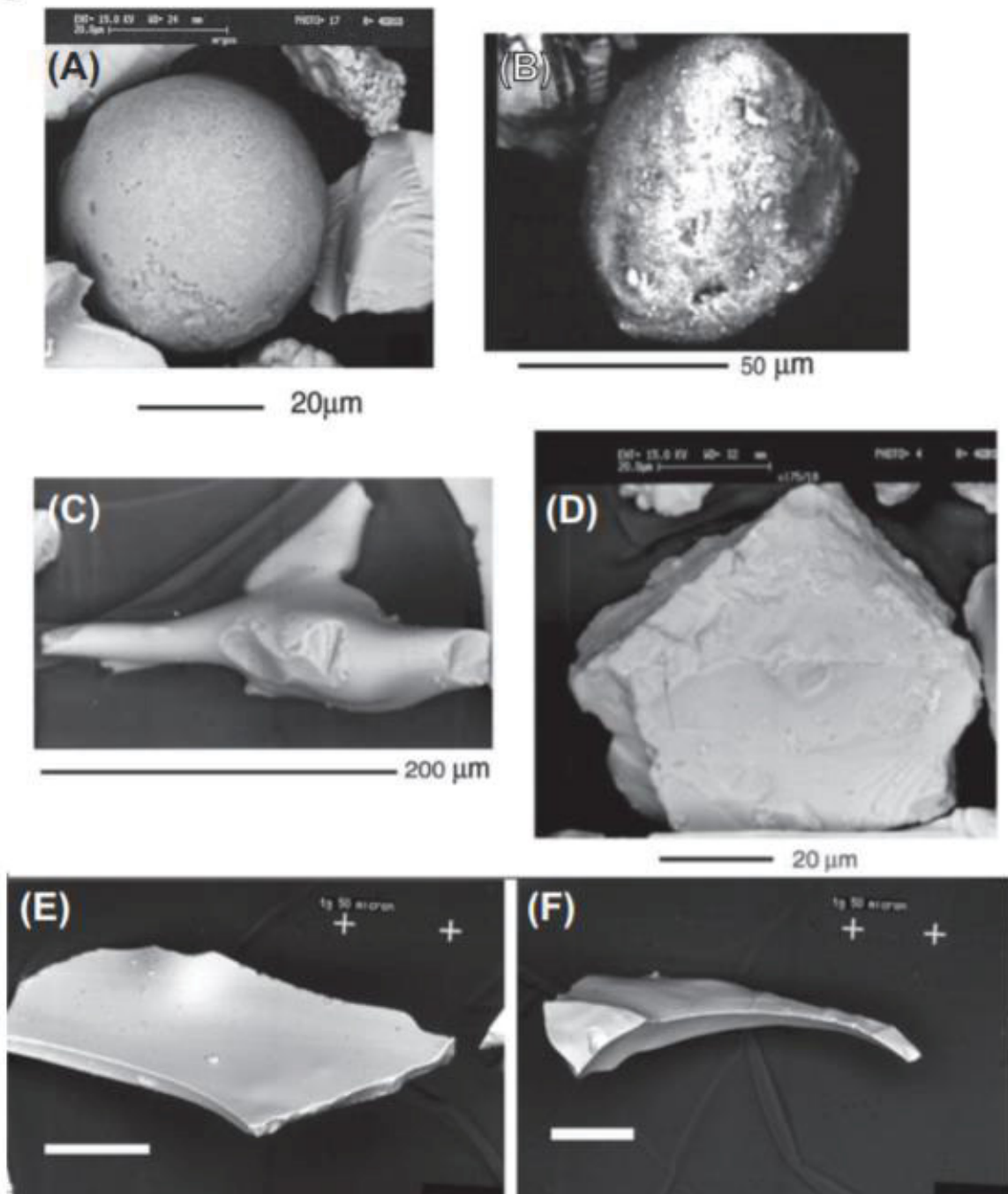
Figura 3.13 – Morfologia de partículas passivas observadas no MEV: A) Partícula arredondada; B) Partícula subarredondada; C) Partícula do tipo "cabelo de *Pele*"; D) Partícula equidimensional em bloco; E) Partícula placoide; F) Fragmento cuspado e delgado. Modificado de Zimanowski *et al.* (2015).

Além da morfologia dos clastos, no entanto, a investigação de depósitos hidrovulcânicos explosivos se baseia em suas características faciológicas gerais (Sohn e Chough, 1989; White, 1991; Vazquez e Ort, 2006; White *et al.*, 2009; Ort *et al.*, 2018; Nemeth e Palmer, 2019). Neste sentido, ressalta-se o estudo da associação entre depósitos hidrovulcânicos originados por condutos monogenéticos

- caracterizados como maares, anéis de tufo e cones de tufo (Figura 3.14, Figura 3.15) – e as condições ambientais que os produzem (Lorenz, 1973, 1986; Wohletz e Sheridan, 1983; Sohn, 1996; White e Ross, 2011; Kereszturi e Nemeth, 2012).
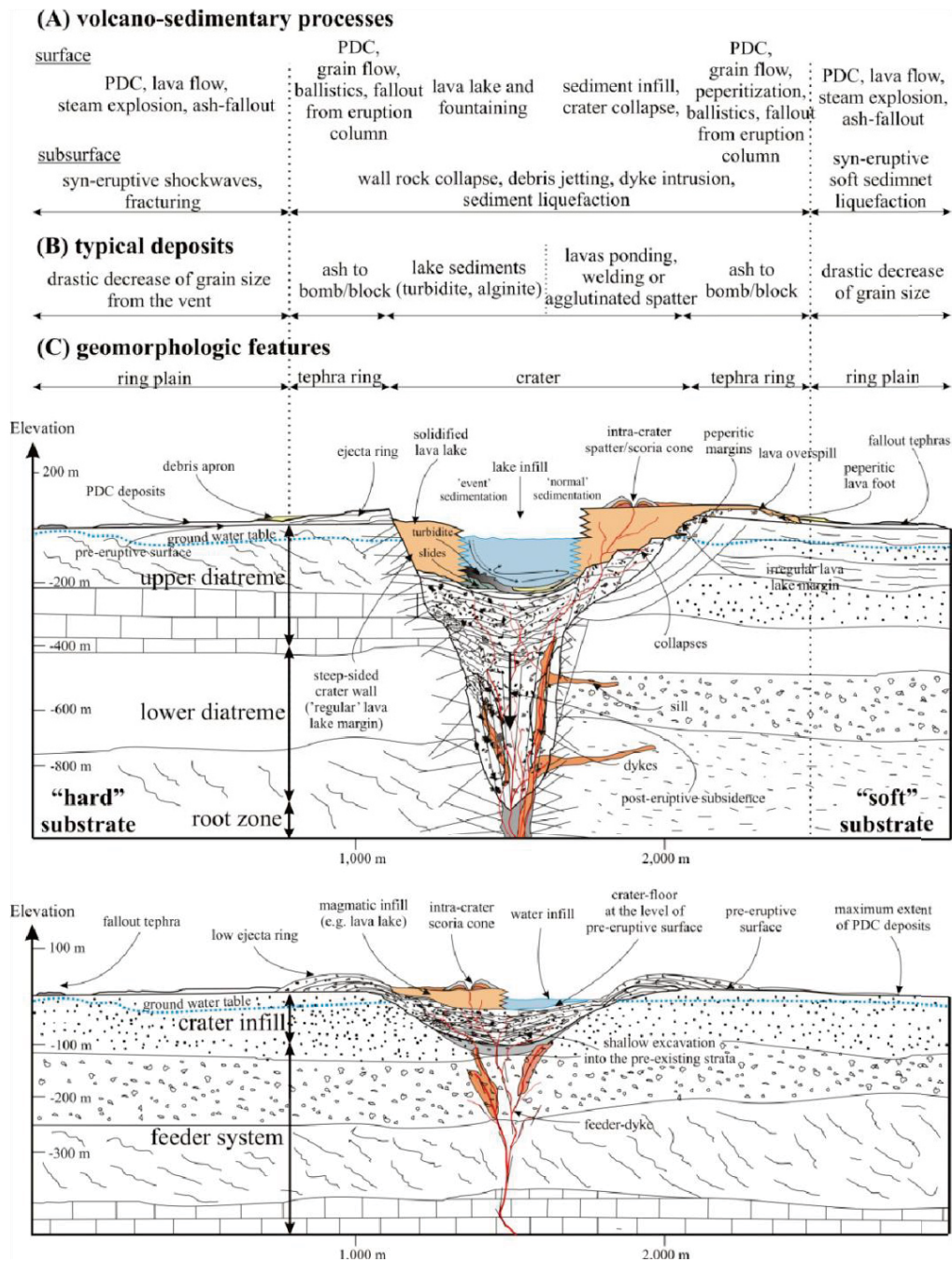
Figura 3.14 – Esquema representando as diferenças geomorfológicas, vulcanológicas e estratigráficas entre maares com diatremas associados (acima) e anéis de tufo (abaixo), de Kereszturi e Nemeth (2012).
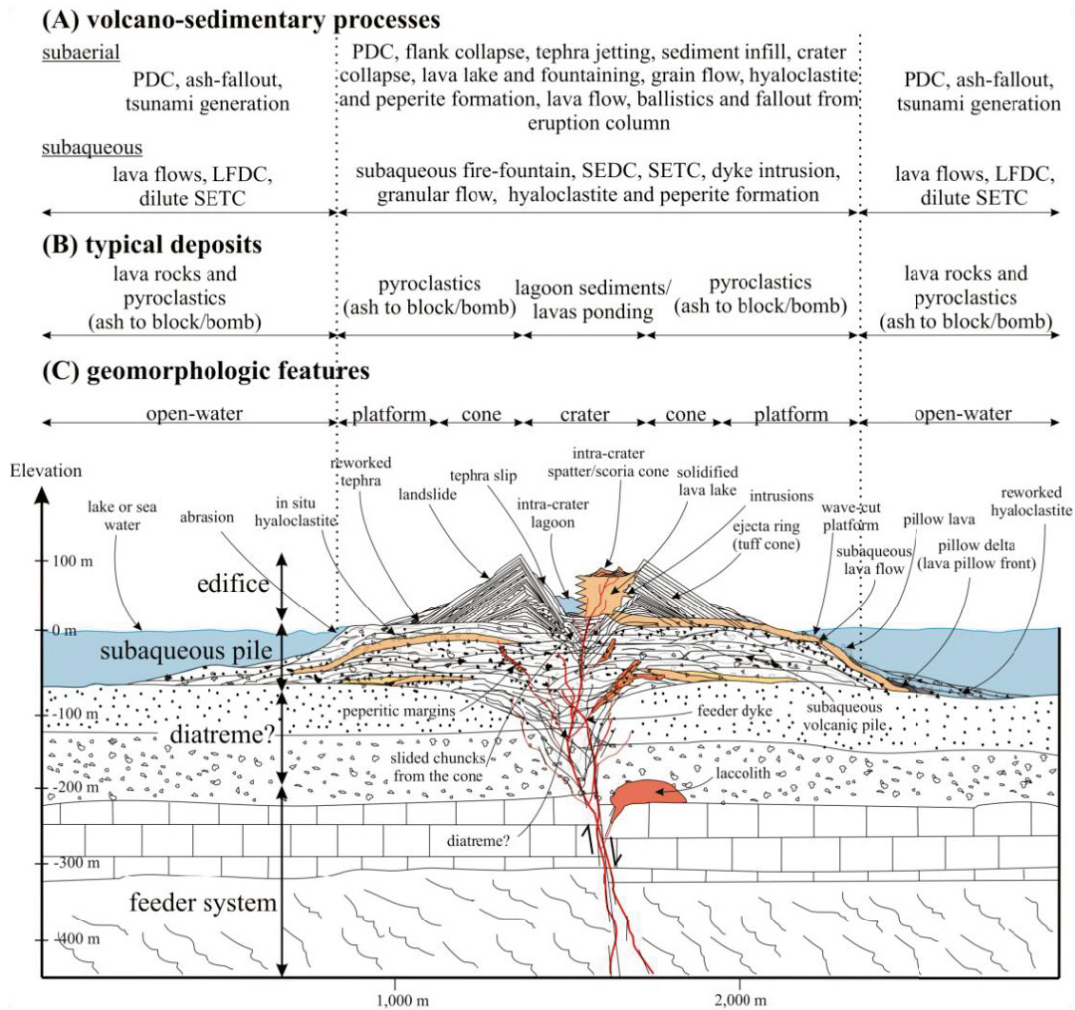
Figura 3.15 – Esquema representando as principais feições geomorfológicas, vulcanológicas e estratigráficas associadas a cones de tuno, de Kereszturi e Nemeth (2012). SEDC – "*subaqueous eruption-fed density current*", SETC – "*subaqueous eruption-fed turbidity current*", LFDC – "*lava flow-fed density current*".

De maneira geral, maares são depressões de centenas de metros a poucos quilômetros de diâmetro com bordas de crateras de elevações sutis, enquanto que anéis de tufo e cones de tufo são feições positivas de diâmetro ligeiramente maior, sendo que a inclinação das camadas de tefra da borda da cratera é progressivamente maior nos cones (Wohletz e Sheridan, 1983; Lorenz, 1986; Sohn e Chough, 1989; Sohn, 1996). Estes sistemas são formados pela deposição a partir de queda piroclástica (controlada por plumas de cinza em suspensão no ar ± cortinas balísticas inerciais) e de correntes piroclásticas de densidade diluídas (*surges* piroclásticos) com variações faciológicas correspondentes a cada tipo (Figura 3.14). Isso se deve, em partes, ao progressivo aumento da "umidade" ("*wetness*") dos depósitos nesse espectro (Wohletz, 1998), sendo os maares os

depósitos mais secos e os cones de tufo os mais úmidos (Wohletz e Sheridan, 1983; Sheridan e Wohletz, 1983; White e Ross, 2011).

Apesar disto, autores como Sohn (1996), Wohletz (2003) e White e Valentine (2016) reiteram que a simples correlação entre razão água/magma total e energia explosiva (Figura 3.11) provavelmente se distancia da realidade observada na maioria dos casos de interações *MFC*, uma vez que nem toda a água disponível no sistema hidrovulcânico é efetivamente envolvida na interação explosiva. Neste sentido, Sohn (1996) e White e Ross (2011) reconhecem que existem diversas variações reais na faciologia dos depósitos hidrovulcânicos de vulcões monogenéticos (*"wet ring, dry cone"*) que não são explicadas pelo modelo típico de Wohletz e Sheridan (1983), sugerindo que os próprios fenômenos de transporte e deposição (queda, *PDC*s, balísticos) possuem maior influência na morfologia dos vulcões. Estes, por sua vez, seriam controlados não só pela razão água/magma total, mas também por fatores como a geometria do conduto, condições de fluxo hidrológico (razão água/magma efetiva, normalmente menor que a total), profundidade das explosões, pressões confinantes e litologia das encaixantes, entre outros.

Recentemente, experimentos, modelos matemáticos e estudos de caso têm mostrado que um controle importante para a faciologia dos depósitos hidrovulcânicos monogenéticos deve incluir as profundidades onde ocorrem as interações *MFC* explosivas, que por sua vez podem variar ao longo de uma mesma erupção (Figura 3.16). De acordo com Valentine e White (2012), Valentine *et al*. (2014, 2015a, 2015b), Graettinger *et al*. (2015) e Graettinger e Valentine (2017), maares são formados por inúmeras explosões que não necessariamente seguem uma tendência de aprofundamento progressivo com o tempo (Lorenz, 1986), e que possuem forte influência na dispersão de partículas. Para esses autores, profundidades grandes (>200 m) favorecem a construção de estruturas como diatremas sem ejeção significativa de material, enquanto que profundidades relativamente mais rasas, entre 10 – 100 m (ligeiramente acima ou dentro da faixa da "profundidade dimensionada ótima", ou *OSD* em inglês) favorecem a deposição de horizontes maciços de cortinas balísticas, *debris jets* e queda piroclástica. Proporcionalmente, erupções produzidas por explosões ligeiramente abaixo da *OSD* (a cerca de 100-200 m, a depender também da consolidação do substrato e energia

da explosão) favorecem a deposição dos típicos depósitos de *PDCs* diluídas (Graettinger *et al.*, 2015; Graettinger e Valentine, 2017).
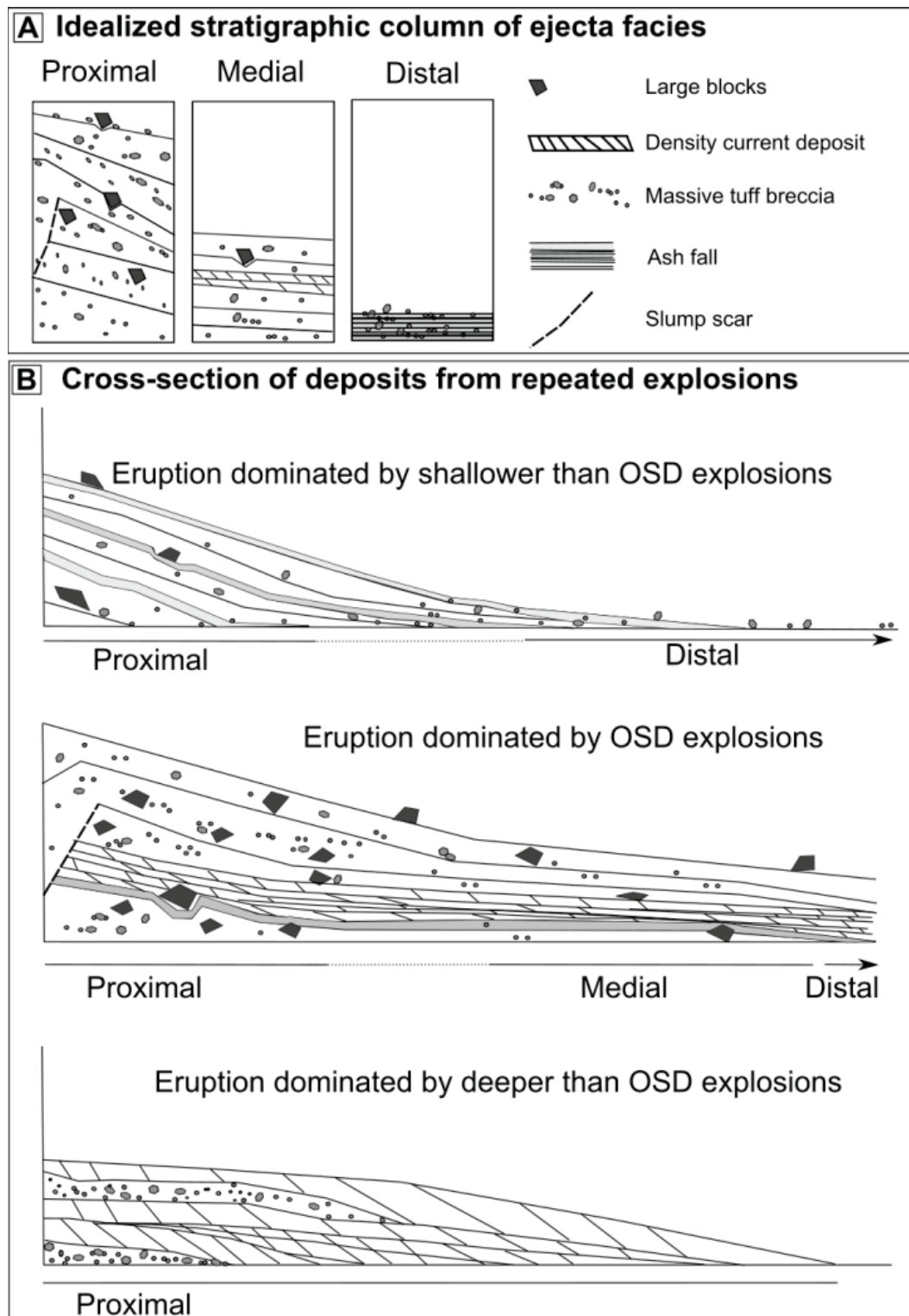
Figura 3.16 – Empilhamento típico de fácies piroclásticas em vulcões "monogenéticos" hidrovulcânicos segundo tendências nas profundidades das explosões (cada erupção é formada por dezenas a centenas de explosões) de Graettinger *et al.* (2015).

Nestes trabalhos, diferenças entre as fácies piroclásticas e condutos hidrovulcânicos monogenéticos são analisadas principalmente sob a ótica da relação entre profundidade e energia da explosão. No entanto, cabe reiterar que a profundidade da explosão também é controlada pelas condições hidrológicas das rochas encaixantes - *e.g.*, profundidade e permeabilidade dos aquíferos ou corpos de água (Valentine e White, 2012; Kurszlaukis e Fulop, 2013), o que acaba por se alinhar à essência fundamental das ideias de Wohletz (1983, 1986) e Wohletz e Sheridan (1983).

Para White e Valentine (2016), independente da ainda controversa relação entre hidrovulcanismo explosivo e parâmetros obscuros da interação MFC em diferentes ambientes geológicos, fenômenos hidrovulcânicos devem continuar a ser distinguidos primeira e principalmente pelas características faciológicas dos depósitos deles resultantes, uma vez que estas se encontram suficientemente bem estabelecidas na literatura.

Em síntese, algumas dessas características incluem a já mencionada predominância da granulação fina dos vitroclastos juvenis e dos depósitos em geral (depósitos de cinza), com clastos líticos associados mais grossos (dependendo da granulação e consolidação das encaixantes regionais) (Cas e Wright, 1987, White e Ross, 2011, Ross *et al*., 2011). *Surges* piroclásticos são típicos, e apresentam estruturas características produzidas por fluxos turbulentos, como dunas, *climbing ripples,* antidunas e ondulações em geral (Schminke, 1973; Sheridan e Wohletz, 1983; Sohn e Chough, 1989; Chough e Sohn, 1990; Sohn, 1996; Wohletz, 1998; Branney e Kokelaar, 2002; Vazquez e Ort, 2006; van Otterloo *et al*., 2013; Smith e Kokelaar, 2013; Jordan *et al*., 2013; Graettinger *et al*., 2013, 2015). São comuns também deformações penecontemporâneas devido ao transporte em sistemas saturados em vapor, bem como a formação de vários tipos de agregados de cinza, como *pellets* de cinza internamente maciços, *lapilli* acrescionário ou encouraçado (*armoured*) (Schumacher e Schminke, 1995; Ellis e Branney, 2010; Brown *et al*., 2010, 2012; Van Eaton e Wilson, 2013). Acredita-se que estes agregados de cinza sejam formados por atração eletroestática, aglutinação e solidificação em nuvens piroclásticas e CDPs, sendo especialmente comuns em erupções úmidas (Chough e Sohn, 1990; Brown *et al*., 2010, Van Eaton e Wilson, 2013; Smith e Kokelaar, 2013). Igualmente importante é a associação com quantidades expressivas de piroclastos

acessórios líticos ou cristalinos derivados das encaixantes (Ross *et al.*, 2005; White e Ross, 2011; Ross *et al.*, 2011; Ort *et al*., 2018).

A pesquisa experimental e petrológica sobre o hidrovulcanismo está diretamente relacionada ao entendimento dos fenômenos que produzem *MVD*s. Conforme mencionado anteriormente, em ambientes hidrovulcânicos típicos interpreta-se que tanto explosões hidrovulcânicas (além de magmáticas *stricto sensu*), como processos autoclásticos e interações passivas entre magma, sedimento e água sejam responsáveis pela geração de complexos arranjos estratigráficos de depósitos vulcanoclásticos, caracterizados por intercalações entre essas diversas litofácies e também diferentes morfologias de clastos juvenis (Ross *et al.* 2005; White e Houghton, 2006; McClintock e White, 2006, McClintock *et al*., 2008; White *et al*., 2009; Sohn e Yoon, 2010; Graettinger *et al*., 2013; Jordan *et al*., 2013; Watton *et al*., 2013; Houghton *et al*., 2015; Valentine *et al*., 2017; Amin e Valentine, 2017) (Figura 3.17).
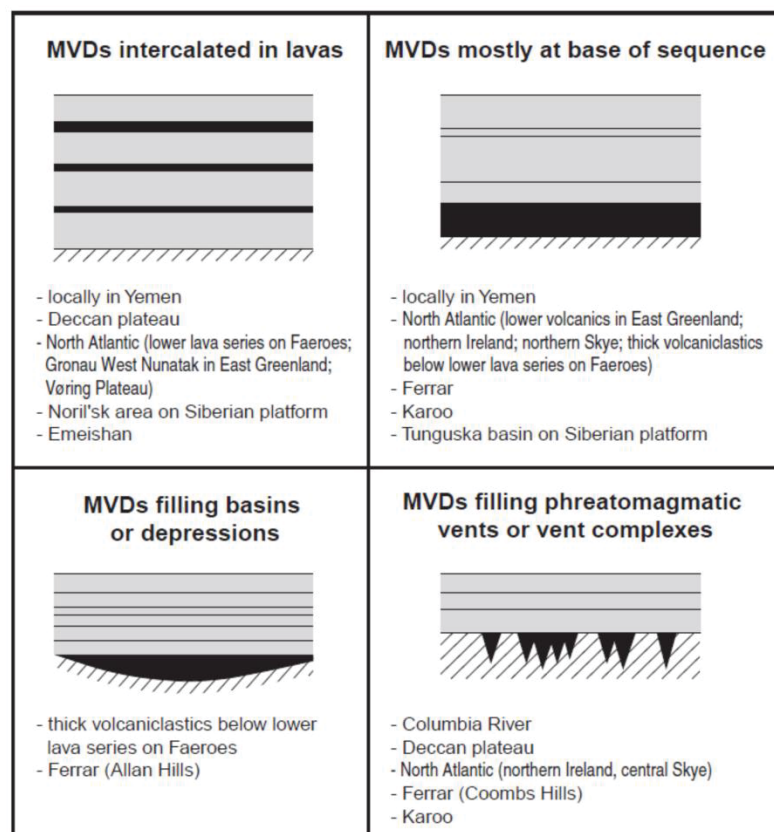
Figura 3.17 – Principais formas de ocorrência de *MVD*s nas diversas PCBs do mundo segundo Ross *et al*. (2005).

Destaca-se ainda a considerável semelhança entre certos aspectos faciológicos e composicionais de depósitos "freatomagmáticos" e de rochas formadas por outras

interações entre magma + sedimento ± água, uma vez que os processos hidrovulcânicos (em especial a *MFCI)* são possíveis e frequentes em essencialmente quaisquer ambientes úmidos, diferindo entre si muitas vezes apenas em intensidade e escala (Martin e Nemeth, 2007; Ross e White, 2012; van Otterloo, 2015; Zimanowski *et al*., 2015). É certo que isto dificulta atualmente a estimativa da real proporção entre as contribuições de diferentes processos vulcanoclásticos atuantes durante a construção da PIP. Por fim, reforça-se aqui que apenas a partir da integração minuciosa entre análises composicionais e faciológicas de camadas interderrames (conforme mencionado nos parágrafos anteriores) esta dificuldade poderá ser contornada.

4 CAPÍTULO IV – "Hydrovolcanic eruptions of the Paraná Igneous Province: insights from mafic volcaniclastic deposits at Sertanópolis, Paraná, Brazil"

Lucas Albanese Valore [a*], Otavio Augusto Boni Licht [a], Eleonora Maria Gouvea Vasconcellos [a]

[a] Universidade Federal do Paraná, Brazil

*Corresponding author: Postgraduate Program in Geology, Universidade Federal do Paraná.

E-mail address: lucasavalore@gmail.com
Phone number: +55 (41) 991961514

4.1 Abstract

In almost all continental flood basalt provinces (CFBPs), volcaniclastic deposits formed by explosive hydrovolcanism have been shown to be significant counterparts of better-known effusive facies, a notion that challenged traditional views of CFB stratigraphy. The only exception to this was the Paraná Igneous Province in South America, part of a larger province that also includes Etendeka in Southwest Africa and several volcanic occurrences in the South Atlantic Ocean. However, mapping campaigns conducted by the geological survey of the State of Paraná provided data for a different perspective, suggesting that many interflow deposits are not sedimentary in nature, but pyroclastic. In order to better characterize and understand this setting, we have studied interflow beds at Sertanópolis, a 250 km² region in northwest Paraná, conducting more detailed geological mapping and petrographic studies. In this area, four interflow units crop out at the transition between the Pitanga and Paranapanema formations, separated by 20-50 m thick effusive basalt intervals. Fine-grained interflow units include frequently vesiculated clastic rocks, which show diffuse stratification to dune-bedding structures, such as decimeter-scale cross laminated sets, wavy lamination and backset-stratification. They are formed mainly by fine quartz grains (20 - 70 %) and extremely fine ash or mud (10 – 30%), followed by hydrothermal mica (<5 – 40%), commonly hydrated (clay-mineral-rich) ash aggregates (<5 – 20%) and lesser amounts of glass and basalt fragments (<5 – 15 %). Additionally, at the eastern portion of the research area, a 4 x 2.5 km area with outcrops of scoriaceous basalt breccias was mapped. These are mostly matrix to clast-supported breccias with finely laminated matrix similar to the fine-grained units. These rocks are interpreted as accessory-rich mafic volcaniclastic beds. Deposits have features that suggest that multiple pyroclastic density currents (PDCs) formed each interflow unit, with minor exclusive fallout contribution in medial successions. Pyroclastic breccias represent proximal PDC and ballistic deposits that help outline a possible conduit, in which magmatic (or "magmatic-like") fragments are dominant as framework clasts. Stratified tuff-breccia strata in medial deposits represent progressive dilution of PDCs and multiple-PDC reworking of scoriaceous fragments. The local stratigraphy is consistent with repeated explosive hydrovolcanic eruptions in maar-like craters. Hydrovolcanic explosions were likely generated by magma-water interaction in confined permeable aquifers below the Sertanópolis units, probably

other clastic interflow units, which are frequent in the Pitanga Formation. This soft-to-mixed wall-rock favored lateral vent migration, leading to a wide and relatively shallow polycyclic crater, similar to hydromagmatic volcanoes in other CFBPs.

KEYWORDS: Flood basalts, physical volcanology, hydrovolcanism.

4.2 Introduction

Mafic volcaniclastic deposits (MVDs) of continental flood basalt provinces (CFBPs) have been the subject of several studies in the whole world (reviews in Ross *et al*., 2005; White *et al*., 2009). Of these, some of the best understood successions include part of the Palaeogene North Atlantic Igneous Province (Ukstins Peate *et al*., 2003; Larsen *et al*., 2003), the Permian – Triassic Siberian Trapps in Russia (Viswanathan and Chandrasekharam, 1981; Czamanske *et al*. 1998) and the Jurassic Karoo-Ferrar Province in Antartica and South Africa (Elliot and Hanson, 2001; White and McClintock, 2001; Ross and White, 2005, 2006; McClintock and White, 2006; McClintock *et al*., 2008). These works have shown that primary volcaniclastic rocks originated mostly by explosive hydromagmatic phenomena can be as volumetrically or stratigraphically important as lava flows in CFBPs, while also providing new links between MVDs, flood basalt volcanism and mass-extinction events (Thordarson and Self, 2003; Ross *et al*., 2005; McClintock and White, 2006)

Up until the review of Ross *et al*. (2005), hydromagmatic deposits in the Cretaceous Paraná Igneous Province (PIP) had been largely overlooked in the international scientific literature, in part because previous research at the province had been more focused on geochemical, petrogenetical and geochronological issues that still needed to be addressed (Mantovani *et al*., 1985; Fodor, 1987; Piccirillo *et al*., 1988; Peate *et al*., 1992). Since then, however, several authors have repeatedly identified mafic volcaniclastic deposits produced essentially by passive hydromagmatic and autoclastic processes (Waichel *et al*., 2006, 2007; Luchetti *et al.*, 2014; Machado *et al*., 2015; Rossetti *et al*., 2018; Moraes e Seer, 2018). Hydromagmatic pyroclastic rocks, which could represent the bulk of MVDs in other provinces (White and McClintock, 2001; Ross *et al*., 2005; White *et al*., 2009), remained only a theoretical implication of the newly discovered hydromagmatic settings in the PIP.

In the last decade, a vastly different situation has been evoked by Licht and Arioli (2011a, 2011b) and Licht *et al*. (2015a). Using data from regional geological mapping campaigns conducted by the late Paraná Geological Survey (formerly Mineropar, now part of the Institute for Land, Cartography and Geology - ITCG), these authors suggested that maar-diatreme volcanism could have played a role as significant in volcaniclastic deposition as in many other CFBPs. For many

researchers, however, this hypothesis remained a controverted issue, being widely disregarded in favor of more traditionalistic views.

In order to further address the full range of possibilities of hydromagmatic interaction in the PIP, we have studied a complex succession of mafic volcaniclastic interflows at Sertanópolis – PR, which was also first uncovered in 2015 during regional mapping campaigns (Valore and Licht, 2016). We have aimed to provide a detailed description of volcaniclastic facies, interflow stratigraphy and physical volcanology, while also discussing observed geological features in light of recently evolving models on continental flood basalts and related volcaniclastic deposition. Our results suggest that the Sertanópolis succession was originated by repeated explosive hydromagmatic eruptions, which likely occurred at a polycyclic maar-like crater complex, similar to those observed in the Karoo-Ferrar CFBP (White and McClintock, 2001; Ross and White, 2005, 2006; McClintock and White, 2006; McClintock *et al.*, 2008).

4.3 Methods

The Sertanópolis interflows outcrop at an escarpement in the rural area between the cities of Sertanópolis, Bela Vista do Paraíso and Primeiro de Maio, in the north of the state of Paraná, in Brazil. We have spent over twenty days in the field conducting geological mapping, with a major focus on the high slope area corresponding to the volcaniclastic interflows. Aerial photographs, satellite images and digital elevation models provided key knowledge on lateral continuity and distribution of interflow deposits, which was derived from interpretation of geomorphic features, following techniques described in Nadalin (2016). Mapped units were divided based on field lithostratigraphic relations. All mapped units can be defined as unconformity-bounded stratigraphic units (UBSUs) (Murphy and Salvador, 1999; Lucchi *et al.*, 2010)

Description of volcaniclastic rocks followed the scheme of White and Houghton (2006), with the division by McPhie *et al.* (1993) for primary volcaniclastic rocks and their resedimented and epiclastic counterparts. Volcaniclastic rocks were divided into lithofacies, following a scheme similar to Sohn (1996) and Branney and Kokelaar (2002). The terms "bed" and "laminae" are used as defined by Campbell (1967). For pyroclast classification, we adopted the scheme of Cas and Wright (1987), with the exclusion of cognate pyroclasts (Múrcia *et al.*, 2013). Detailed petrographic

characterization of about 35 thin sections was conducted with the aid of regular petrographic microscopes. Sorting and modal proportions were estimated visually in outcrops, hand samples and thin sections.

We have also analyzed thin sections, rock chips and hand-milled powder of interflow samples with a scanning electron microscope with coupled electron dispersive spectrometer (SEM-EDS, SEM model JEOL 6010LA, EDS model EX-94410T1L11) at the Laboratory of Mineral and Rock Analysis (LAMIR - UFPR) at Curitiba - PR. Furthermore, whole rock major and trace element geochemistry was used to test the correlation between volcaniclastic deposits and the transition between incompatible-rich high-TiO2 lavas and low-TiO2 lavas, classified as Type 4 and Type 1 (Licht, 2018), respectively. X-ray fluorescence (XRF) analyzes were carried out on fused beads and pressed pellets in the Axios Max (PANalytical, Rh X-ray tube) XRF spectrometer at LAMIR, with previous loss-on-ignition (LOI) at 1000ºC for two hours. We analysed ten samples collected from massive cores of lava flow-units.

4.4 Geological setting

4.4.1 Flood basalt volcanism at the PIP

The extensive volcanic and shallow-intrusive system that comprises the Paraná Igneous Province was originated during the Early Cretaceous, at about 135 – 131 Ma (Renne *et al*., 1992, Thiede and Vasconcelos, 2010; Baksi, 2018) during the continental rifting and breakup event that eventually ended the Pangea supercontinent and led to the formation of the South Atlantic ocean (Szatmari e Milani, 2016; Svensen *et al*., 2018; Foulger, 2018). The PIP extends throughout almost 1 million km² in most of southern Brazil, parts of Argentina, Paraguay and Uruguay, and it is correlated, in western Africa, with the smaller (~ 80,000 km²) Etendeka Igneous Province (Peate *et al*., 1992; Jerram *et al*., 1999; Frank *et al*., 2009, Foulger, 2018). The PIP lavas cover sediments of the Phanerozoic intracratonic Paraná Basin, while shallow-intrusive rocks are extensively present as sills and dyke swarms that cut through the basin and the nearing Precambrian basement (Milani *et al*., 2007; Florisbal *et al*. 2014; Almeida *et al*., 2018, 2019).

The most recent advances in physical volcanology of the PIP lavas (Serra Geral Group, in the stratigraphic lexicon – Rossetti *et al*., 2018) led to the characterization

of a stratigraphic framework similar to other CFBPs, which includes basal compound flow-fields that eventually transition to simple tabular flood basalt facies produced by high effusion rates and overwhelming magmatic activity (Single and Jerram, 2004; Jerram and Widdowson, 2005). Compound flow-fields at the base of the PIP succession have been addressed in the works of Lima *et al*. (2012), Barreto *et al*. (2014), Rossetti *et al*. (2014, 2018) and Machado *et al*. (2015). These authors describe complex braided successions of P-type lobes (*sensu* Walker, 1987; Wilmoth and Walker, 1993) in varied morphologies, including typical sheet lobes, lava toes and lava fingers, produced by less pronounced inflation and low and intermittent effusion rates (Barreto *et al*., 2014; Rossetti *et al*., 2014). Vesicular S-type lobes (Walker, 1989; Wilmoth e Walker, 1993) have also been described by Waichel *et al*. (2006), Lima *et al*. (2012), Barreto *et al*. (2014) and Rossetti *et al*. (2018) in the southern PIP. Compound flow-fields also include thicker (3 – 15 m) inflated sheet lobes with features such as inflation clefts, vesicle horizons, pipe vesicles and vesicle cylinders, formed by lobe coalescence and higher, more continuous effusion rates (Barreto *et al*., 2014; Rossetti *et al*., 2014, 2018). In the southern PIP these flow-units have been shown to become more frequent and thick higher up in stratigraphy (Jerram *et al*. 1999; Lima *et al*., 2012; Rossetti *et al*., 2018), providing their link with more typical flood basalt volcanism. Additionally, in terms of surface morphologies, lavas in these basal successions are classified mostly as typical pahoehoe and slabby pahoehoe, characteristic of low effusion and strain rates (Waichel *et al*., 2006; Barreto *et al*., 2014; Rossetti *et al*., 2014, 2018; Machado *et al*., 2015).

The compound and "transitional" (in the sense of Single and Jerram, 2004) flow-fields that comprise the lower part of the PIP lava successions grade into thicker tabular sheet floods, which have been in many cases termed simple flows (Walker, 1971; Self *et al*. 1998; Jerram and Widdowson, 2005). These laterally extensive and thick sheets are the most remarkable features of the "step-like" stratigraphy of CFBPs (Jerram and Widdowson, 2005). In the southern PIP, described simple flows are associated with rubbly pahoehoe morphologies (Barreto *et al*., 2014; Rossetti *et al*., 2014, 2018), which correspond to tabular flows with cohesive bases and brecciated upper crusts (*sensu* Keszthelyi *et al*., 2001) that have most likely been produced by high effusion, strain and flow rates (Bondre *et al*., 2004; Duraiswami *et al*., 2008; Marshall *et al*., 2016). These were used to define the Vale do Sol Formation in the

state of Rio Grande do Sul (Rossetti *et al*., 2018), although the formation extends as far north as the state of Paraná (Licht and Arioli, 2018).

Recognition of the volcanic systems that produced these tabular sheet floods can be a difficult task, but initial results indicate that certain morphologies, such as breakouts and lava tubes, can be used to trace three-dimensional facies variations in simple flows in a way similar to what is done in compound flow-fields (Thordarson and Self, 1998; Waichel *et al*., 2006; Óskarsson and Riishuus, 2014), which in turn can help establish a sequence stratigraphy framework of CFBPs (Nemeth and Palmer, 2019). In the PIP, efforts in this area are being aided by detailed chemostratigraphy as well (Hartmann *et al*., 2013, Fernandes *et al*., 2018).

4.4.2 Sedimentary and volcaniclastic interflow deposits

Studies that mention interflow deposits in the PIP are known since the beginning of the twentieth century, according to the reviews of Licht (2014) and Cañon-Tapía (2018). Most of these contributions are regional characterizations, which briefly report pyroclastic and sedimentary interbeds located in various regions of the volcanic province (White, 1908; Oliveira, 1916; Washburne, 1930). In the last decades, sedimentary and volcaniclastic interflows have started to regain some attention of researchers working with lava flow stratigraphy (Jerram *et al*., 1999; Waichel *et al*., 2006, Lima *et al*., 2012), and have been recently the subject of more detailed studies (Licht and Ariolli, 2011a, 2011b, Lucchetti *et al*. 2014; Licht *et al*., 2015a; Moraes e Seer, 2018). Most initial studies focused on the interaction between lava flows and aeolian dunes of the Botucatu paleoerg, which were gradually engulfed by the increasingly active lava flow-fields of the Paraná and Etendeka subprovinces (Jerram *et al*., 2000; Scherer, 2002; Jerram e Stollhofen, 2002; Petry *et al*., 2007). It was in this context that authors such as Jerram and Stollhofen (2002) and Petry *et al*. (2007) reported the occurrence of peperite-like rocks derived from the dry interaction of flows and sand dunes in a persisting arid setting, which was widely referenced in order to explain the absence of hydromagmatic deposits in the PIP (Ross *et al*., 2005).

After this, several authors have followed in recognizing peperites throughout the PIP, this time associating them with the interaction between lava flows and wet siltstones, likely deposited in fluvio-lacustrine environments (Waichel *et al*., 2006, 2007; Luccheti *et al*., 2014; Machado *et al*., 2015; Rossetti *et al*., 2018; Moraes and

Seer, 2018). Likewise, exceptional high humidity environments led to some sustained lacustrine sedimentation, which in turn allowed for the local effusion of pillow lavas and deposition of hyaloclastite breccias at the start of the PIP volcanism, in the northern part of the province (Moraes and Seer, 2018).

Traditionally, the Paraná Igneous Province has been regarded as an exception in terms of explosive hydromagmatic deposits (Ross *et al.*, 2005; Waichel *et al.*, 2007). However, Licht and Ariolli (2011a, 2011b) and Licht (2012) have suggested that explosive eruptions originated many mafic tuffs, lapilli-tuffs, tuff-breccias and breccias that the authors have described in the state of Paraná – a hypothesis that actually follows some ideas discussed in the classic paper of Azambuja (1943). It is worth mentioning that in hydromagmatic environments that favor the formation of peperites and hyaloclastites, these same facies can in fact be much less volumetrically important than pyroclastic deposits (Ross *et al.*, 2005). Proportionatelly, this means that the extensive occurrence of passive hydromagmatic rocks could imply that mafic pyroclastic rocks are as frequent in the PIP as in many other CFBPs.

4.5 Stratigraphic framework of Sertanópolis

The studied area encompasses a region close to the transition between high TiO_2 (dominantly Type 4) basalts and low TiO_2 Type 1 (Center-Northern) basalts, according to the chemostratigraphy defined by Licht (2018). However, all analyzed samples were classified as Type 1 (CN) tholeiitic basalts, with the exception of one basaltic andesite (Sup. Table 4.3, Sup. Figure 4.19). This region is marked by the transitional contact between the Pitanga and Paranapanema Formations, as defined in the most recent lithostratigraphic division of the PIP and the Serra Geral Group in Paraná (Licht and Arioli, 2018). In this work, we have identified five diferent units of basalts from both formations, which correspond to two different typical compound flow-fields of the Pitanga Fm. (B1 and B2, Figure 4.1) and three units of tabular flows of the Paranapanema Fm. (B3 to B5). Each of these is accompanied by respective interflow units (I1 to I4), with the exception of B5, which is covered by a sandy-muddy soil on altitudes above 600 m. which might be related to weathering of sedimentary rocks of the overlying Santo Anastácio Formation of the Bauru Basin (Fernandes *et al.* 2015).

Attitudes of tabular flow-units and interflow beds indicate a small (<5º) regional dip to W-SW, although many variations are noticed locally, which could be due to paleotopographic controls on deposition as well as offsets caused by ancient and modern tectonic events (see Section 4.8.3).

Licht & Arioli (2018)			Licht (2018)	This study		
Group	Sub Group	Formation	Geochemical type (main)	Mapping Units	Facies	Sections
Serra Geral	Centern-Northern Serra Geral	Paranapanema	Type 1 (CN)	I4	Tds, LTds, TBs, Bmig, Tlg, Tw	FO, NS, EG, AH
				I3	LTds, Tds, TBs, Tw, LTw, Tp, RTm, LTm, Ss, Bmig,	AM, SI, FO, NS, LG, EG, AH
		Pitanga	Type 4	I2	Western: Tw, LTw, TBs, Bmig, RTm, Ss, Tds, Tp	NS, VV, LG
					Eastern: TBlg, Blg, TBmds, Bmc, Tw, Tlg, LTm, Bmig	AM, SI, CP, CM
				I1	LTds, LTm, Tm, Tds, Tp	RB

Table 4.1 – Summarized characteristics of interflow units, lithostratigraphic and geochemical classification according to Licht and Arioli (2018) and Licht (2018), respectively. Lithofacies code: B – breccia; TB – tuff-breccia; LT – lapilli-tuff; T- tuff; RT - resedimented tuff; S – sandstone; s – stratified; ds – diffusely stratified; p – plane-parallel lamination; w – wavy and cross-lamination; m – massive; c – convoluted; lg – gradational lamination; ig – inversely gradational; t – gradational contact from flow-top. Sections: AH – Água Horizonte; EG – Estância Grevílea; LG – Lourdes Gaspar; VV – Vai-e-Vem; NS – Nossa Senhora Aparecida; FO – Água da Fortuna; RB – Ribeirão do Biguá; CM – Córrego do Macuco; FU – Água da Furna; SI – Santa Isabel; AM – Água da Morena.
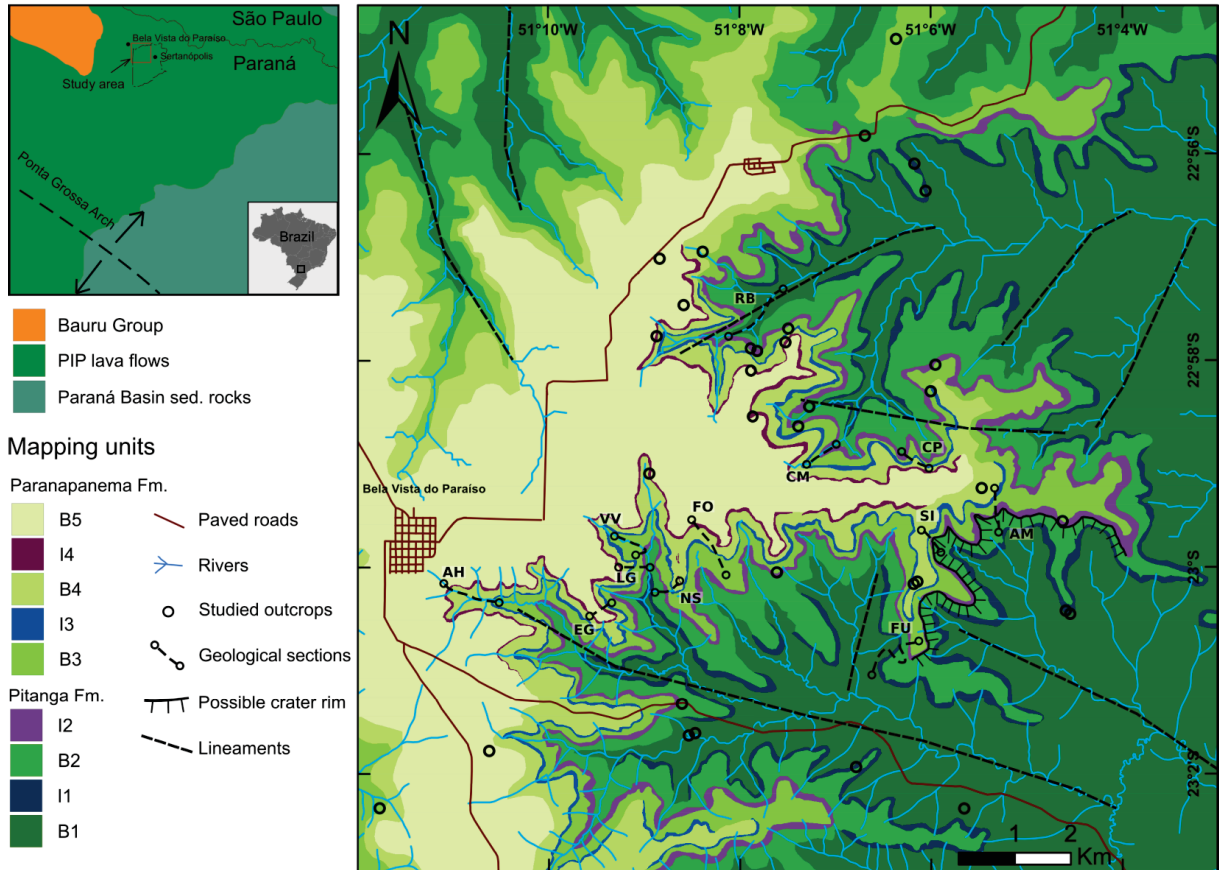
Figure 4.1 – Geological map of the research area. Sections: AH – Água Horizonte; EG – Estância Grevílea; LG – Lourdes Gaspar; VV – Vai-e-Vem; NS – Nossa Senhora Aparecida; FO – Água da Fortuna; RB – Ribeirão do Biguá; CM – Córrego do Macuco; FU – Água da Furna; SI – Santa Isabel; AM – Água da Morena. "Possible crater rim" refers to it's modern day expression.

4.5.1 Overview of interflow facies

In light of the ongoing "controversy" regarding the presence of pyroclastic rocks in the PIP, and because many of our interpretations can be considered novel, lithofacies and their associations will be first described in their lithostratigraphic context (content of units I1 - I4) in the following items, as to initially present our results as objectively as possible and also highlight the interplay between interflows and effusive units. Lithofacies associations will be further referred to in the 4.7.2 item, where they will be interpreted in terms of genesis and stratigraphic significance.

In Sertanópolis, volcaniclastic and sedimentary facies include tuffs/lapilli-tuffs, tuff-breccias, breccias, resedimented volcaniclastic and reworked volcanogenic rocks. General facies characteristics and interpretations are summarized in Table 4.2.

Facies	Textures and structures	Interpretation
TBlg, Blg	Matrix-supported tuff-breccia to breccia in metric successions. Plane-parallel to undulated finely laminated (mm-cm) matrix hosts massive basalt blocks and scoriaceous fragments. Matrix defined by repeated rhythmic alternations of ash and mud. Matrix is similar in composition to the Tlg facies, and is typically vesicular or amygdaloidal. Undulated matrix sometimes shows drapes or mantle-contours over blocks.	Ballistic curtain and fallout (surge modified?) deposit in a near-vent environment. Well developed rhythmic laminae could be due to some degree of subaqueous suspension settling. Concomitant wall rock collapse and gravitational reciclying of clasts could also generate coarse framework.
Bmt	Clast-supported and massive basaltic breccia. Fluidal to angular close-packed framework, usually with <10% matrix. Correlation with fragmented upper flow crusts.	Flow top autoclastic breccia, formed by chilling of juvenile fragments in contact with air. Matrix is both volcanogenic mud produced in situ and clastic material of posterior infill.
Bmig	Inversely graded tuff-breccia to breccia in decimeter thick beds. Oxidized and chilled (quenched) framework in gradational contact with the base of a lava flow. Common pseudonodular texture. Clasts are fluidal to blocky. Matrix commonly includes fluidized extremely fine ash or mud-grade material as "envelopes" surrounding clasts and as veins or irregular, globular injections.	"Close-packed" peperite formed by the passive interaction of a lava flow and wet clastic material. Common extremely fine juvenile ash includes glass fragments and hydrothermal mud.
TBmds, Bmds	Matrix-supported to clast-supported tuff-breccia/breccia in decimetric beds. Massive to diffusely stratified tuff matrix. Frequent ash aggregates (massive or layered), particle clusters and zeolite amygdales in the matrix.	Deposition from proximal wet and relatively concentrated PDC. Lateral transport from proximal plume collapse and fallback (Branney and Kokelaar, 2002; Vazquez and Ort, 2006, Graettinger and Valentine, 2017).
Bmc	Matrix-supported to clast-supported breccia in decametric beds with apparently massive to convoluted matrix, similar to TBmds or TBlg in composition.	Penecontemporaneous fluidization and soft-sediment deformation of TBlg and TBmds due to slumps and hot-fluid–related elutriation.

TBs	Decimetric tuff-breccia horizons interbedded with tuff facies (usually Tw). Isolated outsized blocks of fluidal to angular vesicular basalt blocks hosted by stratified tuff. Some blocks have ragged and irregular shapes and many are rectangular, elongated according to bedding planes. Matrix stratification typically drapes or contours blocks.	Scoria blocks can be medial ballistics, as well as lithics initially transported inside relatively concentrated zones of stratified PDCs (e.g "traction carpets") which were resedimented by the dilute turbulent part of the same surge or by pulsating/multiple PDCs (Sohn, 1997; Vazquez and Ort, 2006; Smith and Kokelaar, 2013).
Tm LTm	Moderately poorly sorted, massive to very crudely bedded tuff to lapilli-tuff that may contain particle clusters. Common matrix-supported coarse ash to lapilli basalt lithics or juvenile clasts, either as crudely defined laminae or dispersed randomly. Usually non vesiculated.	Very rapid sedimentation from collapsing eruption column transitioning to lateral PDC (Branney and Kokelaar, 2002; Vasquez and Ort, 2006).
Tds, LTds	Diffusely stratified (subhorizontal bedding) tuff to lapilli-tuff with frequent massive supported particle clusters (elongated black spikes) and spherical ash aggregates. Vesicles are also common, but not conspicuous.	Deposited by energic, relatively wet, concentrated and cohesive surges in proximal to medial settings (Sohn and Chough, 1989; Sohn, 1996; Vazquez and Ort, 2006; Lube et al., 2014). Particle clusters can be rapidly deposited by drifting plumes, while massive or layered ash aggregates reflect longer residence and reworking in wet plumes and PDCs (Brown et al., 2010, 2012; Van Eaton and Wilson, 2013).
Tw, LTw	Moderately sorted tuff to lapilli-tuff. Decimeter scale cross-laminated sets and ripple-like wavy bedforms (dune-bedding). Frequent matrix-supported mud and ash aggregates (massive or layered) and some juvenile glass shards. Commonly vesiculated.	Deposited by relatively dry traction dominated dilute surge, with sandwave bedforms (Sohn and Chough, 1989; Sohn, 1996; Graettinger and Valentine, 2017). Aggregates deposited from cosurge ash clouds or simultaneous wet plumes in medial settings (Brown et al., 2010, 2012; Van Eaton and Wilson, 2013).

	Description	Interpretation
Tp	Moderately sorted tuff with defined plane-parallel or undulated lamination, with matrix-supported massive ash pellets and particle clusters. Frequently vesiculated.	Deposition by moderately dry and dilute surge in medial to distal settings (Sheridan and Wohletz, 1983, Sohn and Chough, 1989; Sohn, 1996; Vazques and Ort, 2006; Lube *et al.*, 2014), with input from cosurge fallout from a wet plume or ash cloud.
Tlg	Well sorted, mantle bedded and finely laminated "rhythmite"-like tuff, with normal gradational laminae defined by ash-mud couplets. Vesicles and gas escape structures are conspicuous. Ash pellets are absent.	Pyroclastic fallout from relatively medial to distal plumes. Subaqueous deposition or slurry of water-saturated aggregates could help form rhythmite-like fabric.
RTm	Moderately poorly sorted tuff with matrix-supported basalt lapilli, either disperse or in roughly defined laminae. Massive or crudely stratified, non vesiculated and aggregate-less. Occurs isolated as singled-out beds or as lenses that grade into Ss facies.	Syn to post-eruptively resedimented tuff, deposited by concentrated, mud-rich subaqueous flows.
Ss	Stratified and moderately well sorted volcanogenic sandstone. Framework of rounded siliciclastic and volcanogenic material, with lesser amounts of mixed mud than RT. Sometimes includes rounded and altered basalt granules. Frequently shows laminae-scale variations in maturity.	Deposited by post to inter-eruptive shallow subaqueous tractive currents. Sorting variations could be due ephemerous concentrated density flows during transport, interspersed with regular streamflow.

Table 4.2 – Summarized lithofacies descriptions and sedimentological interpretations. Nomenclature as follows: B – breccia; TB – tuff-breccia; LT – lapilli-tuff; T- tuff; RT - resedimented tuff; S – sandstone; s – stratified; ds – diffusely stratified; p – plane-parallel lamination; w – wavy and cross-lamination; m – massive; c – convoluted; lg – gradational lamination; ig – inversely gradational; t – gradational contact from flow-top.

4.5.2 Pitanga Formation

4.5.2.1 Pitanga Formation basalts – B1, B2

The observed flow units of both B1 and B2 include P-type lobes (<1 – 3 m thick) and inflated tabular *pahoehoe* lobes (5-10 m), recognizable at outcrop scale and of difficult lateral correlation. This allows their definition as characteristic compound lava flow-fields (*sensu* Self *et al*., 1997, 1998; Thordarsson and Self, 1998; Jerram and Widdowson, 2005) with some degree of effusion of thicker sheet lobes (especially at the base of B1, Figure 4.2E), similarly to what's observed in other flood basalt compound flow-fields (Thordarson and Self, 1998; Single and Jerram, 2004; Óskarsson and Riishuus, 2013), the southern PIP (Rossetti *et al*., 2014, 2018) and inflated lobes in compound flows in general (Self *et al*., 1998; Hole *et al*., 2013; Perdersen *et al*., 2017).

However, on the top of both B1 and B2, 5 to 15 m thick sequences of interspersed S-type vesicular thin lobes (0.2 to 1 m thick each) are very contrasting breaks from the inflated P-type lobes below (AM, VV, CP, CM, SI sections). These S-type lobes are characterized by decimeter-thick glassy crusts and greenish to reddish (when altered) highly vesicular cores (Figure 4.2D). These sequences are thicker in the southern and southeastern regions of the research area, and tend to be not as well exposed or present in the north.

Above S-type lobes sequences and inflated sheet flows, up to 2 meter thick autoclastic breccias occur locally (figures 4.2A, 4.2C, 4.3). They are characterized by an altered vesicular and amygdaloidal block framework with common jigsaw-fit arrangement of both large (sometimes meter-sized) and also smaller centimeter-sized angular fragments. This indicates somewhat brittle fragmentation and flow top fracturing, although fluidal blocks with characteristic clast face-aligned vesicles are also present, indicating chilling and ductile fragmentation of juvenile lava (Figure 4.2C).

Matrix is sometimes as scarce as 10% of the whole breccia bed. It is commonly composed of altered basalt mud and frequently includes some infill of material from overlying interflow sequences (Figure 4.2C). Breccias rich in <10 cm blocks and coarse lapilli are also locally important (RB section), and could be suggestive of more

efficient and prolonged brecciation during flow emplacement. These are also richer in epigenetic and infilled matrix, likely due to an increased original porosity.
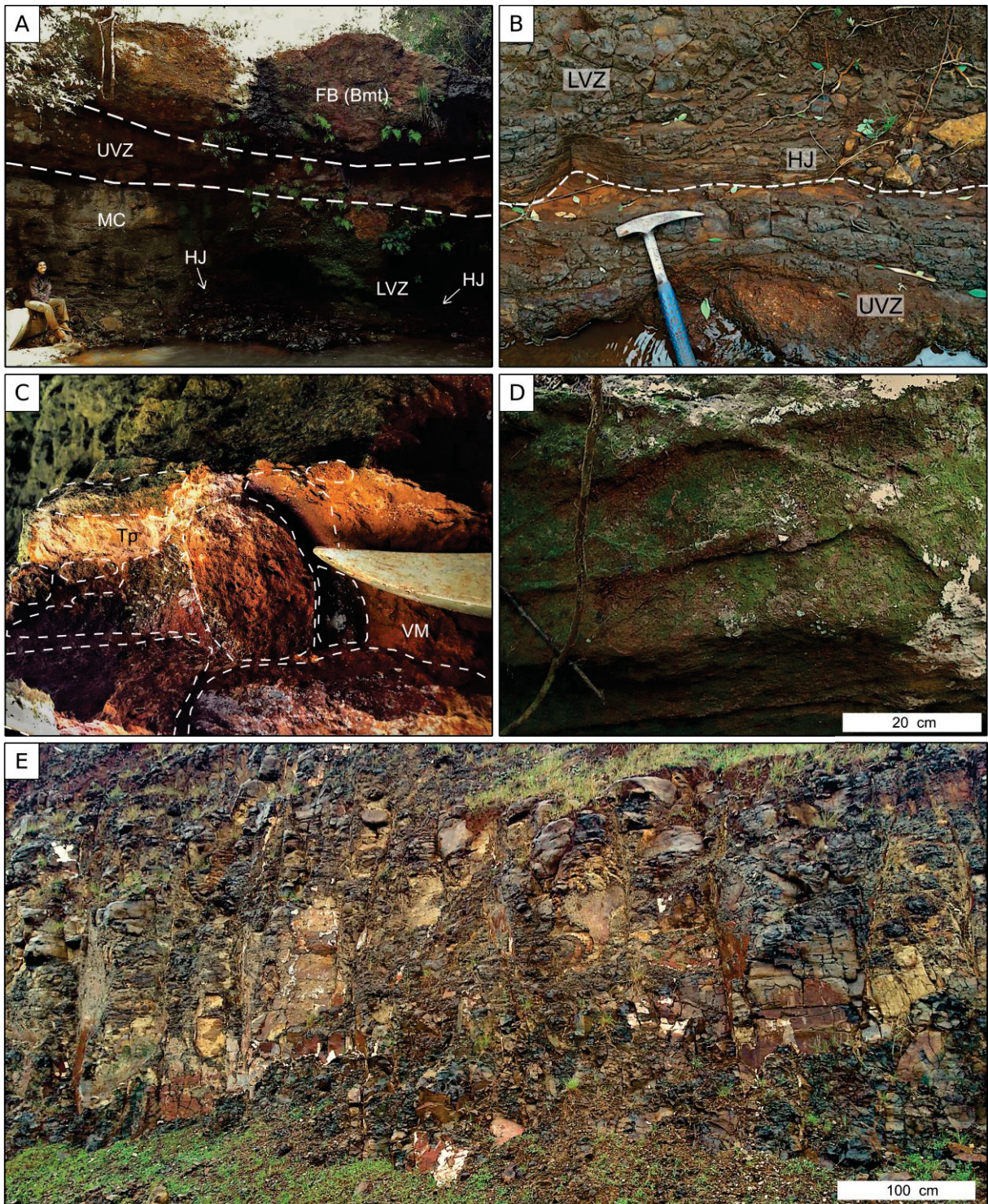
Figure 4.2 – Features of basalt units from Pitanga Formation: A) Outcrop of the RB section, which includes a 5 meter thick inflated sheet flow with a 2 meter thick autoclastic breccia above (B1). LVZ – lower vesicular zone, MC – massive core, UVZ – upper vesicular zone, FB – flow-top breccia, HJ – horizontal jointing; B) Contact between inflated P-lobes of B1 unit; C) Detail of autoclastic breccia, with framework of blocks with very fine vesicles in close-packed fabrics, matrix comprised by reddish and altered volcanogenic mud (VM) and locally tuff infill from I1 unit (Tp facies); D) S-type lobes at the top of the B2 sucession; E) Thick sheet flow in B1 with poorly developed jointing.

Above the autoclastic rubbly *pahoehoe* breccias of B1 and B2, two interflow units of local significance (I1 and I2) and lateral continuity of >15 km are exposed (Figure 4.1) These interflow units will be described in detail in the next sections.

Lower eastern section
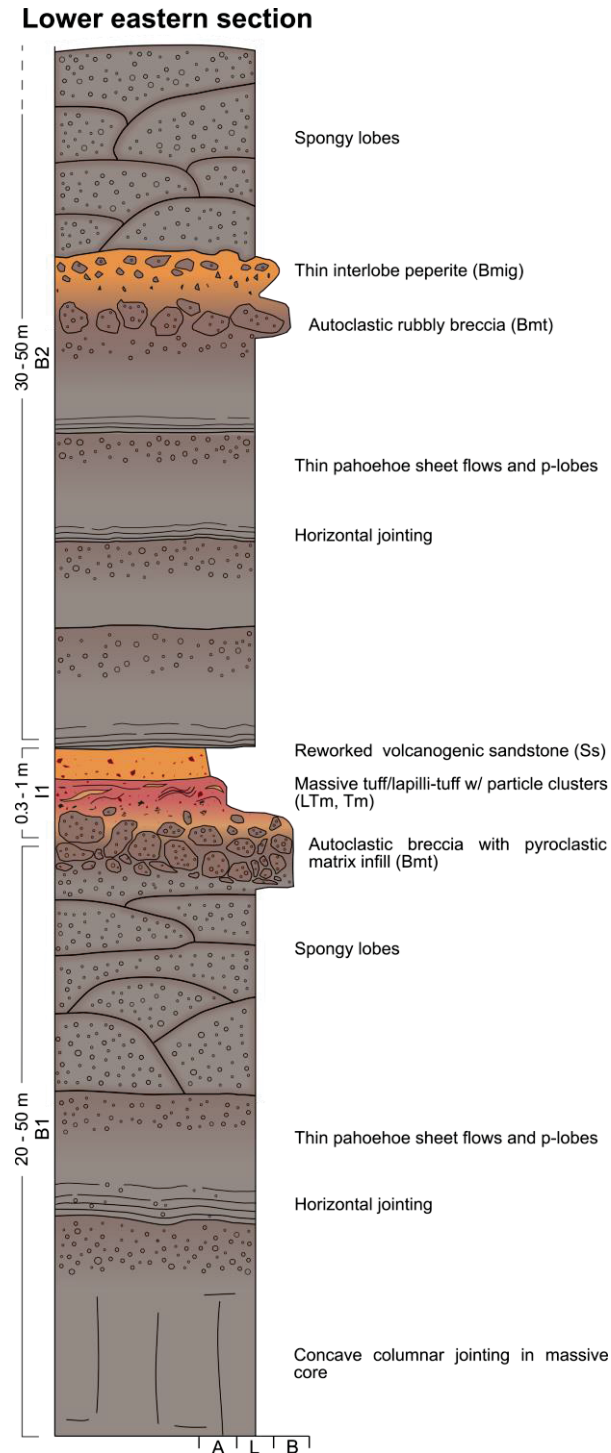
Figure 4.3 – Composite section of B1, I1 and B2 in the eastern (proximal) region of the research area. Legend is the same as 4.8.

Petrographically, flow-unit cores are holocrystalline, aphyric to subaphyric and intergranular (locally subophitic), with 30-45% plagioclase, 20-35% augite, 7-10%

opaque minerals (oxides) and up to 5% exsolution-derived orthopyroxene. Additionally, minor amounts (5-20%) of secondary minerals in diktytaxitic spaces such as chlorite, zeolite and celadonite also occur in massive cores of sheet flows. Clay minerals such as chlorite have been derived from alteration of residual glass, and some of these spaces exhibit few albite spherulites.

4.5.2.2 Pitanga interflow units - I1

The I1 unit includes tuffs and reworked volcaniclastics that are also present as matrix infill in underlying autoclastic breccias of B1 – sometimes exclusively as that (RB section). When exposed as a singled-out bed, I1 is 30 – 100 cm thick and has a moderately undulating and lensoid geometry, outcropping at an altitude range of 430-460 m, which is likely the reason why it's exposure is, to a degree, discontinuous. It is unclear whether this is a depositional feature or if it's due to erosion of the bed before the onset of the B2 volcanic episode.

This is the second least exposed interflow of the region. It is was better followed in the north, but was also correlated to a major topographic break in the south – a feature that is frequently thought to be produced by differential weathering of basalts and much more resistant silicified interflow beds in the PIP (Licht and Arioli, 2018).

The I1 interflow bed is mostly comprised by fine-grained and reddish hardened tuffs of the LTm, Tm and Tds facies. Compositionally, they are formed by almost 35-40% of fine to extremely fine ash-sized angular quartz fragments and ca. 45% red mud-grade ash matrix. This matrix is essentially an oxidized mud that in some thin sections forms poorly defined and convoluted laminae.

In these accessory-crystal-rich tuffs, however, hypohyaline basalt lithic and vitric ash is also present as much as almost 10% of some thin sections. Vitric fragments are usually <100 µm and have blocky and equidimensional shapes. They are formed by translucid sideromelane as well as opaque and oxidized tachylite of basaltic composition (Figure 4.5A). Sideromelane and tachylite are also found in the glassy mesosthasis of lithic basalt fragments (<5%) that are slightly coarser (medium ash) and more irregular. Lithic and vitric fragments show perlitic cracks and oxide microlites. Some glassy fragments have been altered to clay minerals, and fine aligned brown mica flakes (as much as 30% of some thin sections, Tp facies in RB section) are also noted. On at least one location, the I1 bed also includes an even

finer tuff composed majorly of accessory mud-grade ash that exhibits what seem to be many medium ash-sized black "spikes" or irregular and elongated aggregates of oxides/hydroxides. These are similar to particle clusters or massive ash pellets (*sensu* Van Eaton and Wilson, 2013), which are also found in the other interflow units, but are much more altered in I1.

Even though this unit is compositionally similar to siliciclastic detritus, detailed stratigraphic analysis at Sertanópolis has shown this to not be the case. The I1 bed shares many compositional and textural similarities with tuffs in I2, I3 and I4, which are more readily defined as such, and was hence interpreted as a pyroclastic deposit rich in accessory (wall-rock derived) material.

4.5.2.3 Pitanga interflow units – western I2 tuffs

Outcrops of the I2 tuffs are 50 – 200 cm thick, being mostly complete, B2 flow-top – I2 interflow – B3 flow-base sections (VV, NS, LG), typically found in altitude ranges of 490 to 520 m. When thin, these tuff beds are homogeneous and composed of a single facies (typically Tw), but the thickest show more significant vertical variations. The most common occurences are of "dune-bedded", cross-laminated and sandwave bedforms, in which low amplitude ripples and wavy structures are usually decimeter-wide features (figures 4.4A, 4.4C and 4.4D, facies Tw). Wavy structures are also commonly concave, including up to 10 cm thick dunes with preserved stoss-side and lee-side laminations, which were interpreted as antidunes (Schminke *et al*., 1973, Fisher and Schminke, 1984; Valentine, 1987; Slootman and Cartigny, 2019). Due to the inherent difficulty of differing them in the field due to poor exposures, they were all included in the Tw facies, which makes up the bulk of I2. Variations in the succession include rare vertical associations with diffusely stratified centimetric beds or lateral changes into outcrops that show only diffusely stratified (Tds) or plane-parallel to undulated bedforms (Tp).

Massive or diffusely stratified deposits are interpreted as primary features, but many beds are only apparently massive, and structures can be highlighted or obscured by weathering and silicification. Broken fresh rock surfaces of the Tw and Tp facies are commonly apparently massive, while exposed and weathered surfaces show clear stratification. Lastly, contacts between individual beds and facies are gradational; no erosional scours or unconformities were observed.
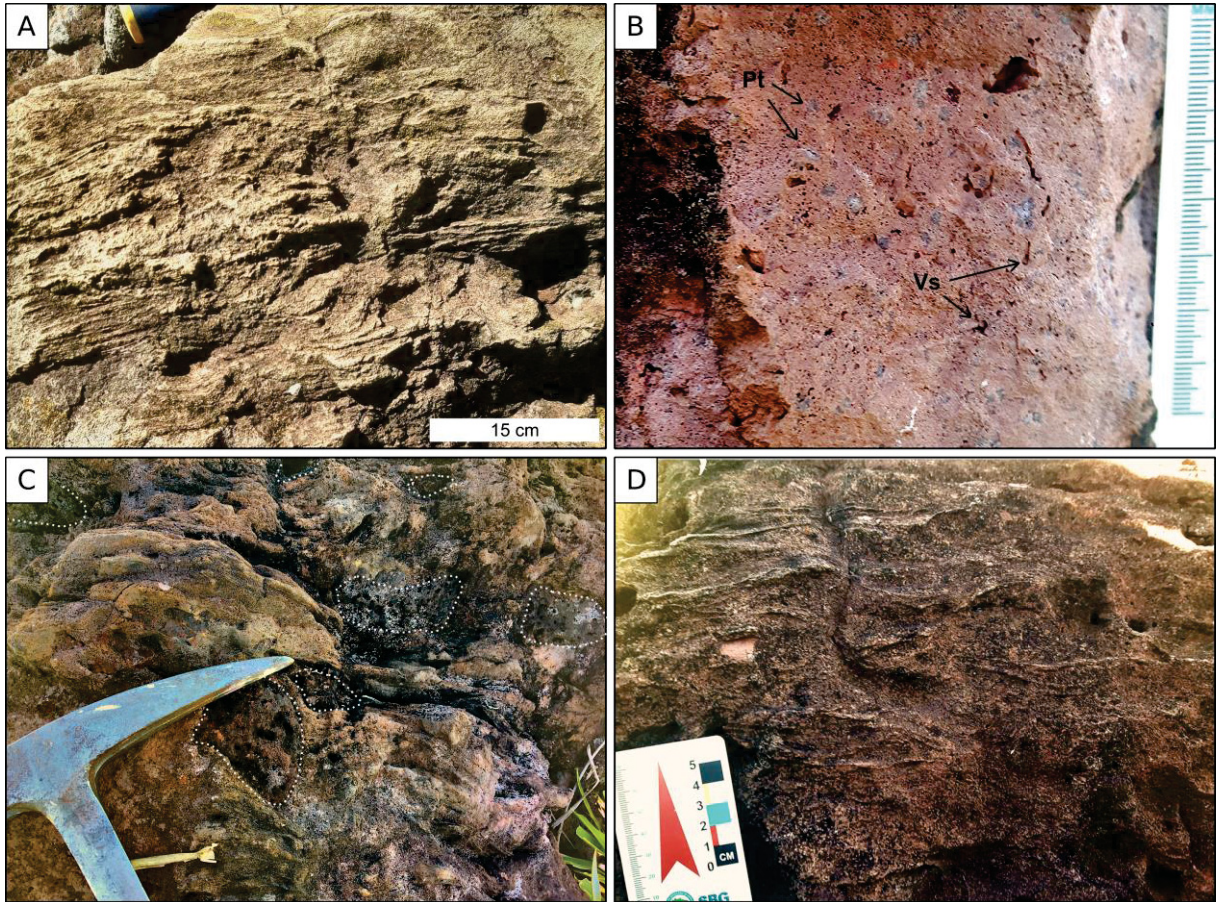
Figure 4.4 – Outcrops of interflow tuffs from Pitanga Formation: A) Low-amplitude (2-3 cm), long wavelength (10-30 cm) wavy and cross-laminated sets of the Tw facies in the I2 unit, NS section; B) Detail of light purple ash pellets (Pt) and vesicles (Vs) in bed of Tw facies, I2 in NS section; C) wavy lamination of Tw facies, holes are eroded basalt clasts, which locally form horizons of TBs facies, I2 in NS section; D) Moderate-amplitude (5-8 cm) and wavelength (10-20 cm) antidunes of the Tw facies, I2 in NS section.

Overall, all occurences of I2 share similar compositions. They are majorly formed by fine ash-sized angular quartz grains (20-50%) and brown mud (5-40%), which are organized in moderately to moderately poorly sorted and mixed fabrics. Some mud size material is concentrated in moderately defined depositional laminae and as diagenetic features. Other crystalloclasts (5-15%) typically include augite, plagioclase, feldspar, biotite, white micas, zircon and opaque minerals. Angular and subrounded crystalloclasts are randomly dispersed, being frequently mixed together.

Mud-grade or extremely fine ash material is also present in mostly massive pellets and aggregates, although some layered ones (similar to aggregates in eastern I2 coarse-grained facies) are also found in tuffs close to the CM section (for detailed description, see Item 4.6.3 and figures 4.15, 4.16). Tw, Tds and Tp facies in I2 show varying proportions (<5 – 20%) of matrix-supported light purple massive ash pellets (Figure 4.4B). Pellet proportions vary vertically, commonly in normally grading

decimeter-thick horizons. There are also common intercalations of pellet-rich and pellet-less laminae in these tuff beds.

In these facies, <1 - 3 mm vesicles are common (Figure 4.4B). These vesicles are sometimes elongated or flattened, with longer axis parallel to stratification, which in turn suggests depositional control on their genesis. Ash pellets and vesicles are always absent in the upper 20 to 30 centimeters of I2.

In NS and VV sections, tuff beds host isolated scoriaceous basalt blocks and coarse lapilli (1 – >10 cm), sometimes in locally relevant proportions (>30%), which characterize them as poorly sorted and stratified tuff-breccia horizons (TBs). Coarse basalt clasts in them are sometimes only partially preserved as deeply eroded holes formed by differential weathering (Figure 4.4C). Overall, I2 tuffs beds also host <1-15% medium ash to fine lapilli fragments of mostly tachylitic hypohyaline basalt, which are internally poorly vesicular but have cuspate and vesicular rims. These are commonly matrix-supported and isolated, homogeneously distributed throughout the succession. In some outcrops, however, there is a marked increase in ash to lapilli size cuspate basalt clasts towards the unit's top (Figure 4.9). I2 beds also show dense extremely fine to medium ash-sized glass shards that are mostly equidimensional and angular, composed of either red sideromelane with oxide microlites or opaque tachylite (Figure 4.5B) in proportions of 5-10%. Some of these finer glassy fragments are platy, cuspate or have subrounded contours.
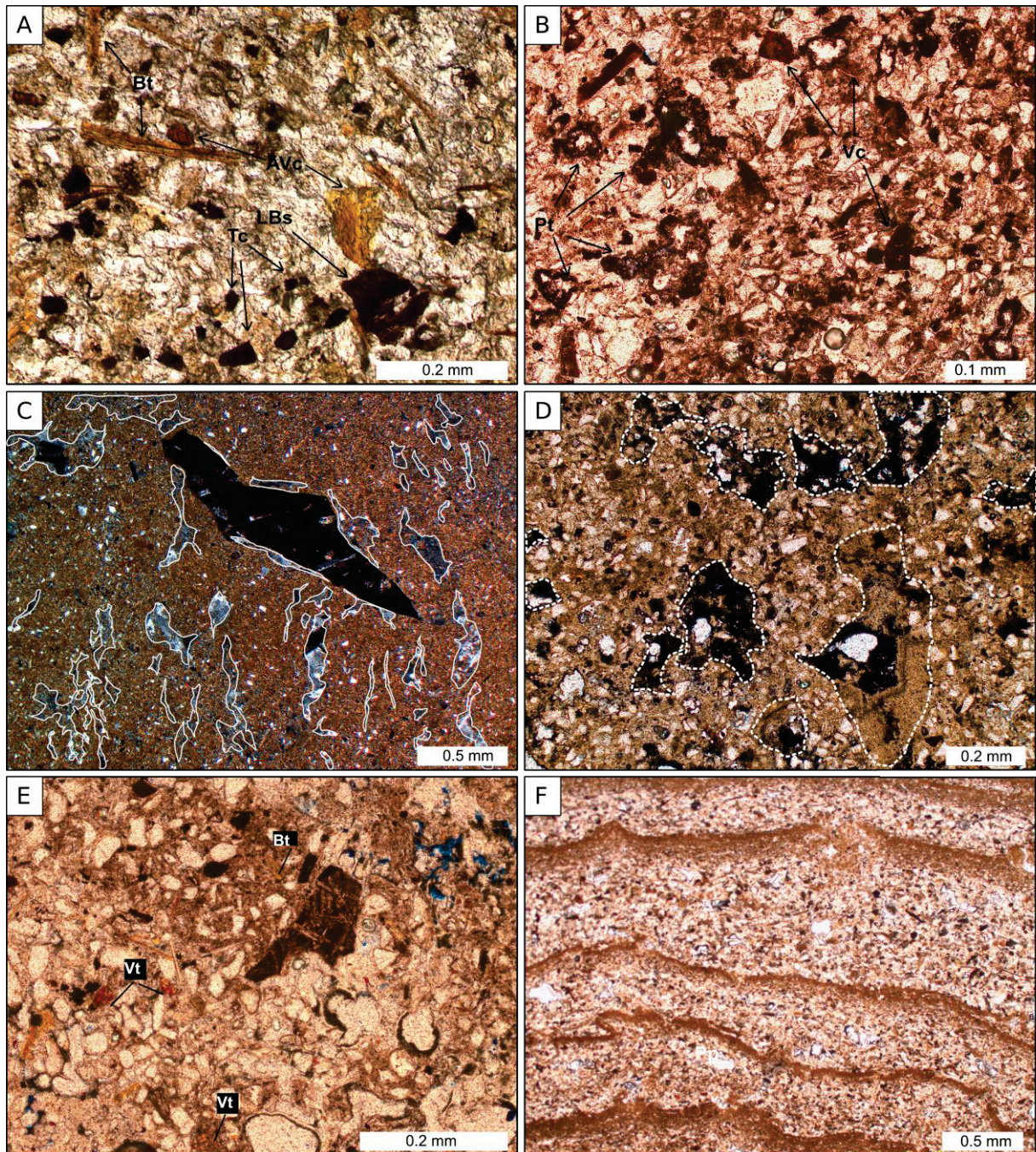
Figure 4.5 – Thin section images of tuffs: A) Altered glass clasts (AVc), opaque tachylite (Tc) (and/or oxides), basalt lithic (LBs) and brown mica (Bt) in I1 tuff, matrix of autoclastic breccia in RB section; B) Dark and ameboidal ash pellets (Pt), brown to reddish devitrified (hydrated?) dense vitric clasts (Vc) with oxide microlites. Tw tuff in LG section. C) Mica rich tuff, with subvertical zeolite amygdales (layer's top up) aligned with plastered and deformed lamination, rotated lithic lapillus. Tds facies, base of I3 in EG section; D) Poorly defined and irregular particle clusters with internal vesicles. Some show irregular rims of extremely fine ash reminiscent of layered aggregates; E) I4 tuff in EG, with very fine red devitrified dense vitric ash (Vt) and medium ash-sized brown cuspate devitrified fragment; F) disturbed rhythmite-like mantle-bedding in I4 Tlg tuff, NS section. Layer's top up.

Overall, this tuff sequence was interpreted as a product of pyroclastic deposition with lesser (<10 – 30%) amounts of juvenile material (Figure 4.5B, Section 4.7.2). However, in some outcrops the upper portion of I2 is marked by roughly bedded or

massive tuff-like rocks without pellets and vesicles, interpreted as reworked volcaniclastic deposits. Distinguishing between these reworked facies and the underlying pyroclastic rocks is not so simple, since they are almost identical compositionally. Some of these beds frequently host subrounded hypocrystalline to glassy basalt fragments (up to 10%), which never have cuspate and salient contours (Ss facies). Other massive, poorly sorted tuff-like rocks are even more similar to the underlying tuffs, as they are rich in seemingly unaltered vitric shards, and have a mud-supported fine ash framework (RTm). Further discussions on these facies are present in the 4.7.3 section.

On the top of I2 (and also I3 and I4) localized and centimeter–thin close-packed breccias are frequent (Figure 4.9). These are interpreted as peperitic domains produced by in situ coarse mingling with overlying lavas (B3, B4 and B5, respectively), with essentially vesicular fluidal blocks and nodules that are sometimes still partially attached to their parent lavas. Centimeter thick portions of the underlying interflow deposits immediately below peperites are hardened and silicified, which also makes them apparently massive, although some original and peperite-related structures can be seen sparsely, especially between blocks on the breccias themselves. These centimeter-thick thermo-metamorphosed regions are largely devoid of ash aggregates, which could be due to intense fluidization, but also a primary feature of either reworked or pyroclastic facies.

4.5.2.4 Pitanga interflow units – eastern I2 breccia sequence

The I2 interflow unit, which lies above the last Pitanga Fm flow-field (B2), is the most complex interflow found in the research area (Figure 4.10). It includes, in the eastern AM, CP and SI sections, a 2-12 m thick (AM) tuff-breccia to breccia sequence that outcrops at an altitude range of 500-525 m, while in the west this sequence correlates to the meter thick tuff and lapilli-tuff beds described in the last item (figures 4.9, 4.10). It is not clear if the breccia sequence indeed has an overall tabular geometry because exposures are somewhat scarce. This sequence is comprised essentially by matrix-supported tuff-breccias and breccias (TBlg, Blg, TBmds, Bmds, Bmc) with a framework of vesicular (scoriaceous) to massive basalt blocks, which are in majority between 10 and 30 cm in size (largest blocks are 60 – 100 cm), and are homogeneously dispersed and hosted by a laminated matrix.

Vesicular blocks are mostly irregular, fluidal or rounded, and massive ones are angular to subrounded. Framework forms 40-60% of the whole tuff-breccia to breccia sequence, and there are lateral and vertical alternations of more close-packed and clast-supported fabrics.
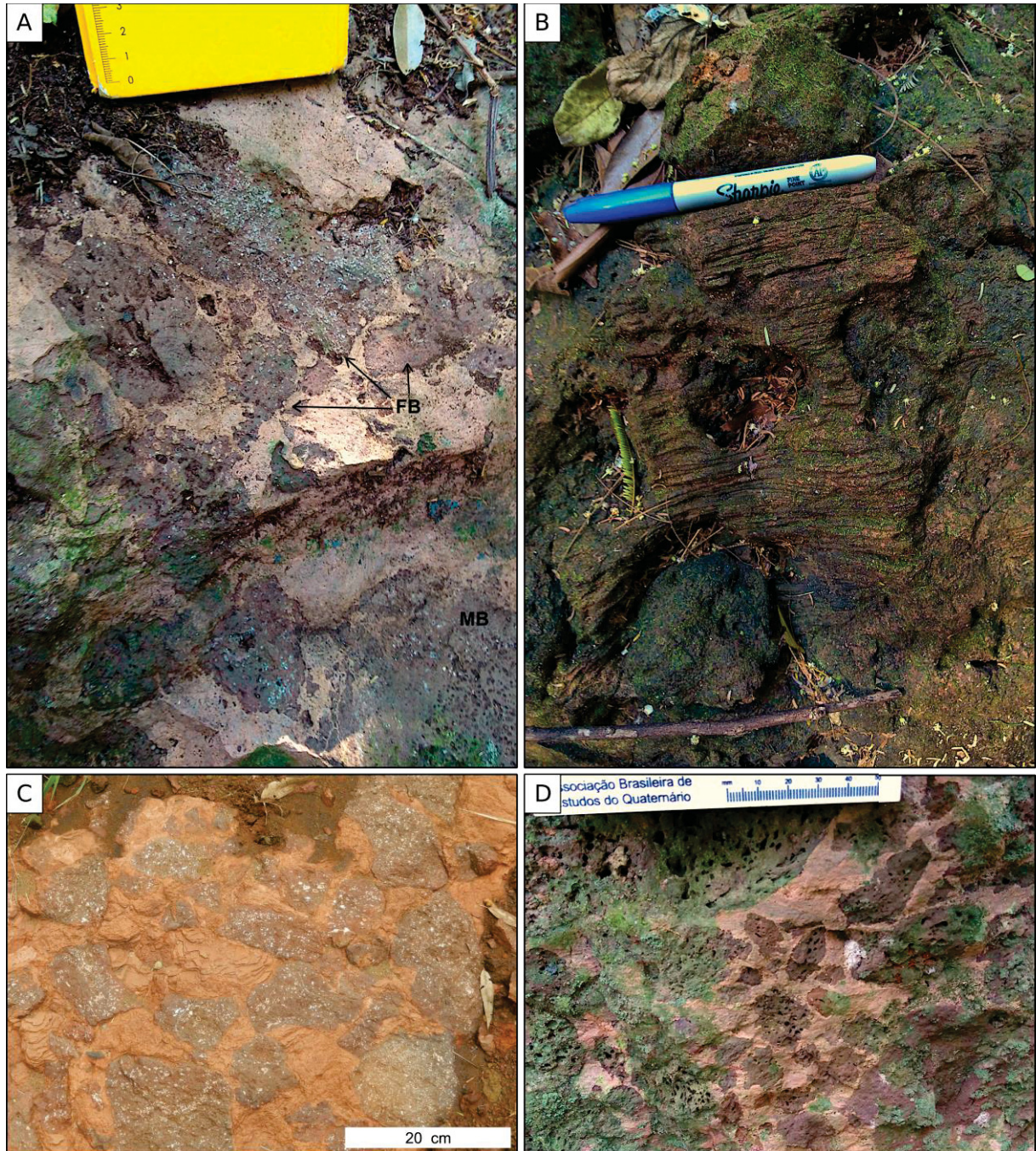
Figure 4.6 – Features of I2 breccias: A) Bed of Bmds facies in SI section, with fluidal bombs and blocks of very variable vesicularity (FB) and "mixed" or composite clasts with vesicular cores and massive rims (MB); B) Bed of the TBlg facies in SI section, with a framework of subrounded to fluidal vesicular blocks and bombs hosted by finely laminated and undulating matrix, which shows laterally consistent bedding; C) Oblique view of TBlg matrix-supported breccia in AM section. Framework of amygdaloidal basalt and laminated matrix of fine accessory ash; D) Lapilli-sized fluidal to angular clasts in Bmds framework, SI section.

Matrix in the TBlg and Blg facies is majorly comprised by heterolithic, rhythmically stacked ash to mud-grade ash couplets. These couplets form millimetric, internally gradational, plane-parallel to slightly undulated laminae (figures 4.6B, 4.6C). This texture is almost constant throughout most of the eastern I2 sequence in AM, although some variations include the presence of thicker (cm) lamination, interbedded tuff or lapilli-tuff lenses with wavy or low angle cross-lamination (Tw, LTw), convoluted, diffusely stratified or massive matrix (Bmc, TBmds facies) and non gradational laminae in the matrix.

These heterolithic couplets are formed by domains of moderately sorted fine to medium ash that grade into extremely fine (mud-grade) ash domains, usually <0.5 mm thick. These coarser ash domains are usually comparatively thicker (0.5 – >3 mm), and the gradational laminae are characterized by correlated exponential upward fining and thinning.

Coarser ash domains are formed mostly by quartz crystalloclasts (up to 50%), followed by significant (up to 20%) augite, plagioclase, opaque minerals (oxides), biotite and white micas, as well as trace amounts of microcline, tourmaline, zircon and rutile. They are hence considerably immature mineralogically. Crystalloclasts themselves are moderately well sorted (fine ash-sized). These same domains host very fine to medium vitric clasts of tachylite and sideromelane with angular shapes and irregular to blocky contours. They also show isolated coarse ash to fine lapilli size basalt fragments that are usually hypohyaline. Lastly, mudstone intraclast-like fine ash-sized fragments and lapilli-sized composite breccia or tuff-like fragments also occur. Some tuff-like lithics are very similar to I1 compositionally and texturally (Figure 4.7D). All lithics and vitric clasts are more poorly sorted than crystalloclasts. Extremely fine ash domains in gradational laminae are dominated by brown, semi-opaque mud and extremely fine crystalloclasts and vitric clasts, but brown mica crystals are also very common in them (figures 4.7B, 4.7C).

Finally, mud-grade or extremely fine ash material is also present in aggregates and pellets, which are well exposed and preserved in I2, especially in facies TBmds (SI section). In I2, these pellets are 1 to 0.2 mm sized spherical layered aggregates or clusters with moderately regular to ameboid contours (figures 4.15A, 4.15B). In the SI section, most have moderately defined rims of light brown mud-grade ash, and

sometimes show cores of fine sideromelane ash and more transparent clay minerals (Figure 4.15C).
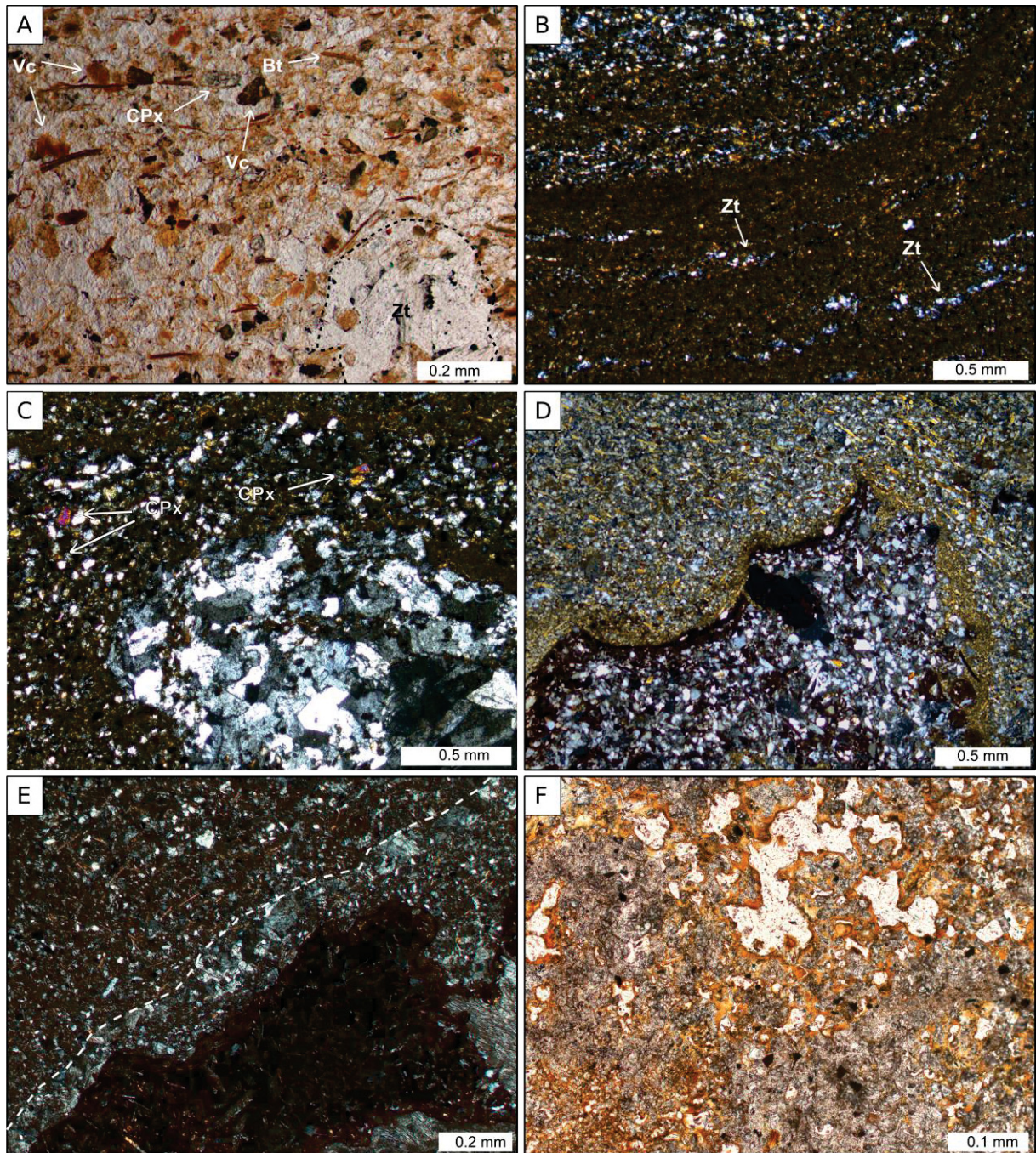
Figure 4.7 – Thin section images of I2 breccias: A) Matrix of TBlg facies. Devitrified brown and red (altered to oxides/clay minerals) vitric clasts (shards), juvenile pyroxene (CPx), and euhedral "biotite" (Bt) crystals; B) Gradational and convoluted mud-grade ash laminae of TBlg, with zeolite amygdales (Zt) aligned to lamination; C) Fine accessory ash domains in TBlg rich in juvenile pyroxene (CPx), large zeolite amygdale with clast inclusions; D) millimeter-sized tuff lithic in matrix of TBlg facies, with angular and cuspate contours and surrounding rim of recrystallized (mica-rich) mud-grade ash (armoured lapilli?), AM section; E) Basalt lithic with zeolite "aureole" in matrix of TBmds facies, SI section; F) vesicles in matrix of TBmds tuff-breccia, with orange clay filling (smectite?).

Texturally, the rhythmite-like fabric in the matrix of TBlg and Blg strongly contrasts with the coarse, poorly sorted and mostly homogeneously arranged block framework. The laminated texture is interrupted by blocks, but lamination remains consistent laterally and vertically (Figure 4.6B).

Some few key features help to classify I2 breccias genetically. These include the presence of: (i) disperse and irregular zeolite amygdales (<0.2 – 1 mm) in the laminated matrix (both with and without inclusions of matrix material, Figure 4.7C); (ii) aligned or elongated fine amygdales and vesicles in coarse ash domains of gradational matrix laminae, separated by vesicleless mud-grade laminae (Figure 4.7B); (iii) zeolite amygdales and "aureoles" attached to basaltic blocks with matrix inclusions; (iv) fine zeolite amygdales inside and also surrounding ash pellets; (v) localized fluidization and soft-bed deformation.

These features were interpreted as indications of syn-depositional to penecontemporaneous hot fluid activity (see Item 4.7). However, the intercalation and spatial association of these features with domains of well-defined rhythmite-like bedding and also with ash pellets strongly indicates that this fluid activity was unrelated to flow peperites. The occurrence of coarse <0.5 – 2 mm ash pellets (which are found in laterally correlated tuff and lapilli-tuff beds of I2) itself is of sheer importance, as they were interpreted as typical pyroclastic ash aggregates (Ellis and Branney, 2010; Brown *et al*. 2010, 2012).

Lastly, outcrops of the I2 breccia sequence have a somewhat radial distribution, collectively covering an area of about 10 km² if the whole eroded region between the most distant outcrops is considered. However, in terms of largest diameter, this radial area is approximately 4 x 2.5 km wide. The I2 breccia sequence is best explained as a proximal pyroclastic deposit and could be considered a diatreme-related breccia, being the closest possible candidate for a near-vent association in the research area. This sequence was correlated with tuffs in isolated outcrops and the westernmost Vai-e-Vem (VV), Nossa Senhora Aparecida (NS), Lourdes Gaspar (LG) and Água da Fortuna (FO) sections (Figure 4.1), which outcrop in a similar topographic break, interpreted as an almost continuous interflow bed that has been partially covered by vegetation and plantation areas (Sup. Figure 4.20).
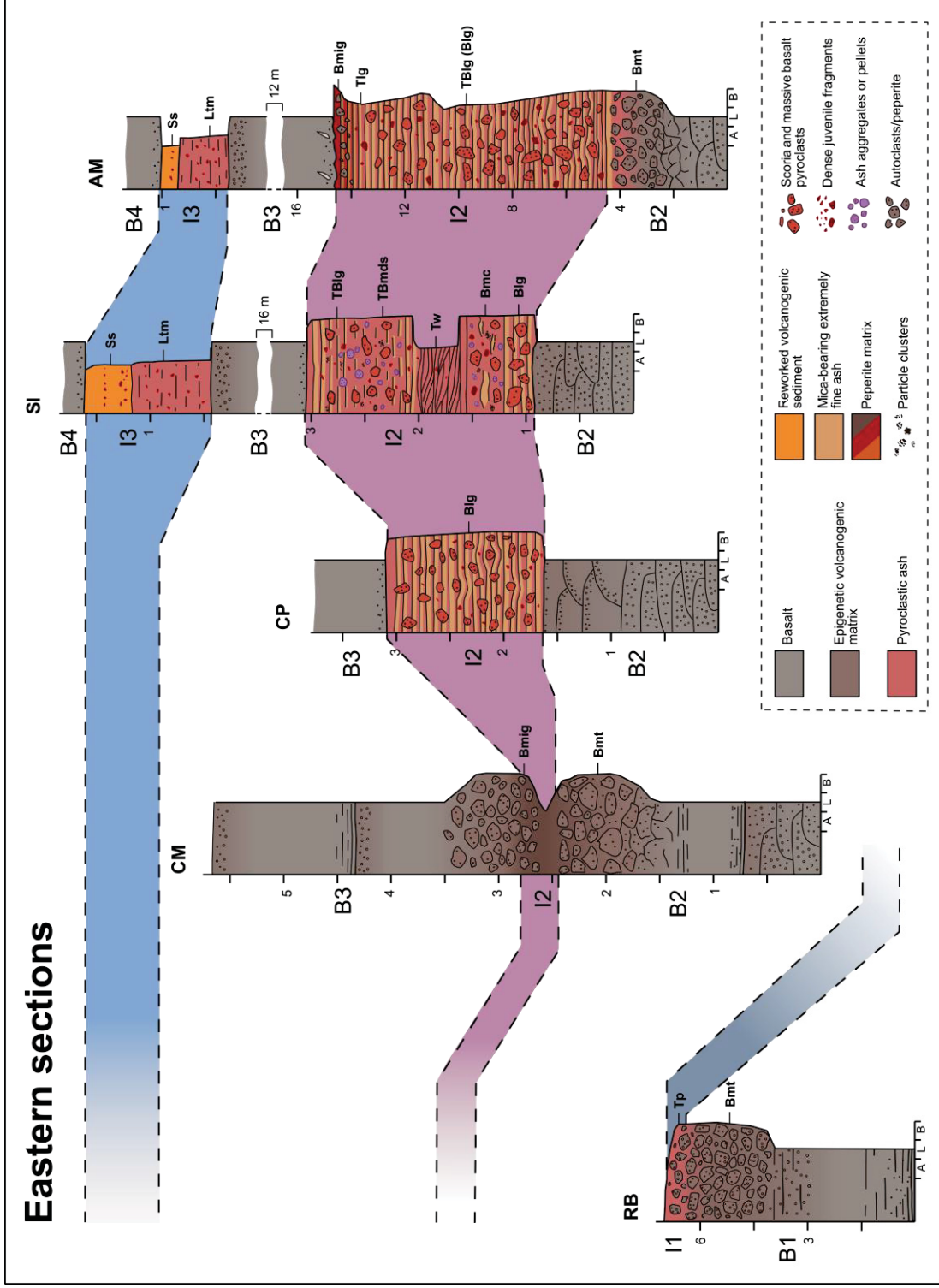
Figure 4.8 – Correlated geological sections from the eastern part of the research area. Scale in meters. Sections were correlated based on geological mapping and unit correspondence to topographic breaks (see Sup. Figure 4.20). Vertical offsets in the image are based on relative altitude offsets measured in the field.
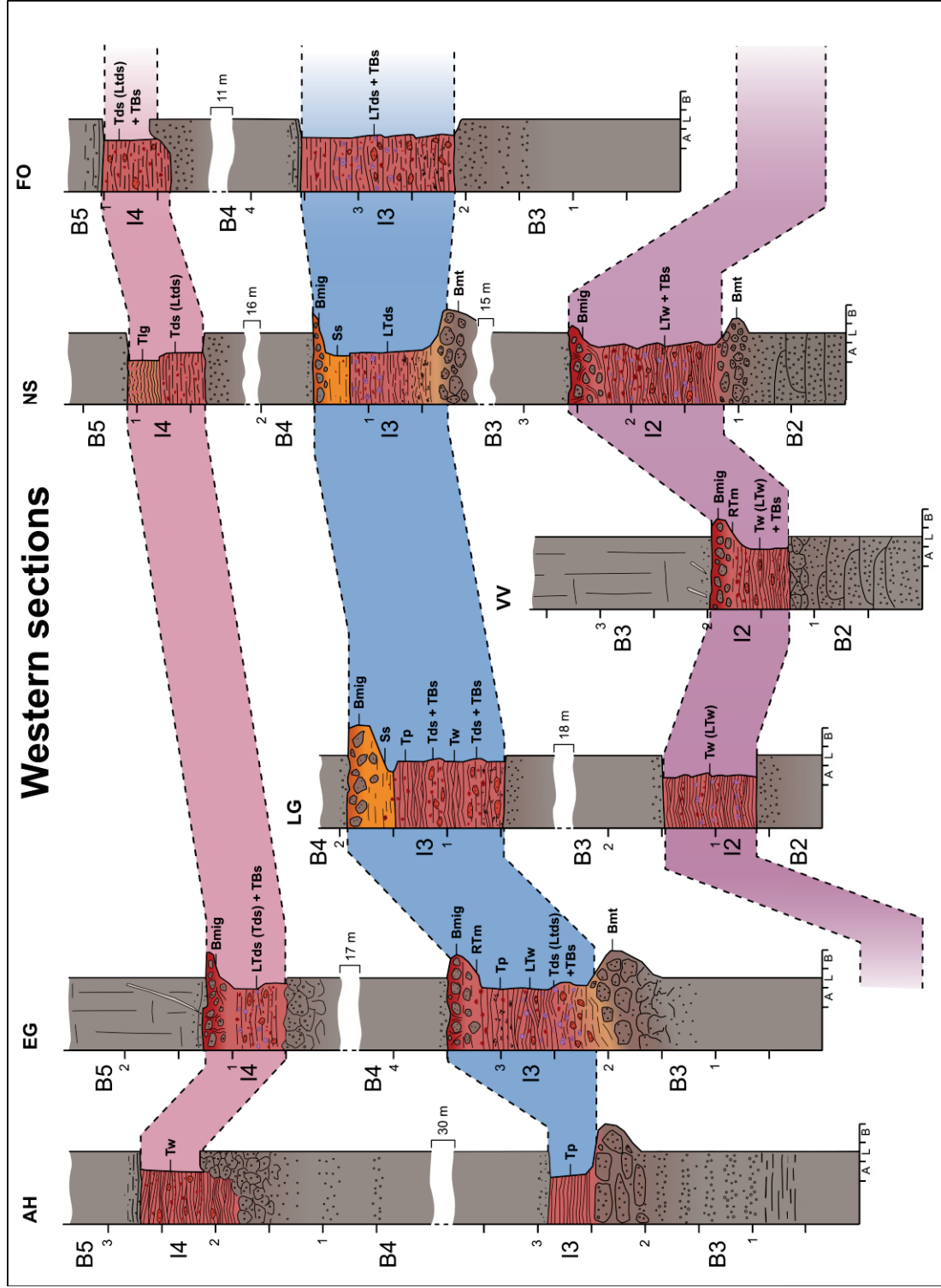
Figure 4.9 – Correlated geological sections of the western region. Scale in meters. Legend is the same as Figure 4.8.
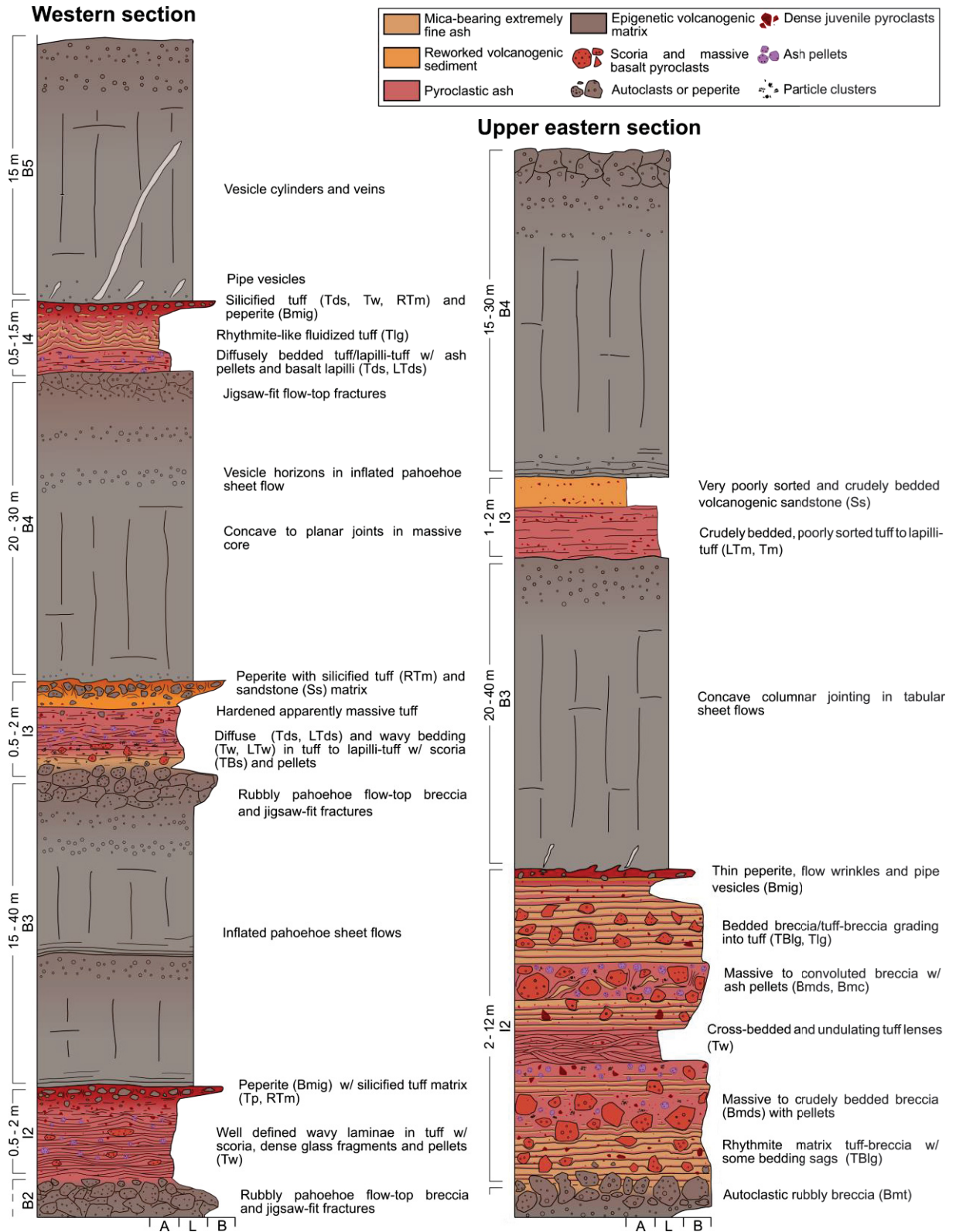
Figure 4.10 – Composite sections of the eastern (proximal) breccias of I2, B3, I3 tuffs and B4 and of the western I2, B3, I3, B4, I4 and B5 units.

4.5.3 Paranapanema Formation

4.5.3.1 Paranapanema Formation basalts - B3, B4 and B5

Above I2, the first flows of Paranapanema Fm in the region were described. These are essentially tabular, 8 to 20 m thick sheet flows, but each unit is not formed necessarily by a single flow (figures 4.9, 4.10), as some interflow beds are locally separated by two or more 10 meter thick tabular flows. These are formed by the typical vertical facies variations of inflated pahoehoe flows, including a lower aphanitic vesicular zone or crust, a fine to medium phaneritic core and an upper aphanitic vesicular crust.

Lower crusts commonly have horizontal joints with cm-thick spacing, similar to flows in B1 and B2. Massive cores typically show moderately developed concave-planar columnar jointing in dm-wide spacing (Figure 4.11A). Upper vesicular zones comprise up to 30% of a single tabular flow, but commonly makes up less than that. They are sometimes brecciated (rubbly pahoehoe breccias) and are usually very fractured, with jigsaw-fit blocks (4.11C). These breccias (Bmt) are very similar in composition and grain-size compared to flow-top breccias of the Pitanga Fm.

In lower vesicular zones, some pipe vesicles were identified. Phaneritic cores also show diktytaxitic cavitites formed by residual melts, which are now filled by clay minerals derived from glass alteration. Upper crusts are many times hypohyaline, and the glassy mesosthasis is formed by cryptocrystalline tachylite. They typically show amalgamated vesicle and amygdale horizons that are sometimes almost indistinguishable from one another (Figure 4.11B).

Massive cores of inflated tabular flows show similar mineral assemblages and textures as Pitanga Fm sheet flows in the area, and intergranular plagioclase (~40%) and augite (30-35%) comprise the most significant mineral phases, with subordinate opaque oxides (10%), secondary chlorite and smectite (5%) in diktytaxitic cavities, as well as minor amounts of semi-devitrified glass (<5%) and orthopyroxene, which occurs as anhedral and intergrown exsolution crystals (<5%). These flows are also majorly equigranular and aphyric, as phenocrysts are only 1.5 or 2 times larger than groundmass (0.1 – 0.2 mm) crystals.
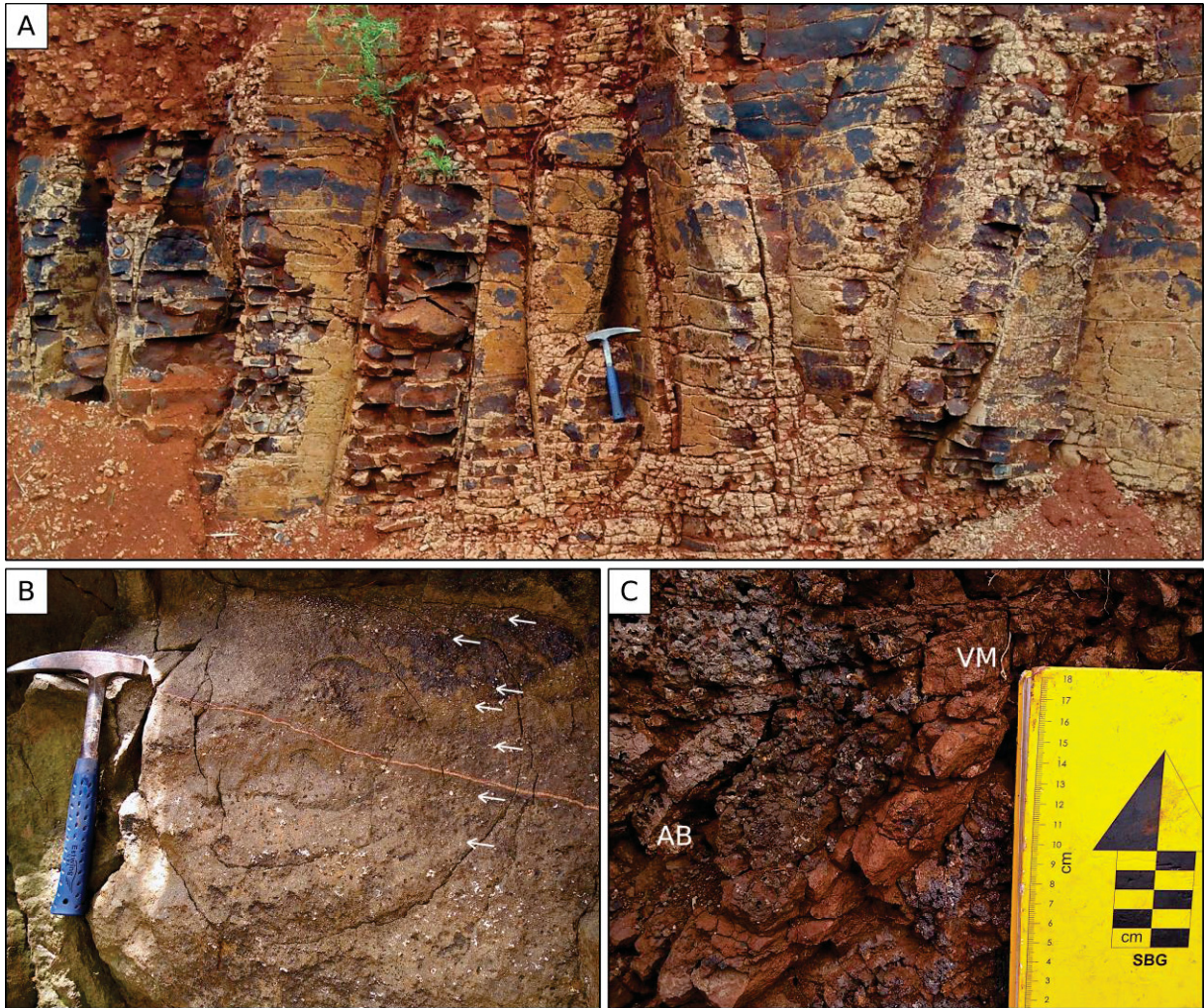
Figure 4.11 – Features of basalt units from Paranapanema Formation: A) Moderately developed concave columnar jointing in flow from B5 unit; B) Vesicle horizons (white arrows) in inflated sheet flow of B3 unit; C) Autoclastic breccia at the top of B3. Blocks (AB) are separated by domains of structureless red lithified clay (VM) that grade into less altered basalt framework. Matrix and framework in autoclastic breccias are frequently almost indistinguishable.

4.5.3.2 Paranapanema interflow units – I3

The I3 interflow unit is found at altitudes ranging between 520-550 m and is typically 50 – 200 cm thick. Differently from I2, in eastern sections (AM, SI) it comprises massive to crudely stratified lapilli-tuffs (LTm) with few to no ash pellets or vesicles (Figure 4.10) in 50 - 100 cm thick beds, capped by dm-thick reworked volcanogenic sandstones (Ss facies, Figure 4.12B). These occurrences are richer (10-20 %) in coarse ash to lapilli-sized (or granule size, in the Ss facies) hypohyalline basalt fragments. Apart from that, they are composed by angular to subrounded crystalloclasts (fine ash-sized) similar to I1 and I2 (50-80 %), mud-grade ash (10-30 %) and very fine sideromelane or tachylite shards, commonly showing devitrification or alteration features (~10%).

Overall, western I3 occurences include mostly intercalations between Tds, LTds and TBs facies, which also differ from the common dune-structures of Tw in western I2 (figures 4.9, 4.10). In the medial NS and FO sections (5 - 6 km west from AM), this unit is formed by a succession of a basal diffusely stratified tuff with black elongate aggregates or spikes, which grades into a tuff with spherical purple ash to lapilli-sized aggregates and conspicuous vesicles (Tds), being capped by reworked volcanogenic sandstones as well.

Closer to the EG and LG sections (7 - 8 km west from the AM section), "dune-bedding" structures of the Tw facies dominate, similarly to the I2 unit in most sections and outcrops. Furthermore, proximal (AM, SI) and medial sections (NS, FO, EG, LG, AH) show similar compositions - differences reside mostly in the presence of vesicles, diffuse stratification and pellets in medial sections.

In the EG section, a complex succession of facies marks I3 (Figure 4.9). This 160 cm thick sequence includes a basal tuff rich in mud-grade ash, brown mica and zeolites, in which bedding is marked by amygdale and vesicle elongation and mica orientation (Figure 4.5C). In this tuff, bedding is sometimes folded, dipping over 45º, with attitudes following the layer's contact with an underlying irregular flow-top breccia. This 15 cm thick plastered layer grades into more typical vesicular crystalloclast-rich tuffs of the Tp and Tw facies that make up the bulk of I3 in EG. These are rich (~20%) in 0.5 to 1 mm ash pellets and show disperse brown mica fragments (<10 %). Pellets increase in proportion up to the 40 – 60 cm mark, above which they become less frequent (< 10%) and smaller than 0,2 mm. In this horizon, black elongate aggregates are also described.
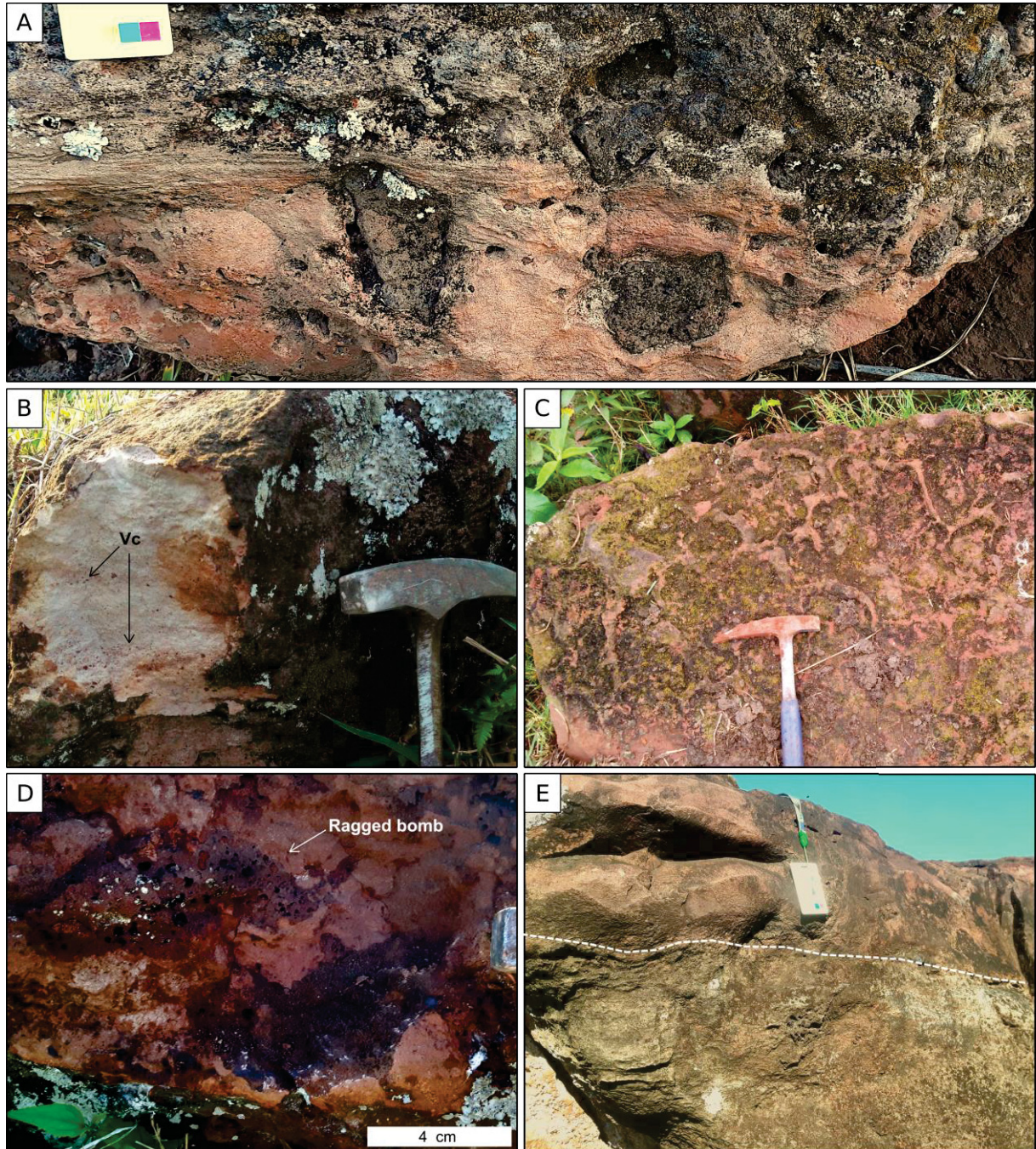
Figure 4.12 – Features from tuff successions from Paranapanema Formation: A) Bed of TBs facies, with matrix draping vertical and imbricated basalt blocks, I3 in EG section; B) Epiclastic and volcanogenic sandstone with crudely defined vitric-clast-rich horizons, I3 in SI section; C) Plan view of peperite, with hardened matrix salient between eroded blocks, I3 in NS section. D) "Ragged" or globular fluidal clasts in TBs facies, I3 in LG section; E) Hardened, massive and salient part of a tuff succession, above beds of Tp facies (exposed faces are also apparently massive here), I3 in EG section.

At about 100 – 120 cm from the base, pellets become completely absent, but texture remains moderately poorly sorted and mud-grade ash rich. This characterizes the overlying reworked or resedimented tuff. The primary tuff and respective resedimented bed are hardened and silicified at the unit's upper 30 - 40 cm (4.12E).

Below the immediate contact with the B4 flow, decimeter-thick peperite horizons are also found. However, most peperite domains are only exposed as plan views where most clasts have been differentially eroded in relation to the underlying hardened interflow matrix (Figure 4.12C). Although this hardened material has become apparently massive, it is possible to observe some preserved primary lamination in portions of the silicified tuff bed. Additionally, features related to the peperite itself include fluidization (or disruption) of the clastic matrix and injections of extremely fine ash (figures 4.12C, 4.14D).

4.5.3.3 Paranapanema interflow units – I4

The last interflow unit of the Sertanópolis succession is also the least defined one, since exposures are sparse. However, it is the unit with the most significantly differing facies architecture. I4 outcrops at an altitude range of 550 – 565 and is usually 50 – 150 cm thick. I4 beds commonly have a channel-like geometry, outcropping as less than 10 m wide lenses, but some exposures are more continuous (EG section). I4 is essentially formed by Tds, Tw and Tlg facies, but since outcrops are sparse, it's difficult to clearly determine their spatial relationships.

Occurences of cm-scale cross-stratified sets and dune-bedding (Tw) seem to be restricted to the westernmost AH section (Figure 4.9). Measurements in cross-stratified beds here indicate NNE and SSW dip directions, but it's difficult to define whether these are antidunes or normal dunes. At this outcrop, there are significant (~15%) isolated vesicular basalt blocks (cm-sized) and also smaller fine lapilli to medium ash basalt fragments. At this section, aggregates are absent in I4.

At the EG and FO sections, I4 is formed by pellet-containing beds of Tds tuffs, with light to dark purple ash pellets (Figure 4.9). Lamination is moderately defined and marked by vesicle elongation, which in turn indicates southward dips. Minor amounts (<10%) of hypohyaline basalt fragments of mostly medium ash to coarse ash size are hosted in the fine ash matrix.
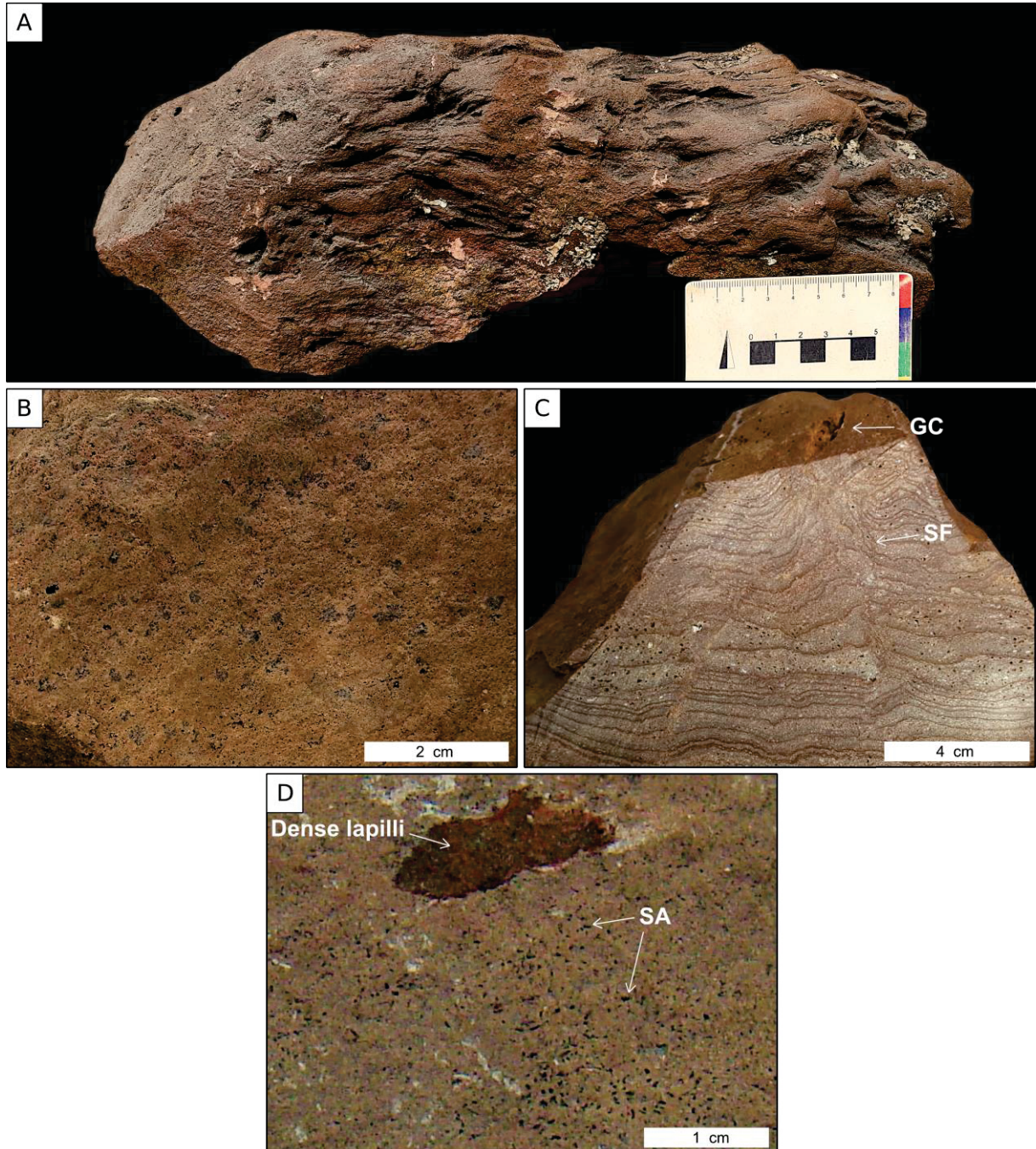
Figure 4.13 – Detailed photos of tuff samples of all units: A) Dune-bedding and waves of Tw facies, sample from I2 in LG section; B) dark purple to black ash pellets in Tds tuff of I3, EG section; C) disturbed vesicular laminae of Tlg tuff, with soft-sediment faults (SF) and gas escape conduits (GC), I4 in NS section; D) Detail of black "spike"-like aggregates and dense basalt lapilli in tuff from I3 unit, LG section.

In all of these occurences, I4 is compositionally similar to other crystalloclastic tuffs rich in accessory quartz and mud (up to 70%). However, one outcrop at the upper end of the NS section is marked by an increase in brown mica proportion (~25%). This exposure of I4 includes a rhythmite-like material similar to the matrix of TBlg breccias (Figure 4.13C). This rhythmite is composed of repeated mm to cm-

scale gradational or internally massive laminae, with moderately sorted crystalloclast-rich bases that grade into mud-grade ash and mica rich domains (Tlg facies). Lamination is plane-parallel and subhorizontal, but with significant wriggles/waves of vertically consistent and regular decimeter-scale undulations (mantle-bedding). Here, vesicles with minor amounts of fine (<0.2 mm) zeolite crystals and carbonate amygdales are conspicuous. Some form thin vesicle sheets aligned with wriggly laminae. These features were interpreted as the result of soft-sediment deformation due to syn-depositional fluid expulsion. Lastly, concentrated subvertical atectonic faults associated with irregular vertically sheared laminae and large coalesced vesicles or openings were interpreted as gas escape conduits. This tuff with disrupted and fluidized mantle-bedding was interpreted as a product of hydromagmatic and water-saturated ash fallout.

4.6 Primary volcaniclastic componentry

4.6.1 Crystalloclasts, lithics and overall accessory material

In all interflow units, tuffs have rather similar compositions, being formed predominantly by siliciclastic-derived fine to extremely fine accessory ash. Accessory crystalloclastic ash (commonly c. 60% volume, sometimes as low as 20%) is comprised mainly by quartz, followed by microcline, opaque oxides and white mica, as well as trace amounts of as rutile, zircon, tourmaline and epidote. Some polymineralic quartz and chert fragments also occur in minor (<5%) amounts. These can arguably be classified as lithics rather than crystalloclasts.

Most crystalloclasts have fragmented contours, being classified as subangular to angular, but some subrounded to rounded and spherical fragments are found randomly mixed with fragmented clasts. These can represent accessory particles with preserved original sedimentary geometries. Overall, crystalloclasts are thought to have been ripped from the wall-rock of the hydromagmatic conduit close to fragmentation levels, which was semi-lithified or silicified at the time.

In some thin sections, lithics include minor amounts (<5%) of ash to lapilli-sized fragments of either crystal-rich tuffs or muddy sandstones. Some light brown mud "clumps" are similar to mudstone intraclasts, and could be accidental fragments derived from mud-rich tuffs or accessory lithics ripped from previous interflow beds in the wall-rock. However, it is also likely that some are semi-consolidated particle

clusters of mud-grade ash or fragments of ash aggregates (Brown *et al.*, 2010, 2012; Van Eaton and Wilson, 2013).

Other constituents are less clearly diagnosed, and can have either an accessory or juvenile (+- hydrothermal) origin. These include fine to very fine ash augite and plagioclase (sometimes as much as 15%), which are likely present as both juvenile and accessory pyroclasts. Distinguishing between these varieties can be significantly difficult with petrographic methods only.

Similarly, basalt fragments include vesicular, massive and mixed or composite varieties (Figure 4.6A). Subrounded to angular blocks are common and predominant in all breccia facies with the exception of Bmig, which is formed mostly by fluidal clasts. Fluidal basalt fragments are present in essentially all tuff-breccia and breccia facies, however. Accessory basalt blocks would be understandingly frequent as wall-rock derived lithics in these explosive hydrovolcanic units, given the stratigraphic context of the area (Gomes *et al.*, 2018). More clearly recognizable lithic basalt blocks are massive and phaneritic, derived from slow-chilled cores of inflated flow-units present in the country-rock of the magmatic system. However, fragments such as these are only present in relatively smaller (20-30% of framework) quantities in proximal I2 breccias overall. Most blocks are vesicular and subrounded to subangular, with various degrees of sphericity.

Spherical and rounded vesicular blocks with no plastic deformation features such as concentric or clast face-aligned vesicle layers are interpreted as wall-rock lithics. Angular lithic (whether massive or vesicular) blocks were likely produced by brittle wall-rock fracturing, while spherical and rounded (mostly vesicular blocks) can be related to block milling during explosive transport inside the vent (Valentine *et al.*, 2015b).

Accessory-like material also includes varying amounts of mud-grade ash (usually between 20-40%), which is sometimes dark red, light brown or dark grey under petrographic microscope. Mud-grade ash typically occurs considerably well mixed with crystalloclasts and other components in most tuff facies, including the resedimented RTm facies, which suggests contemporaneous deposition.

It is difficult to infer whether the nature of this mud-grade or extremely fine ash material is indeed accessory or hydrothermal and juvenile. Hydrothermal mud-grade material is a common byproduct of hydrovolcanic palagonitization and syn-

depositional fluid activity (Capaccioni and Coniglio, 1996). However, it is likely that some of this dark red oxidized mud is volcanogenic in origin and accessory as well.

4.6.2 Juvenile clasts

Dense or poorly vesicular glass shards are found in varied proportions (<5-15 %) in all pyroclastic facies and even in the resedimented tuffs (RTm) and epiclastic sandstones (Ss). Fine ash to extremely fine ash-sized dense fragments range from equidimensional (blocky) to elongate, with angular, subrounded and also cuspate contours (figures 4.5A, 4.5B, 4.5E). Glass shards are commonly formed by slightly altered reddish brown tachylite (blocky to elongate fragments), followed in proportion by reddish to orange devitrified sideromelane (mostly blocky fragments). Altered glass fragments are commonly covered by films of oxides and clay minerals, a common paragenesis in hydrovolcanic environments (Wohletz and Sheridan, 1983). However, this means that many shards (especially tachylite ones) are not clearly distinguishable from hydrothermal brown micas, smectite or accessory oxides in thin sections. Perlitic and hydrothermal alteration features are characteristic of syn-volcanic hydromagmatic fluid activity, which may take place anywhere from inside the eruptive vent (Zimanowski *et al*., 2015) to a water-saturated tephra blanket (Capacionni and Coniglio, 1996).

Dense and subrounded to blocky sideromelane fragments are especially frequent in cores of proximal to medial ash aggregates (figures 4.15C, 4.16B). These very fine-ash fragments usually aren't as devitrified compared to disperse sideromelane shards.

The prevalence of tachylite suggests that erupted juvenile fragments may have been dominated by particles that did not directly interact with water, which can be a rather common feature in hydromagmatic systems (Zimanowski *et al*., 2015; White and Valentine, 2016), and devitrified microlite-bearing fragments can be records of juvenile clast recycling (Graettinger *et al*., 2016).

Medium-ash to lapilli size poorly vesicular glassy fragments also occur in essentially all pyroclastic facies in proportions of <5 - 10%. They are formed by hypohyaline basalt with plagioclase microlites, and show cuspate (vesicular) to rough angular contours. These coarser and cuspate fragments with chilled margins are interpreted as pre-vesiculated juvenile clasts of hydromagmatic (quenching) fragmentation (Graettinger *et al*., 2013; Liu *et al*., 2017, 2018).

It is difficult to define whether vesicular blocks in pyroclastic breccia and tuff-breccia facies (TBlg, TBmds, Bmc, TBs) are simply lithics derived from previous flows or if they are in fact juvenile scoriaceous fragments. Most clearly juvenile bombs are fluidal and show evidences of plastic-deformation during deposition, indicative of a magmatic fragmentative origin such as clast-face aligned vesicles and ragged or globular margins (Figure 4.12D). Fluidal and moderately vesicular clasts are commonly lapilli to block-sized (Figure 4.6). In the proximal breccia and medial tuff sequences, their deposition is simultaneous with clasts of clear hydromagmatic fragmentation, which suggests coeval magmatic and hydromagmatic activity. This mixed Strombolian-like and hydromagmatic character could be explained by the concomitant eruption at more than one type of discrete vent (Kienle *et al*. 1980; Self *et al*. 1980; Valentine and Cortés, 2013; Amin and Valentine, 2017; Ort *et al*. 2018), by mixing of pre-vesiculated lava and water during MFCI (Jordan *et al*., 2014; Liu *et al*., 2017, 2018) or even by simultaneous magmatic volatile-driven and hydromagmatic explosivity in roughly the same source (Houghton *et al*., 1996, 1999; Sottili *et al*., 2009; Murtagh and White, 2013; Valentine *et al*., 2015b; Onken and Forman, 2017).

Furthermore, composite juvenile fragments in tuffs include few occurences of peperite blocks and lapilli, characterized by poorly vesicular tachylitic basalt with entrained mud matrix (Figure 4.14F). These composite fragments are likely preserved records of "time-frozen" MFCI in the diatreme (Martin and Nemeth, 2007), evidencing that tachylitic and poorly vesicular lapilli have indeed been formed by hydromagmatic processes.

Juvenile basalt fragments are also important constituents of flow peperites themselves. These include fluidal hypocrystalline basalt blocks and bombs with quenched margins, as well as minor hypohyaline blocky lapilli and coarse ash. Peperite framework clasts are usually closely related to dark brown mud-rich matrix domains (Figure 4.14C), which includes neoformed clay minerals and oxides (volcanogenic mud) derived of peperite-related hydrothermal alteration (Hole *et al*., 2013).

In some thin sections, this mud-grade material is associated with very dark brown and opaque irregular aggregates of what looks like extremely fine tachylite. This material forms close-packed and jigsaw-fit patches and nodules that seem to have been fragmented *in situ*. This includes coupled/entrained extremely fine ash

glass and volcanogenic mud, derived of intense *in situ* MFCI and hydrothermal alteration (Hole *et al.*, 2013). Additionally, several framework basalt clasts have "envelopes" and rims of more clearly defined disperse fine ash to extremely fine ash juvenile glass fragments, which indicates that MFCI may have been locally explosive even in these peperites (Martin and Nemeth, 2007).

Lastly, petrographic analysis indicates that augite crystalloclasts are present as juvenile pyroclasts in tuffs (<5-10 %) and as crystals derived from juvenile fragments in peperites. Juvenile pyroclastic augite is subhedral to euhedral and subangular when fragmented, while crystals ripped from peperite basaltic framework follow whichever habits they had in correspondent chilled basalt fragments, which are sometimes very anhedral, with apparent rounded contours (Figure 4.14E).

4.6.3 Ash aggregates

Pellets in proximal Bmc and TBmds facies (I2 unit) are yellowish brown in hand sample, with mostly dark brown cores and light orange rims in thin sections (Figure 4.15A). These show moderate enrichment in Ca and Fe and depletion in Si and Al in comparison to surrounding matrix (Sup. Figure 4.23). Rims are formed by amorphous masses of extremely fine ash or mud-grade material. Cores are composed by light to dark brown extremely fine ash material and very fine amygdales (figures 4.15A, 4.16C). It is unclear if these are almost massive pellets with hydrothermally altered rims or if they became layered before deposition, but some subtle concentric color variations are observed in their dark brown cores as well. Semi-quantitative compositional maps also highlight subtle zonations in many of these extremely-fine ash rims (Sup. Figure 4.23). Additionally, some of these pellets are associated with dark brown irregular masses of extremely fine ash that were deposited as either less consolidated particle clusters or as coallesced and liquefied pellets deposited by water-saturated "mudrain" (Rosi, 1992; Brown *et al.*, 2012; Van Eaton et al., 2012; Van Eaton and Wilson, 2013).
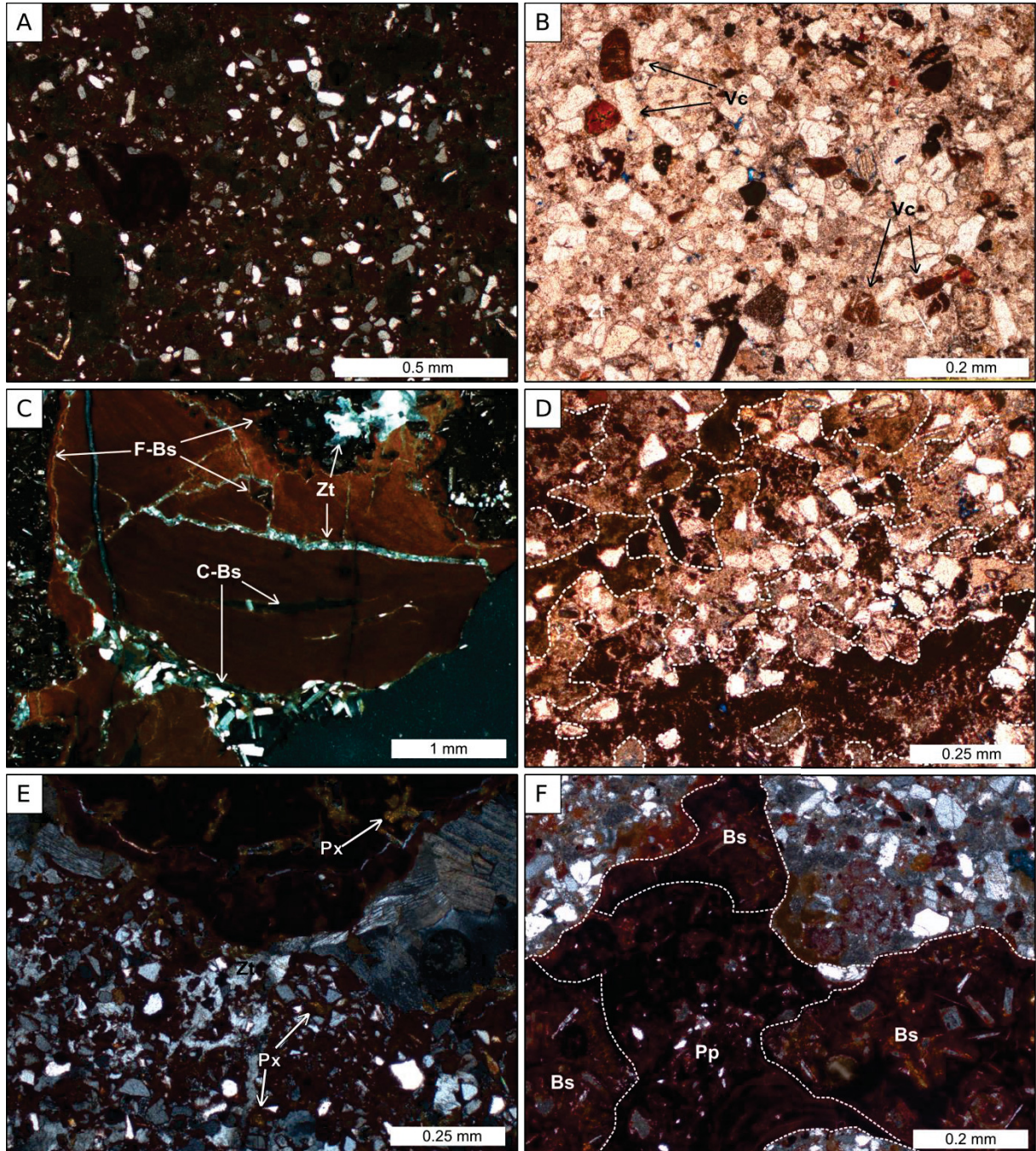
Figure 4.14 – Thin section images of peperites and reworked volcaniclastic rocks. A) Poorly sorted resedimented tuff, rich in mud-grade ash, with angular basalt fragments; B) Epiclastic sandstone, with rounded devitrified red to brown glassy fragments (Vc, reworked juvenile); C) Peperite at the base of B2, with opaque and diffusely laminated mud-grade ash matrix (juvenile + hydrothermal?). At least two generations of juvenile basalt (F-Bs – fine-grained basalt, C-Bs – coarse-grained basalt) and multiple cross-cutting zeolite veins, with ripped and sheared basalt fragments; D) Peperite with epiclastic sandstone matrix, I3 in EG section. Dotted contours mark extent of injections of fragmented extremely fine ash and light brown to yellowish opaque clay minerals; E) Peperite with pyroclastic or resedimented disturbed tuff matrix, with disseminated zeolite cementation (Zt) and juvenile pyroxene ripped from basalt blocks; F) Composite peperite clast in I2 tuff. Basalt block with entrained opaque matrix (Pp) very similar to the juvenile or hydrothermal matrix in image C.

Some aggregates in I2 proximal breccias have more clearly defined compositional layering. These include < 0.5 mm pellets with cores of agglutinated green to brown sideromelane and tachylite shards (< 0.1 mm), zeolite amygdales and red oxidized mud-grade material (Figure 4.15C). Their rims are comprised by an internal layer of opaque extremely fine ash (possibly juvenile tachylite <50 μm) that grades into an external layer of almost amorphous mass of even finer light brown material. This material can include clay minerals related to hydrothermal alteration of juvenile glass.

Similar layered aggregates are found in medial I2 as well. These show either cores of extremely fine sideromelane shards, light brown clay minerals (chlorite from altered glass) and transparent masses of Mg, Fe and Ca-bearing clay minerals (possibly smectites – figures 4.16A, 4.16B, 4.17A and sup. figures 4.24 and 4.25). Their rims are typically composed by well-formed translucid and birefringent Ca and Mg-rich clay minerals (possibly chlorite). In some outcrops, laminae bearing exclusively massive or layered aggregates alternate vertically.

Apart from these layered aggregates, most light to dark purple ash pellets appear black to dark red in thin sections (figures 4.15D, 4.15E). They are usually massive pellets or "particle-cluster"-like aggregates that are not clearly distinguished by BSE-SEM imaging and EDS maps, showing mostly subtle Fe (and sometimes Mg) enrichment and Si and Al depletion in relation to surrounding matrix (Sup. Figure 4.26). They are most likely aggregates of hydrothermal and oxidized volcanogenic mud, with minor quartz silt contribution and in some cases very fine (<<0.1 mm) internal zeolite amygdales. These pellets are conspicuous in many medial to distal beds of the I2, I3 and I4 surge tuffs. The absence of layering and hydrothermal clay mineral alteration along with frequent association with Tw facies suggest that they were deposited by drier eruptions and surges overall.
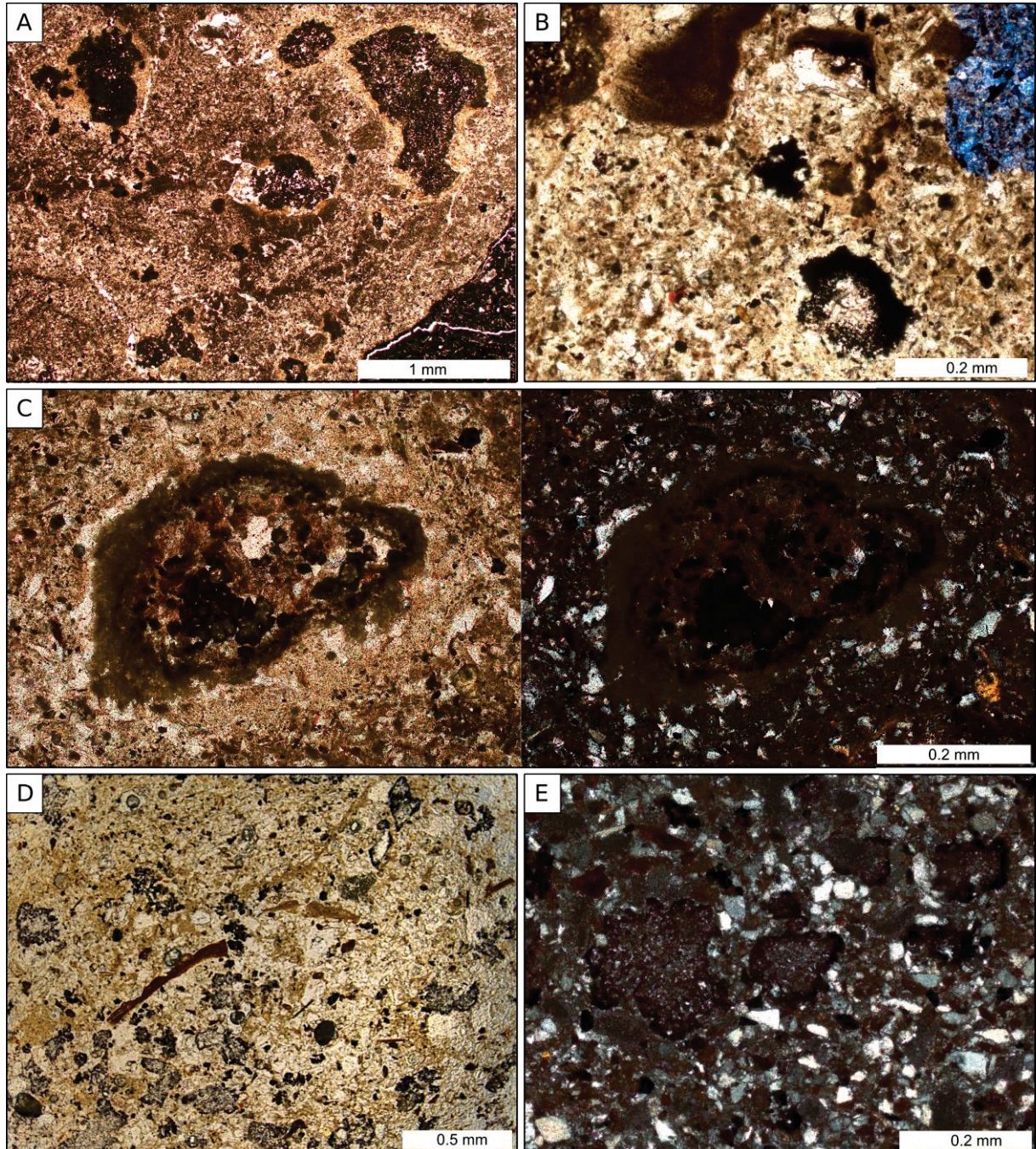
Figure 4.15 – Thin section images of ash aggregates and pellets. A) Layered ("ultrafine rims") and massive pellets in bed of proximal Bmds breccia facies, SI section, I2 unit; B) Deformed and fragmented brown massive pellets and black irregular particle clusters, in the same sample as A; C) Layered aggregate, same sample as in A. Core of very fine sideromelane ash and reddish oxidized mud-grade ash, rim of extremely-fine brown ash. A subtle external "reaction rim" or aureole is marked by zeolites and by a smaller concentration of brown mud-grade ash (Left – natural light; Right – crossed polarizers); D) Black massive pellets and particle clusters in medial tuff, I2 unit; E) Detail of dark red to black massive pellets in I2.

However, the relationship between massive aggregates, particle-cluster-like aggregates and elongate "black spikes" found in I1 and I3 and is not fully understood. Because they are rather similar compositionally, it's possible that the elongate spikes are less consolidated (and hence compacted) and/or wetter and slurried equivalents

of the massive purple pellets. This suggests that dry particle clusters (Van Eaton et al., 2012; Van Eaton and Wilson, 2013) and liquefied aggregates can be harder to distinguish in some settings, in spite of their initially opposite aggregation conditions.

All ash aggregates must have been initially nucleated inside drifting and variably wet ash plumes. This process led to the formation of massive pellets and massive cores of layered aggregates. Concentric cores or rims may be formed by transport inside stratified plumes and/or reworking by ground-hugging density currents (Brown *et al*., 2010) or cosurge clouds (Van Eaton and Wilson, 2013).

Aggregates were incorporated and reworked, after fallout, by different pyroclastic density currents (PDCs) (Ellis and Brown, 2010; Brown *et al*., 2012; Van Eaton and Wilson, 2013), as indicated by facies successions and presence of disrupted aggregate fragments in surge deposits. Those with rims of extremely fine material (<10 μm) efficiently incorporated material lofted from cosurge clouds with 10-15% wt. water ("ultrafine rims" in Van Eaton and Wilson, 2013). Lastly, outcrops showing vertical alternation between laminae with massive and layered aggregates indicate shifts in humidity conditions during deposition, developed due to transport in different, multiple plumes.

4.6.4 Hydrothermal material

Hydrothermal constituents are typical counterparts of hydrovolcanic activity (Wohletz and Sheridan, 1983; Capaccioni and Coniglio, 1996). In the Sertanópolis interflows, these include mostly clay minerals, zeolites, quartz and coarser grained micas in assorted assemblages.

Clay minerals and mud-grade ash are important components in most interflow units. Petrographic evidence indicates that mud-grade ash is present as depositional features, whether intermixed with other coarser ash components (figures 4.5, 4.7), concentrated in aggregates (Figure 4.15) or in mud-rich laminae in some bedded tuffs (figures 4.5F, 4.13C). In many mud-rich tuff successions, spatial associations between masses of semi-opaque brown mud-grade ash and fine reddish brown mica ("biotite") crystals indicate a hydrothermal to thermometamorphic character for the latter, especially because extremely fine and poorly pleochroic crystals, which are intermediate between these two situations, are also frequent. Additionally, some crystals show zonations and fibrous habits, similar to well-formed clay mineral

aggregates (Figure 4.5A). This preserved continuum of crystallization stages suggests a syn-depositional origin for brown mica crystals.
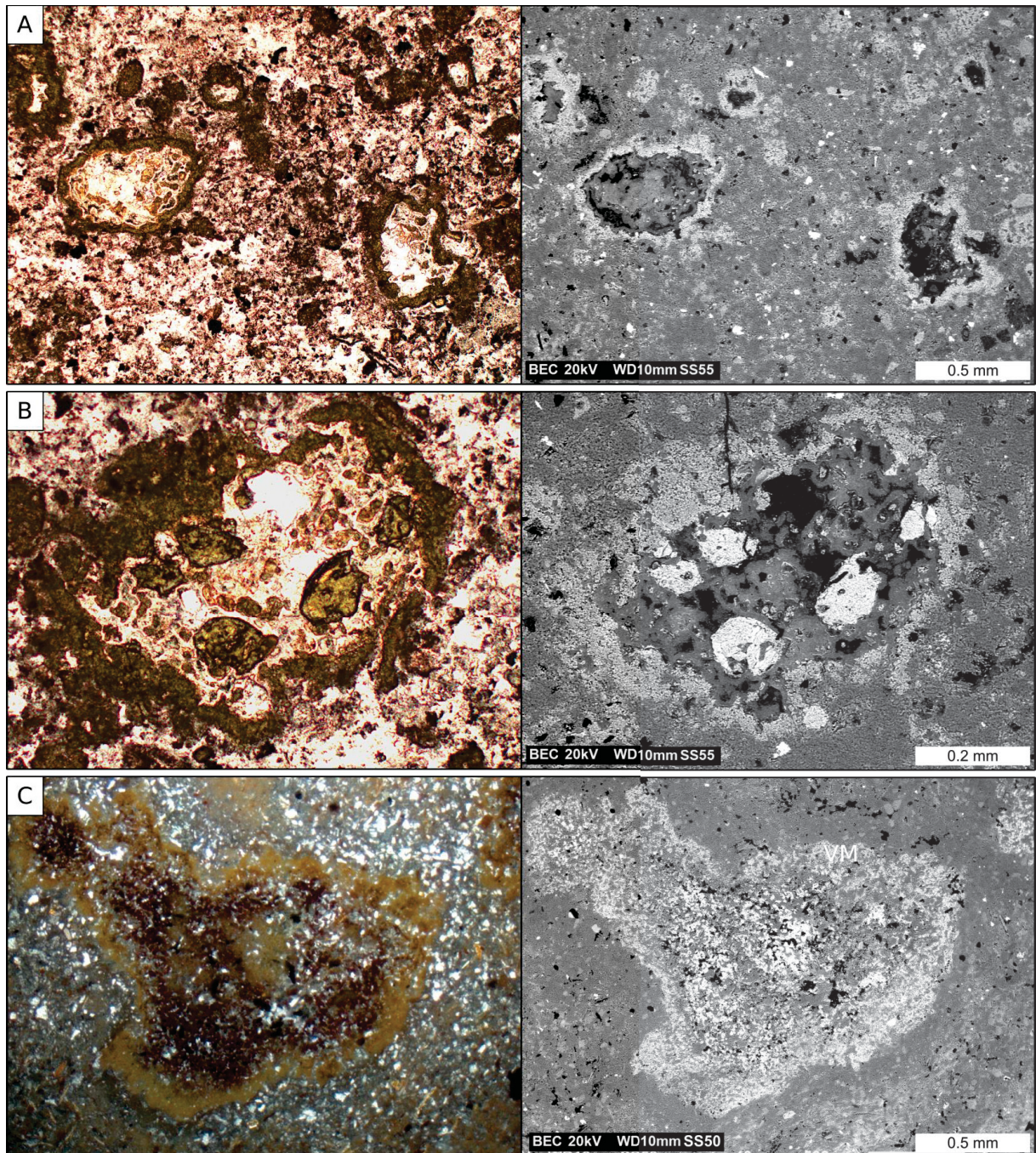
Figure 4.16 – Thin section and correlated BSE-SEM images of ash aggregates. A) Layered aggregates in proximal to medial Tds tuff in I2. Rims composed of green Ca and Mg rich clay minerals; B) Layered aggregate in the same sample, core with green sideromelane fragments (strong contrast in BEC image) and rim of greenish extremely fine ash; C) Layered aggregates in proximal Bmds. Cores of dark red to black extremely fine ash fragments (juvenile and accessory) and light brown rims.

Optical properties of many of these reddish brown mica crystals are similar to biotite and phlogopite, and semi-quantitative compositional maps and EDS analyses indicate K, Fe, Mg and Ti are present. Titanium-rich biotite and Ti-bearing

"oxyphologopite" have been described in hydrothermal parageneses associated with magmatic fluids in basalts (Chukanov *et al*., 2008, 2011), but its genesis is still not well understood in Sertanópolis.

Domains rich in brown mica (around 30-50%) are found in fallout tephra (Tlg, TBlg and also tuffs preserved only as matrix infill in flow-top Bmt breccias) and at the base of some surge successions, in clearly plastered and wet amygdaloidal tuffs. This link between what seem to be water-saturated deposition and mica-rich tuffs suggests that availability of syn-depositional water is directly related with mica-proportion, but it's not clear if the latter is correlated only with wetness of surge or fallout deposits. For instance, a more complex system can include the role played by the remanescent underlying lava flow heat and lava-flow–related fluid circulation as well
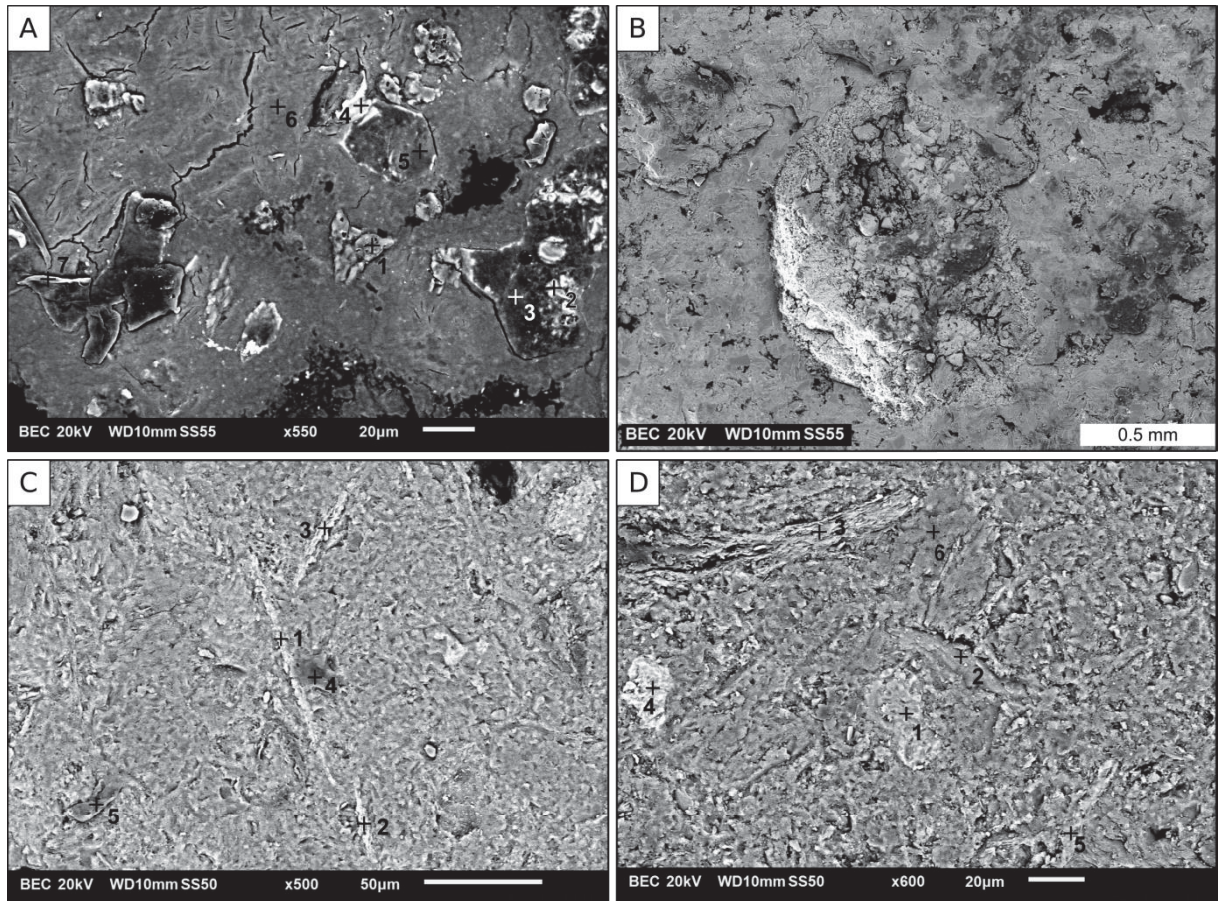
Figure 4.17 – BSE-SEM images of thin sections and rock samples: A) Detailed view of core of a layered aggregate in figure 4.16A. 1 – Silica and zeolites; 2, 4 – Juvenile pyroxene ash. 3, 5, 6, 7 - Altered extremely fine ash and clay minerals; B) Morphology of layered pellet in Bmds facies; C and D) K, Fe, Mg and Ti mica (C – 1, 2, 3; D – 2, 3), oxides (D - 4), quartz (C - 4) and glass fragments (D – 1, 5) in tuffs.

A similar context is highlighted by the presence of semi-opaque mud-grade material and well-formed translucid and birefringent clay mineral rims in vesicles

(orange to red smectite or chlorite), in association with ash aggregates (green Ca and Mg-rich chlorite) and as cohesive disperse fragments (possibly altered vitric clasts). This could indicate that more clearly defined hydromagmatic fluid activity in surge tuffs led to more typical "authigenic" hydrothermal clay mineral assemblages (Capaccioni and Coniglio, 1996). Additionally, well-formed brown mica crystals are present as disperse fragments (ca. 5-10%) in essentially all tuffs that don't have mica-rich domains. In these tuffs, however, a continuum of mica crystallization is not observed, which could imply that mica fragments have been produced in wetter parts of the hydromagmatic system, only to be resedimented by drier PDCs, or even some other process entirely. Data regarding hydrothermal activity related to hydromagmatism in Sertanópolis is still preliminary, and is not clear if this different assemblage is related only to a smaller hydromagmatic water content in tephra, or if such differences are explained by external parameters, such as the ones mentioned before.

Zeolites are found mostly inside amygdales in fallout and surge lithofacies, in basalt fragments and in lava flows as well. They are also less commonly found cementing some proximal tuffs. As amygdales, they usually occur as <0.1 – 1 mm crystals in mosaic-like aggregates, and several amygdales have fine ash inclusions, especially amygdales inside basalt clasts and in zeolite rims around these same clasts. Zeolite rims are also present around many ash aggregates and basalt clasts (figures 4.7E, 4.15C), which evidences their link to a hydromagmatic and syn-depositional paragenesis. However, secondary zeolite veins and amygdales are also described in close association with lava-flow peperites, and should thus be addressed with further caution not only in Sertanópolis, but in other interflow deposits of the PIP, because their presence alone is not diagnostic of either origin (Titon, 2019). On the other hand, syn-depositional zeolite in association with brown mica is only found in pyroclastic facies in Sertanópolis.

Finally, carbonates have been found in close association with zeolite amygdales and in autoclastic breccias as a posterior cavity infill phase. Carbonates in cavities of interflows and in basalts of the PIP have been reported as frequent late to post-magmatic precipitation stages (Gilg *et al*., 2003; Morteani *et al*., 2010; Titon, 2019) In Sertanópolis, this may be linked with overall fluid percolation in hydrothermal volcanic settings, and not specifically with hydromagmatic fluids.

4.7 Magmatic events and associated interflow deposition at Sertanópolis

4.7.1 Physical volcanology of flows

All described flows share morphologies indicative of inflation processes. More typical compound flow-fields of Pitanga Fm. B1 and B2 are very similar to sucessions described in Thordarson and Self (1998) at the Columbia River Province, which include inflated sheet flows and sequences of S and P-type flow-units. The presence of inflated flows at the base of B1 could reflect a local waxing volcanic trend during the main phase of the respective eruption, followed by a waning trend during the B1 to B2 transition, but since flows below this unit were not mapped in detail, this does not necessarily reflect the regional stratigraphy.

S-type lobes at the top of B1 and B2 reflect emplacement by juvenile breakouts and less pronounced inflation, possibly in close to vent areas (Thordarsson and Self, 1998). Clastogenic lava and spatter deposits were not observed, but possibly proximal S-type facies are more frequent and thick in the center – southeast of the research area. This means any magmatic vents could be located near these regions.

S-type lobes that precede interflow units can also indicate that further inflation was hindered by an early shift from effusive to explosive eruption styles. However, it is unclear how continuous volcanic activity was from basalt emplacement to interflow deposition.

At the upper end of B1 and B2, autoclastic breccias overlie S-type lobes and inflated pahoehoe lobes. These autoclastic rocks are essentially rubbly *pahoehoe* breccias, although they do not correspond to thick "simple rubbly *pahoehoe*" flows produced by very high effusion rates (Duraiswami *et al*., 2008; Óskarsson and Riishuus, 2014; Marshall *et al*., 2016; Rossetti *et al*., 2018). Instead, they are better correlated to rubbly and slabby *pahoehoe* in compound and hummocky flows, like some of those described in the Deccan Province (Duraiwsami *et al*., 2014) and in modern lava-flow fields like parts of holocene Holuhraun (Perdersen *et al*., 2017) and 1975-1984 Krafla Fires (Aufaristama, 2015) lavas in Iceland.

However, due to the minimal inflation presumed by S-type lobes, another possibility is that some of these rubbly-like breccias underwent various degrees of weathering and exposure before deposition of the overlying interflow sequences, and hence could also be paleosoil horizons. This interpretation, however, can be masked by conspicuous present day weathering as well (Duraiswami *et al*., 2008).

Because autoclastic breccias are formed simultaneously with lava flows, they were not included as interflow sequences, as these are unconformity bounded units that bear chronostratigraphic significance. Another major difference between autoclastic breccias and true interflow breccias is that the framework of autoclastic breccias was formed by in situ fragmentation and deposition, being essentially autochtonous. In other words, it hasn't undergone major transport after it's parental lava flow has stopped moving, likely retaining most of the original autoclastic clast-supported fabric even after eventual posterior matrix infill and deposition. Minor framework displacement (clast pull-apart) can be caused in situ by sandy matrix infill or mud expansion and contraction, as pointed out by Rosa *et al*. (2016). Original autoclastic fabrics may be significantly modified as well due to posterior alteration (Allen, 1988). However, currents strong enough to significantly displace framework would likely erode an in situ autoclastic breccia and generate a very distinct fabric in a resedimented autoclastic deposit, similarly to what is found in typical associations of in-situ and resedimented hyaloclastite (Kano *et al*., 1991; McPhie *et al*., 1993; Watton *et al*., 2013).

In the Paranapanema Fm. flows, features such as pipe vesicles and vesicle horizons, as well as lateral variations from single to multiple sheet flows in a same unit, suggest that they flows were emplaced as flow-fields similar to B1 and B2, but which otherwise underwent larger degrees of inflation. This is similar to the proposed genesis of many sheet flows in Columbia River (Self *et al*., 1997, 1998; Thordarsson and Self, 1998). More typical "simple flows" could be represented by rubbly pahoehoe flow-units in B3 and B4, but they are lateral variations of unbrecciated sheet flows. These suggest that surges during effusive activity or other local-scale shearing processes were responsible for breccia formation. Conversely, similarly thick flows with thinner vesicular crusts were probably generated by shorter-duration, higher-effusion eruptive episodes.

4.7.2 Hydromagmatic eruptions and tephra deposition

The stratigraphic and sedimentologic characteristics of interflow units indicate that at least four explosive mafic and dominantly hydromagmatic eruptions took place in Sertanópolis, generating most of the facies described in I1, I2, I3 and I4.

4.7.2.1 Sedimentologic and stratigraphic evidences of hydrovolcanism – tuff successions

At the western and eastern sections of the research area, dozens of outcrops of tuffs and lapilli-tuffs (with some horizons of tuff-breccias) were described. These tuff beds were categorized under the I1, I2, I3 and I4 units, which are somewhat regularly separated by 20 - 40 m thick effusive volcanic gaps between them (Figure 4.10) that correspond to basalts of the Pitanga and Panapanema formations.

The various dune-related structures of the Tw and LTw facies include cm-scale foreset and backset cross lamination, as well as ripple drift laminations with preserved low amplitude ripple bedforms and sandwave beds, which can collectively be interpreted as lower and upper flow regime structures produced by concomitant traction (bedload) and suspension deposition by a steam + gas medium. A similar interpretation can be drawn from the undulated and plane-parallel laminae of the Tp facies.

Despite their high content in accessory siliciclastic ash, however, these lithofacies should not be mistakenly interpreted as epiclastic sedimentary deposits. The conspicuous presence of submillimetric and oblate vesicles, clearly distinguishable <0.2 - 2 mm ash aggregates and fine ash to lapilli-size dense basalt and tachylite fragments - in association with dune-related structures -strongly indicates a pyroclastic and hydromagmatic origin for these beds.

These features are typical of traction (turbulence) dominated pyroclastic density currents, which are relatively deflated and dilute. Dilute PDCs (surges) are common in many explosive hydromagmatic deposits, especially the medial tephra blankets associated with monogenetic or "small" volcanoes (White and Ross, 2011), such as maars and tuff rings. In Sertanópolis, the relatively small thickness (1 - 2 m) of the pyroclastic interflow deposits and the facies associations are all consistent with tephra deposited by small hydromagmatic volcanoes. Most interflow units have recorded clearly distinguishable features of such variably dilute PDCs, including the vertical and lateral associations of the Tw, LTw and Tp facies. Likewise, more concentrated and cohseive surge deposits are evidenced by associations of Tm, LTm, Tds, LTds and TBs facies.

The TBs facies is characterized by matrix-supported and usually fluidal blocks and lapilli (1 - >10 cm) in a stratified tuff matrix, which is essentially identical to beds

of Tw and Tp. These isolated blocks are thought to have been transported inside PDCs (Wohletz and Sheridan, 1983; White, 1991; White and Schminke, 1999; Smith and Kokelaar, 2013), rather than being deposited as ballistic ejecta, given the frequent presence of isolated large blocks (>10 cm wide) in tuff beds over 6 km far from the only known vent-like succession. They could be accidental lithics ripped from an underlying volcanic substrate, or could be derived from the mixing between concentrated and dilute turbulent zones in partitioned PDCs or progressive dilution and reworking by multiple PDCs. These tuff-breccia horizons are also different from the massive tuff-breccia facies described in Graettinger and Valentine (2017), which the authors interpret as the initial ballistic deposit produced at the start of a discrete explosion.

Nevertheless, in medial surge beds, more subtle centimeter to decimeter scale variations in grain-size, bedding, componentry and sorting indicate that these were deposited by progressive aggradation related to multiple (and perhaps at some point pulsing and unsteady) PDCs (Vazquez and Ort, 2006; Valentine and White, 2012; Smith and Kokelaar, 2013; Graettinger et al., 2015; Graettinger and Valentine, 2017). Lateral variations in dispersal of energic surge facies, such as TBs and LTds – Tds (which "skip" some of the measured sections, Figure 4.9) also support a scenario of multiple PDC lobes, which must have had variable aspect ratios, covering different depositional areas. This is likewise strongly suggested by laminae-scale variations in ash aggregate proportion, size and componentry, more clearly observed in I2 and I3. These variations were probably produced by different cosurge ash clouds or drifting plumes, related to multiple discrete explosions during each hydromagmatic eruptive episode.

Furthermore, facies characteristics of Tw, LTw, TBs and Tp are consistent with relatively dry surge deposition (Sohn and Chough, 1989; Sohn, 1996), but presence of vesicles has usually been considered a feature of wet deposits (Lorenz, 1974; Wohletz and Sheridan, 1983). Likewise, plastered tuffs rich and mud and mica, which are found at the base of some interflow successions, are indicative of water-saturated deposition (Rosi, 1992). These typically grade into progressively drier, but still vesiculated beds of the aforementioned facies.

The LTm, Tm, LTds and Tds facies are typical of proximal to medial surge deposits, likely produced by collapsing vertical columns transitioning to lateral PDCs (Branney and Kokelaar, 2002; Ross and White, 2005; Vazquez and Ort, 2006) or

directly emplaced by lateral blasts (Belousov *et al*., 2007; Lube *et al*., 2014; Valentine *et al*. 2015a; Graettinger *et al*., 2015). Massive or diffusely stratified tuffs are usually considered to be the products of wetter surges (Sohn and Chough, 1989; Sohn, 1996) but vesicles are absent in many Tm and LTm outcrops. This can be tentatively related to effective slurrying of ash in water-saturated conditions, followed by rapid solidification and hardening, leaving no time for vesicle entrapment. However, the presence of "dry" particle-cluster-like aggregates and absence of mica further complicates interpretations regarding Tm facies in Sertanópolis.

However, the dispersal of these facies, which are thought to be produced by relatively cohesive and energic currents, helps indicate provenance from a conduit near the eastern sections, where LTm is the dominant interflow lithofacies in I1 and I3. Lateral facies variations into LTds and Tds (NS and FO sections) in I3 suggest progressive dilution to the west, at about 6-7 km from a possible conduit. If a similar polycyclic conduit is considered for I2 (see Section 4.7.2.3), then it can be said that these relatively concentrated surges progressed further west in I3 than during the eruption of I2, which is marked by beds of the Tw and Tp facies near the NS section. Likewise, I4, even if now poorly exposed, may have been produced by the most energic of all eruptions, since beds of the Tds facies are found up to ~7 km away from the AM section, with a transition to relatively drier and less cohesive surges only somewhere close to AH (Figure 4.9), 8 km west from AM and SI.

Although this general trend may imply that explosions became more violent from I2 to I4, this interpretation must be considered cautiously, as the lack of more continuous exposures or closely spaced outcrops render it rather imprecise. This is further complicated because outcrops of near-vent successions, which should be used to calibrate this hypothesis, are scarce. Likewise, conclusions of the same nature are not easily drawn from the I1 bed, not only because outcrops of the unit are sparse, but also because it's primary features may have been significantly altered by post-depositional hardening and weathering.

Furthermore, singled-out and clearly distinguishable fallout tuffs are not considerably frequent in Sertanópolis, perhaps due to erosion of the top of pyroclastic depositional sequences, which frequently include them (Smith and Kokelaar, 2013; Lucchi *et al*., 2018). Fallout tuffs (Tlg) are characterized by a rhythmite-like stacking of gradational laminae, which includes a repeated pattern of vesicular regions in the coarser ash domains of each lamina, which are separated by

vesicle-less mud-grade domains. Vesicles are elongated parallel to the somewhat disturbed and wriggly mantle-bedding. Syn-depositional fluids, responsible for vesicle formation, eventually managed to escape through localized soft-sediment faults, forming gas-escape conduits and larger, coalesced bubbles that sometimes seem to have "popped out" of tuff beds.

Vesicles in some medial to distal tuffs have been explained as products of deposition by "mudrain" and fallout of water-saturated aggregates (coalesced pellets according to Van Eaton and Wilson, 2013), which were eventually liquefied by syn-depositional fluid percolation and slurrying, resulting in the respective vesiculated fabric (Rosi, 1992). Bedding in these deposits has been interpreted as the result of splashing of less consolidated "mud droplets". Considering that wet plumes are efficient ash aggregate factories, the liquefaction hypothesis can indeed partially explain the fabric in Tlg tuffs, and in any case a nearly water-saturated origin is highly likely for these beds (Lorenz, 1974; Wohletz and Sheridan, 1983; Rosi, 1992; Capacionni and Coniglio, 1996). We also note that the rhythmite-like structure is suggestive of an even greater degree of free-water activity, which could perhaps be responsible for complete liquefaction and slurrying of any aggregates, with consequent suspension settling controlled sedimentation.

Lastly, cm-thick close-packed and fluidal clast breccias on the contact between lava flows and underlying interflow beds were interpreted as flow peperites, produced by the dynamic hydrovolcanic interaction between wet, unconsolidated interflow tuffs (or commonly reworked beds of Ss and RTm facies) and inflating lava flows. Peperite-related features include: chilled fluidal clast margins; fluidized clastic matrix; deformed matrix lamination, which is frequently squeezed between blocks; local neoformed clay mineral or mud matrix - which commonly forms laminae and "envelopes" that mark the extent of interaction; overlapping veins or injections with zeolites or extremely fine ash matrix.

It is important to note that peperite-related fluidization has formed a considerably different fabric than fluidization related to wet hydromagmatic deposition. Additionally, although vesicle formation is a common phenomenon in the clastic matrix of some peperites (White *et al*., 2000; Skilling *et al*., 2002), it does not explain vesiculation both in the medial interflows and in the eastern I2 breccia sequence. Vesicles are present throughout entire tuff beds, in portions that are otherwise clearly unaffected by any peperites, such as above the contact with

underlying flow-top breccias. Peperite domains, however, are restricted to cm-thick regions on the top of interflow units, immediatelly below the contact with overlying basalts. Conversely, vesicle horizons are conspicuous in both fallout tuffs (Figure 4.13C) and surge-related tuffs (Figure 4.4B). Additionally, matrix in peperite domains has commonly partially undergone contact metamorphism and recrystallization, becoming a massive quartzite-like material, devoid of any vesicles or mantle-bedding like structure.

4.7.2.2 Sedimentologic and stratigraphic evidences of hydrovolcanism – near-vent breccia successions

The occurence of dilute PDC tuffs in interflows is a compelling evidence that repeated hydromagmatic deposition intercalated with effusive volcanic activity took place at Sertanópolis. In this context, the best candidates for near-vent records of the systems that fed these eruptions are the scoriaceous breccia beds in eastern I2 sections.

In these proximal I2 beds, it can be very difficult to distinguish between scoriaceous juvenile blocks/bombs and vesicular basalt lithics, but detailed petrographic analysis indicates that both are present (Item 4.6). So far, one of the best possibilities is that the pyroclastic breccia facies are analogous to transitional magmatic to hydromagmatic tephra such as the scoria-rich beds of the Rothenberg volcano in Eifel (Houghton and Schminke, 1986), Lake Purrumbete Maar (Jordan *et al*., 2013), Ukinrek Maar (Self *et al*., 1980, Ort *et al*., 2018), Mt. Gambier Maar Complex (van Otterloo *et al*., 2013, 2014) and the Hopi Buttes Volcanic Field (White, 1991, Graettinger and Valentine, 2017). These deposits collectively indicate a previously overlooked synchronism of magmatic and hydromagmatic activity in many maar-like volcanoes, as well as an overlap of features of hydromagmatic and supposedly typically magmatic fragmentation in particles of their deposits (Ross and White, 2012; Liu *et al*., 2017; Amin and Valentine, 2017; Valentine *et al*., 2017).

However, the sequence of proximal facies in I2 contrasts considerably with other typical proximal high-energy hydromagmatic breccia deposits. Important differences include the fact that structureless block and lapilli dominated sets or matrix-supported massive breccia domains are not frequent in the sequence – only some dm-thick beds of the Bmds, TBmds and Bmc facies are present in the SI section, and similar features have been found in laterally correlated tuffs. In this

context, massive or crudely bedded matrix domains (TBmds) were interpreted as the result of PDC-related deposition, instead of more typical *en masse* massive breccia deposition by ballistic curtains, debris jets and/or fallback. Breccias with convoluted matrix (Bmc) are interspersed with well-bedded rocks, and therefore cannot be related to peperite domains, which do occur on the top of the proximal I2 succession (Figure 4.10). These are hence thought to be the products of syn-depositional fluidization related to water-saturated and pyroclastic sedimentation.

Wall-rock collapse events, common in hydromagmatic vents, tend to form similar localized matrix-supported lithic breccia fabrics, but these are usually found as somewhat singled-out horizons in near-vent sequences (Nemeth *et al*., 2010). Some laminated matrix breccia beds are also described in some proximal maar sequences (Weinstein, 2007) but these typically form individual horizons in the middle of finer-grained tuff or lapilli-tuff deposits.

The remarkable sets of the TBlg facies are also different from typical bedded diatreme facies, which are usually formed by better sorted lapilli and ash-dominated fallout and surge deposits (White e Ross, 2011; Ross *et al*., 2013; Bélanger and Ross, 2018) or, as proposed recently, couplets of massive tuff-breccias and stratified tuffs, generated by ballistic curtains trailed by dilute PDCs (Graettinger and Valentine, 2017). The rhythmic character of TBlg beds can be compared to the latter, but lamination here is much finer than the cyclic stacking of dm-thick couplets as described in Graettinger and Valentine (2017).

The bimodal and independent character of textures in TBlg - namely the laminated matrix and coarse block framework - suggest that distinct styles of deposition were involved in their formation. This is similarly the case of underlying autoclastic breccias (Bmt), which typically includes an essentially autochtonous framework and matrix of posterior transport and infill. Differently from Bmt, the matrix-supported texture and frequently dispersed or contactless blocks in TBlg indicate allochtonous origin for the framework as well, besides transport and deposition conditions somewhat distinct from the rhythmite-like matrix.

Furthermore, the bimodal and independent matrix and framework fabrics suggest an overlap of additional controls other than the recurrence of cycles of discrete explosions. In this context, beds of TBlg may have been deposited by processes comparable to PDC modified proximal fallout (White, 1991; White and Schminke, 1999; Jordan *et al*., 2013) – which is probably similar in parts to what has

been described in Graettinger and Valentine (2017). Mixed fallout and wind-directed PDCs (Ort *et al.*, 2018), or even "expulsion-driven" PDCs (Graettinger *et al.*, 2015; Valentine *et al.*, 2015a, 2015b; Ort *et al.*, 2018) are other processes that could perhaps be responsible for deposition of the conflicting simultaneously poorly sorted framework and better sorted rhythmite-like matrix. So far, strictly in terms of facies characteristics, one of the best analogues for the TBlg fabric seems to be the succession of matrix-rich beds with isolated blocks of the upper rim sequence in the Hoyo Negro tephra ring, as described in White and Schminke (1999).

The well developed rhythmite-like gradational matrix is an intriguing feature, usually better understood as a product of effective and cyclic deposition by suspension settling. In other words, it could be the product of some degree of subaqueous tephra resedimentation.

Syn-eruptive resedimentation (McPhie *et al.*, 1993; Nemeth and Palmer, 2019) is usually observed in the tephra rings of hydromagmatic edifices, and normally consists in processes governed by gravitational transport (Sohn, 1996, White and Ross, 2011; Kurszlaukis and Fulop, 2013). Tephra resedimentation inside the actual maar craters, with the exception of wall-rock collapse events, is reportedly more frequent as a post-eruptive phenomenon, which typically starts with mass transport deposition and eventually grades into calmer fluvio-lacustrine sedimentation (Kurszlaukis and Fulop, 2013, Onken and Forman, 2017). Presence of water in the crater is therefore a typical condition of post-eruptive settings. However, water-filled craters have been described in some syn-eruptive phases as well (White and Ross, 2011). Furthermore, evidences of primary pyroclastic deposition such as the vesicular/amygdaloidal matrix and presence of well preserved ash pellets in TBlg and TBmds suggest that any resedimentation could have been strictly syn-eruptive.

It is still unclear which of the reported phenomena could have originated conspicuous laminated-matrix breccia deposition like the one recorded in I2. Nonetheless, a hydromagmatic origin is strongly favored for this succession.

Regardless of depositional processes, it is clear that in Sertanópolis very coarse basalt fragments were abundant during at least some parts of the related hydromagmatic events. However, as mentioned in the 4.6 section and in the above paragraphs, it is not very clear how abundant ballistic ejecta were. Although some cm-scale impact sags are apparent in the proximal succession, evidences of ballistic impacts are not inambiguous. In light of the previous discussion, this could be due to

a number of different reasons. The first is that some blocks could have indeed been transported inside PDCs along with ash and lapilli (White, 1991; White and Schminke, 1999, Smith and Kokelaar, 2013), as seems to have been the case in PDC-related proximal TBmds and Bmds facies. Medial surge sequences also show fluidal scoria lapilli and lithic blocks in some horizons with poorly defined or absent bedding sags (TBs facies), probably transported inside the surges as well. This reiterates their correlation with the proximal scoriaceous beds, besides indicating the same degree of "magmatic" influence in the medial surge deposition. However, in the proximal TBlg succession, it is possible that the development of bedding sags related to ballistic ejecta was hindered by the abundant presence of blocks in the substrate, which may render it less deformable than loose ash.

Finally, it is also worth noting that the fabric in TBlg facies, which makes up the bulk of proximal I2 discussed above, is interestingly similar to that observed in sediments of the modern drainage systems found now in the studied area, which consist in muddy-sandy river beds and alluvial bars where some basaltic pebbles have also been simultaneously deposited by gravitational (colluvial) transport. This modern depositional setting is continually producing a somewhat resembling matrix-supported breccia fabric, which includes laminated and moderately well sorted sandy-muddy matrix that hosts a framework of isolated clasts. Considering how pyroclastic fallout and ballistic curtains are processes controlled by gravity, this otherwise strictly sedimentary subaerial gravitational + subaqueous tractive origin can be, in physical essence, similar to that of the I2 breccias. This is an interesting observation on how mixed-origin beds can be formed by the dynamic interaction of two or more transport and deposition mechanisms in both primary volcaniclastic and solely post-eruptive contexts. In the author's view, this is an issue that warrants further studies and comparisons in the Paraná Igneous Province, because these related depositional processes can be confused in the absence of unambiguous evidence of one origin or the other.

4.7.2.3 Conduit geometry and cyclic eruptions

The main breccia sequence of I2 has a radial distribution of about 4 x 2.5 km. In the Água da Morena section (AM) it reaches a maximum measured thickness of about 12 meters, while most other outcrops show few meters thick exposures (Figure 4.8). The only few reliable proximal bedding measurements available indicate <10-

20º dips to W and SW in general, which are mostly consistent with the strikes of laterally correlated tuff beds (which tend to be more subhorizontal).

The proximal I2 tephra thickness and bedding measurements are similar to some reported maars, but the maximum measured thickness can now be smaller than pre-erosional and pre-compaction tephra ring or diatreme thicknesses. The overall volcanic stratigraphy indicates that the main proximal breccia sequence is part of a hydromagmatic volcanic edifice similar to a maar or tuff ring, although original vent or diatreme geometries are obscure. Because of such constraints, it is difficult to infer parameters such as crater diameter/depth and complete diatreme facies architecture. Additionally, possible proximal volcanic facies of B1 and B2 indicate a similar provenance, which may not be fortuitous. However, further information is needed for any inferences regarding this matter.

The proximal or near-diatreme facies succession reveals a prevalence of bedded units, which could represent shallow fragmentation levels (White and Ross, 2011). Facies from a typical deep diatreme weren't observed as of yet, and may be entirely absent in the area, which is consistent with other complexes of shallow coalesced and laterally-migrating maars (Carrasco-Núñez *et al*., 2007; Ort and Carrasco-Núñez, 2009; Jordan *et al*., 2013, Chako Tchamabé *et al*., 2014, 2015). Additionally, the recurrence of intermittent medial pyroclastic surge deposition alternated with effusive activity also suggests polycyclic maar activity. Modern day extension of proximal breccia beds are likewise indicative of vent coalescence, which resulted in a larger than usual complex of craters ("phreatocauldron", as in White and McClintock, 2001, Ross *et al*., 2008; McClintock *et al*., 2008).

The eastern breccia sequence was correlated to the medial and distal tuffs that make up the bulk of the I2 bed in part because of how it grades upward into a fallout tuff (Tlg) directly below B3, a contact that was followed regionally, which means that stratigraphy of the lava flows and remote sensing also helped define this correlation. Additionally, it is still is not clear whether the I2 breccia sequence is part of only an external tephra ring, an upper diatreme or both. If the latter is the case, then subsidence was minor, given that the beds of the proximal and medial I2 outcrop at a similar altitude range. However, due to this polycyclic character, it is possible that part of this breccia sequence was at least in part affected by other hydromagmatic explosions (White and Ross, 2011), and, with further detailed mapping, could potentially be correlated to interflow units I3 and I4 as well. It must be noted that

other clearly proximal regions of I3 and I4 haven't been distinguished yet, and paleocurrent data (even if small) do indicate flows from E to W in I2, I3 and I4 surge beds west of the AM and SI breccia sections as well. Additionally, close to AM and SI sections, limited massive breccia beds cross-cutting B3 basalts are exposed in altitudes above I2, which indicates that some portions of overlying or laterally cross-cutting diatreme/vent facies could still be undiscovered.
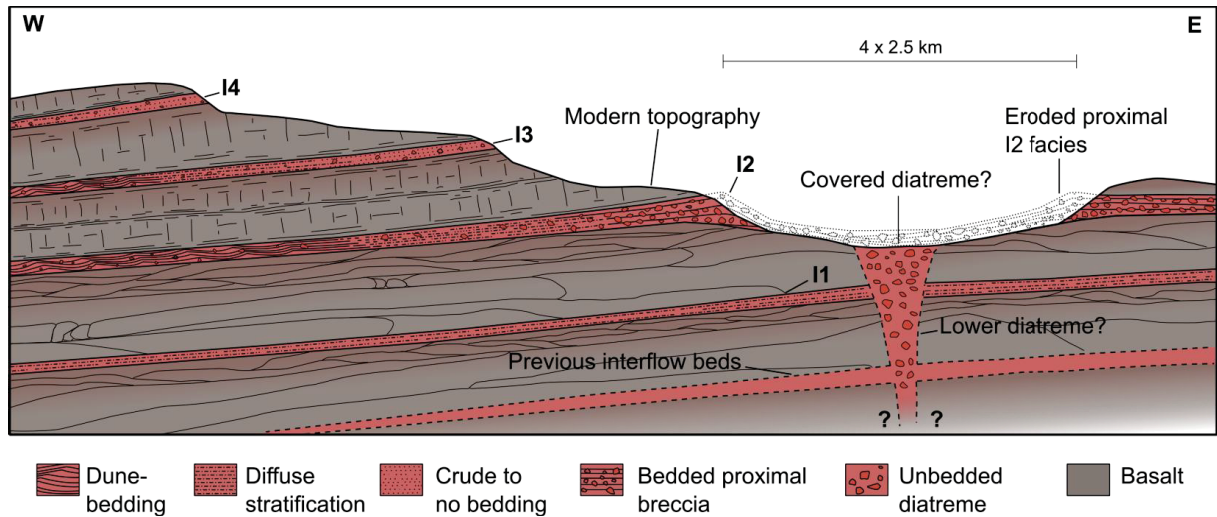
Figure 4.18 – Schematic drawing of proximal facies and possible diatreme geometry during the deposition of I2, considering modern topography.

4.7.3 Reworked volcaniclastic rocks

Reworked volcaniclastic rocks (in broad definition) at Sertanópolis include secondary resedimented tuffs and volcanogenic (epiclastic) sediments. These occur as centimeter to decimeter- thick beds at the upper end of interflow successions, and are frequently involved as matrix in peperites. The RTm facies is texturally very similar to underlying primary surge tuffs, being characterized by mixed mud and variably angular fine accessory ash with matrix-supported lapilli-sized basalt fragments. Lapilli-sized fragments are present in varied proportions in resedimented and epiclastic beds (Figure 4.12B), and in resedimented tuffs they are identical to underlying primary pyroclasts (Figure 4.14A).

Differently from cosurge fallout beds, these massive beds have no preserved aggregates or vesicles, a feature that was interpreted as the result of transport and deposition by sedimentary processes. However, small degrees of reworking and gradual transitions from underlying primary tuffs suggest that these have been syn to post-eruptively resedimented.

Facies characteristics are consistent with deposition by moderately cohesive and concentrated flows. In a hydromagmatic setting, syn to post-eruptive resedimentation may include the occurrence of mudflows and sheetwash derived from water-saturated primary deposits (Walker, 1981; Wohletz and Sheridan, 1983).

The most clearly distinguishable reworked volcaniclastic rocks typically occur as centimeter to decimeter thick epiclastic sandstone (Ss) beds above primary tuff successions in interflow outcrops (figures 4.12B, 4.14B). They are comprised by siliciclastic fragments similar to underlying tuffs, but sand size quartz and vitric clasts are usually subrounded and better sorted. Well sorted portions and rounded fragments are present in underlying pyroclastic tuffs, but in reworked beds they form well defined laminae, while in tuffs they are randomly mixed with other less sorted crystalloclasts and mud grade-ash. Lapilli-sized basalt fragments in epiclastic sandstones are subrounded and never show cuspate or vesicular margins. They also typically include more crystalline basalt lithics, likely derived from erosion of lava flows.

Epiclastic deposits, differently from resedimented ones, must have been formed by longer-lasting background sedimentation processes in inter-eruptive times (Kataoka *et al*., 2009; Nemeth and Palmer, 2019). Sedimentological evidence suggests that in Sertanópolis they were at least partially formed by subaqueous tractive currents with frequent variations in flow competence, responsible for intercalation of well sorted fine sand and less sorted granule-bearing laminae. These variations have been interpreted as the result of fluctuations in regular stream flow or ephemerous concentrated flows in fluvial settings. Additionally, some authors have reported a fluvio-aeolian origin for interflow beds of the Serra Geral Group (da Cruz, 2019). At Sertanópolis, aeolian beds have not been identified.

Reworked volcaniclastic deposits are common accompaniements to pyroclastic deposits in all volcanic environments, including CFBPs (White *et al*., 2009, White and Ross, 2011) - which is a depositional result of the very sudden increase in sediment supply rates in such settings (Kataoka, 2005; Kataoka *et al*., 2009; Manvile *et al*., 2009; Nemeth and Palmer, 2019). This abnormal increase in sedimentation rate is characteristic of syn-eruptive to immediately post-eruptive periods, and may in some times result in a better record of regular depositional processes than actual background sedimentation (Sohn and Yoon, 2010). In Sertanópolis, the scarcity of clearly defined background sediment deposits complicates this comparison, while

further suggesting that inter-eruptive times were dominated by erosion rather than deposition.

According to some authors, the fluvial facies of some post-volcanic Bauru Group sedimentary rocks have been deposited by southwestward flowing rivers much like the modern drainage systems, which flow away from the sea due to a regional dip towards the basin centre and the uplift of the Serra do Mar region, to the east of the Paraná and Bauru basins (Fernandes *et al.*, 2015). However, the Serra do Mar uplift only occurred during the sedimentation of the Bauru Basin, which means that syn-volcanic rivers must have flowed east, towards the opening South Atlantic Sea – an interpretation that is supported by the stratigraphy of the marginal Santos basin (Moreira *et al.*, 2007).

In Sertanópolis, the only recorded drainage systems must not have been very extensive, having carried essentially intrabasinal (volcanogenic) material, which is consistent with a degradational and low accomodation setting with intermittent fluvial activity. This contrasts considerably with the fault-bounded epiclastic deposits of the Jacuí Group, which overlie the main PIP lavas in the state of Rio Grande do Sul (Riccomini *et al.*, 2016).

4.8 Discussion

4.8.1 Sourcing of accessory siliciclastic material and wall-rock lithics

The lesser contribution of massive basalt blocks, along with the predominance of siliciclastic accessory ash suggests explosion *loci* may have been restricted to horizons of more porous vesicular basalts and previous unconsolidated to consolidated interflow deposits, which is also evidenced by the occurrence of tuff lithics. Such horizons must have acted as aquifers confined between less permeable massive basalt zones that must have allowed for effective hydromagmatic fragmentation of both accessory and juvenile material. It is likely that hydromagmatic fragmentation was hindered when magma columns reached less permeable levels, and volcanic activity changed to magmatic lava fountaining or simply to effusive lava flowage (Valentine and White, 2012; Kereszturi and Nemeth, 2012; Onken and Forman, 2017). This general setting is consistent with restricted vertical migration of explosion *loci* during individual eruptive episodes. Similarly, lateral migration is a typical feature of coalesced maars in soft-substrate (White and McClintock, 2001;

Sohn and Park, 2005; Nemeth *et al*., 2010) or mixed-substrate settings (Ort and Carrasco-Núñez, 2009).

In Sertanópolis, siliciclastics are records of intrabasinal and pyroclastic transport deposition, and siliciclastic-rich sedimentary beds are actually reworked volcanogenic deposits. This contrasts with the interpreted origin of Jacuí Group epiclastic deposits in Riccomini *et al*. (2016), which consider them to be mixtures of extrabasinal (siliciclastic) and intrabasinal (volcanogenic) material.

In Sertanópois, this accessory material was derived from previous interflows, which may have been deposited in settings similar to Sertanópolis or in other sorts of inter-eruptive environments. Tephra rings in monogenetic (or small) hydromagmatic volcanoes have been shown to be usually formed by explosions at smaller than ~250 m depths (Valentine *et al*., 2014; Graettinger *et al*., 2015; Valentine *et al*., 2017), which means that deposition of the first mapped tuffs (I1 and I2) probably involved fragmentation levels at the previous last interflows of the Pitanga formation (not mapped), with this recycling trend continuing during I3 and I4.

The provenance of siliciclastic material in these other interflows is more obscure. Mineral assemblages suggest extrabasinal sources, perhaps similar to the sources of the pre and post volcanic Botucatu and Bauru lithostratigraphic units, which were deposited in mainly arid and semiarid environments, respectively (Scherer, 2002; Fernandes *et al*., 2015). This has been shown to be true for the first aeolian sandstone interflows of the Serra Geral Group, produced by the remnants of the once large Botucatu erg, which was gradually buried by the PIP lavas (Jerram *et al*. 2000; Jerram and Stollhofen, 2002; Scherer, 2002). However, data regarding palaeoenvironments and sedimentary provenance in more intermediate PIP interflows is lacking, and a connection between these sources cannot be sufficiently well established as of now.

4.8.2 Volcanic palaeoenvironments and water availability

In Sertanópolis, the hiatuses between effusive volcanic activity have been marked by explosive hydromagmatic deposition. A progressive aggradation by discrete explosions and multiple PDCs origin is supported by observed facies characteristics, which is consistent with several authors' observations on "monogenetic" hydrovolcanism (White and McClintock, 2001; McClintock *et al*., 2008; Valentine and White, 2012; Graettinger and Valentine, 2017; Onken and Forman,

2017). The absence of clear depositional gaps (such as paleosoils) in the middle of pyroclastic successions suggest that no significant eruptive pauses occurred during the respective sedimentation of each unit; however, such unconformities could well have been wiped by post-eruptive erosion.

Time breaks between single-vent eruptions in Cenozoic polycyclic maar-like volcanoes have been reported at a very wide range, from days or months (Self *et al*., 1980; Kienle *et al*., 1980; Leat and Thompson, 1988; White and Houghton, 2000; White and Ross, 2011; Ort *et al*., 2018) to tens -hundreds of thousand years (Freda *et al*., 2006; Sottili *et al*., 2009; Chako Tchamabé *et al*., 2015). In Sertanópolis, it is possible that individual eruptive episodes lasted for a few days at minimum (following Kienle *et al*., 1980; Leat and Thompson, 1988), each resulting in the deposition of a respective interflow unit. Individual eruptions were comprised by several discrete explosions, which produced at least up to 1.5 m thick surge deposits as far as 6-7 km away from the only known possible vent in the region. Breaks between eruptive episodes corresponded to periods of overall volcanic quiescence that may have lasted for as much as tens to hundreds of thousand years (Hole *et al*., 2013), resulting in reworking and erosion of the tuff successions in degradational settings and likely removing part of the original tephra thicknesses.

We infer that explosive eruptions were controlled by subterranean water availability in up to 250 m deep aquifers. Arid settings are typically characterized by depleted water tables at depths that may be as large as >250 m (Bonsor and MacDonald, 2011; MacDonald *et al*., 2012), but which can be abruptly changed by flash floods (Grosjean *et al*., 1997; Houston, 2002; Grosjean and Veit, 2005). In the Atacama Desert, one of the driest in the modern world, a mean annual rainfall of <10 mm.year^{-1} was registered from 1975 to 1991 in altitudes below 2000 m (Houston, 2002, Nester *et al*., 2007). Considerably higher precipitation rates are focused on intense torrents that typically last for several days, resulting in mean rainfall rates of > 20 mm.day^{-1}. In the Chacarilla catchment, in Atacama, flash floods caused by this magnitude of rainfall have reportedly resulted in aquifer recharge volumes of up to 25,000,000 m³ (Houston, 2002).

In the Eastern Desert in Egypt, similar recharge volumes are believed to be supplied by floods that occur roughly every 40 months (Gheith and Sultan, 2002). In the PIP, if sufficient infiltration was possible, water recharge of this same order might have been enough to create the settings required for magma-water interaction during

similarly seasonal events. Considering the whole span of geological time encompassed by this igneous province, it seems likely that overall arid settings would not have obligatorily precluded explosive hydromagmatism.

However, arid settings weren't necessarily dominant during syn-volcanic times altogether. This is highlighted by the conspicuous presence of interflow deposits that, in one way or the other, must have been deposited in somewhat humid settings (Waichel *et al*., 2006, 2007; Luccheti *et al*., 2014; Machado *et al*., 2015; Rossetti *et al*., 2018; Moraes and Seer, 2018). We reiterate that further studies are needed if we are to better understand the origin of the water that was unquestionably part of syn-volcanic history. This is especially important because this environmental change may have been related to the volcanic systems themselves, possibly in ways similar to the phenomena referred to in Hartmann *et al*. (2012) and Hole *et al*. (2013), which include expulsion of deep aquifer water in hydrothermal springs in the PIP and the North Atlantic Igneous Province, respectively.

4.8.3 Tectonic controls on emplacement and current geometry of the Sertanópolis deposit

The current geometry and exposure of the Sertanópolis interflow beds is a result of the interplay between (i) syn-depositional tectonics and sediment supply rates and (ii) post-depositional deformation, uplift and erosion. Like all magmatic activity in the Paraná province, eruption of the Sertanópolis maar-like craters was likely conditioned by major volcanic lineaments. At the PIP, most models have considered that regional structures that are perpendicular to the initial Paraná Basin rift axis controlled most of the fissural magmatic activity (Szatmari and Milani, 2016; Foulger, 2018). This includes the predominantly NW-SE faults of the Ponta Grossa Arch in Paraná. However, some alternative models have questioned the prevalence of NW-SE structures as the predominant magmatic conduits (Licht and Arioli, 2018).

In Sertanópolis, NW-SE, NE-SW and E-W directions show major structures, while N-S structures are smaller aligned lineaments, probably related to Cenozoic intraplate distension in South Brazil overall (Sowinski, 2016). NW-SE structures could be related to post-volcanic distension in the Ponta Grossa Arch (Gomes *et al*., 2018), while NNE and NE lineaments are likely the result of tectonic movements according to Precambrian basement beneath the basin (regardless of timing). In the syn to

post-volcanic Jacui Group, a continental-rift–related NE-SW trough has likely conditioned pyroclastic and volcanogenic sedimentation (Riccomini *et al*., 2016).

This discussion lies beyond the scope of this work, but it must be noted that tectonic controls must have varied considerably from the full-on continental rifting at modern day continent margins to more restricted lineament-bound tectonically active zones in the continent interior, resulting in rather complex interplays of uplift and subsidence (Ukstins Peate *et al*., 2003; Milani, 2004). This likely played a big role in constraining depositional and vulcanological activity, while also creating the offsets that now complicate much of the regional stratigraphic correlations between lava piles (Gomes *et al*., 2018).

4.8.4 Regional stratigraphic significance

Interflow deposits of the Paraná Igneous Province have been widely regarded as either products of aeolian deposition continued from the desertic settings of the underlying Botucatu Formation (Jerram and Stollhofen, 2002; Petry *et al*., 2007), peperites derived from passive lava flow – wet sediment interaction (Waichel *et al*., 2007; Luchetti *et al*., 2014), restricted fluvio-lacustrine sedimentation (Waichel *et al*., 2007; Ricommini *et al*., 2016; Moraes and Seer, 2018) and overall sedimentary infill of matrix in autoclastic breccias (Rossetti *et al*., 2018).

The data we present here suggests a rather different perspective, which favors the hypothesis of significantly larger involvement of explosive hydromagmatic deposition controlled by maar-like volcanism (Licht, 2012). This approximates the volcanic history of the Paraná province to that of other CFBPs in the world (White and McClintock, 2001; Ross *et al*., 2005). Additionally, we suggest that some previous interflow characterizations may need to be reassessed in light of this hypothesis, and that hydromagmatic deposits are underrepresented in many of them.

Some of the diagnostic features of explosive hydromagmatic deposits in Sertanópolis have in fact been observed in other interflow deposits in the PIP. This includes the occurrence of various types of ash aggregates, poorly sorted basaltic breccias with siliciclastic matrix and diffusely to well stratified and vesiculated surge and fallout deposits (Licht and Arioli, 2011, 2018; Licht, 2012). Furthermore, in many of these reported volcaniclastic deposits, the prevalence of tuffs with rather constant proportions of dominant fragmented siliciclastic accessory ash (commonly 60-80%), mud-grade or extremely fine ash (5-40%) and subordinate juvenile material in the

form of dense tachylite and sideromelane (5-20%) suggest that most explosive hydromagmatic eruptions were generated by similar hydrological conditions (Chako Tchamabé *et al*., 2015; Valentine *et al*., 2015a), possibily during specific time periods of the PIP evolution.

Is has been evoked that the transition from high-TiO_2 (Type 4) to low-TiO_2 (Type 1 CN) lavas in the state of Paraná strongly accompanies these conditions (Valore *et al*., 2017; Licht, 2018), possibly due to an external control exerted by excess fluorine, which is turn correlated with increased fluidity, external water absorption capability and inherent explosiveness of basaltic melts (Martini, 1984; Licht *et al*., 2015b).

The latest efforts in regional geological mapping of the PIP in Paraná follow a similar reasoning (Licht and Arioli, 2018), indicating a prevalence of explosive hydromagmatism in the lowermost Pitanga Formation and during its transition to the Paranapanema Formation, after which explosive hydrovolcanism was precluded. In the future, if more detailed stratigraphic data on these mafic pyroclastic interflows becomes available, further subdivisions will be necessary to better represent any possible spatial and temporal correlations established between them.

4.9 Conclusions

The geological mapping of mafic volcaniclastic deposits revealed that explosive hydrovolcanism was the dominant supply of clastic material for interflow deposition at Sertanópolis, in the northern Paraná. From this, some key concluding remarks are highlighted:

- Mafic pyroclastic breccias outcrop at a 4 x 2.5 km region. These were interpreted to represent proximal facies of a hydromagmatic volcano. One facies of pyroclastic breccia suggests mixed controls on framework and matrix deposition (TBlg), which could be represented by pyroclastic ballistic fallout with subordinate surge or syn-eruptive resedimentation.

- At least in Sertanópolis, siliciclastic material present in both mafic pyroclastic deposits and their reworked counterparts has not been brought from extrabasinal sedimentary systems, and is in fact accessory ash derived from the wall-rock of maar-like craters, most likely from previous interflow deposits. Furthermore, rounding of siliciclastic grains in these reworked deposits is not a good proxy for degree of reworking. Other textural characteristics of reworked deposits can be used to

distinguish them from primary pyroclastics, such as sorting, proportion of mud and absence of vesicles and aggregates.

- Pyroclastic interflows may be mistaken for sedimentary rocks due to a high content in accessory ash (He *et al.* 2003; White *et al.*, 2009). In some cases, if only resedimented or reworked volcanogenic deposits are present as interflow beds, they can be virtually undistinguishable from extrabasinal sedimentary rocks with lesser volcanogenic (epiclastic) contributions.

- Permeable interflow deposits below the Sertanópolis stratigraphic succession may have controlled hydrological conditions that favored subterranean explosive hydromagmatic interactions. Data suggests that polycyclic maar activity was controlled by lateral vent migration in mixed-substrate settings, which must have resulted in a shallow but wide complex of maar-like craters ("phreatocauldron").

- Ejected tephra rings were likely produced by shallower than ~250 m explosions (Valentine *et al.*, 2014, 2015a; Graettinger *et al.*, 2014; 2015). Facies characteristics of the pyroclastic successions relate them to deeper-than-OSD dominated maars in Graettinger *et al.* (2015). Each eruption was marked by cycles of discrete explosions, producing multiple PDCs ("flow-units").

- Onlap and matrix infill in autoclastic breccias is likely a common feature of volcanic successions in the Paraná Igneous Province. However, it is very unlikely that this process produced matrix-supported fabrics such as the ones in the pyroclastic TBlg and TBmds facies.

- Hydrovolcanic products in Sertanópolis do in fact include flow peperites produced by the interaction between the B2, B3, B4 and B5 lava flows and respective underlying interflow tuffs (Bmig facies). These peperites are generally characterized by a moderately sorted framework, hardened and/or disrupted matrix and cm-thick close-packed beds. They are clearly distinguished from the underlying pyroclastic successions even when these include breccias or tuff-breccias, especially because of their immediate contact with a disrupted parent basalt flow.

4.10 Supplementary material

	34	81	82	35	37	49	50	51	60	68
Sample number	34	81	82	35	37	49	50	51	60	68
Formation	Pitanga					Paranapanema				
Unit	B1		-	B2		B3				
Section	FU			FU		VV			NS	AH
Type	Sheet lobe, top of B1	Thick sheet flow, base of B1	Sheet lobe + S lobes top of B1	Sheet lobe group 1 (first of B2)	Sheet lobe group 2	Thick sheet flow, first of B3	Thick sheet flow, first of B3	Thick sheet flow, first of B3	Thick sheet flow (only B3 flow locally)	Thick sheet flow, top of B3
SiO_2	51,38	50,6	50,34	51,53	52,45	51,53	51,04	50,9	51	48,97
Al_2O_3	12,93	12,53	12,97	12,82	12,96	12,29	12,45	11,62	10,93	10,5
Fe_2O_3	15,34	14,94	15,67	15,18	13,46	15,84	16,68	16,91	16,77	17,19
CaO	9,43	8,86	8,65	9,35	9,17	8,42	9,06	8,66	8,52	8,66
MgO	5,11	4,78	4,79	4,93	4,94	4,75	4,91	5,5	6,18	6,88
K_2O	0,61	1,29	1,48	0,78	0,97	1,22	0,79	1,43	1,29	1,12
Na_2O	2,4	2,39	2,53	2,29	1,96	2,28	2,33	2,27	2,21	1,79
TiO_2	2,1	2,05	2,15	2,2	1,86	2,42	2,48	2,23	2,52	2,39
MnO	0,23	0,21	0,19	0,21	0,18	0,24	0,25	0,22	0,25	0,29
P_2O_5	0,24	0,24	0,25	0,26	0,21	0,29	0,29	0,26	0,31	0,28
LOI	0,78	1,83	0,78	0,87	2,15	0,73	0,23	0,48	0,43	2,42
Total	100,55	99,72	99,81	100,43	100,31	100,01	100,51	100,48	100,42	100,49
Ba	284	268	266	277	241	343	287	248	290	311
Cr	43	44	39	63	77	24	25	62	120	146
Cu	202	214	222	205	198	228	173	143	342	251
Nb	14	13	14	15	13	16	16	14	16	15
Ni	34	32	30	37	40	33	29	39	64	69
Rb	22	29	46	13	46	29	12	46	35	28
Sr	239	233	232	274	309	221	216	196	180	173
Y	38	34	35	35	30	35	34	35	47	35
Zn	109	115	114	111	90	106	113	101	122	117
Zr	153	158	165	168	138	185	181	170	207	176

Table 4.3 – Geochemical data of analyzed basalt samples. Oxides in %, trace elements in ppm.

.
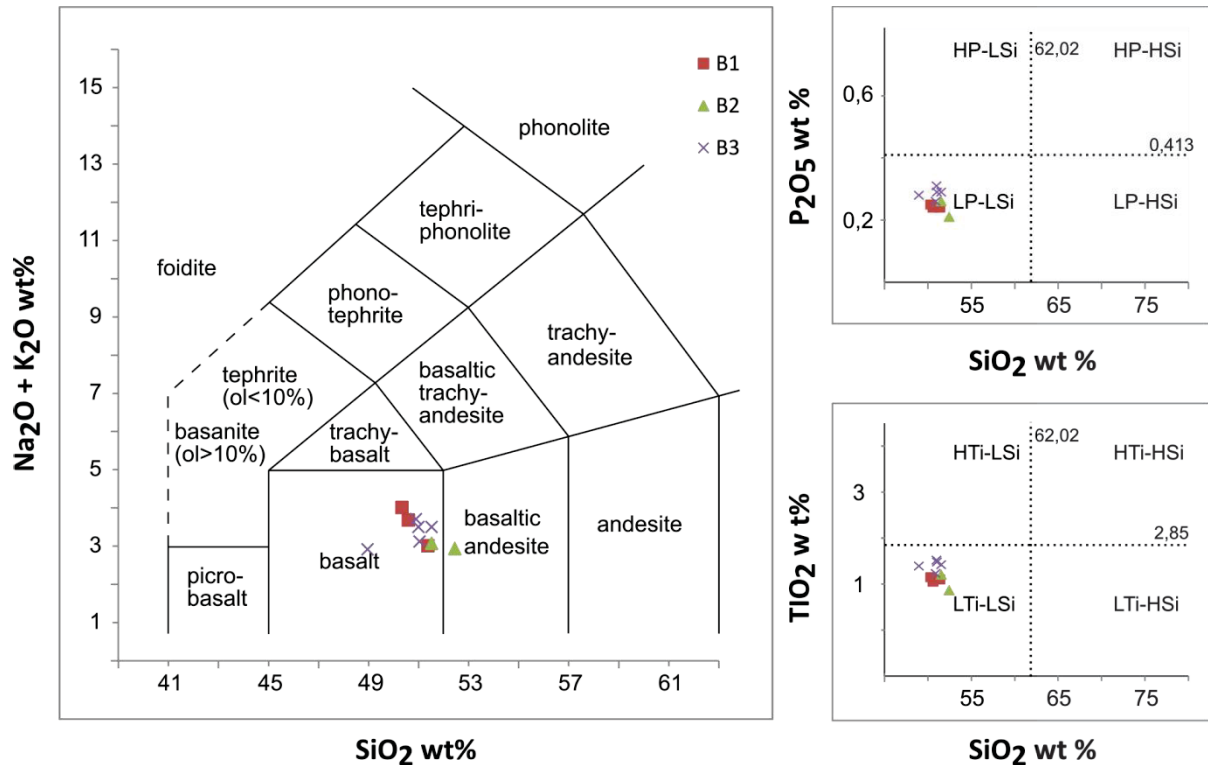
Figure 4.19 – Total alkali *vs* silica (left) classification and division according to the proposed scheme of Licht, 2018 (right).

All analyzed basalt samples were classified as low TiO_2 and low P_2O_5 Type 1 basalts according to the classification scheme of Licht (2018). This contrasts with the regional chemostratigraphic division proposed in that work and in Licht and Arioli (2018), which show incompatible-element-rich types extending as far up in the lava pile as the contact between Pitanga and Paranapanema formations. However, this is simply a matter of scale-related generalization, as lithostratigraphic characteristics of the mapped units in Sertanópolis conform to notions established in the regional lithostratigraphic division of Licht and Arioli (2018). Additionally, lithochemical assemblages may show mixtures and variations between the exact low and high TiO_2 end-members in this division (Gomes et al., 2018; Licht, 2018).

4.20 – Photographs of typical interflow exposures in pasture areas. Note that not all topographic breaks are interflow units.
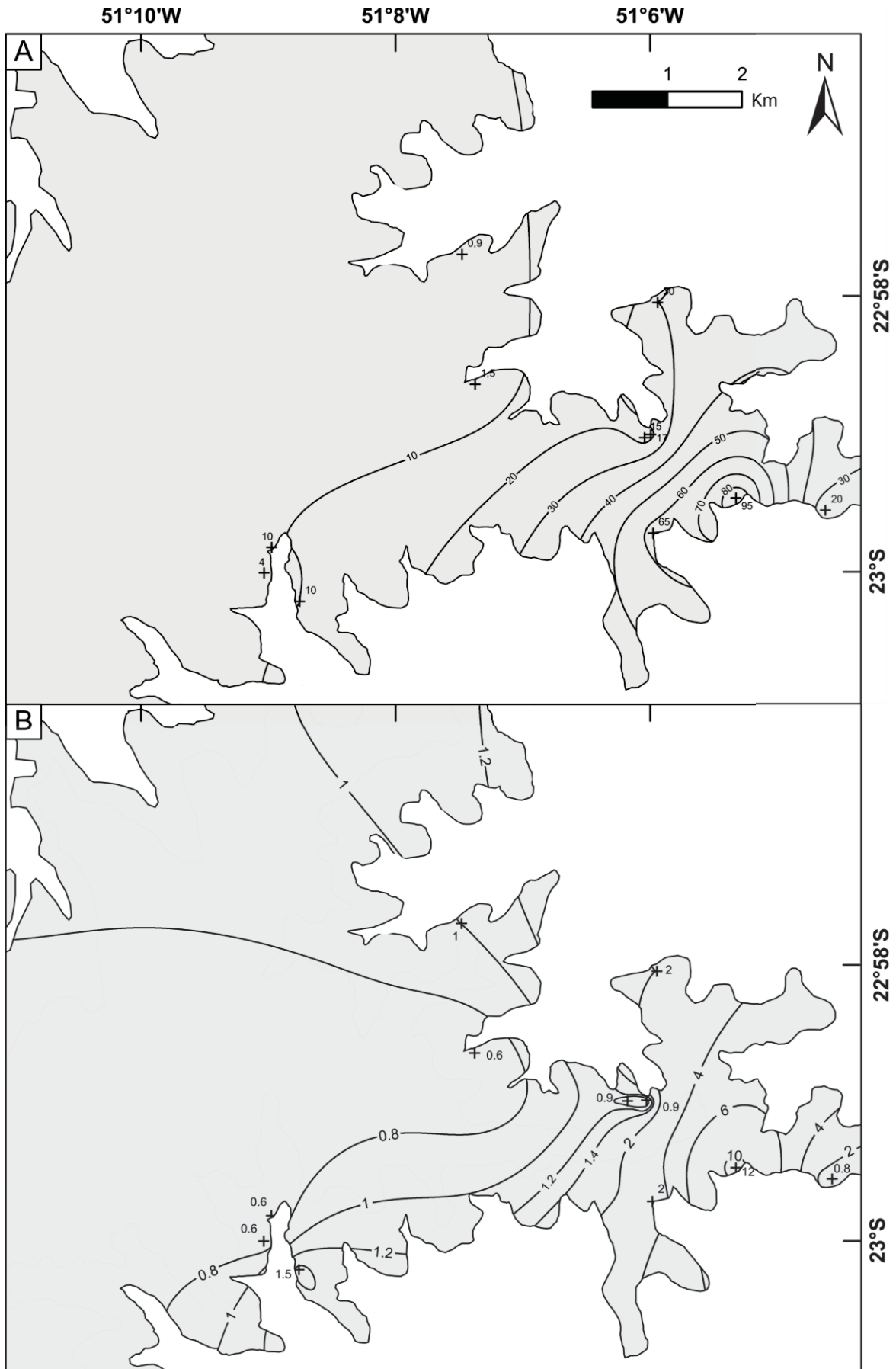
Figure 4.21 – Isopleth of average largest clasts (A, centimeters) and isopach (B, meters) maps of I2.
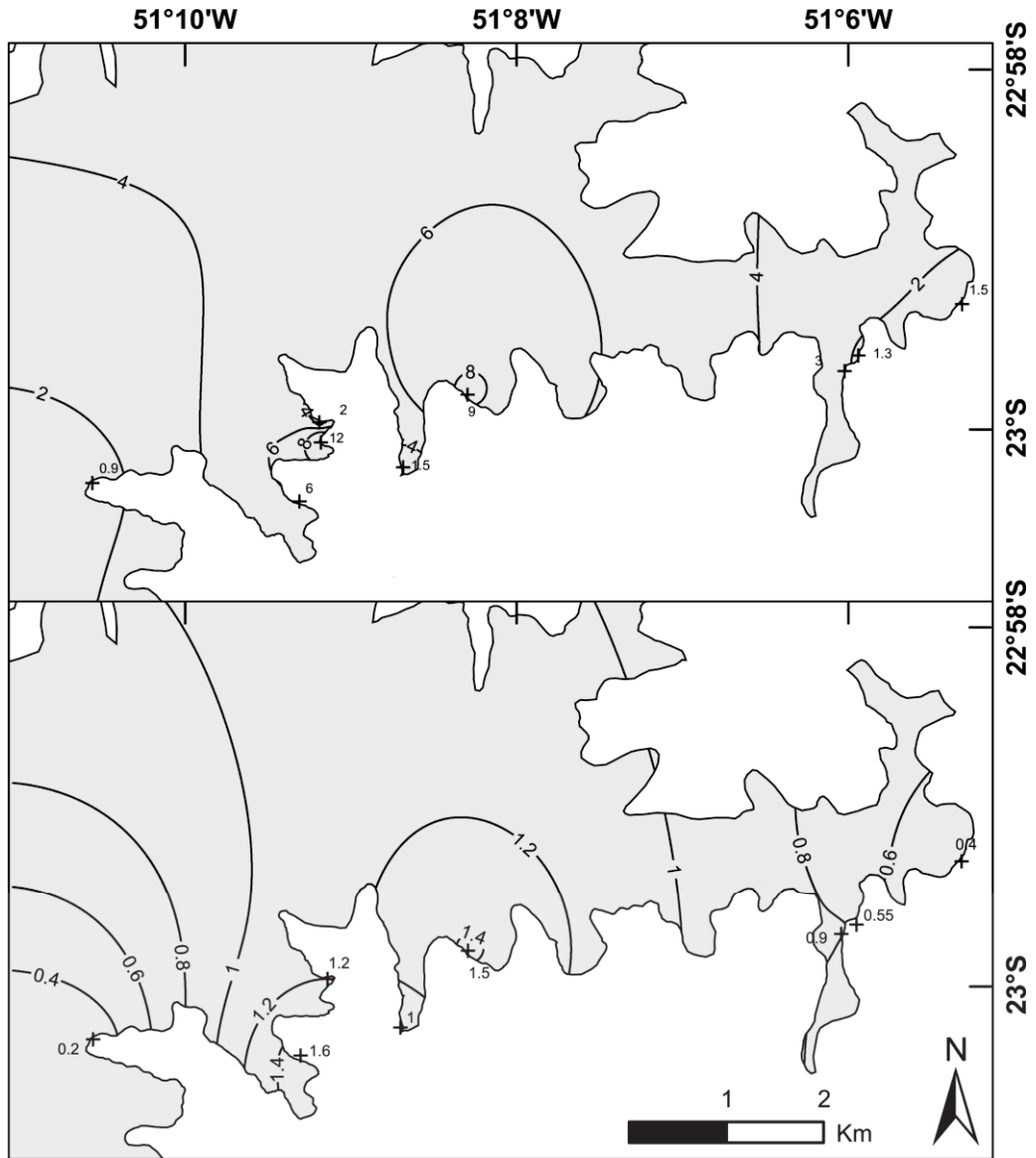
Figure 4.22 - Isopleth of average largest clasts (A, in centimeters) and isopach (B, in meters) maps of I3.
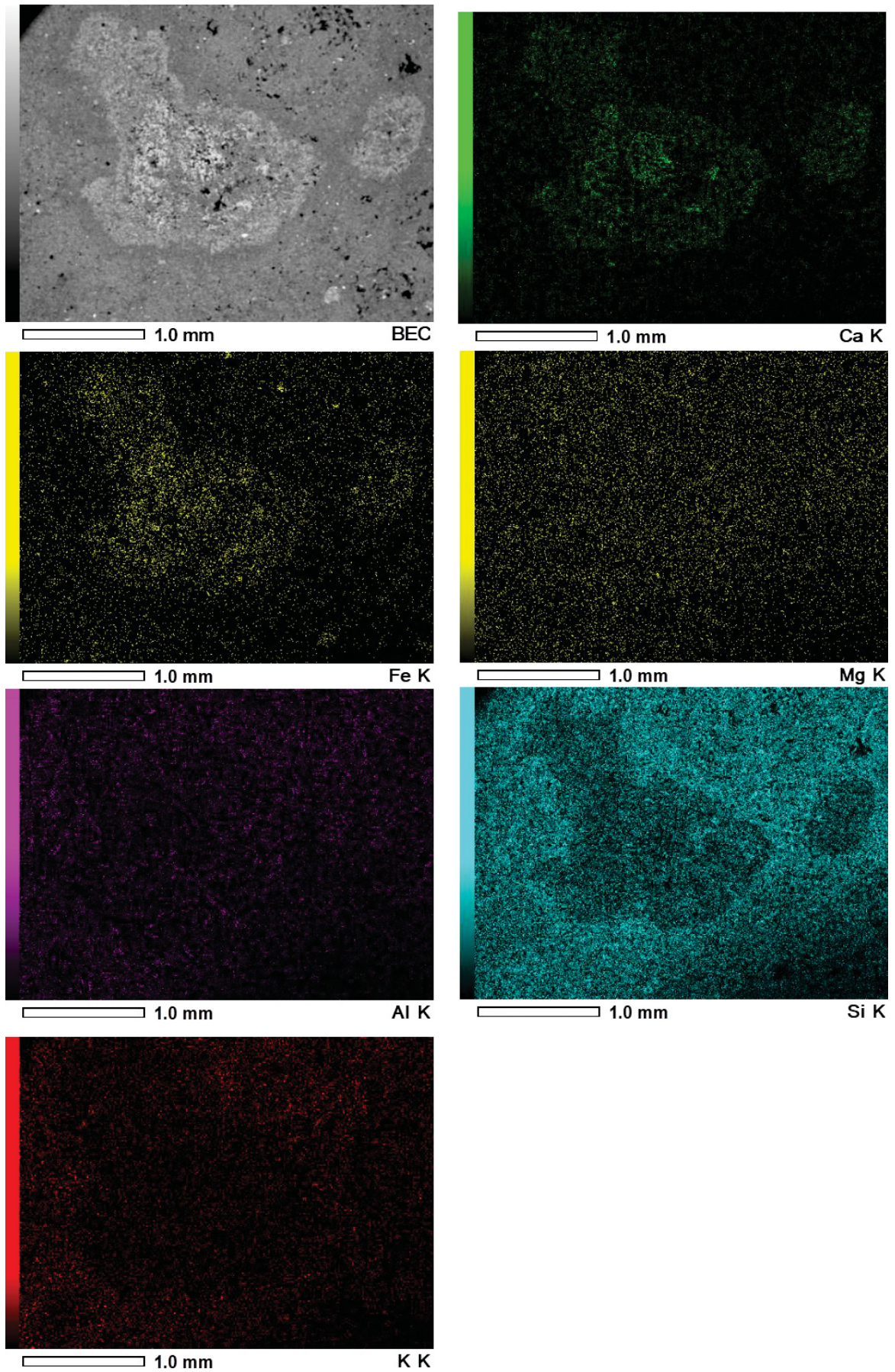
Figure 4.23 – EDS compositional maps in layered aggregate sample from I2 breccia.
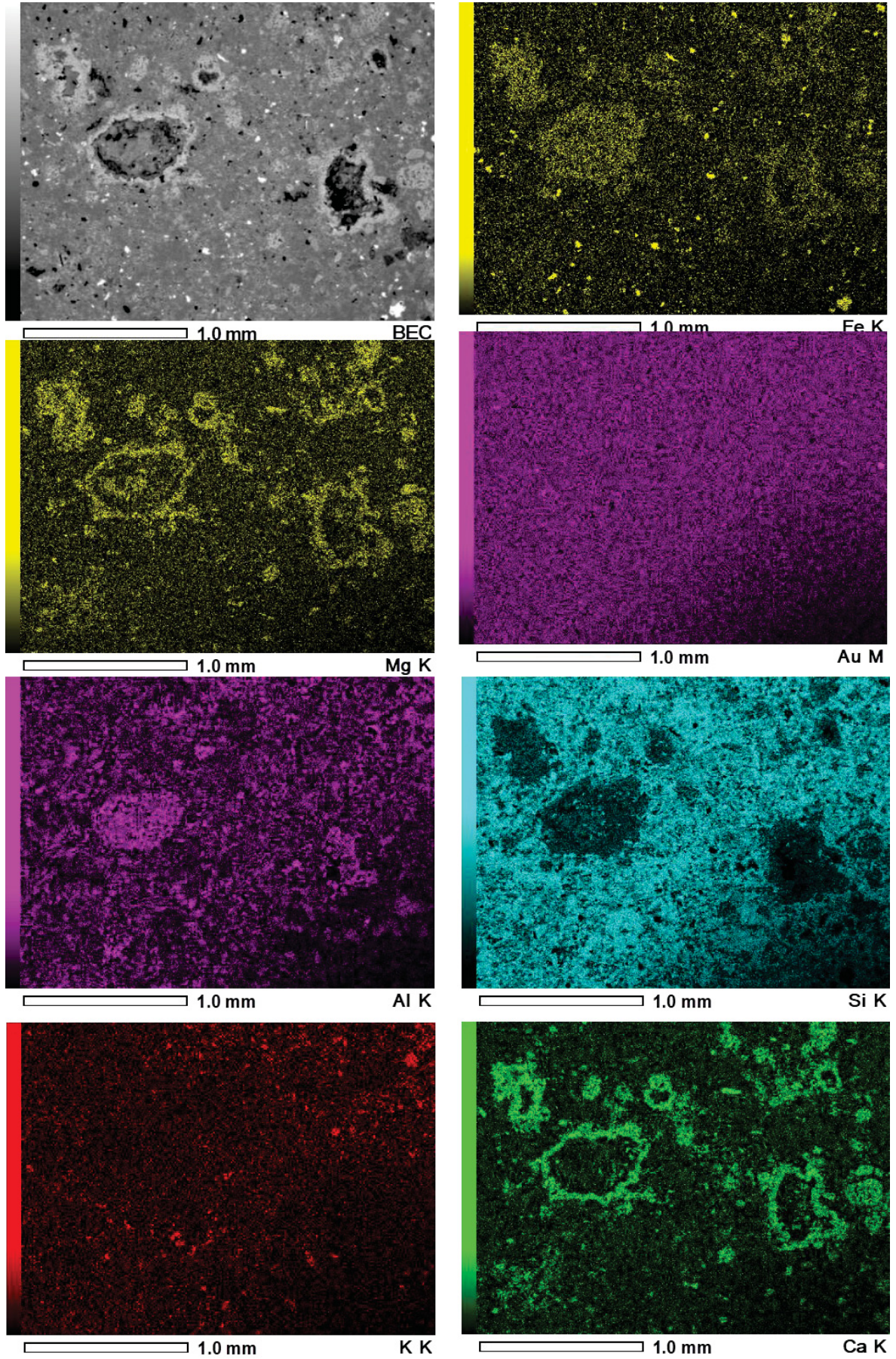
Figure 4.24 – EDS compositional maps from layered aggregates of proximal I2 tuffs.
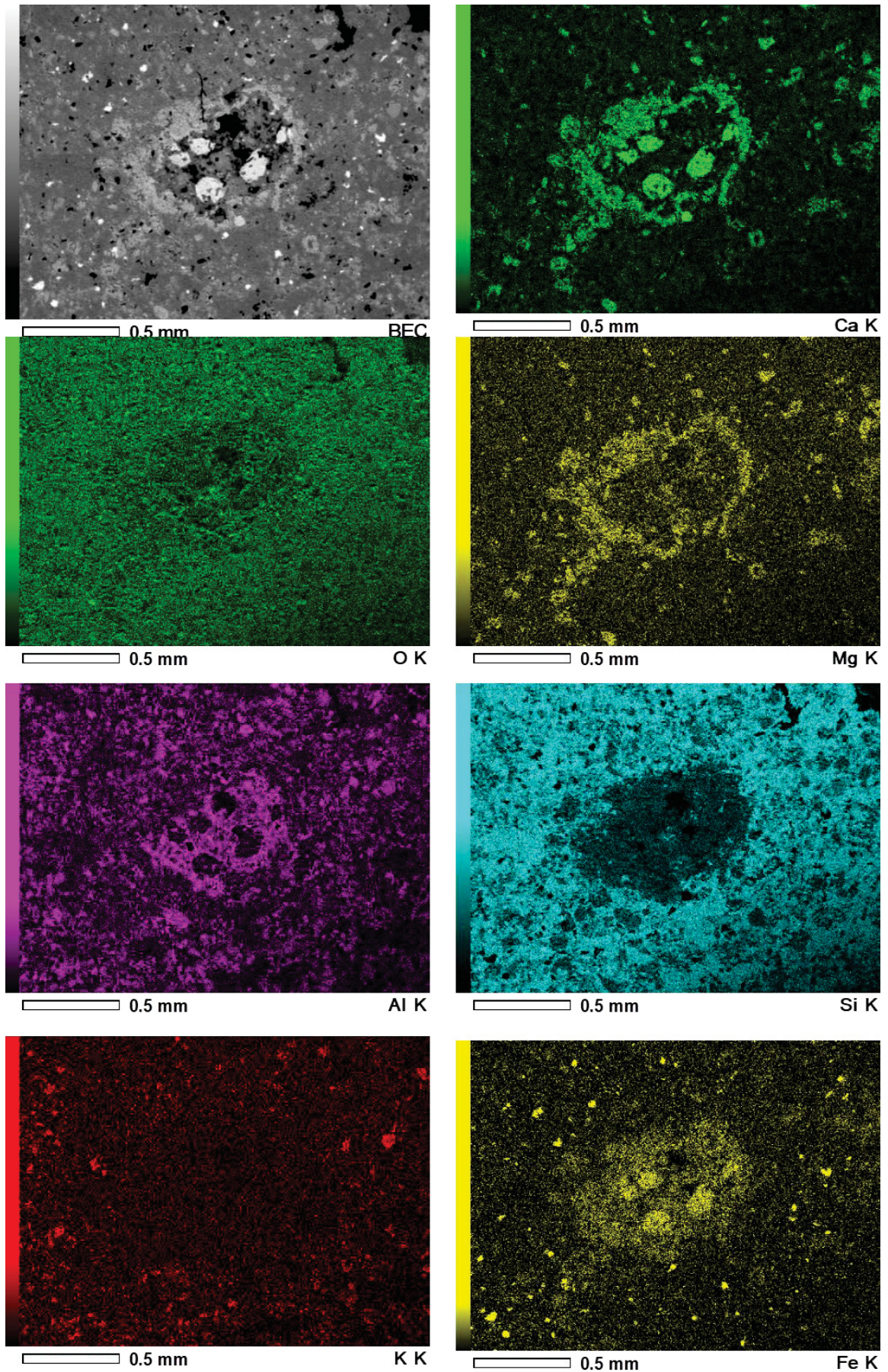
Figure 4.25 – EDS compositional maps of layered aggregates of proximal I2 tuffs.
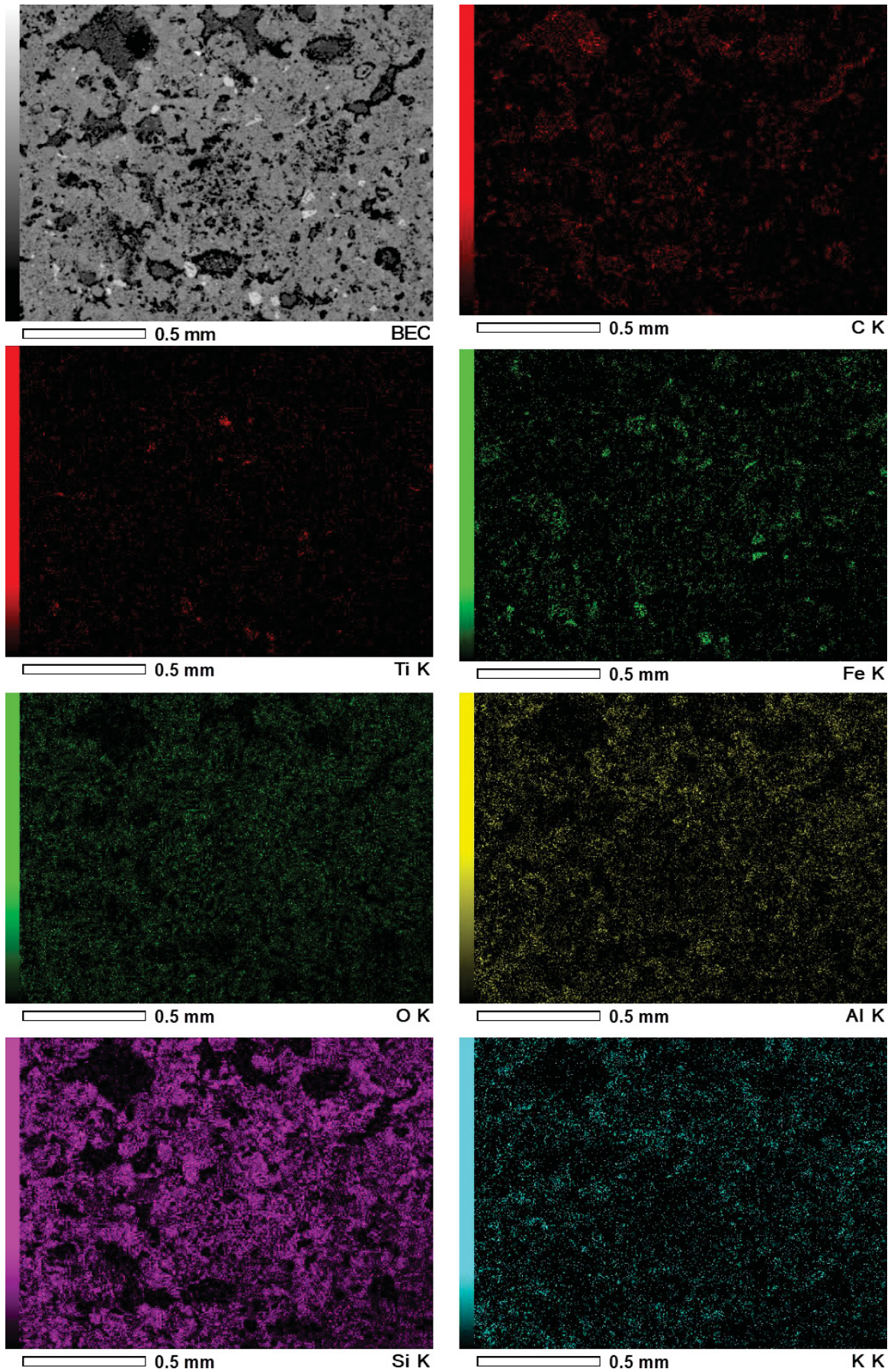
Figure 4.26 – EDS compositional maps from massive aggregates of medial I2 tuff.

4.11 References

Aufaristama, M. 2015. Mapping and Assessing Surface Morphology of Holocene Lava Flow in Krafla, NE Iceland, Using Remote Sensing. Dissertação (Mestrado em Ciência da Geoinformação). Escola de Engenharia e Ciências Naturais. Universidade da Islândia, Reykjavik. 119p.

Allen, R.L. 1988. False pyroclastic textures in altered silicic lavas, with implications for volcanic-associated mineralization. **Economic Geology**, 83: 1424–1446. https://doi.org/10.2113/gsecongeo.83.7.1424.

Almeida, V.V., Janasi, V.A., Heaman, L.M., Shaulis, B.J., Hollanda, M.H.B.M., Renne, P.R. 2018. Contemporaneous alkaline and tholeiitic magmatism in the Ponta Grossa Arch, Paraná-Etendeka Magmatic Province: Constraints from U–Pb zircon/baddeleyite and 40Ar/39Ar phlogopite dating of the José Fernandes Gabbro and mafic dykes. **Journal of Volcanology and Geothermal Research**, 355: 55–65. https://doi.org/10.1016/j.jvolgeores.2017.01.018.

Almeida, V.V., Janasi, V.A, Azzone, R.G., Faleiros, F.M. 2019. Crustal contamination and genesis of transitional alkaline-tholeiitic intrusions: Insights from the José Fernandes Suite, Paraná Magmatic Province, Brazil. **Lithos**, 342–343: 59–75. https://doi.org/10.1016/j.lithos.2019.05.023.

Amin, J., Valentine, G.A. 2017. Compound maar crater and co-eruptive scoria cone in the Lunar Crater Volcanic Field (Nevada, USA). **Journal of Volcanology and Geothermal Research**, 339: 41–51. https://doi.org/10.1016/j.jvolgeores.2017.05.002.

Azambuja Jr., J. R. A. 1943. Arenito Vulcano-clástico intertrapeano de Iraí, R. G do Sul. **Mineração e Metalurgia,** 7(41**)**: 361-364.

Baksi, A.K. 2018. Paraná flood basalt volcanism primarily limited to ~ 1 Myr beginning at 135 Ma: New 40Ar/39Ar ages for rocks from Rio Grande do Sul, and critical evaluation of published radiometric data. **Journal of Volcanology and Geothermal Research**, 355: 66–77. https://doi.org/10.1016/j.jvolgeores.2017.02.016.

Barreto, C.J.S., de Lima, E.F., Scherer, C.M., Rossetti, L. de M.M. 2014. Lithofacies analysis of basic lava flows of the Paraná igneous province in the south hinge of Torres Syncline, Southern Brazil. **Journal of Volcanology and Geothermal Research**, 285: 81–99. https://doi.org/10.1016/j.jvolgeores.2014.08.008.

Bélanger, C., Ross, P.S. 2018. Origin of nonbedded pyroclastic rocks in the Cathedral Cliff diatreme, Navajo volcanic field, New Mexico. **Bulletin of Volcanology**, 80: 61. https://doi.org/10.1007/s00445-018-1234-0.

Belousov, A., Voight, B., Belousova, M. 2007. Directed blasts and blast-generated pyroclastic density currents: a comparison of the Bezymianny 1956, Mount St Helens 1980, and Soufrière Hills, Montserrat 1997 eruptions and deposits. **Bulletin of Volcanology**, *69*(7): 701.

Bondre, N.R., Duraiswami, R.A., Dole, G. 2004. Morphology and emplacement of flows from the Deccan Volcanic Province, India. **Bulletin of Volcanology**, 66: 29–45. https://doi.org/10.1007/s00445-003-0294-x.

Bonsor, H. C., MacDonald, A. M. 2011. An initial estimate of depth to groundwater across Africa. British Geological Survey Open Report OR/11/067.

Branney, M.J., Kokelaar, P., 2002. Pyroclastic Density Currents and the Sedimentation of Ignimbrites. The Geological Society, London.

Brown, R.J., Bonadonna, C., Durant, A.J. 2012. A review of volcanic ash aggregation. **Physics and Chemistry of the Earth**, 45–46: 65–78. https://doi.org/10.1016/j.pce.2011.11.001.

Brown, R.J., Branney, M.J., Maher, C., Dávila-Harris, P. 2010. Origin of accretionary lapilli within ground-hugging density currents: Evidence from pyroclastic couplets on Tenerife. **Bulletin of the Geological Society of America**, 122: 305–320. https://doi.org/10.1130/B26449.1.

Buckley, J.P., Bosence, D., Elders, C. 2015. Tectonic setting and stratigraphic architecture of an Early Cretaceous lacustrine carbonate platform, Sugar Loaf High, Santos Basin, Brazil. **Geological Society Special Publication**, 418: 175–191. https://doi.org/10.1144/SP418.13.

Campbell, C. V. 1967. Lamina, laminaset, bed and bedset. **Sedimentology,** *8*(1): 7-26.

Cañón-Tapia, E. 2018. The Paraná-Etendeka Continental Flood Basalt Province: A historical perspective of current knowledge and future research trends. **Journal of Volcanology and Geothermal Research**, 355: 287–303. https://doi.org/10.1016/j.jvolgeores.2017.11.011.

Capaccioni, B., Coniglio, S. 1996. Varicolored and vesiculated tuffs from La Fossa volcano, Vulcano Island (Aeolian Archipelago, Italy): evidence of syndepositional alteration processes. **Bulletin of Volcanology**, 57: 61–70. https://doi.org/10.1007/BF00298708.

Carrasco-Núñez, G., Ort, M.H., Romero, C. 2007. Evolution and hydrological conditions of a maar volcano (Atexcac crater, Eastern Mexico). **Journal of Volcanology and Geothermal Research**, 159: 179–197. https://doi.org/10.1016/j.jvolgeores.2006.07.001.

Cas, R. A. F.; Wright, J. V. 1987. Volcanic successions: modern and ancient. Chapman & Hall, Londres, 528 p.

Chako Tchamabé, B.C., Ohba, T., Issa, Ooki, S., Youmen, D., Owona, S., Tanyileke, G., Hell, J.V. 2014. Temporal Evolution of the Barombi Mbo Maar, a Polygenetic Maar-Diatreme Volcano of the Cameroon Volcanic Line. **International Journal of Geosciences**, 05: 1315–1323. https://doi.org/10.4236/ijg.2014.511108.

Chako Tchamabe, B., Ohba, T., Kereszturi, G., Németh, K., Aka, F.T., Youmen, D., Issa, Miyabuchi, Y., Ooki, S., Tanyileke, G., Hell, J.V. 2015. Towards the reconstruction of the shallow plumbing system of the Barombi Mbo Maar (Cameroon) implications for diatreme growth processes of a polygenetic maar volcano. **Journal of Volcanology**

and Geothermal Research, 301: 293–313. https://doi.org/10.1016/j.jvolgeores.2015.06.004.

Chough, S.K., Sohn, Y.K. 1990. Depositional mechanics and sequences of base surges, Songaksan tuff ring, Cheju Island, Korea. **Sedimentology**, 37: 1115–1135. https://doi.org/10.1111/j.1365-3091.1990.tb01849.x.

Chukanov, N.V., Mukhanova, A.A., Rastsvetaeva, R.K., Belakovsky, D.I., Möckel, S., Karimova, O.V., Britvin, S.N., Krivovichev, S.V. 2011. Oxyphlogopite K(Mg,Ti,Fe)3[(Si,Al)4O10](O,F)2: A new mineral species of the mica group. **Geology of Ore Deposits**, 53: 583–590. https://doi.org/10.1134/S1075701511070063.

Czamanske, G.K., Gurevitch, A.B., Fedorenko, V., Simonov, O., 1998. Demise of the Siberian plume: paleogeographic and paleotectonic reconstruction from the prevolcanic and volcanic record, North-Central Siberia. **Int. Geol. Rev.,** 40: 95–115.

da Cruz, V.G.P. 2019. Rochas siliciclásticas e vulcanoclásticas associadas do Grupo Serra Geral na Calha De Torres (RS). BSc monography. Universidade Federal do Rio Grande do Sul – Porto Alegre - RS.

Duraiswami, R.A., Bondre, N.R., Managave, S. 2008. Morphology of rubbly pahoehoe (simple) flows from the Deccan Volcanic Province: Implications for style of emplacement. **Journal of Volcanology and Geothermal Research**, 177: 822–836. https://doi.org/10.1016/j.jvolgeores.2008.01.048.

Duraiswami, R.A., Gadpallu, P., Shaikh, T.N., Cardin, N. 2014. Pahoehoe-a'a transitions in the lava flow fields of the western Deccan Traps, India-implications for emplacement dynamics, flood basalt architecture and volcanic stratigraphy. **Journal of Asian Earth Sciences**, 84: 146–166. https://doi.org/10.1016/j.jseaes.2013.08.025.

Elliot, D.H., Hanson, R.E., 2001. Origin of widespread, exception- ally thick basaltic phreatomagmatic tuff breccia in the middle Jurassic Prebble and Mawson Formations, Antarctica. **Journal of Volcanology and Geothermal Research**, 111: 183–201.

Ellis, B., Branney, M.J. 2010. Silicic phreatomagmatism in the Snake River Plain: The Deadeye Member. **Bulletin of Volcanology**, 72: 1241–1257. https://doi.org/10.1007/s00445-010-0400-9.

Fernandes, A.J., De Assis Negri, F., Sobrinho, J.M.A., De Assis Janasi, V. 2018. Local geological sections and regional stratigraphy based on physical geology and chemical stratigraphy of the Serra Geral Group from Araraquara to Avaré, SP. **Brazilian Journal of Geology**, 48: 243–261. https://doi.org/10.1590/2317-4889201720180093.

Fernandes, L.A., Magalhães Ribeiro, C.M. 2015. Evolution and palaeoenvironment of the Bauru Basin (Upper Cretaceous, Brazil). **Journal of South American Earth Sciences**, 61: 71–90. https://doi.org/10.1016/j.jsames.2014.11.007.

Fisher, R. V., Schmincke, H. -U. 1984. Pyroclastic rocks. Springer-Verlag, Berlin, 472 p.

Florisbal, L.M., Heaman, L.M., de Assis Janasi, V., de Fatima Bitencourt, M. 2014. Tectonic significance of the Florianópolis Dyke Swarm, Paraná-Etendeka Magmatic Province: A reappraisal based on precise U-Pb dating. **Journal of Volcanology and Geothermal Research**, 289: 140–150. https://doi.org/10.1016/j.jvolgeores.2014.11.007.

Fodor, R.V. 1987. Low- and high-TiO2 flood basalts of southern Brazil: origin from picritic parentage and a common mantle source. **Earth and Planetary Science Letters**, 84: 423–430. https://doi.org/10.1016/0012-821X(87)90007-0.

Foulger, G.R. 2018. Origin of the South Atlantic igneous province. **Journal of Volcanology and Geothermal Research**, 355: 2–20. https://doi.org/10.1016/j.jvolgeores.2017.09.004.

Frank, H.T., Gomes, M.E.B., Formoso, M.L.L. 2009. Revisão da extensão areal e do volume da formação serra geral, Bacia do paraná, América do Sul. **Pesquisas em Geociencias**, 36: 49–57. https://doi.org/10.22456/1807-9806.17874.

Freda, C., Gaeta, M., Karner, D.B., Marra, F., Renne, P.R., Taddeucci, J., Scarlato, P., Christensen, J.N., Dallai, L. 2006. Eruptive history and petrologic evolution of the Albano multiple maar (Alban Hills, Central Italy). **Bulletin of Volcanology**, 68: 567–591. https://doi.org/10.1007/s00445-005-0033-6.

Gheith, H., Sultan, M. 2002. Construction of a hydrologic model for estimating Wadi runoff and groundwater recharge in the Eastern Desert, Egypt. **Journal of Hydrology**, 263: 36–55. https://doi.org/10.1016/S0022-1694(02)00027-6.

Gilg, H.A.; Morteani, G.; Kostitsyn, Y.; Preinfalk, C.; Gatter, I.; Strieder, A.J. 2003. Genesis of amethyst geodes in basaltic rocks of the Serra Geral Formation (Ametista do Sul, Rio Grande do Sul, Brazil): a fluid inclusion, REE, oxygen, carbon, and Sr isotope study on basalt, quartz, and calcite. **Mineralium Deposita**, 38:1009–1025.

Gomes, A.S., Licht, O.A.B., Vasconcellos, E.M.G., Soares, J.S. 2018. Chemostratigraphy and evolution of the Paraná Igneous Province volcanism in the central portion of the state of Paraná Southern Brazil. **Journal of Volcanology and Geothermal Research**, 355: 253–269. https://doi.org/10.1016/j.jvolgeores.2017.09.002.

Graettinger, Alison H., Skilling, I., McGarvie, D., Höskuldsson, Á. 2013. Subaqueous basaltic magmatic explosions trigger phreatomagmatism: A case study from Askja, Iceland. **Journal of Volcanology and Geothermal Research**, 264: 17–35. https://doi.org/10.1016/j.jvolgeores.2013.08.001.

Graettinger, A.H., Valentine, G.A. 2017. Evidence for the relative depths and energies of phreatomagmatic explosions recorded in tephra rings. **Bulletin of Volcanology**, 79: 88. https://doi.org/10.1007/s00445-017-1177-x.

Graettinger, A.H., Valentine, G.A., Sonder, I. 2016. Recycling in debris-filled volcanic vents. **Geology**, 44: 811–814. https://doi.org/10.1130/G38081.1.

Graettinger, A.H., Valentine, G.A., Sonder, I., Ross, P.S., White, J.D.L. 2015. Facies distribution of ejecta in analog tephra rings from experiments with single and multiple subsurface explosions. **Bulletin of Volcanology**, 77: 1–12. https://doi.org/10.1007/s00445-015-0951-x.

Graettinger, A.H., Valentine, G.A., Sonder, I., Ross, P.S., White, J.D.L., Taddeucci, J. 2014. Maar-diatreme geometry and deposits: Subsurface blast experiments with variable explosion depth. **Geochemistry, Geophysics, Geosystems**, 15: 740–764. https://doi.org/10.1002/2013GC005198.

Grosjean, M., Núñez, L., Cartajena, I., Messerli, B. 1997. Mid-Holocene climate and culture change in the Atacama Desert, Northern Chile. **Quaternary Research**, 48: 239–246. https://doi.org/10.1006/qres.1997.1917.

Grosjean, M., Veit, H. 2005. Water Resources in the Arid Mountains of the Atacama Desert (Northern Chile): Past Climate Changes and Modern Conflicts. pp. 93–104. https://doi.org/10.1007/1-4020-3508-X_10.

Hartmann, L.A., Arena, K.R., Duarte, S.K. 2012. Geological relationships of basalts, andesites and sand injectites at the base of the Paraná volcanic province, Torres, Brazil. **Journal of Volcanology and Geothermal Research**, 237–238: 97–111. https://doi.org/10.1016/j.jvolgeores.2012.05.017.

Hartmann, L.A., Arena, K.R., Duarte, S.K., Pertille, J. 2013. Long-distance lava correlation in the Paraná volcanic province along the Serra Geral cuesta, southeastern Brazil. **International Journal of Earth Sciences**, 102: 1655–1669. https://doi.org/10.1007/s00531-013-0899-z.

He, B., Xu, Y.-G., Chung, S.-L., Xiao, L., Wang, Y., 2003. Sedimentary evidence for a rapid, kilometer-scale crustal doming prior to the eruption of the Emeishan flood basalts. **Earth Planet. Sci. Lett.** 213: 391–405.

Hole, M., Jolley, D., Hartley, A., Leleu, S., John, N., Ball, M. 2013. Lava-sediment interactions in an Old Red Sandstone basin, NE Scotland. **Journal of the Geological Society**, 170: 641–655. https://doi.org/10.1144/jgs2012-107.

Houghton, B.F., Schmincke, H.U. 1986. Mixed deposits of simultaneous strombolian and phreatomagmatic volcanism: Rothenberg volcano, east Eifel volcanic field. **Journal of Volcanology and Geothermal Research**, 30: 117–130. https://doi.org/10.1016/0377-0273(86)90069-7.

Houghton, B.F., Wilson, C.J.N., Rosenberg, M.D., Smith, I.E.M., Parker, R.J. 1996. Mixed deposits of complex magmatic and phreatomagmatic volcanism: An example from Crater Hill, Auckland, New Zealand. **Bulletin of Volcanology**, 58: 59–66. https://doi.org/10.1007/s004450050126.

Houghton, B. F., Wilson, C. J. N., Smith, I. E. M. 1999. Shallow-seated controls on styles of explosive basaltic volcanism: a case study from New Zealand. **Journal of Volcanology and Geothermal Research**, *91*(1): 97-120.

Houston, J. 2002. Groundwater recharge through an alluvial fan in the Atacama Desert, northern Chile: mechanisms, magnitudes and causes. **Hydrological processes**, 16(15): 3019-3035.

Schipper, I.C., White, J.D.L. 2016. Magma-slurry interaction in Surtseyan eruptions. **Geology**, 44: 195–198. https://doi.org/10.1130/G37480.1.

Jerram, D.A, Mountney, N.P, Holzförster, F., Stollhofen, H. 1999. Internal stratigraphic relationships in the Etendeka Group in the Huab Basin, NW Namibia: Understanding the onset of flood volcanism. **Journal of Geodynamics**, 28: 393–418. https://doi.org/10.1016/S0264-3707(99)00018-6.

Jerram, D.A., 2002. Volcanology and facies architecture of flood basalts. In: Menzies, M.A., Klemperer, S.L., Ebinger, C.J., Baker. Volcanic Rifted Margins. **Spec. Pap.-Geol. Soc. Am**. 362: 121–135.

Jerram, D.A., Mountney, N.P., Howell, J.A., Long, D., Stollhofen, H., 2000. Death of a sand sea: an active aeolian erg system- atically buried by the Etendeka flood basalts of NW Namibia. J. Geol. Soc. (Lond.) 157, 513–516.

Jerram, D.A., Stollhofen, H. 2002. Lava-sediment interaction in desert settings; are all peperite-like textures the result of magma-water interaction? **Journal of Volcanology and Geothermal Research**, 114: 231–249. https://doi.org/10.1016/S0377-0273(01)00279-7.

Jerram, D.A., Widdowson, M. 2005. The anatomy of Continental Flood Basalt Provinces: Geological constraints on the processes and products of flood volcanism. **Lithos**, 79: 385–405. https://doi.org/10.1016/j.lithos.2004.09.009.

Jordan, S.C., Cas, R.A.F., Hayman, P.C. 2013. The origin of a large (\textgreater3km) maar volcano by coalescence of multiple shallow craters: Lake Purrumbete maar, southeastern Australia. **Journal of Volcanology and Geothermal Research**, 254: 5–22. https://doi.org/10.1016/j.jvolgeores.2012.12.019.

Jordan, S.C., Dürig, T., Cas, R.A.F., Zimanowski, B. 2014. Processes controlling the shape of ash particles: Results of statistical IPA. **Journal of Volcanology and Geothermal Research**, 288: 19–27. https://doi.org/10.1016/j.jvolgeores.2014.09.012.

Kano, K., Takeuchi, K., Yamamoto, T., Hoshizumi, H. 1991. Subaqueous rhyolite block lavas in the Miocene Ushikiri formation, Shimane Peninsula, SW Japan. **Journal of volcanology and geothermal research,** *46*(3-4): 241-253.

Kataoka, K. 2005. Distal fluvio-lacustrine volcaniclastic resedimentation in response to an explosive silicic eruption: The Pliocene Mushono tephra bed, central Japan. **Bulletin of the Geological Society of America**, 117: 3–17. https://doi.org/10.1130/B25379.1.

Kataoka, K.S., Manville, V., Nakajo, T., Urabe, A. 2009. Impacts of explosive volcanism on distal alluvial sedimentation: Examples from the Pliocene-Holocene volcaniclastic successions of Japan. **Sedimentary Geology**, 220: 306–317. https://doi.org/10.1016/j.sedgeo.2009.04.016.

Kereszturi, G., Nmeth, K. 2012. Monogenetic Basaltic Volcanoes: Genetic Classification, Growth, Geomorphology and Degradation, In: Updates in Volcanology - New Advances in Understanding Volcanic Systems. InTech. https://doi.org/10.5772/51387.

Keszthelyi, L., Keszthelyi, L., Thordarson, T., Self, S. 2001. Rubbly Pahoehoe: Implication for Flood Basalt Eruptions and their Atmospheric Effects. **AGU Fall Meeting** 2001: V52A–1050.

Kienle, J., Kyle, P.R., Self, S., Motyka, R.J., Lorenz, V., 1980. Ukinrek Maars, Alaska, I. April 1977 eruption sequence, petrology and tectonic setting. **J. Volcanol. Geotherm. Res**. 7: 11-37.

Kurszlaukis, S., Fulop, A. 2013. Factors controlling the internal facies architecture of maar-diatreme volcanoes. **Bulletin of Volcanology**, 75: 1–12. https://doi.org/10.1007/s00445-013-0761-y.

Larsen, L.M., Fitton, J.G., Pedersen, A.K., 2003. Paleogene volcanic ash layers in the Danish Basin: compositions and source areas in the North Atlantic igneous province. **Lithos,** 71: 47–80.

Leat, P.T., Thompson, R.N. 1988. Miocene hydrovolcanism in NW Colorado, USA, fuelled by explosive mixing of basic magma and wet unconsolidated sediment. **Bulletin of Volcanology**, 50: 229–243. https://doi.org/10.1007/BF01047486.

Licht, O.A.B., Arioli, E.E. 2011. Evidências de eventos explosivos - hidrovulcanismo - na Formação Serra Geral, Estado do Paraná, Brasil. Proc.... V° Simpósio de Vulcanismo e Ambientes Associados. SBG. Goiás.

Licht, O.A.B., Arioli, E.E. 2011b. Hidrovulcanismo, um modelo eruptivo para a Formação Serra Geral. Proc.... V° Simpósio de Vulcanismo e Ambientes Associados. SBG. Goiás.

Licht, O. A. B. 2012. Estudo de produtos hidrovulcânicos no sudoeste do Paraná. Serviço Geológico do Paraná - MINEROPAR, Curitiba, 314 p.

Licht, O. A . B., Arioli, E. E. 2018. Mapa geológico do Grupo Serra Geral no Estado do Paraná. Instituto de Terras, Cartografia e Geologia – ITCG, Curitiba, v.1, 318 p.

Licht, O.A.B. 2014. a Evolução Do Conhecimento Sobre a Província Ígnea Do Paraná - Dos Primórdios Até 1950. **Revista do Instituto Geológico**, 35: 71–106. https://doi.org/10.5935/0100-929x.20140010.

Licht, O.A.B. 2018. A revised chemo-chrono-stratigraphic 4-D model for the extrusive rocks of the Paraná Igneous Province. **Journal of Volcanology and Geothermal Research**, 355: 32–54. https://doi.org/10.1016/j.jvolgeores.2016.12.003.

Licht, O. A. B., Valore, L. A., Szatmari, P. 2015a. Faciology and stratigraphy of Mafic Volcaniclastic Deposits (MVDs), Serra Geral Group Saudade do Iguaçu-Coronel Vivida region, State of Paraná, Brazil. *Proc...*VI Simpósio de Vulcanismo e Ambientes Associados, SBG, São Paulo.

Licht, O. A. B., Gomes, A. S., Vasconcellos, E. M. 2015b. The role played by fluorine in the Serra Geral volcanics, Paraná Igneous Province: a first glance. *Proc....*XV Congresso Brasileiro de Geoquímica, SBGq, Brasília.

Lima, E.F., Waichel, B.L., De Magalhães May Rossetti, L., Viana, A.R., Scherer, C.M., Bueno, G.V., Dutra, G. 2012. Morphological and petrographic patterns of the pahoehoe and a'a flows of the Serra Geral Formation in the Torres Syncline (Rio Grande do sul state Brazil). **Revista Brasileira de Geociencias**, 42: 744–753. https://doi.org/10.5327/Z0375-75362012000400007.

Liu, E.J., Cashman, K.V., Rust, A.C., Edmonds, M. 2018. Insights into the dynamics of mafic magmatic-hydromagmatic eruptions from volatile degassing behaviour: The Hverfjall Fires, Iceland. **Journal of Volcanology and Geothermal Research**, 358: 228–240. https://doi.org/10.1016/j.jvolgeores.2018.05.016.

Liu, E.J., Cashman, K.V., Rust, A.C., Höskuldsson, A. 2017. Contrasting mechanisms of magma fragmentation during coeval magmatic and hydromagmatic activity: the Hverfjall Fires fissure eruption, Iceland. **Bulletin of Volcanology**, 79: . https://doi.org/10.1007/s00445-017-1150-8.

Lorenz, V. 1974. Vesiculated tuffs and associated features. **Sedimentology**, 21: 273–291. https://doi.org/10.1111/j.1365-3091.1974.tb02059.x.

Lucchi, F., Francalanci, L., De Astis, G., Tranne, C.A., Braschi, E., Klaver, M. 2018. Geological evidence for recurrent collapse-driven phreatomagmatic pyroclastic density currents in the Holocene activity of Stromboli volcano, Italy. **Journal of Volcanology and Geothermal Research**, 385: 81–102. https://doi.org/10.1016/j.jvolgeores.2018.10.024.

Lucchi, F., Tranne, C.A., Rossi, P.L. 2010. Stratigraphic approach to geological mapping of the late quaternary volcanic island of Lipari (Aeolian archipelago, southern Italy), In: Special Paper of the Geological Society of America. Geological Society of America, pp. 1–32. https://doi.org/10.1130/2010.2464(01).

Luchetti, A.C.F., Nardy, A.J.R., Machado, F.B., Madeira, J.E.O., Arnosio, J.M. 2014. New insights on the occurrence of peperites and sedimentary deposits within the silicic volcanic sequences of the Paraná Magmatic Province, Brazil. **Solid Earth**, 5: 121–130. https://doi.org/10.5194/se-5-121-2014.

MacDonald, A.M., Bonsor, H.C., Dochartaigh, B.É.Ó., Taylor, R.G. 2012. Quantitative maps of groundwater resources in Africa. Institute of Physics Publishing.

Machado, F.B., Rocha-Júnior, E.R.V., Marques, L.S., Nardy, A.J.R. 2015. Volcanological aspects of the northwest region of Paraná continental flood basalts (Brazil). **Solid Earth**, 6: 227–241. https://doi.org/10.5194/se-6-227-2015.

Mantovani, M.S.M., Marques, L.S., De Sousa, M.A., Civetta, L., Atalla, L., Innocenti, F., 1985. Trace elements and strontium isotope constraints on the origin and evolution of Paraná continental flood basalts of Santa Catarina State (Southern Brazil). **J. Petrol**. 26: 187–209.

Manville, V., Németh, K., Kano, K. 2009. Source to sink: A review of three decades of progress in the understanding of volcaniclastic processes, deposits, and hazards. **Sedimentary Geology**, 220: 136–161. https://doi.org/10.1016/j.sedgeo.2009.04.022.

Marshall, P.E., Widdowson, M., Murphy, D.T. 2016. The Giant Lavas of Kalkarindji: Rubbly pāhoehoe lava in an ancient continental flood basalt province. **Palaeogeography, Palaeoclimatology, Palaeoecology**, 441: 22–37. https://doi.org/10.1016/j.palaeo.2015.05.006.

Martin, U., Németh, K. 2007. Blocky versus fluidal peperite textures developed in volcanic conduits, vents and crater lakes of phreatomagmatic volcanoes in Mio/Pliocene

volcanic fields of Western Hungary. **Journal of Volcanology and Geothermal Research**, 159: 164–178. https://doi.org/10.1016/j.jvolgeores.2006.06.010.

Martini, M. 1984. On the behaviour of fluorine in volcanic processes. **Bulletin Volcanologique,** *47*(3): 483-489.

McClintock, M., White, J.D.L. 2006. Large phreatomagmatic vent complex at Coombs Hills, Antarctica: Wet, explosive initiation of flood basalt volcanism in the Ferrar-Karoo LIP. **Bulletin of Volcanology**, 68: 215–239. https://doi.org/10.1007/s00445-005-0001-1.

McClintock, M., White, J.D.L., Houghton, B.F., Skilling, I.P. 2008. Physical volcanology of a large crater-complex formed during the initial stages of Karoo flood basalt volcanism, Sterkspruit, Eastern Cape, South Africa. **Journal of Volcanology and Geothermal Research**, 172: 93–111. https://doi.org/10.1016/j.jvolgeores.2005.11.012.

McPhie, J., Doyle, M., and Allen, R., 1993, Volcanic textures: A guide to the interpretation of textures in volcanic rocks: Hobart, CODES Key Centre, University of Tasmania, 196 p.

Milani, E.J., Rangel, H.D., Bueno, G.V., Stica, J.M., Winter, W.R., Caixeta, J.M., Da Cruz Pessoa Neto, O. 2007. Brazilian sedimentary basins - Stratigraphic charts | Bacias sedimentares brasileiras - Cartas estratigráficas. **Boletim de Geociencias da Petrobras**, 15: 183–205.

Milani, E.J., 2004. Comentários sobre a origem e a evolução tectônica da Bacia do Paraná. In: Montesso-Neto, V., Bartorelli, A., Carneiro, C.D.R., Brito-Neves, B.B. (Eds.), Geologia do Continente Sul-Americano – evolução da obra de Fernando Flávio Marques de Almeida. Ed. Becca, pp. 265–279.

Moraes, L.C., Seer, H.J. 2018. Pillow lavas and fluvio-lacustrine deposits in the northeast of Paraná Continental Magmatic Province, Brazil. **Journal of Volcanology and Geothermal Research**, 355: 78–86. https://doi.org/10.1016/j.jvolgeores.2017.03.024.

Moreira, J.L.P., Madeira, C.V., Gil, J.A., Machado, M.A.P. 2007. Santos basin | Bacia de Santos. **Boletim de Geociencias da Petrobras**, 15: 531–549.

Morteani, G.; Kostitsyn, Y.; Preinfalk, C.; Gilg, H.A. 2010. The genesis of the amethyst geodes at Artigas (Uruguay) and the paleohydrology of the Guaraní aquifer: structural, geochemical, oxygen, carbon, strontium isotope and fluid inclusion study. **International Journal of Earth Sciences**, 99: 927–947.

Murcia, H.F., Borrero, C.A., Pardo, N., Alvarado, G.E., Arnosio, M., Scolamacchia, T. 2013. Depósitos Volcaniclásticos: Términos Y Conceptos Para Una Clasificación En Español Volcaniclastic Deposits: Terminology and Concepts for a Classification in Spanish. **Revista Geológica de América Central**, 48: 15–39. https://doi.org/10.15517/rgac.v0i48.12211.

Murphy, M. A., Salvador, A. 1999. International subcommission on stratigraphic classification of IUGS international commission on stratigraphy-international stratigraphic guide-an abridged version. **Episodes,** 22(4): 255-271.

Murtagh, R.M., White, J.D.L. 2013. Pyroclast characteristics of a subaqueous to emergent Surtseyan eruption, black point volcano, california. **Journal of Volcanology and Geothermal Research**, 267: 75–91. https://doi.org/10.1016/j.jvolgeores.2013.08.015.

Németh, K., Cronin, S., Haller, M., Brenna, M., Csillag, G. 2010. Modern analogues for Miocene to Pleistocene alkali basaltic phreatomagmatic fields in the Pannonian Basin: "Soft-substrate" to "combined" aquifer controlled phreatomagmatism in intraplate volcanic fields. **Central European Journal of Geosciences**, 2: 339–361. https://doi.org/10.2478/v10085-010-0013-8.

Németh, K., Palmer, J. 2019. Geological mapping of volcanic terrains: Discussion on concepts, facies models, scales, and resolutions from New Zealand perspective. **Journal of Volcanology and Geothermal Research**, 385: 27-45

Nester, P. L., Gayo, E., Latorre, C., Jordan, T. E., Blanco, N. 2007. Perennial stream discharge in the hyperarid Atacama Desert of northern Chile during the latest Pleistocene. **Proceedings of the National Academy of Sciences**, 104(50): 19724-19729.

Oliveira, E.P. 1916. Geologia do Estado do Paraná. Ministério da Agricultura, Industria e Commercio, Rio de Janeiro, **Bol**. 5, 1: p. 67-143.

Onken, J., Forman, S. 2017. Terminal Pleistocene to early Holocene volcanic eruptions at Zuni Salt Lake, west-central New Mexico, USA. **Bulletin of Volcanology**, 79: 10. https://doi.org/10.1007/s00445-016-1089-1.

Ort, M. H., Carrasco-Núñez, G. 2009. Lateral vent migration during phreatomagmatic and magmatic eruptions at Tecuitlapa Maar, east-central Mexico. **Journal of Volcanology and Geothermal Research,** 181(1-2): 67-77.

Ort, M.H., Lefebvre, N.S., Neal, C.A., McConnell, V.S., Wohletz, K.H. 2018. Linking the Ukinrek 1977 maar-eruption observations to the tephra deposits: New insights into maar depositional processes. **Journal of Volcanology and Geothermal Research**, 360: 36–60. https://doi.org/10.1016/j.jvolgeores.2018.07.005.

Óskarsson, B.V., Riishuus, M.S. 2014. The mode of emplacement of Neogene flood basalts in eastern Iceland: Facies architecture and structure of simple aphyric basalt groups. **Journal of Volcanology and Geothermal Research**, 289: 170–192. https://doi.org/10.1016/j.jvolgeores.2014.11.009.

Peate, D. W.; Hawkesworth, C. J.; Mantovani, M. S. M. 1992. Chemical stratigraphy of the Paraná lavas (South America): classification of magma types and their spatial distribution. **Bulletin of Volcanology**, 55: 119-139.

Pedersen, G.B.M., Höskuldsson, A., Dürig, T., Thordarson, T., Jónsdóttir, I., Riishuus, M.S., Óskarsson, B.V., Dumont, S., Magnusson, E., Gudmundsson, M.T., Sigmundsson, F., Drouin, V.J.P.B., Gallagher, C., Askew, R., Gudnason, J., Moreland, W.M., Nikkola, P., Reynolds, H.I., Schmith, J. 2017. Lava field evolution

and emplacement dynamics of the 2014–2015 basaltic fissure eruption at Holuhraun, Iceland. **Journal of Volcanology and Geothermal Research**, 340: 155–169. https://doi.org/10.1016/j.jvolgeores.2017.02.027.

Petry, K., Jerram, D. A., De Almeida, D. D. P. M., Zerfass, H. 2007. Volcanic-sedimentary features in the Serra Geral Fm., Paraná Basin, southern Brazil: examples of dynamic lava-sediment interactions in an arid setting. **Journal of Volcanology and Geothermal Research,** 159**:** 313–325.

Piccirillo, E.M., Melfi, A.J., Comin-Chiaramonti, P., Bellieni, G., Ernesto, M., Marques, L.S., Nardy, A.J.R., Pacca, I.G., Roisenberg, A., Stolfa, D., 1988. Continental flood volcanism from the Paraná Basin (Brazil). In: MacDougall, J.D. (Ed.), Continental Flood Basalts. Kluwer Acad. Publ., pp. 195–238.

Renne, P. R., Ernesto, M., Pacca, I. G., Coe, R. S., Glen, J. M.,Prévot, M., Perrin, M. 1992. The age of Parana flood volcanism, rifting of Gondwanaland, and the Jurassic Cretaceous boundary. **Science**, 258: 975–979.

Riccomini, C., Sant'Anna, L.G., Fambrini, G.L. 2016. The Early Cretaceous Jacuí Group, a newly discovered volcaniclastic-epiclastic accumulation at the top of the Paraná Basin, southern Brazil. **Cretaceous Research**, 59: 111–128. https://doi.org/10.1016/j.cretres.2015.10.020.

Rosa, C. J. P., McPhie, J., Relvas, J. M. R. S. 2016. Distinguishing peperite from other sediment-matrix igneous breccias: Lessons from the Iberian Pyrite Belt. **Journal of Volcanology and Geothermal Research**, 315: 28-39.

Rosi, M. 1992. A model for the formation of vesiculated tuff by the coalescence of accretionary lapilli. **Bulletin of Volcanology**, 54: 429–434. https://doi.org/10.1007/BF00312323.

Ross, P.S., Delpit, S., Haller, M.J., Németh, K., Corbella, H. 2011. Influence of the substrate on maar-diatreme volcanoes - An example of a mixed setting from the Pali Aike volcanic field, Argentina. **Journal of Volcanology and Geothermal Research**, 201: 253–271. https://doi.org/10.1016/j.jvolgeores.2010.07.018.

Ross, P.S., Ukstins Peate, I., McClintock, M.K., Xu, Y.G., Skilling, I.P., White, J.D.L., Houghton, B.F. 2005. Mafic volcaniclastic deposits in flood basalt provinces: A review. **Journal of Volcanology and Geothermal Research**, 145: 281–314. https://doi.org/10.1016/j.jvolgeores.2005.02.003.

Ross, P.S., White, J.D.L. 2005. Mafic, large-volume, pyroclastic density current deposits from phreatomagmatic eruptions in the ferrar large igneous province, Antarctica. **Journal of Geology**, 113: 627–649. https://doi.org/10.1086/449324.

Ross, P.S., White, J.D.L. 2006. Debris jets in continental phreatomagmatic volcanoes: A field study of their subterranean deposits in the Coombs Hills vent complex, Antarctica. **Journal of Volcanology and Geothermal Research**, 149: 62–84. https://doi.org/10.1016/j.jvolgeores.2005.06.007.

Ross, P.S., White, J.D.L. 2012. Quantification of vesicle characteristics in some diatreme-filling deposits, and the explosivity levels of magma-water interactions within

diatremes. **Journal of Volcanology and Geothermal Research**, 245–246: 55–67. https://doi.org/10.1016/j.jvolgeores.2012.07.006.

Ross, P.S., White, J.D.L., McClintock, M. 2008. Geological evolution of the Coombs-Allan Hills area, Ferrar large igneous province, Antarctica: Debris avalanches, mafic pyroclastic density currents, phreatocauldrons. **Journal of Volcanology and Geothermal Research**, 172: 38–60. https://doi.org/10.1016/j.jvolgeores.2005.11.011.

Ross, P.S., White, J.D.L., Valentine, G.A., Taddeucci, J., Sonder, I., Andrews, R.G. 2013. Experimental birth of a maar-diatreme volcano. **Journal of Volcanology and Geothermal Research**, 260: 1–12. https://doi.org/10.1016/j.jvolgeores.2013.05.005.

Rossetti, L., Lima, E.F., Waichel, B.L., Hole, M.J., Simões, M.S., Scherer, C.M.S. 2018. Lithostratigraphy and volcanology of the Serra Geral Group, Paraná-Etendeka Igneous Province in Southern Brazil: Towards a formal stratigraphical framework. **Journal of Volcanology and Geothermal Research**, 355: 98–114. https://doi.org/10.1016/j.jvolgeores.2017.05.008.

Rossetti, L.M., Lima, E.F., Waichel, B.L., Scherer, C.M., Barreto, C.J. 2014. Stratigraphical framework of basaltic lavas in Torres Syncline main valley, southern Parana-Etendeka Volcanic Province. **Journal of South American Earth Sciences**, 56: 409–421. https://doi.org/10.1016/j.jsames.2014.09.025.

Scherer, C. M. S. 2002. Preservation of aeolian genetic units by lava flow in the Lower Cretaceous of the Paraná Basin, southern Brazil. **Sedimentology**, 49: 97-116.

Schmincke, H. -U, Fisher, R.V., Waters, A.C. 1973. Antidune and chute and pool structures in the base surge deposits of the Laacher See area, Germany. **Sedimentology**, 20: 553–574. https://doi.org/10.1111/j.1365-3091.1973.tb01632.x.

Self, S., Keszthelyi, L., Thordarson, T. 1998. The importance of pāhoehoe. **Annual Review of Earth and Planetary Sciences**, *26*(1): 81-110.

Self, S., Thordarson, T., Keszthelyi, L. 1997. Emplacement of continental flood basalt lava flows. Geophysical Monograph - American Geophysical Union, 100: 381-410.

Self, S., Thordarson, T., Keszthelyi, L., Walker, G.P.L., Hon, K., Murphy, M.T., Long, P., Finnemore, S. 1996. A new model for the emplacement of Columbia River basalts as large, inflated pahoehoe lava flow fields. **Geophysical Research Letters**, 23: 2689–2692. https://doi.org/10.1029/96GL02450.

Self, S., Kienle, J., Huot, J. P. 1980. Ukinrek Maars, Alaska, II. Deposits and formation of the 1977 craters. **Journal of Volcanology and Geothermal Research**, 7(1-2): 39-65.

Sheridan, M.F., Wohletz, K.H. 1983. Hydrovolcanism: Basic considerations and review. **Journal of Volcanology and Geothermal Research**, 17: 1–29. https://doi.org/10.1016/0377-0273(83)90060-4.

Single, R., Jerram, D., 2004. The 3D facies architecture of flood basalt provinces and their internal heterogeneity: examples from the Palaeogene Skye Lava Field. J. Geol. Soc. London. 161, 911–926.

Skilling, I.P., White, J.D.L., McPhie, J. 2002. Peperite: A review of magma-sediment mingling. **Journal of Volcanology and Geothermal Research**, 114: 1–17. https://doi.org/10.1016/S0377-0273(01)00278-5.

Slootman, A., Cartigny, M.J.B. 2020. Cyclic steps: Review and aggradation-based classification.

Smith, N.J., Kokelaar, B.P. 2013. Proximal record of the 273 ka Poris caldera-forming eruption, Las Cañadas, Tenerife. **Bulletin of Volcanology**, 75: 1–21. https://doi.org/10.1007/s00445-013-0768-4.

Sohn, Y.K. 1996. Hydrovolcanic processes forming basaltic tuff rings and cones on Cheju Island, Korea. **Bulletin of the Geological Society of America**, 108: 1199–1211. https://doi.org/10.1130/0016-7606(1996)108<1199:HPFBTR>2.3.CO;2.

Sohn, Y. K. 1997. On traction-carpet sedimentation. J**ournal of Sedimentary Research**, 67(3): 502-509.

Sohn, Y.K., Chough, S.K. 1989. Depositional processes of the Suwolbong tuff ring, Cheju Island (Korea). **Sedimentology**, 36: 837–855. https://doi.org/10.1111/j.1365-3091.1989.tb01749.x.

Sohn, Y.K., Park, K.H. 2005. Composite tuff ring/cone complexes in Jeju Island, Korea: Possible consequences of substrate collapse and vent migration. **Journal of Volcanology and Geothermal Research**, 141: 157–175. https://doi.org/10.1016/j.jvolgeores.2004.10.003.

Sohn, Y.K., Yoon, S.H. 2010. Shallow-marine records of pyroclastic surges and fallouts over water in Jeju Island, Korea, and their stratigraphic implications. **Geology**, 38: 763–766. https://doi.org/10.1130/G30952.1.

Sottili, G., Taddeucci, J., Palladino, D. M., Gaeta, M., Scarlato, P., Ventura, G. 2009. Sub-surface dynamics and eruptive styles of maars in the Colli Albani Volcanic District, Central Italy. **Journal of Volcanology and Geothermal Research**, *180*(2-4): 189-202.

Sowinski, A. C. B. 2016. Estudo das paleotensões na Região de Londrina, Paraná. Trabalho de Conclusão de Curso. Setor de Ciências da Terra. Universidade Federal do Paraná, Curitiba. 43 p.

Svensen, H.H., Torsvik, T.H., Callegaro, S., Augland, L., Heimdal, T.H., Jerram, D.A., Planke, S., Pereira, E. 2018. Gondwana Large Igneous Provinces: Plate reconstructions, volcanic basins and sill volumes. **Geological Society Special Publication**, 463: 17–40. https://doi.org/10.1144/SP463.7.

Szatmari, P., Milani, E.J. 2016. Tectonic control of the oil-rich large igneous-carbonate-salt province of the South Atlantic rift. **Marine and Petroleum Geology**, 77: 567–596. https://doi.org/10.1016/j.marpetgeo.2016.06.004.

Thiede, D. S., Vasconcellos, P. M., 2010. Paraná flood basalts: rapid extrusion hypothesis confirmed by new 40Ar/39Ar results. **Geology**, 38 (8);: 747–750.

Thordarson, T., Self, S. 1998. The Roza Member, Columbia River Basalt Group: A gigantic pahoehoe lava flow field formed by endogenous processes? **Journal of**

Geophysical Research: Solid Earth, 103: 27411–27445. https://doi.org/10.1029/98jb01355.

Thordarson, T., Self, S., 2003. Atmospheric and environmental effects of the 1783–1784 Laki eruption: a review and reassessment. **J. Geophys. Res.,** 108 art. no. 4011.

Titon, B. G. 2019. Controles geoquímicos e mineralógicos na formação de minerais secundários na Província Ígnea do Paraná, noroeste do Estado do Paraná. MSc thesis. Setor de Ciências da Terra, Universidade Federal do Paraná, Curitiba. 136 p.

Ukstins Peate, I., Larsen, M., Lesher, C.E. 2003. The transition from sedimentation to flood volcanism in the Kangerlussuaq Basin, East Greenland: Basaltic pyroclastic volcanism during initial Palaeogene continental break-up. **Journal of the Geological Society**, 160: 759–772. https://doi.org/10.1144/0016-764902-071.

Valentine, G.A. 1987. Stratified flow in pyroclastic surges. **Bulletin of Volcanology**, 49(4): 616-630.

Valentine, G.A., Cortés, J.A. 2013. Time and space variations in magmatic and phreatomagmatic eruptive processes at Easy Chair (Lunar Crater Volcanic Field, Nevada, USA). **Bulletin of Volcanology**, 75: 1–13. https://doi.org/10.1007/s00445-013-0752-z.

Valentine, G.A., Graettinger, A.H., Macorps, É., Ross, P.S., White, J.D.L., Döhring, E., Sonder, I. 2015a. Experiments with vertically and laterally migrating subsurface explosions with applications to the geology of phreatomagmatic and hydrothermal explosion craters and diatremes. **Bulletin of Volcanology**, 77: 1–17. https://doi.org/10.1007/s00445-015-0901-7.

Valentine, G.A., Graettinger, A.H., Sonder, I. 2014. Explosion depths for phreatomagmatic eruptions. **Geophysical Research Letters**, 41: 3045–3051. https://doi.org/10.1002/2014GL060096.

Valentine, G.A., Sottili, G., Palladino, D.M., Taddeucci, J. 2015b. Tephra ring interpretation in light of evolving maar-diatreme concepts: Stracciacappa maar (central Italy). **Journal of Volcanology and Geothermal Research**, 308: 19–29. https://doi.org/10.1016/j.jvolgeores.2015.10.010.

Valentine, G.A., van Wyk de Vries, B. 2014. Unconventional maar diatreme and associated intrusions in the soft sediment-hosted Mardoux structure (Gergovie, France). **Bulletin of Volcanology**, 76: 1–16. https://doi.org/10.1007/s00445-014-0807-9.

Valentine, G.A., White, J.D.L. 2012. Revised conceptual model for maar-diatremes: Subsurface processes, energetics, and eruptive products. **Geology**, 40: 1111–1114. https://doi.org/10.1130/G33411.1.

Valentine, G.A., White, J.D.L., Ross, P.-S., Graettinger, A.H., Sonder, I. 2017. Updates to Concepts on Phreatomagmatic Maar-Diatremes and Their Pyroclastic Deposits. **Frontiers in Earth Science**, 5: 68. https://doi.org/10.3389/feart.2017.00068.

Valore, L.A., Licht, O.A.B., 2016. A mafic volcaniclastic deposit (MVD) of the Serra Geral Group, Sertanópolis, State of Paraná. Proc… 48th Brazilian Geological Congress, SBG, Porto Alegre, Brazil.

Van Eaton, A. R., Muirhead, J. D., Wilson, C. J. N., Cimarelli, C. 2012. Growth of volcanic ash aggregates in the presence of liquid water and ice: an experimental approach. **Bulletin of Volcanology,** 74(9): 1963 – 1984.

Van Eaton, A.R., Wilson, C.J.N. 2013. The nature, origins and distribution of ash aggregates in a large-scale wet eruption deposit: Oruanui, New Zealand. **Journal of Volcanology and Geothermal Research**, 250: 129–154. https://doi.org/10.1016/j.jvolgeores.2012.10.016.

Van Otterloo, J., Cas, R.A.F., Scutter, C.R. 2015. The fracture behaviour of volcanic glass and relevance to quench fragmentation during formation of hyaloclastite and phreatomagmatism. **Earth-Science Reviews,** 151: 79-116.

Van Otterloo, J., Cas, R.A.F., Sheard, M.J. 2013. Eruption processes and deposit characteristics at the monogenetic Mt. Gambier Volcanic Complex, SE Australia: Implications for alternating magmatic and phreatomagmatic activity. **Bulletin of Volcanology**, 75: 1–21. https://doi.org/10.1007/s00445-013-0737-y.

Van Otterloo, J., Raveggi, M., Cas, R. A. F., Maas, R. 2014. Polymagmatic activity at the monogenetic Mt Gambier volcanic complex in the Newer Volcanics Province, SE Australia: new insights into the occurrence of intraplate volcanic activity in Australia. **Journal of Petrology**, *55*(7): 1317-1351.

Vazquez, J.A., Ort, M.H. 2006. Facies variation of eruption units produced by the passage of single pyroclastic surge currents, Hopi Buttes volcanic field, USA. **Journal of Volcanology and Geothermal Research**, 154: 222–236. https://doi.org/10.1016/j.jvolgeores.2006.01.003.

Viswanathan, S., Chandrasekharam, D., 1981. Geochemical comparison of the Siberian and Deccan traps. In: Subbaroa, K.V., Sukheswala, R.N. (Eds.), Deccan Volcanism and Related Basalt Provinces of the World. **Mem.-Geol. Soc. India** 3: 460–471.

Waichel, B.L., de Lima, E.F., Lubachesky, R., Sommer, C.A. 2006. Pahoehoe flows from the central Paraná Continental Flood Basalts. **Bulletin of Volcanology**, 68: 599–610. https://doi.org/10.1007/s00445-005-0034-5.

Waichel, B.L., de Lima, E.F., Sommer, C.A., Lubachesky, R. 2007. Peperite formed by lava flows over sediments: An example from the central Paraná Continental Flood Basalts, Brazil. **Journal of Volcanology and Geothermal Research**, 159: 343–354. https://doi.org/10.1016/j.jvolgeores.2006.07.009.

Waichel, B.L., de Lima, E.F., Viana, A.R., Scherer, C.M., Bueno, G.V., Dutra, G. 2012. Stratigraphy and volcanic facies architecture of the Torres Syncline, Southern Brazil, and its role in understanding the Paraná-Etendeka Continental Flood Basalt Province. **Journal of Volcanology and Geothermal Research**, 215–216: 74–82. https://doi.org/10.1016/j.jvolgeores.2011.12.004.

Walker, G.P.L. 1971. Compound and simple lava flows and flood basalts. **Bulletin Volcanologique**, 35: 579–590. https://doi.org/10.1007/BF02596829.

Walker, G.P.L. 1981. Characteristics of two phreatoplinian ashes, and their water-flushed origin. **Journal of Volcanology and Geothermal Research**, 9: 395–407. https://doi.org/10.1016/0377-0273(81)90046-9.

Walker, G. P. 1987. Pipe vesicles in Hawaiian basaltic lavas: Their origin and potential as paleoslope indicators. **Geology,** *15*(1): 84-87.

Walker, G.P.L. 1989. Spongy pahoehoe in Hawaii: A study of vesicle-distribution patterns in basalt and their significance. **Bulletin of Volcanology**, 51: 199–209. https://doi.org/10.1007/BF01067956

Washburne, Ch. W. 1930. Petroleum geology of the State of São Paulo. Comissão Geográfica e Geológica do Estado de São Paulo, São Paulo, **Bol.** 22, 282 p.

Watton, T.J., Jerram, D.A., Thordarson, T., Davies, R.J. 2013. Three-dimensional lithofacies variations in hyaloclastite deposits. **Journal of Volcanology and Geothermal Research**, 250: 19–33. https://doi.org/10.1016/j.jvolgeores.2012.10.011.

Weinstein, Y. 2007. A transition from strombolian to phreatomagmatic activity induced by a lava flow damming water in a valley. **Journal of Volcanology and Geothermal Research**, 159: 267–284. https://doi.org/10.1016/j.jvolgeores.2006.06.015.

Wentworth, C.K.. 1922. A scale of grade and class terms for clastic sediments. **The Journal of Geology**, 30: 377–392.

White, J.D. 1991. Maar-diatreme phreatomagmatism at Hopi Buttes, Navajo Nation (Arizona), USA. **Bulletin of Volcanology**, 53: 239–258. https://doi.org/10.1007/BF00414522.

White, J.D.L., Bryan, S.E., Ross, P.S., Self, S., Thordarson, T. 2009. Physical volcanology of continental large igneous provinces: Update and review. **Studies in volcanology: the legacy of George Walker. Special Publications of IAVCEI,** 2: 291-321. https://doi.org/10.1144/iavcel002.15.

White, J. D. L., Houghton, B. 2000. Surtseyan and related phreatomagmatic eruptions. In: Sigurdsson, H., Houghton, B., McNutt, S., Rymer, H., Stix, J. Encyclopedia of volcanoes. Academic press. San Diego, 495-513.

White, J.D.L., Houghton, B.F. 2006. Primary volcaniclastic rocks. **Geology**, 34: 677–680. https://doi.org/10.1130/G22346.1.

White, J.D.L., McClintock, M.K. 2001. Immense vent complex marks flood-basalt eruption in a wet, failed rift: Coombs Hills, Antarctica. **Geology**, 29: 935–938. https://doi.org/10.1130/0091-7613(2001)029<0935:IVCMFB>2.0.CO;2

White, J.D.L., McPhie, J., and Skilling, I., 2000, Peperite: A useful genetic term. **Bulletin of Volcanology**, 62: 65–66. doi: 10.1007/s004450050293.

White, J.D.L., Ross, P.S. 2011. Maar-diatreme volcanoes: A review. **Journal of Volcanology and Geothermal Research**, 201: 1–29. https://doi.org/10.1016/j.jvolgeores.2011.01.010.

White, J.D.L., Schmincke, H.U. 1999. Phreatomagmatic eruptive and depositional processes during the 1949 eruption on La Palma (Canary Islands). **Journal of Volcanology and Geothermal Research**, 94: 283–304. https://doi.org/10.1016/S0377-0273(99)00108-0.

White, J.D.L., Valentine, G.A. 2016. Magmatic versus phreatomagmatic fragmentation: Absence of evidence is not evidence of absence. **Geosphere**, 12: 1478–1488. https://doi.org/10.1130/GES01337.1.

White, I.C. 1908. Comissão de Estudos das Minas de Carvão de Pedra do Brazil – Relatório Final. In: CPRM. 2008. Edição comemorativa: 100 anos do Relatório White. Edição fac-similar, Imprensa Nacional, Rio de Janeiro, 617 p.

Wilmoth, R.A., Walker, G.P.L. 1993. P-type and S-type pahoehoe: a study of vesicle distribution patterns in Hawaiian lava flows. **Journal of Volcanology and Geothermal Research**, 55: 129–142. https://doi.org/10.1016/0377-0273(93)90094-8.

Wohletz, K.H., Sheridan, M.F. 1983. Hydrovolcanic explosions II. Evolution of basaltic tuff rings and tuff cones. **American Journal of Science**, 283: 385–413. https://doi.org/10.2475/ajs.283.5.385.

Zimanowski, B., Büttner, R., Dellino, P., White, J.D.L., Wohletz, K.H. 2015. Magma–Water Interaction and Phreatomagmatic Fragmentation. **The Encyclopedia of Volcanoes**, 473–484. https://doi.org/10.1016/b978-0-12-385938-9.00026-2.

5 CAPÍTULO V – CONCLUSÃO

5.1 Considerações finais

Em Sertanópolis, as características das fácies interderrames mapeadas permitem associá-las ao modelo dos aparelhos hidrovulcânicos "monogenéticos" dos maares a anéis de tufos. Muitas dessas características incluem feições já observadas em interderrames de outras regiões da PIP no Paraná, como: agregados de cinza; vesículas sin-deposicionais em tufos; estruturas sedimentares características de depósitos de queda ou fluxo; presença de vitroclastos juvenis de morfologias sugestivas de *quenching* e interação *MFC* explosiva (Licht, 2012; Licht e Arioli, 2013, 2018; Licht *et al*., 2015; Valore *et al*., 2017).

Devido à alta proporção de cinza acessória siliclástica, estas camadas podem ser confundidas à primeira vista com arenitos e siltitos sedimentares. Por causa disso, é necessária atenção à observação de feições como as reportadas acima - o que pode ser consideravelmente dificultado pela qualidade das exposições interderrames ou silicificação avançada em alguns casos. É inteiramente possível que muitas sucessões interderrames reportadas como sedimentos com contribuição vulcanogênica sejam na realidade depósitos piroclásticos primários. Conforme demonstrado nesta caracterização, isso inclui o material que comumente preenche a porosidade primária em brechas autoclásticas, dando origem a uma fácies mista de extrema importância para interpretações paleoambientais, uma vez que frequentemente apenas este material se encontra preservado em sucessões interderrames.

Neste mesmo contexto, a observação de brechas cujas características sedimentológicas dificilmente são explicadas por fenômenos de deposição autoclástica realça a necessidade de atenção para este mesmo tema. Conforme o panorama que vêm se estabelecendo no estudo de depósitos vulcanoclásticos, fenômenos de transporte e deposição de natureza extremamente distinta por vezes geram fácies de arranjos muito semelhantes, que só podem ser distinguidas por investigações com sólidas bases sedimentológicas - ou podem se tornar essencialmente indiferenciáveis devido à sobreposição de processos diagenéticos, deformacionais ou intempéricos, especialmente em sucessões mais antigas (Allen, 1988; McPhie *et al*., 1993; Rosa *et al*., 2016). No entanto, isto também significa que

depósitos cujas características permitem claros diagnósticos vulcanológicos devem ser excepcionalmente bem estudados. Além disso, de maneira semelhante ao que ocorre na sedimentologia regular, estudos sobre fácies vulcanoclásticas em depósitos recentes devem sempre ser calibrados por observações a respeito de fatores de preservação e representatividade no registro geológico.

Na Província Ígnea do Paraná, o estudo de camadas interderrames e especialmente depósitos vulcanoclásticos máficos pode melhorar significativamente o entendimento a respeito de processos vulcanológicos (efusivos e explosivos), paleoambientes sin-vulcânicos, estratigrafia de PCBs e tectônica de *rifts* continentais. Os melhores resultados possíveis serão obtidos a partir da integração de diversas abordagens, como por exemplo:

- análises vulcanológicas diversas, que busquem a conexão entre controles eruptivos/magmáticos, processos de geração de fragmentos vulcanoclásticos, distribuição de fácies vulcânicas e interações com sistemas sedimentares;
- análises paleoambientais, por meio da palinologia, geoquímica de sedimentos e também biomarcadores, por exemplo;
- análises paleogeográficas, baseadas na continuidade de campanhas de mapeamento geológico regional e detalhado em rochas vulcânicas e interderrames;
- análises tectonoestratigráficas, que devem partir de um arcabouço estratigráfico obtido pelo emprego dos métodos acima, sendo então extrapolado e correlacionado em subsuperfície com auxílio de dados estruturais da sequência vulcânica.

REFERÊNCIAS

Allen, R.L. 1988. False pyroclastic textures in altered silicic lavas, with implications for volcanic-associated mineralization. **Economic Geology**, 83: 1424–1446. https://doi.org/10.2113/gsecongeo.83.7.1424.

Almeida, F.F.M. de, Carneiro, C., dal, R., Mizusaki, A.M.P., 1996. Correlação do magmatismo das bacias da margem continental brasileira com o das áreas emersas adjacentes. **Rev. Bras. Geociencias**, 26: 125–138.

Almeida F. F. M., Carneiro, C. S. R., Bartorelli, A. 2012. Magmatismo pós-paleozoico no Brasil, in: Geologia do Brasil. In: Hasui, Y., Carneiro, C. D. R., Almeida F. F. M., Bartorelli, A. (Eds.), Beca Ed., 430–452,

Almeida, V.V., Janasi, V.A., Heaman, L.M., Shaulis, B.J., Hollanda, M.H.B.M., Renne, P.R. 2018. Contemporaneous alkaline and tholeiitic magmatism in the Ponta Grossa Arch, Paraná-Etendeka Magmatic Province: Constraints from U–Pb zircon/baddeleyite and 40Ar/39Ar phlogopite dating of the José Fernandes Gabbro and mafic dykes. **Journal of Volcanology and Geothermal Research**, 355: 55–65. https://doi.org/10.1016/j.jvolgeores.2017.01.018.

Almeida, V.V., Janasi, V.A, Azzone, R.G., Faleiros, F.M. 2019. Crustal contamination and genesis of transitional alkaline-tholeiitic intrusions: Insights from the José Fernandes Suite, Paraná Magmatic Province, Brazil. **Lithos**, 342–343: 59–75. https://doi.org/10.1016/j.lithos.2019.05.023.

Amin, J., Valentine, G.A. 2017. Compound maar crater and co-eruptive scoria cone in the Lunar Crater Volcanic Field (Nevada, USA). **Journal of Volcanology and Geothermal Research**, 339: 41–51. https://doi.org/10.1016/j.jvolgeores.2017.05.002.

Anderson, D.L. 2005. Large Igneous Provinces, Delamination, and Fertile Mantle. **Elements**, 1: 271–275. https://doi.org/10.2113/gselements.1.5.271.

Anderson, D. L. 2007. The eclogite engine: Chemical geodynamics as a Galileo thermometer. **Special Papers Geological Society Of America**, 430.

Assine, M. L. Aspectos da estratigrafia das seqüências pré-carboníferas da Bacia do Paraná no Brasil. 1996. Tese (Doutorado) - Universidade de São Paulo, São Paulo.

Azambuja Jr., J. R. A. 1943. Arenito Vulcano-clástico intertrapeano de Iraí, R. G do Sul. **Mineração e Metalurgia**, 7(41): 361-364.

Baker, C.L., 1923. The lava fields of the Paraná Basin, South America. **J. Geol**. 31: 66–79.

Baksi, A.K. 2018. Paraná flood basalt volcanism primarily limited to ~ 1 Myr beginning at 135 Ma: New 40Ar/39Ar ages for rocks from Rio Grande do Sul, and critical evaluation of published radiometric data. **Journal of Volcanology and Geothermal Research**, 355: 66–77. https://doi.org/10.1016/j.jvolgeores.2017.02.016.

Barreto, C.J.S., de Lima, E.F., Scherer, C.M., Rossetti, L. de M.M. 2014. Lithofacies analysis of basic lava flows of the Paraná igneous province in the south hinge of Torres Syncline, Southern Brazil. **Journal of Volcanology and Geothermal Research**, 285: 81–99. https://doi.org/10.1016/j.jvolgeores.2014.08.008.

Barreto, C. J. S., Lafon, J. M., Lima, E. F., Sommer, C. A. 2016. Geochemical and Sr-Nd-Pb isotopic insight into the low-Ti basalts from Southern Paraná Igneous Province, Brazil: The role of crustal contamination. International Geology Review, 58(11): 1324-1349.

Bellieni, G., Brotzu, P., Comin-Chiaramonti, P., Ernesto, M., Melfi, A. J., Pacca, I. G., and Piccirillo, E. M. 1984. Flood basalt to rhyolites suites in the southern Paraná plateau (Brazil): paleomagnetism, petrogenis and geodynamic implications, J. Petrol., 25, 579–618.

Bigarella, J. J. 1970. Continental drift and paleocurrent analysis (a comparison between Africa and South America). **Bol. Paranaense Geoci**. 30: 73 - 97.

Bigarella, J. J., Van Eeden, O. R. 1970. Mesozoic palaeowind patterns and the problem of continental drift. **Boletim Paranaense de Geociências,** 28/29: 115-144.

Black, B. A., Weiss, B. P., Elkins-Tanton, L. T., Veselovskiy, R. V., Latyshev, A. 2015. Siberian Traps volcaniclastic rocks and the role of magma-water interactions. **Geological Society of America Bulletin,** 127(9-10): 1437-1452.

Bondre, N.R., Duraiswami, R.A., Dole, G. 2004. Morphology and emplacement of flows from the Deccan Volcanic Province, India. **Bulletin of Volcanology**, 66: 29–45. https://doi.org/10.1007/s00445-003-0294-x.

Branney, M.J., Kokelaar, P., 2002. Pyroclastic Density Currents and the Sedimentation of Ignimbrites. The Geological Society, London.

Brown, R.J., Bonadonna, C., Durant, A.J. 2012. A review of volcanic ash aggregation. **Physics and Chemistry of the Earth**, 45–46: 65–78. https://doi.org/10.1016/j.pce.2011.11.001.

Brown, R.J., Branney, M.J., Maher, C., Dávila-Harris, P. 2010. Origin of accretionary lapilli within ground-hugging density currents: Evidence from pyroclastic couplets on Tenerife. **Bulletin of the Geological Society of America**, 122: 305–320. https://doi.org/10.1130/B26449.1.

Bryan, S.E., Ernst, R.E. 2008. Revised definition of Large Igneous Provinces (LIPs). **Earth-Science Reviews**, 86: 175–202. https://doi.org/10.1016/j.earscirev.2007.08.008.

Busby-Spera, C.J., White, J.D.L. 1987. Variation in peperite textures associated with differing host-sediment properties. **Bulletin of Volcanology,** 49(6): 765-776.

Büttner, R., Dellino, P., La Volpe, L., Lorenz, V., Zimanowski, B. 2002. Thermohydraulic explosions in phreatomagmatic eruptions as evidenced by the comparison between pyroclasts and products from Molten Fuel Coolant Interaction experiments. **Journal of Geophysical Research: Solid Earth**, 107: ECV 5–1–ECV 5–14. https://doi.org/10.1029/2001jb000511.

Campbell, I.H., 2007. Testing the plume theory. **Chem. Geol**., 241:153–176.

Cañón-Tapia, E. 2018. The Paraná-Etendeka Continental Flood Basalt Province: A historical perspective of current knowledge and future research trends. **Journal of Volcanology and Geothermal Research**, 355: 287–303. https://doi.org/10.1016/j.jvolgeores.2017.11.011.

Capaccioni, B., Coniglio, S. 1995. Varicolored and vesiculated tuffs from La Fossa volcano, Vulcano Island (Aeolian Archipelago, Italy): evidence of syndepositional alteration processes. **Bulletin of Volcanology**, 57: 61–70. https://doi.org/10.1007/BF00298708.

Cashman, K.V., Thornber, C., Kauahikaua, J.P. 1999. Cooling and crystallization of lava in open channels, and the transition of Pāhoehoe Lava to 'A'ā. **Bulletin of Volcanology**, 61: 306–323. https://doi.org/10.1007/s004450050299.

Chough, S.K., Sohn, Y.K. 1990. Depositional mechanics and sequences of base surges, Songaksan tuff ring, Cheju Island, Korea. **Sedimentology**, 37: 1115–1135. https://doi.org/10.1111/j.1365-3091.1990.tb01849.x.

Coffin, M. F, Eldholm, O. 1994. Large Igneous Provinces: Crustal structure, dimensions, and external consequences. **Rev. Geophys.,** 32: 1–36.

Cordani, U.G., Neves, B.B.B., Fuck, R.A., Porto, R., Thomaz Filho, A., Cunha, F.M.B.d., 1984. Estudo preliminar de integração do Pré-cambriano com os eventos tectônicos das bacias sedimentares brasileiras. Ciênc. Téc. Petról. 1–70

Creer, K.M., Miller, J.A., Smith, A.G. 1965. Radiometric age of the Serra Geral Formation [4]. **Nature**, 207: 282–283. https://doi.org/10.1038/207282a0.

De Min, A., Callegaro, S., Marzoli, A., Nardy, A.J., Chiaradia, M., Marques, L.S., Gabbarrini, I. 2018. Insights into the petrogenesis of low- and high-Ti basalts: Stratigraphy and geochemistry of four lava sequences from the central Paraná basin. **Journal of Volcanology and Geothermal Research**, 355: 232–252. https://doi.org/10.1016/j.jvolgeores.2017.08.009.

Dellino, P., Isaia, R., Volpe, L.L., Orsi, G. 2001. Statistical analysis of textural data from complex pyroclastic sequences: Implications for fragmentation processes of the Agnano-Monte Spina Tephra (4.1 ka), Phlegraean Fields, southern Italy. **Bulletin of Volcanology**, 63: 443–461. https://doi.org/10.1007/s004450100163.

Derby, O.A., 1878. A geologia da região diamantífera da Província do Paraná no Brasil. Rio de Janeiro. Archivos do Museu Nacional do Rio de Janeiro III (3/4), 87–98.

Duraiswami, R.A., Bondre, N.R., Managave, S. 2008. Morphology of rubbly pahoehoe (simple) flows from the Deccan Volcanic Province: Implications for style of emplacement. **Journal of Volcanology and Geothermal Research**, 177: 822–836. https://doi.org/10.1016/j.jvolgeores.2008.01.048.

Duraiswami, R.A., Gadpallu, P., Shaikh, T.N., Cardin, N. 2014. Pahoehoe-a'a transitions in the lava flow fields of the western Deccan Traps, India-implications for emplacement dynamics, flood basalt architecture and volcanic stratigraphy. **Journal of Asian Earth Sciences**, 84: 146–166. https://doi.org/10.1016/j.jseaes.2013.08.025.

Dürig, T., Zimanowski, B. 2012. "Breaking news" on the formation of volcanic ash: Fracture dynamics in silicate glass. **Earth and Planetary Science Letters**, 335–336: 1–8. https://doi.org/10.1016/j.epsl.2012.05.001.

Du Toit, A. L. 1927. A geological comparison of South America with South Africa. The Carnegie Institution, Washington, Publication 381.

Du Toit, A. L. 1937. Our wandering continents. Oliver and Boyd, Edinburgh.

Ellis, B., Branney, M.J. 2010. Silicic phreatomagmatism in the Snake River Plain: The Deadeye Member. **Bulletin of Volcanology**, 72: 1241–1257. https://doi.org/10.1007/s00445-010-0400-9.

Erlank, A.J., Marsh, J.S., Duncan, A.R., Miller, R.M., Hawkesworth, C.J., Betton, P.J., Rex, D.C., 1984. Geochemistry and petrogenesis of Etendeka volcanic rocks from SW A/ Namibia. In: Erlank, A.J. (Ed.), Petrogenesis of Volcanic Rocks of the Karoo Province. Geological Society of Sud Africa, pp. 195–247.

Ernst, R.E., Buchan, K.L., Campbell, I.H. 2005. Frontiers in Large Igneous Province research. **Lithos**, 79: 271–297. https://doi.org/10.1016/j.lithos.2004.09.004.

Fernandes, A.J., De Assis Negri, F., Sobrinho, J.M.A., De Assis Janasi, V. 2018. Local geological sections and regional stratigraphy based on physical geology and chemical stratigraphy of the Serra Geral Group from Araraquara to Avaré, SP. **Brazilian Journal of Geology**, 48: 243–261. https://doi.org/10.1590/2317-4889201720180093.

Fernandes, L. A., Coimbra, A. M. 1996. Bacia Bauru (Cretáceo Superior, Brasil). **Anais da Academia Brasileira de Ciências**: 68(2): 195-205.

Fernandes, L. A., Coimbra, A. M. 2000. The Late Cretaceous Caiuá Desert (Bauru Basin, Brazil). International Geological Congress Vol. 31.

Fernandes, L.A., Magalhães Ribeiro, C.M. 2015. Evolution and palaeoenvironment of the Bauru Basin (Upper Cretaceous, Brazil). **Journal of South American Earth Sciences**, 61: 71–90. https://doi.org/10.1016/j.jsames.2014.11.007.

Fisher, R.V. 1961. Proposed classification of volcaniclastic sediments and rocks. **Geological Society of America Bulletin**, 72: 1409–1414.

Fisher, R. V., Schmincke, H. -U. 1984. Pyroclastic rocks. Springer-Verlag, Berlin, 472 p.

Florisbal, L.M., Heaman, L.M., de Assis Janasi, V., de Fatima Bitencourt, M. 2014. Tectonic significance of the Florianópolis Dyke Swarm, Paraná-Etendeka Magmatic Province: A reappraisal based on precise U-Pb dating. **Journal of Volcanology and Geothermal Research**, 289: 140–150. https://doi.org/10.1016/j.jvolgeores.2014.11.007.

Fodor, R.V. 1987. Low- and high-TiO2 flood basalts of southern Brazil: origin from picritic parentage and a common mantle source. **Earth and Planetary Science Letters**, 84: 423–430. https://doi.org/10.1016/0012-821X(87)90007-0.

Fodor, R.V., Corwin, C., Roisenberg, A. 1985a. Petrology of Serra Geral (Paraná) continental flood basalts, southern Brazil: crustal contamination, source material, and South Atlantic magmatism. **Contributions to Mineralogy and Petrology**, 91: 54–65. https://doi.org/10.1007/BF00429427.

Fodor, R.V., Corwin, C., Sial, A.N. 1985b. Crustal signatures in the Serra Geral flood-basalt province, southern Brazil: O- and Sr-isotope evidence. **Geology**, 13: 763–765. https://doi.org/10.1130/0091-7613(1985)13<763:CSITSG>2.0.CO;2.

Fornero, S. A., Marins, G. M., Lobo, J. T., Freire, A. F. M., Lima, E. F. 2019. Characterization of subaerial volcanic facies using acoustic image logs: Lithofacies and log-facies of a lava-flow deposit in the Brazilian pre-salt, deepwater of Santos Basin. **Marine and Petroleum Geology**, 99: 156-174.

Foulger, G.R. 2018. Origin of the South Atlantic igneous province. **Journal of Volcanology and Geothermal Research**, 355: 2–20. https://doi.org/10.1016/j.jvolgeores.2017.09.004.

Frank, H.T., Gomes, M.E.B., Formoso, M.L.L. 2009. Revisão da extensão areal e do volume da formação serra geral, Bacia do paraná, América do Sul. **Pesquisas em Geociencias**, 36: 49–57. https://doi.org/10.22456/1807-9806.17874.

Goldberg, K., Kuchle, J., Scherer, C., Alvarenga, R., Ene, P.L., Armelenti, G., De Ros, L.F. 2017. Re-sedimented deposits in the rift section of the Campos Basin. **Marine and Petroleum Geology**, 80: 412–431. https://doi.org/10.1016/j.marpetgeo.2016.11.022.

Gomes, A.S., Licht, O.A.B., Vasconcellos, E.M.G., Soares, J.S. 2018. Chemostratigraphy and evolution of the Paraná Igneous Province volcanism in the central portion of the state of Paraná Southern Brazil. **Journal of Volcanology and Geothermal Research**, 355: 253–269. https://doi.org/10.1016/j.jvolgeores.2017.09.002.

Graettinger, Alison H., Skilling, I., McGarvie, D., Höskuldsson, Á. 2013. Subaqueous basaltic magmatic explosions trigger phreatomagmatism: A case study from Askja, Iceland. **Journal of Volcanology and Geothermal Research**, 264: 17–35. https://doi.org/10.1016/j.jvolgeores.2013.08.001.

Graettinger, A.H., Valentine, G.A. 2017. Evidence for the relative depths and energies of phreatomagmatic explosions recorded in tephra rings. **Bulletin of Volcanology**, 79: 88. https://doi.org/10.1007/s00445-017-1177-x.

Graettinger, A.H., Valentine, G.A., Sonder, I., Ross, P.S., White, J.D.L. 2015. Facies distribution of ejecta in analog tephra rings from experiments with single and multiple subsurface explosions. **Bulletin of Volcanology**, 77: 1–12. https://doi.org/10.1007/s00445-015-0951-x.

Gregg, T.K.P. 2017. Patterns and processes: Subaerial lava flow morphologies: A review. **Journal of Volcanology and Geothermal Research**, 342: 3-12.

Harris, A. J. L., Rowland, S. K. 2009. Effusion rate controls on lava flow length and the role of heat loss: a review. **Studies in volcanology: the legacy of George Walker**. **Special Publications of IAVCEI**, 2: 33-51.

Hartmann, L.A., Arena, K.R., Duarte, S.K., Pertille, J. 2013. Long-distance lava correlation in the Paraná volcanic province along the Serra Geral cuesta, southeastern Brazil. **International Journal of Earth Sciences**, 102: 1655–1669. https://doi.org/10.1007/s00531-013-0899-z.

Hawkesworth, C., Mantovani, M., Peate, D. 1988. Lithosphere remobilization during parana cfb magmatism. **Journal of Petrology**, Special_Volume: 205–223. https://doi.org/10.1093/petrology/Special_Volume.1.205.

Hawkesworth, C.J., Gallagher, K., Kelley, S., Mantovani, M., Peate, D.W., Regelous, M., Rogers, N.W. 1992. Paraná magmatism and the opening of the South Atlantic. **Geological Society Special Publication**, 68: 221–240. https://doi.org/10.1144/GSL.SP.1992.068.01.14.

Heiken, G. H. 1972. Morphology and petrology of volcanic ash. **Geological Society of America Bulletin**, 83: 1961–1988.

Hon, K., Kauahikaua, J., Denlinger, R., Mackay, K. 1994. Emplacement and inflation of pahoehoe sheet flows: observations and measurements of active lava flows on Kilauea volcano, Hawaii. **Geological Society of America Bulletin**, 106: 351–370. https://doi.org/10.1130/0016-7606(1994)106<0351:EAIOPS>2.3.CO;2.

Houghton, B. F., Swanson, D. A., Rausch, J., Carey, R. J., Fagents, S. A., Orr, T. R. 2013. Pushing the Volcanic Explosivity Index to its limit and beyond: Constraints from exceptionally weak explosive eruptions at Kīlauea in 2008. **Geology**, 41(6): 627-630.

Houghton, B.F., White, J. D. L., Van Eaton, A. R. 2015. Phreatomagmatic and related eruption styles. In: Sigurdsson, H., Houghton, B., McNutt, S., Rymer, H., Stix, J. (Eds.). The encyclopedia of volcanoes (pp. 537-552). Academic Press.

Jerram, D.A, Mountney, N.P, Holzförster, F., Stollhofen, H. 1999. Internal stratigraphic relationships in the Etendeka Group in the Huab Basin, NW Namibia: Understanding the onset of flood volcanism. **Journal of Geodynamics**, 28: 393–418. https://doi.org/10.1016/S0264-3707(99)00018-6.

Jerram, D.A., Mountney, N.P., Howell, J.A., Long, D., Stollhofen, H., 2000. Death of a sand sea: an active aeolian erg system- atically buried by the Etendeka flood basalts of NW Namibia. **J. Geol. Soc. (Lond.)** 157: 513–516.

Jerram, D.A., Stollhofen, H. 2002. Lava-sediment interaction in desert settings; are all peperite-like textures the result of magma-water interaction? **Journal of Volcanology and Geothermal Research**, 114: 231–249. https://doi.org/10.1016/S0377-0273(01)00279-7.

Jerram, D.A., Svensen, H.H., Planke, S., Polozov, A.G., Torsvik, T.H. 2016. The onset of flood volcanism in the north-western part of the Siberian Traps: Explosive volcanism versus effusive lava flows. **Palaeogeography, Palaeoclimatology, Palaeoecology**, 441: 38–50. https://doi.org/10.1016/j.palaeo.2015.04.022.

Jerram, D.A., Widdowson, M. 2005. The anatomy of Continental Flood Basalt Provinces: Geological constraints on the processes and products of flood volcanism. **Lithos**, 79: 385–405. https://doi.org/10.1016/j.lithos.2004.09.009.

Jordan, S.C., Cas, R.A.F., Hayman, P.C. 2013. The origin of a large (\textgreater3km) maar volcano by coalescence of multiple shallow craters: Lake Purrumbete maar, southeastern Australia. **Journal of Volcanology and Geothermal Research**, 254: 5–22. https://doi.org/10.1016/j.jvolgeores.2012.12.019.

Jordan, S.C., Dürig, T., Cas, R.A.F., Zimanowski, B. 2014. Processes controlling the shape of ash particles: Results of statistical IPA. **Journal of Volcanology and**

Geothermal Research, 288: 19–27. https://doi.org/10.1016/j.jvolgeores.2014.09.012.

Kauahikaua, J., Cashman, K.V., Mattox, T.N., Heliker, C.C., Hon, K.A., Mangan, M.T., Thornber, C.R. 1998. Observations on basaltic lava streams in tubes from Kilauea Volcano, island of Hawai'i. **Journal of Geophysical Research: Solid Earth**, 103: 27303–27323. https://doi.org/10.1029/97jb03576.

Kereszturi, G., Nemeth, K. 2012. Monogenetic Basaltic Volcanoes: Genetic Classification, Growth, Geomorphology and Degradation, In: Updates in Volcanology - New Advances in Understanding Volcanic Systems. InTech. https://doi.org/10.5772/51387.

Keszthelyi, L., Keszthelyi, L., Thordarson, T., Self, S. 2001. Rubbly Pahoehoe: Implication for Flood Basalt Eruptions and their Atmospheric Effects. **Agufm**, 2001: V52A–1050.

Kokelaar, B.P., 1986. Magma-water interactions in subaqueous and emergent basaltic volcanism. **Bull. Volcanol.,** 48: 275- 289.

Kurszlaukis, S., Fulop, A. 2013. Factors controlling the internal facies architecture of maar-diatreme volcanoes. **Bulletin of Volcanology**, 75: 1–12. https://doi.org/10.1007/s00445-013-0761-y.

Licht,O.A.B., Arioli,E.E. 2011. Evidências de eventos explosivos - hidrovulcanismo - na Formação Serra Geral, Estado do Paraná, Brasil. Proc.... V° Simpósio de Vulcanismo e Ambientes Associados. SBG. Goiás.

Licht,O.A.B., Arioli,E.E. 2011. Hidrovulcanismo, um modelo eruptivo para a Formação Serra Geral. Proc.... V° Simpósio de Vulcanismo e Ambientes Associados. SBG. Goiás.

Licht, O. A. B., Arioli, E. E. 2013. O Grupo Serra Geral no Estado do Paraná: Mapeamento geológico das cartas 1:250.000 de Guaíra, Cascavel, Campo Mourão, Foz do Iguaçu, Guaraniaçu, Guarapuava, Pato Branco e Clevelândia. Serviço Geológico do Paraná - MINEROPAR, Curitiba, v. 1 (texto), 451 p.

Licht, O. A . B., Arioli, E. E. 2018. Mapa geológico do Grupo Serra Geral no Estado do Paraná. Instituto de Terras, Cartografia e Geologia – ITCG, Curitiba, v.1, 318 p.

Licht, O. A. B., Valore, L. A., Szatmari, P. 2015. Faciology and stratigraphy of Mafic Volcaniclastic Deposits (MVDs), Serra Geral Group Saudade do Iguaçu-Coronel Vivida region, State of Paraná, Brazil. Proc...VI Simpósio de Vulcanismo e Ambientes Associados, SBG, São Paulo.

Licht, O. A. B. 2012. Estudo de produtos hidrovulcânicos no sudoeste do Paraná. Serviço Geológico do Paraná - MINEROPAR, Curitiba, 314 p.

Licht, O. A. B. 2014. A evolução do conhecimento sobre a Província Ígnea do Paraná – dos primórdios até 1950. **Revista do Instituto Geológico (São Paulo),** 35(2): 71-106.

Licht, O.A.B. 2018. A revised chemo-chrono-stratigraphic 4-D model for the extrusive rocks of the Paraná Igneous Province. **Journal of Volcanology and Geothermal Research**, 355: 32–54. https://doi.org/10.1016/j.jvolgeores.2016.12.003.

Lima, E.F., Waichel, B.L., De Magalhães May Rossetti, L., Viana, A.R., Scherer, C.M., Bueno, G.V., Dutra, G. 2012. Morphological and petrographic patterns of the pahoehoe and a'a flows of the Serra Geral Formation in the Torres Syncline (Rio Grande do sul state Brazil). **Revista Brasileira de Geociencias**, 42: 744–753. https://doi.org/10.5327/Z0375-75362012000400007.

Liu, E.J., Cashman, K.V., Rust, A.C., Höskuldsson, A. 2017. Contrasting mechanisms of magma fragmentation during coeval magmatic and hydromagmatic activity: the Hverfjall Fires fissure eruption, Iceland. **Bulletin of Volcanology**, 79: . https://doi.org/10.1007/s00445-017-1150-8.

Lobo, J. T., Duarte, B. P., Szatmari, P., Castro Valente, S. 2016. Basaltos continentais do Cretáceo Inferior da bacia de Campos, SE do Brasil: compilação de dados e petrogênese. **Revista Brasileira de Geociências, 37(2**): 204-236.

Lorenz, V. 1973. On the formation of maars. **Bulletin Volcanologique**, 37: 183–204. https://doi.org/10.1007/BF02597130.

Lorenz, V. 1986. On the growth of maars and diatremes and its relevance to the formation of tuff rings. **Bulletin of Volcanology**, 48: 265–274. https://doi.org/10.1007/BF01081755.

Luchetti, A.C.F., Nardy, A.J.R., Machado, F.B., Madeira, J.E.O., Arnosio, J.M. 2014. New insights on the occurrence of peperites and sedimentary deposits within the silicic volcanic sequences of the Paraná Magmatic Province, Brazil. **Solid Earth**, 5: 121–130. https://doi.org/10.5194/se-5-121-2014.

Maack, R. 1947. Breves notícias sobre a geologia dos estados de Santa Catarina e Paraná. **Arquivos de Biologia e Tecnologia**, 2: 65-154.

Machado, F. B., Rocha-Júnior, E.R.V., Marques, L.S., Nardy, A.J.R. 2015. Volcanological aspects of the northwest region of Paraná continental flood basalts (Brazil). **Solid Earth**, 6: 227–241. https://doi.org/10.5194/se-6-227-2015.

Mantovani, M.S.M., Marques, L.S., De Sousa, M.A., Civetta, L., Atalla, L., Innocenti, F., 1985. Trace elements and strontium isotope constraints on the origin and evolution of Paraná continental flood basalts of Santa Catarina State (Southern Brazil). **J. Petrol**. 26: 187–209.

Mantovani, M.S.M., Peate, D.W., Hawkesworth, C.J., 1988. Geochemical stratigraphy of Paraná Continental Flood Basalts: a contribution from borehole samples. In: Piccirillo, E.M., Melfi, A.J. (Eds.), The Mesozoic Flood Volcanism of the Paraná Basin. Inst. Astron. Geofísico, Univ. São Paulo, São Paulo, 15–24.

Manville, V., Németh, K., Kano, K. 2009. Source to sink: A review of three decades of progress in the understanding of volcaniclastic processes, deposits, and hazards. **Sedimentary Geology**, 220: 136–161. https://doi.org/10.1016/j.sedgeo.2009.04.022.

Marques, L.S., De Min, A., Rocha-Júnior, E.R.V., Babinski, M., Bellieni, G., Figueiredo, A.M.G. 2018. Elemental and Sr-Nd-Pb isotope geochemistry of the Florianópolis Dyke Swarm (Paraná Magmatic Province): crustal contamination and mantle source constraints. **Journal of Volcanology and Geothermal Research**, 355: 149–164. https://doi.org/10.1016/j.jvolgeores.2017.07.005.

Marques, L.S., Ernesto, M. 2004. O magmatismo toleítico da Bacia do Paraná. **Geologia do Continente Sul-Americano: evolução da obra de Fernando Flávio Marques de Almeida**, 245–263.

Marques, L.S., Rocha-Júnior, E.R.V., Babinski, M., Carvas, K.Z., Petronilho, L.A., De Min, A. 2016. Lead isotope constraints on the mantle sources involved in the genesis of Mesozoic high-Ti tholeiite dykes (Urubici type) from the São Francisco Craton (Southern Espinhaço, Brazil). **Brazilian Journal of Geology**, 46: 105–122. https://doi.org/10.1590/2317-4889201620150010.

Marshall, P.E., Widdowson, M., Murphy, D.T. 2016. The Giant Lavas of Kalkarindji: Rubbly pāhoehoe lava in an ancient continental flood basalt province. **Palaeogeography, Palaeoclimatology, Palaeoecology**, 441: 22–37. https://doi.org/10.1016/j.palaeo.2015.05.006.

Martí, J., Groppelli, G., Brum da Silveira, A. 2018. Volcanic stratigraphy: A review. **Journal of Volcanology and Geothermal Research**, 357: 68-91.

Martin, U., Németh, K. 2004. Peperitic lava lake-fed sills at Ság-hegy, western Hungary: A complex interaction of a wet tephra ring and lava. **Geological Society Special Publication**, 234: 33–50. https://doi.org/10.1144/GSL.SP.2004.234.01.04.

Martin, U., Németh, K. 2007. Blocky versus fluidal peperite textures developed in volcanic conduits, vents and crater lakes of phreatomagmatic volcanoes in Mio/Pliocene volcanic fields of Western Hungary. **Journal of Volcanology and Geothermal Research**, 159: 164–178. https://doi.org/10.1016/j.jvolgeores.2006.06.010.

McClintock, M., White, J.D.L. 2006. Large phreatomagmatic vent complex at Coombs Hills, Antarctica: Wet, explosive initiation of flood basalt volcanism in the Ferrar-Karoo LIP. **Bulletin of Volcanology**, 68: 215–239. https://doi.org/10.1007/s00445-005-0001-1.

McClintock, M., White, J.D.L., Houghton, B.F., Skilling, I.P. 2008. Physical volcanology of a large crater-complex formed during the initial stages of Karoo flood basalt volcanism, Sterkspruit, Eastern Cape, South Africa. **Journal of Volcanology and Geothermal Research**, 172: 93–111. https://doi.org/10.1016/j.jvolgeores.2005.11.012.

McDougall, I., Rüegg, N.R. 1966. Potassium-argon dates on the Serra Geral Formation of South America. **Geochimica et Cosmochimica Acta**, 30: 191–195. https://doi.org/10.1016/0016-7037(66)90106-2.

Milani, E. J. 1997. Evolução tectono-estratigráfica da Baciado Paraná e seu relacionamento com a geodinâmica fanerozóica do Gondwana sul-ocidental. Tese (Doutorado) - Universidade Federal do Rio Grande do Sul, Porto Alegre, 2v.

Milani, E.J., 2004. Comentários sobre a origem e a evolução tectônica da Bacia do Paraná. In: Montesso-Neto, V., Bartorelli, A., Carneiro, C.D.R., Brito-Neves, B.B. (Eds.), Geologia do Continente Sul-Americano – evolução da obra de Fernando Flávio Marques de Almeida. Ed. Becca, pp. 265–279.

Milani, E.J., De Wit, M.J. 2008. Correlations between the classic Paraná and Cape-Karoo sequences of South America and southern Africa and their basin infills flanking the Gondwanides: Du Toit revisited. **Geological Society Special Publication**, 294: 319–342. https://doi.org/10.1144/SP294.17.

Milani, E. J., Faccini, U. F., Scherer, C. M., Araújo, L. M. D., Cupertino, J. A. 1998. Sequences and stratigraphic hierarchy of the Paraná Basin (Ordovician to Cretaceous), southern Brazil. **Boletim IG-USP**, 29: 125-173.

Milani, E.J., Ramos, V.A. 1998. Paleozoic orogenies in southwestern Gondwana and the subsidence cycles of the Parana Basin. Orogenias paleozoicas no dominio sul-ocidental do Gondwana e os cicios de subsidencia da bacia do Parana. **Revista Brasileira de Geociencias**, 28: 473–484. https://doi.org/10.5327/rbg.v28i4.651.

Milani, E.J., Rangel, H.D., Bueno, G.V., Stica, J.M., Winter, W.R., Caixeta, J.M., Da Cruz Pessoa Neto, O. 2007. Brazilian sedimentary basins - Stratigraphic charts | Bacias sedimentares brasileiras - Cartas estratigráficas. **Boletim de Geociencias da Petrobras**, 15: 183–205.

Millett, J.M., Wilkins, A.D., Campbell, E., Hole, M.J., Taylor, R.A., Healy, D., Jerram, D.A., Jolley, D.W., Planke, S., Archer, S.G., Blischke, A., 2016. The geology of off-shore drilling through basalt sequences: Understanding operational complications to improve efficiency. **Mar. Petrol. Geol**. 77: 1177–1192. https://doi.org/10.1016/j.marpetgeo.2016.08.010.

Milner, S.C., Duncan, A.R., Whittingham, A.M., Ewart, A., 1995. Trans-Atlantic correla- tion of eruptive sequences and individual silicic volcanic units within the

Paraná- Etendeka igneous province. **J. Volcanol. Geoth. Res**. 69: 137–157. https://doi.org/10. 1016/0377-0273(95)00040-2.

Mohriak, W.U., Rosendahl, B.R., Turner, J.P., Valente, S.C., 2002. Crustal architecture of South Atlantic volcanic margins. **Geol. Soc. Am. Spec. Pap.** 362: 159–202. https:// doi.org/10.1130/0-8137-2362-0.159.

Mohriak, W., Nemčok, M., Enciso, G. 2008. South Atlantic divergent margin evolution: rift-border uplift and salt tectonics in the basins of SE Brazil. **Geological Society, London, Special Publications**, 294(1): 365-398.

Moraes, L.C., Seer, H.J. 2018. Pillow lavas and fluvio-lacustrine deposits in the northeast of Paraná Continental Magmatic Province, Brazil. **Journal of Volcanology and Geothermal Research**, 355: 78–86. https://doi.org/10.1016/j.jvolgeores.2017.03.024.

Moraes, L.C., Seer, H.J., Marques, L.S. 2018. Geology, geochemistry and petrology of basalts from Paraná Continental Magmatic Province in the Araguari, Uberlândia, Uberaba and Sacramento regions, Minas Gerais state, Brazil. **Brazilian Journal of Geology**, 48: 221–241. https://doi.org/10.1590/2317-4889201820170091.

Muffler, L. P., White, D. E., Truesdell, A. H. 1971. Hydrothermal explosion craters in yellowstone National Park. **Geological Society of America Bulletin**, 82(3): 723-740.

Morrissey M., Zimanowski B., Wohletz K.H., Büttner R. 2000. Phreatomagmatic Fragmentation. In: Sigurdsson, H., Houghton, B., McNutt, S., Rymer, H., Stix, J. Encyclopedia of Volcanoes, Academic Press, San Diego, p. 431-446.

Mueller, W.U., Garde, A.A., Stendal, H. 2000. Shallow-water, eruption-fed, mafic pyroclastic deposits along a Paleoproterozoic coastline: Kangerluluk volcano-sedimentary sequence, southeast Greenland (No. 2–4).

Murcia, H.F., Borrero, C.A., Pardo, N., Alvarado, G.E., Arnosio, M., Scolamacchia, T. 2013. Depósitos Volcaniclásticos: Términos Y Conceptos Para Una Clasificación En Español Volcaniclastic Deposits: Terminology and Concepts for a Classification in Spanish. **Revista Geológica de América Central**, 48: 15–39. https://doi.org/10.15517/rgac.v0i48.12211.

Nadalin, R. J. 2016. Tópicos especiais em cartografia geológica. Universidade Federal do Paraná.

Németh, K., Palmer, J. 2019. Geological mapping of volcanic terrains: Discussion on concepts, facies models, scales, and resolutions from New Zealand perspective. **Journal of Volcanology and Geothermal Research**, 385: 27-45

Newhall, C.G., Self, S. 1982. The volcanic explosivity index (VEI): an estimate of explosive magnitude for historical volcanism. **Journal of Geophysical Research**, 87: 123–1238. https://doi.org/10.1029/jc087ic02p01231.

Ort, M.H., Lefebvre, N.S., Neal, C.A., McConnell, V.S., Wohletz, K.H. 2018. Linking the Ukinrek 1977 maar-eruption observations to the tephra deposits: New insights into maar depositional processes. **Journal of Volcanology and Geothermal Research**, 360: 36–60. https://doi.org/10.1016/j.jvolgeores.2018.07.005.

Óskarsson, B.V., Riishuus, M.S. 2014. The mode of emplacement of Neogene flood basalts in eastern Iceland: Facies architecture and structure of simple aphyric basalt groups. **Journal of Volcanology and Geothermal Research**, 289: 170–192. https://doi.org/10.1016/j.jvolgeores.2014.11.009.

Pacheco, F. E. R. C., Caxito, F. A, Moraes, L. C., Marangoni, Y. R., Santos, R. P. Z., Pedrosa-Soares, A. C. 2018. Basaltic ring structures of the Serra Geral Formation at the southern Triângulo Mineiro, Água Vermelha region, Brazil. **Journal of Volcanology and Geothermal Research**, 355: 136-148.

Peate, D. W. 1989. Stratigraphy and petrogenesis of the Parana Continental Flood Basalts, Southern Brazil. Tese (Doutorado). Open University. 359 pg.

Peate, D. W. 1997. The Paraná-Etendeka Province. In: Mahoney, J.J., Coffin, M.F. (Eds.), Large Igneous Provinces: Continental, Oceanic, and Planetary Food Volcanism. **Am. Geophys. Union Geophys. Monogr**. 100: 217-246.

Peate, D. W.; Hawkesworth, C. J.; Mantovani, M. S. M. 1992. Chemical stratigraphy of the Paraná lavas (South America): classification of magma types and their spatial distribution, **Bulletin of Volcanology**, 55:119-139.

Petersohn, E. 2018. Potencial petrolífero brasileiro e as rodadas de licitações da ANP. Apresentação, disponível em: http://www.anp.gov.br/images/Palestras/SDB_011.2018_potencial_petrolifero_brasileiro.pdf

Petry, K., Jerram, D. A., De Almeida, D. D. P. M., Zerfass, H. 2007. Volcanic-sedimentary features in the Serra Geral Fm., Paraná Basin, southern Brazil: examples of dynamic lava-sediment interactions in an arid setting. **Journal of Volcanology and Geothermal Research**, 159: 313–325.

Postek, M. T., Howard, K. S., Johnson, A. H., McMichael, K. L. 1980. Scanning electron microscopy. A student's handbook. Ladd Research Industries. Inc.

Piccirillo, E.M., Melfi, A.J. (Eds.). 1988. The Mesozoic Flood Volcanism of the Paraná Basin. Inst. Astron. Geofísico, Univ. São Paulo, São Paulo, 600 pg.

Piccirillo, E.M., Melfi, A.J., Comin-Chiaramonti, P., Bellieni, G., Ernesto, M., Marques, L.S., Nardy, A.J.R., Pacca, I.G., Roisenberg, A., Stolfa, D., 1988. Continental flood volcanism from the Paraná Basin (Brazil). In: MacDougall, J.D. (Ed.), Continental Flood Basalts. Kluwer Acad. Publ., 195–238.

Pinto, V.M., Hartmann, L.A., Santos, J.O.S., McNaughton, N.J., Wildner, W., 2011. Zircon U-Pb geochronology from the Paraná bimodal volcanic province support a brief eruptive cycle at ~135 Ma. **Chem. Geol**. 281: 93–102.

Reading, H. R. 1996. Sedimentary Environments: Processes, Facies and Stratigraphy. Blackwell, Oxford

Renne, P. R., Ernesto, M., Pacca, I. G., Coe, R. S., Glen, J. M.,Prévot, M., Perrin, M. 1992. The age of Parana flood volcanism, rifting of Gondwanaland, and the Jurassic Cretaceous boundary. **Science:** 258, 975–979.

Riccomini, C., Sant'Anna, L.G., Fambrini, G.L. 2016. The Early Cretaceous Jacuí Group, a newly discovered volcaniclastic-epiclastic accumulation at the top of the Paraná Basin, southern Brazil. **Cretaceous Research**, 59: 111–128. https://doi.org/10.1016/j.cretres.2015.10.020.

Rocha-Júnior, E.R.V., Marques, L.S., Babinski, M., Nardy, A.J.R., Figueiredo, A.M.G., Machado, F.B. 2013. Sr-Nd-Pb isotopic constraints on the nature of the mantle sources involved in the genesis of the high-Ti tholeiites from northern Paraná Continental Flood Basalts (Brazil). **Journal of South American Earth Sciences**, 46: 9–25. https://doi.org/10.1016/j.jsames.2013.04.004.

Rocha-Júnior, E.R.V., Puchtel, I.S., Marques, L.S., Walker, R.J., Machado, F.B., Nardy, A.J.R., Babinski, M., Figueiredo, A.M.G. 2012. Re-Os isotope and highly siderophile element systematics of the Paraná continental flood basalts (Brazil). **Earth and Planetary Science Letters**, 337–338: 164–173. https://doi.org/10.1016/j.epsl.2012.04.050.

Rogerson, M., Mercedes-Martín, R., Brasier, A. T., McGill, R. A., Prior, T. J., Vonhof, H., Fellows, S. M, Reijmer, J. G., McClymont, E., Billing, I., Matthews, A. Pedley, H. M. 2017. Are spherulitic lacustrine carbonates an expression of large-scale mineral carbonation? A case study from the East Kirkton Limestone, Scotland. **Gondwana Research**, *48*: 101-109.

Ross, P.S., Delpit, S., Haller, M.J., Németh, K., Corbella, H. 2011. Influence of the substrate on maar-diatreme volcanoes - An example of a mixed setting from the Pali Aike volcanic field, Argentina. **Journal of Volcanology and Geothermal Research**, 201: 253–271. https://doi.org/10.1016/j.jvolgeores.2010.07.018.

Ross, P.S., Ukstins Peate, I., McClintock, M.K., Xu, Y.G., Skilling, I.P., White, J.D.L., Houghton, B.F. 2005. Mafic volcaniclastic deposits in flood basalt provinces: A review. **Journal of Volcanology and Geothermal Research**, 145: 281–314. https://doi.org/10.1016/j.jvolgeores.2005.02.003.

Ross, P.S., White, J.D.L. 2005. Mafic, large-volume, pyroclastic density current deposits from phreatomagmatic eruptions in the ferrar large igneous province, Antarctica. **Journal of Geology**, 113: 627–649. https://doi.org/10.1086/449324.

Ross, P.S., White, J.D.L. 2006. Debris jets in continental phreatomagmatic volcanoes: A field study of their subterranean deposits in the Coombs Hills vent complex, Antarctica. **Journal of Volcanology and Geothermal Research**, 149: 62–84. https://doi.org/10.1016/j.jvolgeores.2005.06.007.

Ross, P.S., White, J.D.L. 2012. Quantification of vesicle characteristics in some diatreme-filling deposits, and the explosivity levels of magma-water interactions within diatremes. **Journal of Volcanology and Geothermal Research**, 245–246: 55–67. https://doi.org/10.1016/j.jvolgeores.2012.07.006.

Ross, P.S., White, J.D.L., McClintock, M. 2008. Geological evolution of the Coombs-Allan Hills area, Ferrar large igneous province, Antarctica: Debris avalanches, mafic pyroclastic density currents, phreatocauldrons. **Journal of Volcanology and Geothermal Research**, 172: 38–60. https://doi.org/10.1016/j.jvolgeores.2005.11.011.

Rossetti, L., Lima, E.F., Waichel, B.L., Hole, M.J., Simões, M.S., Scherer, C.M.S. 2018. Lithostratigraphy and volcanology of the Serra Geral Group, Paraná-Etendeka Igneous Province in Southern Brazil: Towards a formal stratigraphical framework. **Journal of Volcanology and Geothermal Research**, 355: 98–114. https://doi.org/10.1016/j.jvolgeores.2017.05.008.

Rossetti, L.M., Healy, D., Hole, M.J., Millett, J.M., de Lima, E.F., Jerram, D.A., Rossetti, M.M.M. 2019. Evaluating petrophysical properties of volcano-sedimentary sequences: A case study in the Paraná-Etendeka Large Igneous Province. **Marine and Petroleum Geology**, 102: 638–656. https://doi.org/10.1016/j.marpetgeo.2019.01.028.

Rossetti, L.M., Lima, E.F., Waichel, B.L., Scherer, C.M., Barreto, C.J. 2014. Stratigraphical framework of basaltic lavas in Torres Syncline main valley, southern Parana-Etendeka Volcanic Province. **Journal of South American Earth Sciences**, 56: 409–421. https://doi.org/10.1016/j.jsames.2014.09.025.

Rowland, S.K., Walker, G.P. 1990. Pahoehoe and aa in Hawaii: volumetric flow rate controls the lava structure. **Bulletin of Volcanology**, 52: 615–628. https://doi.org/10.1007/BF00301212.

Rüegg, N.R., 1970. A composição química das rochas basálticas da Bacia do Paraná (América do Sul) e de outras províncias gonduânicas equivalentes. Mus. Labor. Mineral. Geol., Univ. Coimbra. Coimbra, **Memória e Notícias,** 70: 26–85.

Scherer, C.M.S., 2002. Preservation of aeolian genetic units by lava flows in the Lower Cretaceous of the Paran Basin, southern Brazil. **Sedimentology** 49: 97–116. https:// doi.org/10.1046/j.1365-3091.2002.00434.x.

Schipper, I.C., White, J.D.L. 2016. Magma-slurry interaction in Surtseyan eruptions. **Geology**, 44: 195–198. https://doi.org/10.1130/G37480.1.

Schmincke, H. -U, Fisher, R.V., Waters, A.C. 1973. Antidune and chute and pool structures in the base surge deposits of the Laacher See area, Germany. **Sedimentology**, 20: 553–574. https://doi.org/10.1111/j.1365-3091.1973.tb01632.x.

Schneider, R. L., Mühlmann, H., Tommasi, E., Medeiros, R. A., Daemon, R. F., Nogueira, A. A. 1974. Revisão estratigráfica da Bacia do Paraná. *Anais*....Congresso Brasileiro de Geologia, 28, Porto Alegre. São Paulo: Sociedade Brasileira de Geologia, 1: 41-65.

Schumacher, R., Schmincke, H.U. 1995. Models for the origin of accretionary lapilli. **Bulletin of Volcanology**, 56: 626–639. https://doi.org/10.1007/BF00301467.

Self, S., Keszthelyi, L., Thordarson, T. 1998. The importance of pāhoehoe. **Annual Review of Earth and Planetary Sciences**, *26*(1): 81-110.

Self, S., Sparks, R.S.J., 1978. Characteristics of widespread pyroclastic deposits formed by the interaction of silicic magma and water. **Bull. Volcanol.,** 41: 196-212.

Self, S., Thordarson, T., Keszthelyi, L. 1997. Emplacement of continental flood basalt lava flows. Geophysical Monograph - American Geophysical Union, 100: 381-410.

Self, S., Thordarson, T., Keszthelyi, L., Walker, G.P.L., Hon, K., Murphy, M.T., Long, P., Finnemore, S. 1996. A new model for the emplacement of Columbia River basalts as large, inflated pahoehoe lava flow fields. **Geophysical Research Letters**, 23: 2689–2692. https://doi.org/10.1029/96GL02450.

Sheridan, M.F., Wohletz, K.H. 1983. Hydrovolcanism: Basic considerations and review. **Journal of Volcanology and Geothermal Research**, 17: 1–29. https://doi.org/10.1016/0377-0273(83)90060-4.

Silver, P., Behn, M.D., Kelley, K., Schmitz, M., Savage, B. 2006. Understanding cratonic flood basalts. **Earth and Planetary Science Letters**, 245: 190–201. https://doi.org/10.1016/j.epsl.2006.01.050.

Single, R., Jerram, D., 2004. The 3D facies architecture of flood basalt provinces and their internal heterogeneity: examples from the Palaeogene Skye Lava Field. J. Geol. Soc. London. 161, 911–926.

Skilling, I.P., White, J.D.L., McPhie, J. 2002. Peperite: A review of magma-sediment mingling. **Journal of Volcanology and Geothermal Research**, 114: 1–17. https://doi.org/10.1016/S0377-0273(01)00278-5.

Smith, N.J., Kokelaar, B.P. 2013. Proximal record of the 273 ka Poris caldera-forming eruption, Las Cañadas, Tenerife. **Bulletin of Volcanology**, 75: 1–21. https://doi.org/10.1007/s00445-013-0768-4.

Soares, P. C., Landim, P. M. B., Fulfaro, V. J. 1978. Tectonic cycles and sedimentary sequences in the Brazilian intracratonic basins. **Geological Society of America Bulletin**, 89(2):181-191.

Sohn, Y.K. 1996. Hydrovolcanic processes forming basaltic tuff rings and cones on Cheju Island, Korea. **Bulletin of the Geological Society of America**, 108: 1199–1211. https://doi.org/10.1130/0016-7606(1996)108<1199:HPFBTR>2.3.CO;2.

Sohn, Y.K., Chough, S.K. 1989. Depositional processes of the Suwolbong tuff ring, Cheju Island (Korea). **Sedimentology**, 36: 837–855. https://doi.org/10.1111/j.1365-3091.1989.tb01749.x.

Sohn, Y.K., Yoon, S.H. 2010. Shallow-marine records of pyroclastic surges and fallouts over water in Jeju Island, Korea, and their stratigraphic implications. **Geology**, 38: 763–766. https://doi.org/10.1130/G30952.1.

Sottili, G., Taddeucci, J., Palladino, D. M., Gaeta, M., Scarlato, P., Ventura, G. 2009. Sub-surface dynamics and eruptive styles of maars in the Colli Albani Volcanic District, Central Italy. **Journal of Volcanology and Geothermal Research**, *180*(2-4): 189-202.

Stearns, H. T., Macdonald, G. A. 1946. Geology and ground-water resources of the island of Hawaii. **Hawaii Div. Hydrol. Bull**., 67: 3-49.

Stica, J.M., Zalán, P.V., Ferrari, A.L., 2014. The evolution of rifting on the volcanic margin of the Pelotas Basin and the contextualization of the Paraná–Etendeka LIP in the separation of Gondwana in the South Atlantic. **Mar. Petrol. Geol**. 50: 1–21. https://doi.org/10.1016/j.marpetgeo.2013.10.015.

Svensen, H., Planke, S., Polozov, A.G., Schmidbauer, N., Corfu, F., Podladchikov, Y.Y., Jamtveit, B. 2009. Siberian gas venting and the end-Permian environmental crisis. **Earth and Planetary Science Letters**, 277: 490–500. https://doi.org/10.1016/j.epsl.2008.11.015.

Svensen, H.H., Torsvik, T.H., Callegaro, S., Augland, L., Heimdal, T.H., Jerram, D.A., Planke, S., Pereira, E. 2018. Gondwana Large Igneous Provinces: Plate reconstructions, volcanic basins and sill volumes. **Geological Society Special Publication**, 463: 17–40. https://doi.org/10.1144/SP463.7.

Shaw, H. R., Swanson, D. A. 1970. Eruption and flow rates of flood basalts. *Proc….* Second Columbia River Basalt*,* Eastern Washington State College Press Cheney.

Swanson, D.A., Wright, T.L., Helz, R.T. 1975. Linear vent systems and estimated rates of magma production and eruption for the Yakima Basalt on the Columbia Plateau. **American Journal of Science**, 275: 877–905. https://doi.org/10.2475/ajs.275.8.877.

Szatmari, P., Milani, E.J., 2016. Tectonic control of the oil-rich large igneous-carbonate-salt province of the South Atlantic rift. **Marine and Petroleum Geology**, 77: 567–596. https://doi.org/10.1016/j.marpetgeo.2016.06.004.

Thomaz, L.V., Lobo, J.T., Roisenberg, A. 2015. An integrated methodology to evaluate the basaltic volcanism environment: a petroleum exploration approach. Proc.... Simpósio de Vulcanismo e Ambientes Associados, São Paulo, Brasil.

Thompson, D. L., Stilwell, J. D., Hall, M. 2015. Lacustrine carbonate reservoirs from Early Cretaceous rift lakes of Western Gondwana: Pre-salt coquinas of Brazil and West Africa. **Gondwana Research**, 28(1): 26-51.

Thordarson, T., Self, S. 1998. The Roza Member, Columbia River Basalt Group: A gigantic pahoehoe lava flow field formed by endogenous processes? **Journal of Geophysical Research: Solid Earth**, 103: 27411–27445. https://doi.org/10.1029/98jb01355.

Tucker, M. E. 2001. Sedimentary petrology: an introduction to the origin of sedimentary rocks. John Wiley & Sons.

Ukstins Peate, I., Larsen, M., Lesher, C.E. 2003. The transition from sedimentation to flood volcanism in the Kangerlussuaq Basin, East Greenland: Basaltic pyroclastic volcanism during initial Palaeogene continental break-up. **Journal of the Geological Society**, 160: 759–772. https://doi.org/10.1144/0016-764902-071.

Vail, P. R., Mitchum Jr, R. M., Thompson III, S. 1977. Seismic stratigraphy and global changes of sea level: Part 4. Global cycles of relative changes of sea level.: Section 2. Application of seismic reflection configuration to stratigraphic interpretation.

Valentine, G.A. 1987. Stratified flow in pyroclastic surges. *Bulletin of Volcanology*, *49*(4), 616-630.

Valentine, G.A., Graettinger, A.H., Macorps, É., Ross, P.S., White, J.D.L., Döhring, E., Sonder, I. 2015a. Experiments with vertically and laterally migrating subsurface explosions with applications to the geology of phreatomagmatic and hydrothermal explosion craters and diatremes. **Bulletin of Volcanology**, 77: 1–17. https://doi.org/10.1007/s00445-015-0901-7.

Valentine, G.A., Graettinger, A.H., Sonder, I. 2014. Explosion depths for phreatomagmatic eruptions. **Geophysical Research Letters**, 41: 3045–3051. https://doi.org/10.1002/2014GL060096.

Valentine, G.A., Sottili, G., Palladino, D.M., Taddeucci, J. 2015b. Tephra ring interpretation in light of evolving maar-diatreme concepts: Stracciacappa maar (central Italy). **Journal of Volcanology and Geothermal Research**, 308: 19–29. https://doi.org/10.1016/j.jvolgeores.2015.10.010.

Valentine, G.A., White, J.D.L. 2012. Revised conceptual model for maar-diatremes: Subsurface processes, energetics, and eruptive products. **Geology**, 40: 1111–1114. https://doi.org/10.1130/G33411.1.

Valentine, G.A., White, J.D.L., Ross, P.-S., Graettinger, A.H., Sonder, I. 2017. Updates to Concepts on Phreatomagmatic Maar-Diatremes and Their Pyroclastic Deposits. **Frontiers in Earth Science**, 5: 68. https://doi.org/10.3389/feart.2017.00068.

Valore, L.A., Licht, O.A.B., 2016. A mafic volcaniclastic deposit (MVD) of the Serra Geral Group, Sertanópolis, State of Paraná. Anais... 48º Congresso Brasileiro de Geologia, SBG, Porto Alegre.

Valore, L. A., Licht, O. A. B, Höfig, D. F., Vasconcellos, E. M. G., Ukstins Peate, I., Óskarsson, B. V. 2017. Mafic volcaniclastic deposits of the Paraná Igneous Province and their correlation to chemostratigraphy - State of Paraná, Brazil. Anais...X Simpósio Sul Brasileiro de Geologia, SBG, Curitiba.

Van Eaton, A.R., Wilson, C.J.N. 2013. The nature, origins and distribution of ash aggregates in a large-scale wet eruption deposit: Oruanui, New Zealand. **Journal of Volcanology and Geothermal Research**, 250: 129–154. https://doi.org/10.1016/j.jvolgeores.2012.10.016.

van Otterloo, J., Cas, R.A.F., Scutter, C.R. 2015. The fracture behaviour of volcanic glass and relevance to quench fragmentation during formation of hyaloclastite and phreatomagmatism. **Earth-Science Reviews,** 151,: 79-116.

van Otterloo, J., Cas, R.A.F., Sheard, M.J. 2013. Eruption processes and deposit characteristics at the monogenetic Mt. Gambier Volcanic Complex, SE Australia: Implications for alternating magmatic and phreatomagmatic activity. **Bulletin of Volcanology**, 75: 1–21. https://doi.org/10.1007/s00445-013-0737-y.

Vazquez, J.A., Ort, M.H. 2006. Facies variation of eruption units produced by the passage of single pyroclastic surge currents, Hopi Buttes volcanic field, USA. **Journal of Volcanology and Geothermal Research**, 154: 222–236. https://doi.org/10.1016/j.jvolgeores.2006.01.003.

Waichel, B.L., de Lima, E.F., Lubachesky, R., Sommer, C.A. 2006. Pahoehoe flows from the central Paraná Continental Flood Basalts. **Bulletin of Volcanology**, 68: 599–610. https://doi.org/10.1007/s00445-005-0034-5.

Waichel, B.L., de Lima, E.F., Sommer, C.A., Lubachesky, R. 2007. Peperite formed by lava flows over sediments: An example from the central Paraná Continental Flood Basalts, Brazil. **Journal of Volcanology and Geothermal Research**, 159: 343–354. https://doi.org/10.1016/j.jvolgeores.2006.07.009.

Waichel, B.L., de Lima, E.F., Viana, A.R., Scherer, C.M., Bueno, G.V., Dutra, G. 2012. Stratigraphy and volcanic facies architecture of the Torres Syncline, Southern Brazil, and its role in understanding the Paraná-Etendeka Continental Flood Basalt Province. **Journal of Volcanology and Geothermal Research**, 215–216: 74–82. https://doi.org/10.1016/j.jvolgeores.2011.12.004.

Walker, G.P.L. 1971. Compound and simple lava flows and flood basalts. **Bulletin Volcanologique**, 35: 579–590. https://doi.org/10.1007/BF02596829.

Walker, G. P. L. 1973. Mount Etna and the 1971 eruption-Lengths of lava flows. **Philosophical Transactions of the Royal Society of London**. Series A, Mathematical and Physical Sciences, 274(1238): 107-118.

Walker, G.P.L. 1981. Characteristics of two phreatoplinian ashes, and their water-flushed origin. **Journal of Volcanology and Geothermal Research**, 9: 395–407. https://doi.org/10.1016/0377-0273(81)90046-9.

Walker, G. P. 1987. Pipe vesicles in Hawaiian basaltic lavas: Their origin and potential as paleoslope indicators. **Geology,** *15*(1): 84-87.

Walker, G.P.L. 1989. Spongy pahoehoe in Hawaii: A study of vesicle-distribution patterns in basalt and their significance. **Bulletin of Volcanology**, 51: 199–209. https://doi.org/10.1007/BF01067956.

Walker, G. P. 1991. Structure, and origin by injection of lava under surface crust, of tumuli,"lava rises","lava-rise pits", and "lava-inflation clefts" in Hawaii. **Bulletin of Volcanology,** *53*(7): 546-558.

Walker, R.G., James, N. P. 1992, Facies Models: response to sea level change. Geol Assoc Can.

Washburne, Ch. W. 1930. Petroleum geology of the State of São Paulo. Comissão Geográfica e Geológica do Estado de São Paulo, São Paulo, **Bol.** 22, 282 p.

Watton, T.J., Jerram, D.A., Thordarson, T., Davies, R.J. 2013. Three-dimensional lithofacies variations in hyaloclastite deposits. **Journal of Volcanology and Geothermal Research**, 250: 19–33. https://doi.org/10.1016/j.jvolgeores.2012.10.011.

Wentworth, C.K.. 1922. A scale of grade and class terms for clastic sediments. The **Journal of Geology**, 30: 377–392.

White, I.C. 1908. Comissão de Estudos das Minas de Carvão de Pedra do Brazil – Relatório Final. In: CPRM. 2008. Edição comemorativa: 100 anos do Relatório White. Edição fac-similar, Imprensa Nacional, Rio de Janeiro, 617 p.

White, J.D. 1991. Maar-diatreme phreatomagmatism at Hopi Buttes, Navajo Nation (Arizona), USA. **Bulletin of Volcanology**, 53: 239–258. https://doi.org/10.1007/BF00414522.

White, J. D. 1996. Impure coolants and interaction dynamics of phreatomagmatic eruptions. **Journal of Volcanology and Geothermal Research**, *74*(3-4): 155-170.

White, J.D.L., Bryan, S.E., Ross, P.S., Self, S., Thordarson, T. 2009. Physical volcanology of continental large igneous provinces: Update and review. **Studies in volcanology: the legacy of George Walker. Special Publications of IAVCEI,** 2: 291-321. https://doi.org/10.1144/iavcel002.15.

White, J.D.L., Houghton, B.F. 2006. Primary volcaniclastic rocks. **Geology**, 34: 677–680. https://doi.org/10.1130/G22346.1.

White, J.D.L., McClintock, M.K. 2001. Immense vent complex marks flood-basalt eruption in a wet, failed rift: Coombs Hills, Antarctica. **Geology**, 29: 935–938. https://doi.org/10.1130/0091-7613(2001)029<0935:IVCMFB>2.0.CO;2.

White, J.D.L., McPhie, J., and Skilling, I., 2000, Peperite: A useful genetic term. **Bulletin of Volcanology**, 62: 65–66, doi: 10.1007/s004450050293.

White, J. D. L., Houghton, B. 2000. Surtseyan and related phreatomagmatic eruptions. In: Sigurdsson, H., Houghton, B., McNutt, S., Rymer, H., Stix, J. Encyclopedia of volcanoes. Academic press. San Diego, 495-513.

White, J.D.L., Ross, P.S. 2011. Maar-diatreme volcanoes: A review. **Journal of Volcanology and Geothermal Research**, 201: 1–29. https://doi.org/10.1016/j.jvolgeores.2011.01.010.

White, J.D.L., Valentine, G.A. 2016. Magmatic versus phreatomagmatic fragmentation: Absence of evidence is not evidence of absence. **Geosphere**, 12: 1478–1488. https://doi.org/10.1130/GES01337.1.

Wilmoth, R.A., Walker, G.P.L. 1993. P-type and S-type pahoehoe: a study of vesicle distribution patterns in Hawaiian lava flows. **Journal of Volcanology and Geothermal Research**, 55: 129–142. https://doi.org/10.1016/0377-0273(93)90094-8.

Williamson, I. T., Bell, B. R. 1994. The Palaeocene lava field of west-central Skye, Scotland: Stratigraphy, palaeogeography and structure. **Earth and Environmental Science Transactions of The Royal Society of Edinburgh**, 85(1): 39-75.

Wohletz, K.H. 1983. Mechanisms of hydrovolcanic pyroclast formation: Grain-size, scanning electron microscopy, and experimental studies. **Journal of Volcanology and Geothermal Research**, 17: 31–63. https://doi.org/10.1016/0377-0273(83)90061-6.

Wohletz, K. H. 1986. Explosive magma-water interactions: Thermodynamics, explosion mechanisms, and field studies. **Bulletin of Volcanology**, 48: 245-264.

Wohletz, K. H. 1998. Pyroclastic surges and two-phase compressible flows. In: Freundt, A., Rosi, M. From magma to tephra: modelling physical processes of explosive volcanic eruptions (No. 4). Elsevier, Amsterdam. p. 247-312.

Wohletz, K.H. 2002. Water/magma interaction: Some theory and experiments on peperite formation. **Journal of Volcanology and Geothermal Research**, 114: 19–35. https://doi.org/10.1016/S0377-0273(01)00280-3.

Wohletz, K.H. 2003. Water/magma interaction: Physical considerations for the deep submarine environment, In: Geophysical Monograph Series. Blackwell Publishing Ltd, pp. 25–49. https://doi.org/10.1029/140GM02.

Wohletz, K.H., Sheridan, M.F. 1983. Hydrovolcanic explosions II. Evolution of basaltic tuff rings and tuff cones. **American Journal of Science**, 283: 385–413. https://doi.org/10.2475/ajs.283.5.385.

Zalán, P. V., Wolff, S., Conceição, J. D. J., Astolfi, M. A. M., Vieira, I. S., Appi, V. T., Zanotto, O. A. 1987. Tectônica e sedimentação da Bacia do Paraná. 3ºSimpósio Sul-Brasileiro de Geologia,p 441-473.

Zalán, P.V., Wolff, S., Astolfi, M.A.M., et al., 1990. The Paraná Basin, Brazil. In: In: Leighton, M.W., Kolata, D.R., Oltz, D.F., Eidel, J.J. (Eds.), Interior Cratonic Basins, vol. 51. American Association of Petroleum Geologists Memoir, pp. 683–708.

Zalán, P. V. 1991. Influence of pre-Andean orogenies on the Paleozoic intracratonic basins of South America. 4th Simposio Bolivariano-Exploracion Petrolera en las Cuencas Subandinas. Asociación Colombiana de Geólogos y Geofisicos del Petróleo – ACGGP.

Zimanowski, B., Büttner, R., Dellino, P., White, J.D.L., Wohletz, K.H. 2015. Magma–Water Interaction and Phreatomagmatic Fragmentation. In: Sigurdsson, H., Houghton, B., McNutt, S., Rymer, H., Stix, J. The Encyclopedia of Volcanoes, 473–484. https://doi.org/10.1016/b978-0-12-385938-9.00026-2.

Zimanowski, B, Büttner, R., Lorenz, V., Häfele, H.-G. 1997. Fragmentation of basaltic melt in the course of explosive volcanism. **Journal of Geophysical Research: Solid Earth**, 102: 803–814. https://doi.org/10.1029/96jb02935.